

Mechanistic Studies of the Class I Ribonucleotide
Reductase from *Escherichia coli*

by

Erin Jelena Artin

Submitted to the Department of Chemistry
in partial fulfillment of the requirements for the degree of

Doctor of Science in Biochemistry

at the

MASSACHUSETTS INSTITUTE OF TECHNOLOGY

June 2006

© Massachusetts Institute of Technology 2006. All rights reserved.

Author
Department of Chemistry
May 15, 2006

Certified by
Daniel S. Kemp
Professor of Chemistry

Accepted by
Robert W. Field
Chairman, Department Committee on Graduate Students

This doctoral thesis has been examined by a committee of the Department of Chemistry as follows:

Professor Daniel S. Kemp.....
Committee Chair

Professor Catherine L. Drennan.....

Professor Robert G. Griffin

Mechanistic Studies of the Class I Ribonucleotide Reductase from *Escherichia coli*

by
Erin Jelena Artin

Submitted to the Department of Chemistry
on May 15, 2006, in partial fulfillment of the
requirements for the degree of
Doctor of Science in Biochemistry

Abstract

Ribonucleotide reductases (RNRs) catalyze the conversion of nucleotides to deoxynucleotides, providing the monomeric precursors required for DNA replication and repair. The class I RNRs are found in many bacteria, DNA viruses, and all eukaryotes including humans, and are composed of two homodimeric subunits: R1 and R2. RNR from *Escherichia coli* (*E. coli*) serves as the prototype of this class. R1 has the active site where nucleotide reduction occurs, and R2 contains the diferric-tyrosyl radical ($Y\cdot$) cofactor essential for radical initiation on R1. The rate-determining step in *E. coli* RNR has recently been shown to be a physical step prior to generation of the putative thiyl radical ($S\cdot$) on C439. Thus, the chemistry of nucleotide reduction is kinetically invisible, which has precluded detection of intermediates in the reduction process with the normal substrate. Perturbation of the system using mechanism-based inhibitors and site-directed mutants of R1 and R2 has provided the bulk of the insight into the reduction mechanism by inference.

The work described in this thesis makes use of two mechanism-based inhibitors, 2'-azido-2'-deoxyuridine-5'-diphosphate (N_3 UDP) and 2'-deoxy-2',2'-difluorocytidine-5'-diphosphate (dFdCDP), and one active site mutant, E441Q R1, to further our understanding of the catalytic capabilities of RNR. The results provide strong support for a 3'-ketodeoxynucleotide intermediate postulated to lie on the normal reduction pathway, as well as for the elimination of nitrogenous base in the active site of R1 during inhibition. The studies further show that under physiologically relevant reducing conditions, inhibition of RNR by the clinically important nucleotide analog dFdCDP is a result of covalent modification. An essential part of these studies was the development of a robust, high-yielding enzymatic method for the selective 5'-phosphorylation of cytidine, 2'-deoxycytidine, 2'-deoxyuridine and their analogs that are not amenable to standard chemical phosphorylation methods.

Thesis Supervisor: JoAnne S. Stubbe

Title: Novartis Professor of Chemistry and Professor of Biology

Acknowledgments

I am grateful to Isaac Colbert and Toni Robinson for the help, support and encouragement they have given me, and for their personal integrity. Professors Catherine Drennan, Sylvia Ceyer, and Stuart Licht guided me through the graduation process within the Chemistry Department. I thank the members of my thesis committee, Professors Catherine Drennan, Robert Griffin, and Daniel Kemp for their advice, care, and time.

Many of the accomplishments described in this thesis would not have been possible without the involvement of colleagues and collaborators. John Robblee, Jie Ge, Deborah Perlstein, Debora Martino, Galit Bar, Nicholas Lees, Gregory Lohman, Mohammad Seyed-sayamdost, Aaron Hoskins, Stanislaw Wnuk, Jörg Fritscher, Yongting Wang, and Bernd Giese were always ready to share their expertise and provide encouragement. I thank them for helping me become a better scientist.

The manuscript itself has been immeasurably improved by Christopher Wipf's insightful comments, suggestions on style, and his knowledge of English grammar. When I grow up, I hope to be able to write like he.

Helpful comments on parts of this manuscript were supplied by friends and colleagues. I am most grateful to them all: John Robblee, Debora Martino, Danil Suits, and Jun Wang. I owe a special debt to John Robblee for his technical input on Chapters 2, 4, and 5.

Completion of this manuscript would not have been possible without Ben Artin's contribution to the figures and formatting. That I felt that I could rely on him with complete confidence was a gift for which I am grateful.

Professor Catherine Drennan spent many hours proofreading this manuscript and steering it through many stages of completion.

Ben Artin, Christopher Wipf, and Tijana Antonić advised me, inspired me, encouraged me, and sustained me. Most of all, they believed in me at times when I didn't think it was at all clear that confidence was warranted.

This thesis is dedicated to Budimka and Tripko Milićević, my grandparents, who introduced me to the joy of understanding the world, with gratitude, admiration, and love.

Contents

1	Introduction	17
1.1	General background	17
1.2	Structure	18
1.3	Kinetic model for <i>E. coli</i> RNR	20
1.4	Proposed mechanism of ribonucleotide reduction	21
1.5	Mechanism-based inhibition of RNR	22
1.6	Evidence for the proposed mechanism of ribonucleotide reduction	23
1.7	Scope of this thesis	23
	Bibliography	25
2	Structure of the nitrogen-centered radical formed during inactivation of Class I <i>Escherichia coli</i> ribonucleotide reductase by 2'-azido-2'-deoxyuridine-5'-diphosphate: trapping of the 3'-ketonucleotide	29
2.1	Introduction	29
2.2	Materials and methods	31
2.2.1	Purchased materials and materials obtained as gifts	31
2.2.2	Protein overexpression, purification, and activity assays	31
2.2.3	Examination of the reaction of N ₃ UDP and RNR by 9 GHz EPR spectroscopy	32
2.2.4	Examination of the reaction of N ₃ UDP and RNR by 140 GHz EPR spectroscopy	32
2.2.5	Simulations of the EPR spectra	33
2.2.6	Computational methods	33
2.3	Results	33
2.3.1	9 GHz EPR experiments	34
2.3.2	140 GHz EPR experiments	35
2.3.3	Quantum chemical calculations to assign the structure of N·	36
2.4	Discussion	40
2.4.1	Structural assignment of N·	40
2.4.2	Mechanistic implications	42
2.5	Acknowledgments	44
	Bibliography	44

3	Development of a high-yielding enzymatic method for the 5'-phosphorylation of C, dC, dU and their 2'-analogs	49
3.1	Introduction	49
3.2	Materials and methods	52
3.2.1	Purchased materials and materials obtained as gifts	52
3.2.2	Growth and induction of 6xHis-HdCK expression strain	52
3.2.3	Purification of 6xHis-HdCK	53
3.2.4	Spectrophotometric and radioactive assays of 6xHis-HdCK	54
3.2.5	Growth and induction of human GST-UMP-CMP kinase	54
3.2.6	Purification of human GST-UMP-CMP kinase	55
3.2.7	Assay of human GST-UMP-CMP kinase	55
3.2.8	Formation of nucleoside monophosphates	55
3.2.9	Formation of nucleoside diphosphates	56
3.2.10	Purification of dCDP, dUDP, and their 2'-analogs after enzymatic diphosphorylation	56
3.2.11	Purification of CDP after enzymatic diphosphorylation	57
3.3	Results	57
3.3.1	Growth and induction of 6xHis-HdCK expression strain	57
3.3.2	Purification and activity assays of 6xHis-HdCK	58
3.3.3	Growth and induction of human GST-UMP-CMP kinase	60
3.3.4	Purification and activity assays of human GST-UMP-CMP kinase	60
3.3.5	Formation of nucleoside monophosphates	61
3.3.6	Formation of nucleoside diphosphates	62
3.3.7	Purification of dCDP, dUDP, and their 2'-analogs after enzymatic diphosphorylation	62
3.3.8	Purification of CDP after enzymatic diphosphorylation	63
3.4	Discussion	64
	Bibliography	66
4	Effect of removing the general acid/base catalyst E441 from the RNR reaction: evidence for the formation of an α,β-unsaturated 2'-ketyl radical anion	69
4.1	Introduction	69
4.2	Materials and methods	73
4.2.1	Purchased materials and materials obtained as gifts	73
4.2.2	Protein overexpression, purification, and activity assays	73
4.2.3	Tyrosyl radical loss on R2	76
4.2.4	Synthesis of 5,6-dideuteriocytidine	76
4.2.5	Synthesis of [2'- ² H]-cytidine	77
4.2.6	Enzymatic phosphorylation of specifically deuterated cytidine analogs	77
4.2.7	9 GHz EPR experiments and simulations	79
4.2.8	140 EPR experiments	80

4.2.9	35 GHz ENDOR experiments	81
4.3	Results	82
4.4	Discussion	94
4.5	Acknowledgments	97
	Bibliography	97
5	Inactivation of aerobic <i>Escherichia coli</i> ribonucleotide reductase by 2',2'-difluoro-2'-deoxycytidine-5'-diphosphate: studies on the structure of a substrate-based radical and evidence for covalent modification	101
5.1	Introduction	101
5.2	Materials and methods	103
5.2.1	Purchased materials and materials obtained as gifts	103
5.2.2	Protein overexpression, purification, and activity assays	104
5.2.3	Time-dependent inactivation of R1 and R2 by dFdCDP in the presence and absence of reductants	108
5.2.4	Tyrosyl radical loss on R2 in the presence of dFdCDP	109
5.2.5	Phosphorylation of [5- ³ H]-dFdC to form [5- ³ H]-dFdCMP	109
5.2.6	Phosphorylation of [5- ³ H]-dFdCMP to form [5- ³ H]-dFdCDP	109
5.2.7	Phosphorylation of [1'- ² H]-dFdC to form [1'- ² H]-dFdCMP	110
5.2.8	Phosphorylation of [1'- ² H]-dFdCMP to form [1'- ² H]-dFdCDP	111
5.2.9	Size-exclusion experiments with radio-labeled dFdCDP to look for evidence of covalent modification	112
5.2.10	Identification of non-covalent products generated during inactivation of RNR by dFdCDP	112
5.2.11	Tryptic digest of wt-RNR inhibited by [1'- ³ H]-dFdCDP in the presence of DTT	114
5.2.12	9 GHz EPR experiments and simulations of the reaction of RNR with dFdCDP	115
5.2.13	140 GHz EPR experiments of the reaction of RNR with dFdCDP	116
5.3	Results	116
5.3.1	Protein purification and assays	116
5.3.2	Time-dependent inactivation of RNR subunits by dFdCDP at 3 μM enzyme concentration	120
5.3.3	Quantification of end products of inactivation and size-exclusion experiments with radiolabeled dFdCDP	122
5.3.4	Tryptic digest of wt-RNR inhibited by [1'- ³ H]-dFdCDP in the presence of DTT	124
5.3.5	Studies on the structure of the radical formed in the absence of reductants	125
5.3.6	C225 is necessary for the mode of inactivation observed in the presence of reductants	127
5.3.7	9 GHz EPR measurements aimed at looking for fluorine hyperfine interactions	132

5.3.8	9 GHz simulations	132
5.4	Discussion	133
	Bibliography	135
A	9 GHz EPR experiments on the time-course of <i>E. coli</i> RNR inactivation by N₃NDPs: optimization of conditions for PELDOR measurements	139
A.1	Introduction	139
A.2	Calculations used for measuring distances between Y122 in each monomer of R2	140
A.3	Phosphorylation of 2' - azido - 2' - deoxyuridine and 2' - azido - 2' - deoxycytidine	143
A.4	Results of N ₃ NDP inactivation studies	143
	Bibliography	157
B	<i>Ab initio</i> coupled cluster (CCSD(T)) calculations on HO-N•-SH and HO-CH₂-N•-SH structures	159

List of Figures

1.1	Reaction catalyzed by RNR	17
1.2	Docking model of the R1/R2 complex	19
1.3	Proposed pathway of communication between Y122 on R2 and C439 on R1	20
1.4	Mechanistic model for the reaction catalyzed by RNR	21
1.5	Mechanistic model for RNR inactivation by 2'-substituted nucleotide analogs	22
1.6	Proposed α,β -unsaturated ketyl radical anion formed in the active site of R1 during the reaction of E441Q-R1, wt-R2, TTP, DTT and CDP (Chapter 4)	24
2.1	Pathways for the generation of two previously proposed structures for $N\cdot$. The blue pathway is proposed based on theoretical studies. The black pathways were proposed by van der Donk <i>et al.</i>	30
2.2	9 GHz EPR spectra of $N\cdot$ formed during inactivation of RNR by [3'- ^{16}O]- N_3UDP and $46 \pm 2\%$ enriched [3'- ^{17}O]- N_3UDP	34
2.3	Derivative line shapes of the 140 GHz pulsed EPR spectra of $N\cdot$ formed during inactivation of RNR by [3'- ^{16}O]- N_3UDP and $46 \pm 2\%$ enriched [3'- ^{17}O]- N_3UDP	35
2.4	Structural models of $N\cdot$ used in DFT calculations	36
2.5	Definition of φ and ψ angles in the CNS structural model	38
2.6	Structure of the $N\cdot$ radical with the CNS_{140}^* conformation	40
3.1	6xHis-HdCK induction gel	58
3.2	6xHis-HdCK purification gel by the procedure of Usova <i>et al.</i>	59
3.3	6xHis-HdCK purification gel by the optimized procedure	59
3.4	Human GST-UMP-CMP kinase induction gel	60
3.5	Human GST-UMP-CMP kinase purification gel	61
3.6	Purification of dFdCMP	62
3.7	First purification of dFdCDP	63
3.8	Second purification of dFdCDP	64
3.9	First purification of CDP	65
3.10	Second purification of CDP	65
4.1	Mechanistic model for the reaction catalyzed by RNR	70
4.2	Structures of model ketyl radicals	71
4.3	Proposed mechanism for the formation of α,β -unsaturated ketyl radical anion in the active site of R1	72
4.4	Nucleotide nomenclature	82

4.5	9 GHz EPR spectra of the E441Q-R1, R2, [5'- ² H]-CDP, TTP and DTT reaction (blue), scaled tyrosyl radical (red), and the result of subtraction as explained in the text (purple)	83
4.6	Formation and base-trapping of the 4'-ketyl radical (hydrogens shown in red are at position 5 and 6 of the base)	83
4.7	Formation of the thioether crosslink between C439 and Y730 of E441Q-R1	84
4.8	HPLC separation of peptides from the tryptic digest of [β - ² H]-tyrosine E441Q-R1	84
4.9	HPLC separation of peptides from the tryptic digest of wt <i>E. coli</i> R1	85
4.10	140 GHz EPR spectra of unlabeled or deuterated reactions of E441Q-R1, R2, CDP, TTP, and DTT	86
4.11	Formation of the 2'-ketyl radical	88
4.12	9 GHz EPR spectra of the E441Q-R1, R2, [1'- ² H]-CDP, TTP and DTT reaction, scaled tyrosyl radical, and results of subtraction	89
4.13	9 GHz EPR spectra of the E441Q-R1, R2, [2'- ² H]-CDP, TTP and DTT reaction, scaled tyrosyl radical, and results of subtraction	89
4.14	9 GHz EPR spectra of the E441Q-R1, R2, TTP, DTT and CDP reactions after Y \cdot subtraction	90
4.15	140 GHz EPR spectra of unlabeled or deuterated reactions of E441Q-R1, R2, CDP, TTP, and DTT	91
4.16	9 GHz EPR spectra of the E441Q-R1, R2, [4'- ² H]-CDP, TTP and DTT reaction, scaled tyrosyl radical, and results of subtraction	92
4.17	Deuterium ENDOR spectra of reactions of E441Q-R1, R2, TTP, and DTT with unlabeled or [2'- ² H]-CDP	93
4.18	Deuterium ENDOR spectra of reactions of E441Q-R1, R2, TTP, and DTT with [1'- ² H]-CDP or [5'- ² H]-CDP	94
4.19	Formation of the radical cation in the absence of general base	95
4.20	Resonance structures for the radical cation formed in Figure 4.19	95
5.1	Gemcitabine metabolism	102
5.2	Induction of R2 in deuterated media	117
5.3	SDS-PAGE of purified perdeuterated R2	118
5.4	6xHis-R2 induction gel	119
5.5	6xHis-R2 purification gel	119
5.6	Time-dependent inactivation of R1 in the absence of reductants	120
5.7	Time-dependent inactivation of R2 in the absence of reductants	121
5.8	Time-dependent inactivation of R1 in the presence of reductants	121
5.9	Time-dependent inactivation of R2 in the presence of reductants	122
5.10	Loss of A _{410 nm} in the presence of [5- ³ H]-dFdCDP	123
5.11	Tryptic digest of RNR labeled with [1'- ³ H]-dFdCDP in the presence of DTT and radioactivity profile	125

5.12	Tryptic digest of RNR labeled with [1' - ³ H] - dFdCDP in the presence of DTT and [CH ₃ CN]	126
5.13	9 GHz EPR spectra of the reaction of wt - R1, wt - R2, and ATP with dFdCDP, scaled Y · , and the result of subtraction	127
5.14	9 GHz EPR spectra of the reaction of wt - R1, wt - R2, and ATP with [1' - ² H] - dFdCDP, scaled Y · , and the result of subtraction	128
5.15	Comparison of the new radical from the reaction of wt - R1, wt - R2, and ATP with dFdCDP and [1' - ² H] - dFdCDP	129
5.16	R2 activity loss with wt - R1	130
5.17	R2 activity loss with C225S - R1	130
5.18	9 GHz EPR spectra of the reaction of C225S - R1, wt - R2, and ATP with dFdCDP, scaled Y · , and the result of subtraction	131
5.19	9 GHz EPR spectra of the reaction of C225S - R1, wt - R2, and ATP with [1' - ² H] - dFdCDP, scaled Y · , and the result of subtraction	132
A.1	9 GHz EPR spectra of the reaction of wt <i>E. coli</i> RNR with N ₃ UDP as a function of time	144
A.2	N · spectra in the reaction of wt <i>E. coli</i> RNR with N ₃ UDP as a function of time	145
A.3	Decay curves for radical species in the reaction of wt <i>E. coli</i> RNR with N ₃ UDP	145
A.4	9 GHz EPR spectra of the reaction of wt R1/C268S - R2 <i>E. coli</i> RNR with N ₃ UDP as a function of time	147
A.5	N · spectra in the reaction of wt R1/C268S - R2 <i>E. coli</i> RNR with N ₃ UDP as a function of time	148
A.6	Decay curves for radical species in the reaction of wt R1/C268S - R2 with N ₃ UDP	149
A.7	9 GHz EPR spectra of the reaction of wt <i>E. coli</i> RNR with N ₃ CDP as a function of time	150
A.8	N · spectra in the reaction of wt <i>E. coli</i> RNR with N ₃ CDP as a function of time	151
A.9	Decay curves for radical species in the reaction of wt <i>E. coli</i> RNR with N ₃ CDP	151
A.10	9 GHz EPR spectra of the reaction of wt <i>E. coli</i> RNR with N ₃ UDP as a function of time in the presence of DTT	152
A.11	N · spectra in the reaction of wt <i>E. coli</i> RNR with N ₃ UDP as a function of time in the presence of DTT	153
A.12	Decay curves for radical species in the reaction of wt <i>E. coli</i> RNR with N ₃ UDP in the presence of DTT	154
A.13	Decay curves for total radical in the reaction of RNR with N ₃ NDP	155
A.14	Decay curves for Y · radical in the reaction of RNR with N ₃ NDP	155
A.15	Decay curves for N · in the reaction of RNR with N ₃ NDP	156
A.16	Decay curves for N · / Y · ratio in the reaction of RNR with N ₃ NDP	156

List of Tables

2.1	Calculated HFC tensors and selected N – H distances of structural models of N \cdot	37
2.2	Hyperfine coupling tensors, molecular energies, and selected N – H distances for different conformers of the CNS model	39
3.1	Summary of yields and characterization of compounds made by the enzymatic method	66
4.1	g_{av} and hyperfine coupling constant in G for model ketyl radicals in Figure 4.2	71
4.2	Amino acid composition of the minimal medium	74
4.3	Nitrogenous base composition of the minimal medium	75
4.4	Other components of the minimal medium	75
4.5	Analysis by ESI mass spectrometry of the F688-R703 peptide	85
5.1	Results of single turnover experiments	117
5.2	Results of product identification studies with dFdCDP	124
5.3	Comparison of g-values for wt - RNR plus dFdCDP, and 3 min E441Q - R1/wt - R2 plus CDP radicals	125
A.1	π spin density distributions on Y122 of <i>E. coli</i> R2	141
A.2	Distances between the csd on Y122 of each monomer or between individual atoms for 1RIB	142
A.3	Distances between the csd on Y122 of each monomer or between individual atoms for 1PFR	142
A.4	Distances between the csd on Y122 of each monomer or between individual atoms for 1AV8	143
A.5	Distances between the csd on Y122 of each monomer or between individual atoms for 1MXR	143
A.6	Time-course of the wt RNR reaction with N $_3$ UDP	146
A.7	Time-course of the wt R1/C268S - R2 RNR reaction with N $_3$ UDP	147
A.8	Timecourse of the wt RNR reaction with N $_3$ CDP	148
A.9	Time-course of the wt RNR reaction with N $_3$ UDP in the presence of DTT	148

B.1	Comparison between isotropic (A_{iso}) and dipolar (T_{ii}) hyperfine coupling constants obtained by UB3PW91/IGLO-II and IGLO-III and by <i>ab initio</i> CCSD(T)/IGLO-III calculations for ONS and CNS model substructures	160
-----	---	-----

Chapter 1

Introduction

1.1 General background

The reaction in which purine and pyrimidine ribonucleotides are reduced to deoxyribonucleotides (Figure 1.1) is catalyzed by ribonucleotide reductases (RNRs) and is life's only known pathway for generating deoxyribonucleotides *de novo*.^{1,2} It thus serves as a source of the monomeric precursors required for DNA replication and DNA repair. The central role of RNRs in nucleic acid metabolism has made them the successful target of antiviral and antitumor agents, two of which are used clinically in the treatment of AIDS and cancer: hydroxyurea and gemcitabine.^{3,4}

RNRs serve as a paradigm for understanding free radical reactions in biology involving stable and transient protein- and nucleotide-based radical intermediates and for understanding long range proton coupled electron transfer (PCET).⁵ They have further been of interest because of the unusual diferric-tyrosyl radical ($Y\cdot$) cofactor in one class of reductases;⁶ the formation of this cofactor involves controlled delivery of ferrous iron and is linked to understanding transition metal homeostasis *in vivo*. Additionally, layered RNR regulation *in vivo*, which ensures balanced deoxyribonucleotide pools and is essential for the fidelity of DNA replication and repair, is a challenging problem whose mechanisms remain to be understood.

RNRs have been divided into three classes based on the metallo-cofactors used to initiate the complex radical chemistry of the nucleotide reduction process.⁵ The class I enzymes

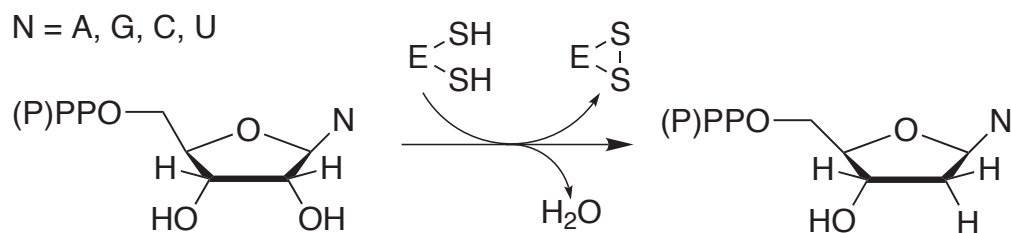


Figure 1.1: Reaction catalyzed by RNR

are found in many bacteria, DNA viruses, and all eukaryotes including humans and use a diferric tyrosyl radical ($Y\cdot$). The class II RNRs are found in bacteria, archaea, and algae, and use adenosylcobalamin. The class III RNRs are found in bacteria which can survive under anaerobic conditions, and use a glycy radical generated by an activating enzyme that utilizes a 4Fe4S cluster and S-adenosylmethionine. Recently, a class I subfamily has been identified in *Chlamydia trachomatis*.⁷ Its structure revealed no oxidizable tyrosine (Y) adjacent to the di-iron center. This RNR is proposed to use a $[Fe^{4+} - Fe^{3+}]$ di-iron cluster. A similar intermediate has been identified during *in vitro* assembly of the diferric- $Y\cdot$ cofactor in *E. coli*.^{8,9} The function of the metallo-cofactor in all cases is proposed to be the generation of a transient thiyl radical ($S\cdot$) that initiates nucleotide reduction.¹ Although the structures of radical initiators used by three classes of RNRs are different, the proteins share a structurally homologous catalytic subunit, designated R1 in *E. coli* RNR, and use mechanistically similar chemistry.¹⁰⁻¹²

1.2 Structure

The class I RNR from *E. coli* is the focus of this thesis. This reductase serves as the prototype of eukaryotic enzymes. It is composed of two homodimeric subunits: R1 (α_2) and R2 (β_2).¹³ R1 contains the active site where nucleotide reduction occurs and where three cysteines, one glutamate, and one asparagine essential for catalysis are located. One of the cysteines, C439, becomes the putative $S\cdot$. The remaining two cysteines, C225 and C462, are oxidized concomitantly with substrate reduction. Additionally, there are two cysteines in the C-terminus of R1, C754 and C759, that re-reduce the active-site disulfide after each turnover, and which are themselves reduced by an external protein reducing system such as thioredoxin or glutaredoxin.

R1 also contains the allosteric effector binding sites.¹³ The specificity site (s-site) where dNTPs and ATP can bind controls which of the nucleotides (ADP, GDP, CDP, or UDP) is reduced in the active site. The activity site (a-site) is present in a subclass of class I RNRs (class Ia) and binds ATP or dATP; this site controls the overall rate of nucleotide reduction. In the mouse R1, a third site (h-site) has been identified recently which binds ATP and induces higher order oligomer (α_6) formation.¹⁴ The presence and location of this site in other class I RNRs have not been determined.

R2 contains the diferric- $Y\cdot$ metallo-cofactor which is essential for catalysis in class I RNRs and serves as the initiator of radical-based nucleotide reduction chemistry on R1.^{15,16} Recombinantly expressed R2 contains 1.2 $Y\cdot$ and 3.6 irons per dimer.⁸

The active form of the enzyme has long been thought to be a symmetrical 1:1 complex of the two subunits.¹⁷ Structures at atomic resolution of R1 and R2 have been reported,^{12,15} as well as an asymmetric co-crystal structure of R1 and R2 in which the C-terminal end of one of the R2 monomers makes contact with R1.¹⁸ However, an active complex of R1 and R2 has not yet been crystallographically characterized. Based on shape complementarity of the structures of R1 and R2, a docking model for the R1/R2 complex has been proposed which places Y122 on R2 ~ 35 Å away from C439 on R1, Figure 1.2.¹² The docking model and

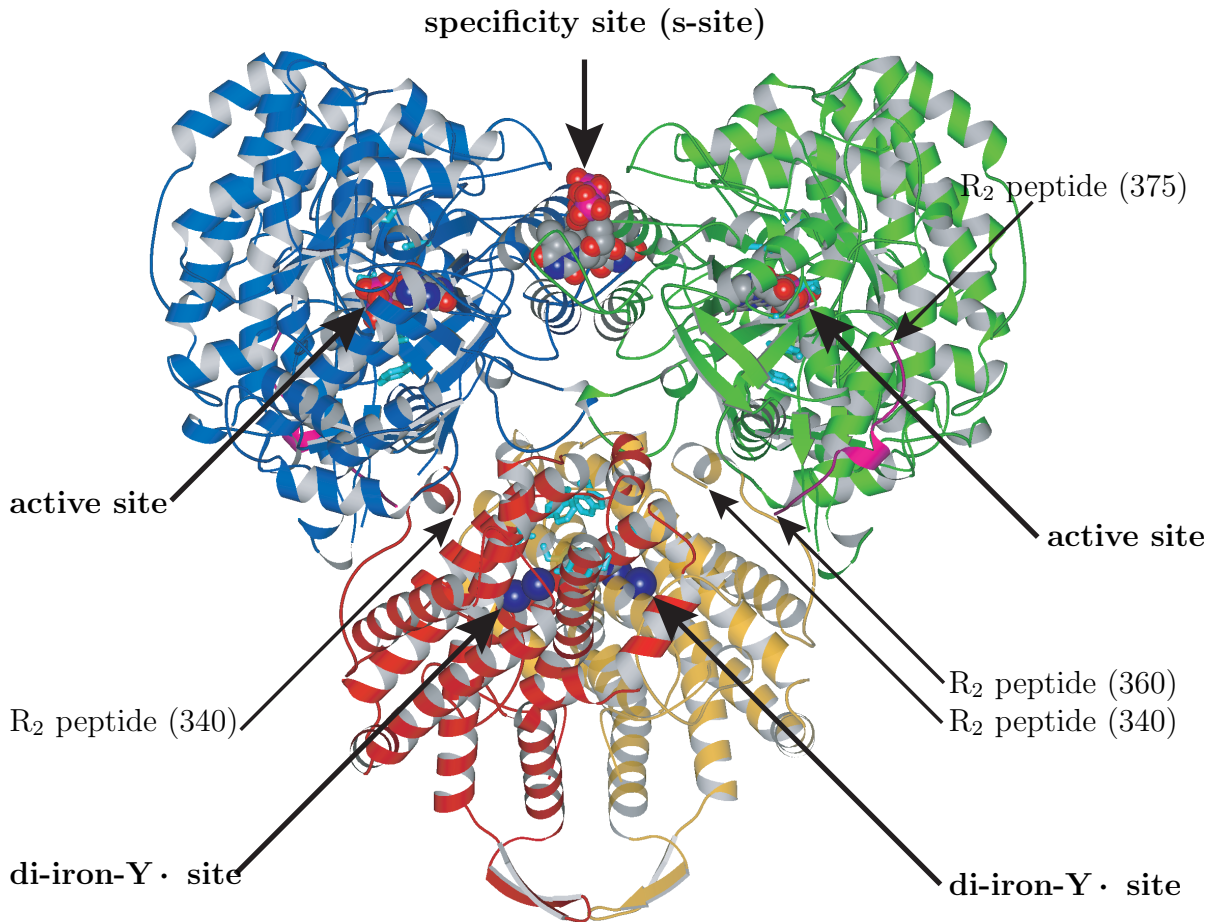


Figure 1.2: Docking model of the R1/R2 complex

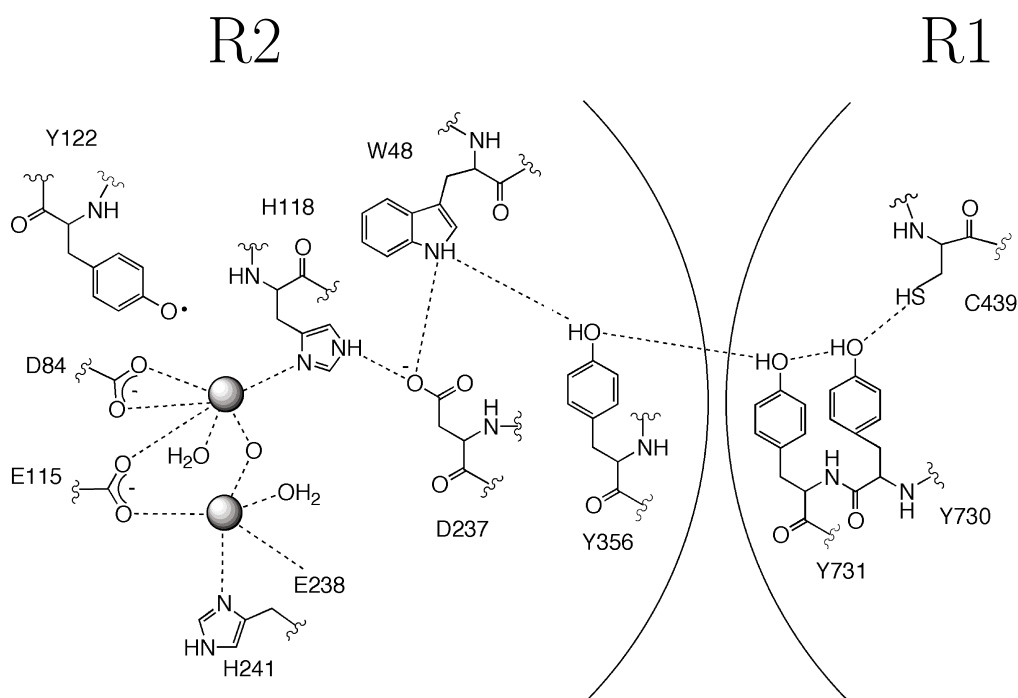


Figure 1.3: Proposed pathway of communication between Y122 on R2 and C439 on R1

the absolute conservation of amino acid residues from 40 sequences of RNRs have provided grounds for a pathway model for communication between Y122 on R2 and C439 on R1, Figure 1.3. The postulated mechanisms for the long-range generation of a putative transient $S\cdot$ on R1 by $Y\cdot$ on R2 have recently been reviewed.¹⁹

1.3 Kinetic model for *E. coli* RNR

In order to determine which step or steps are rate-limiting during *E. coli* RNR turnover, two groups have carried out pre-steady state experiments monitoring dNDP and disulfide formation, or changes in $Y\cdot$ concentration. Ge *et al.*²⁰ have used stopped flow (SF) Vis spectroscopy to monitor changes in the $Y\cdot$ concentration ($A_{410\text{ nm}}$) and rapid chemical quench (RCQ) methodology to monitor dNDP formation. Erickson has used RCQ and immunoabsorption chromatography with antibodies raised to peptide sequences around C225, and C754/C759 to monitor disulfide bond formation.^{21,22} Studies by Ge *et al.* with pre-reduced R1/R2, CDP as substrate, ATP as the effector, and no external reductant showed that 1.7 equivalents of dCDP were produced in a single kinetic phase (k_{obs} of 9 s^{-1}). This result indicates that each monomer of R1 is active. SF experiments monitoring $Y\cdot$ failed to reveal any changes from 2 ms to s, demonstrating that the participation of $Y\cdot$ in the radical prop-

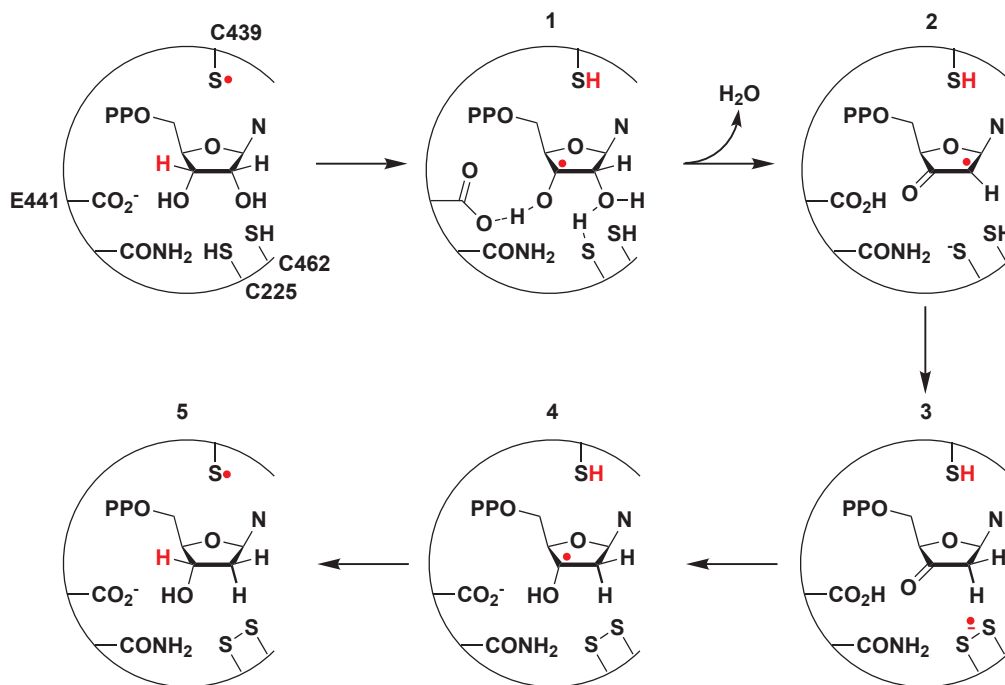


Figure 1.4: Mechanistic model for the reaction catalyzed by RNR

agation process is kinetically invisible. Erickson reported that disulfide formation between C225 and C462 occurred at 8 s^{-1} . Together, the results suggest that the rate-determining step is a physical step prior to rapid nucleotide reduction. Thus, the chemistry of nucleotide reduction is kinetically invisible, which has precluded detection of intermediates in the reduction process with the normal substrate. Perturbation of the system using mechanism-based inhibitors and site-directed mutants of R1 and R2 has provided the bulk of insight into the reduction mechanism by inference.

1.4 Proposed mechanism of ribonucleotide reduction

The proposed mechanism for nucleotide reduction is shown in Figure 1.4.¹ In the first step, the metallo-cofactor (diferric $Y\cdot$ in the case of *E. coli* RNR) generates the putative transient thiyl radical $S\cdot$ on C439 in the active site of R1. The thiyl radical is proposed to initiate catalysis by abstraction of the 3'-hydrogen of the substrate to generate a 3'-nucleotide radical intermediate, 1 in Figure 1.4. This intermediate is proposed to rapidly lose its 2'-hydroxyl group as water and the proton from its 3'-hydroxyl group to glutamate 441 (E441), forming a 3'-keto-2'-deoxynucleotide radical, 2 in Figure 1.4. Reduction is proposed to proceed by a single electron transfer from C225 located on the α face of the nucleotide concomitantly with rapid proton transfer to generate 3'-keto-2'-deoxynucleotide and a disulfide radical anion between C225 and C462, 3 in Figure 1.4. A second one-

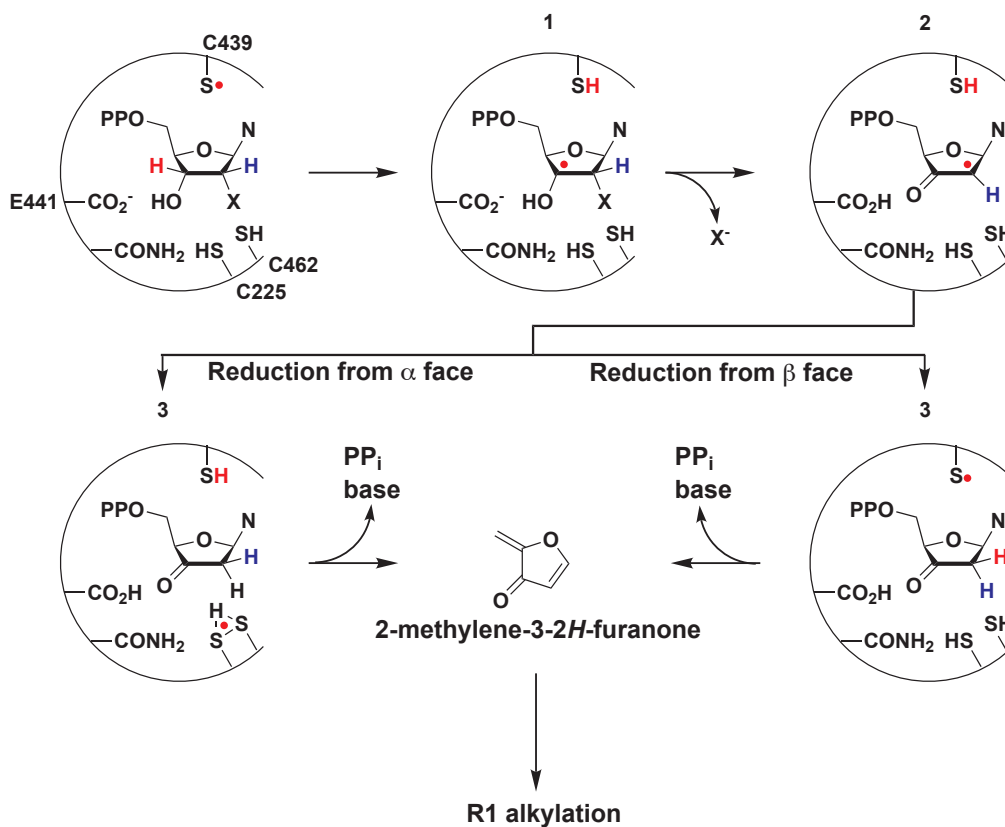


Figure 1.5: Mechanistic model for RNR inactivation by 2'-substituted nucleotide analogs

electron reduction of the putative 3'-keto-2'-deoxynucleotide by the disulfide radical anion is proposed to occur concomitantly with proton transfer from E441 to the 3'-oxygen, to form 3'-(2'-deoxy)nucleotide radical and regenerate the anionic form of E441, 4 in Figure 1.4. Subsequent reabstraction of a hydrogen atom from C439 by the 3'-(2'-deoxy)nucleotide radical results in formation of the deoxynucleotide product, regenerates the thiyl radical and thus the Y•, and completes turnover, 5 in Figure 1.4. In order for the next turnover to take place, the disulfide formed between C225 and C462 must be reduced.

1.5 Mechanism-based inhibition of RNR

Any mechanism proposed for the nucleotide reduction process must also account for the observations made with 2'-substituted nucleotide analogs and with site-directed mutants of RNR. In 1976 Thelander and Eckstein reported that 2'-chloro-2'-deoxynucleotides and 2'-azido-2'-deoxynucleotides were potent inactivators of RNRs.²³ A mechanistic paradigm has evolved over the years to explain the results observed during RNR inhibition by these analogs, Figure 1.5.¹ The initial step, as with NDP reduction, is the abstraction of the 3'-

hydrogen atom by the putative $S\cdot$ on C439. Deprotonation of the 3'-hydroxyl by E441 concomitantly with the loss of the 2'-leaving group (X), results in the formation of the 3'-keto-2'-deoxynucleotide radical (2, Figure 1.5), an intermediate also proposed to be on the normal reduction pathway (2, Figure 1.4). To explain the difference in results observed with 2'-substituted analogs compared to NDP, the 2'-substituent (X, Figure 1.5) is proposed to depart without the requirement for protonation. Thus, both thiols on the α face of the nucleotide remain protonated. The 3'-keto-2'-deoxynucleotide radical can then be reduced by hydrogen atom transfer as opposed to electron transfer followed by proton transfer as in the case of NDP. Reduction from the β face allows the regeneration of the thiyl radical and consequently the tyrosyl radical on R2; reduction from the α face forms the disulfide radical. In both cases, the product is the 3'-keto-2'-deoxynucleotide. This compound is unstable and decomposes to give a nitrogenous base (N), inorganic pyrophosphate, and 2-methylene-3-2H-furanone. The latter is activated toward nucleophilic addition, and inactivates RNR by non-specific alkylation. Additionally, it has been shown that NDPs can become mechanism based inhibitors when catalytically essential residues in the active site of R1 (C225, N437, E441, or C462) are mutated.

1.6 Evidence for the proposed mechanism of ribonucleotide reduction

EPR methods have been essential in the deconvolution of the complex mechanism of the ribonucleotide reduction process. Studies on the interaction of 2'-vinylfluorocytidine-5'-diphosphate with *E. coli* RNR demonstrated that the enzyme could generate a 3'-allyl nucleotide radical.^{24,25} This experiment, along with V/K isotope effects measured with [3'-³H]-NDPs,^{26,27} provided evidence that RNRs can abstract a 3'-hydrogen atom from a nucleotide substrate. Studies with an active site mutant of R1, E441Q, and substrate CDP resulted in conversion of the normal substrate into a putative 3'-ketodeoxynucleotide concomitantly with the buildup of a disulfide radical anion.²⁸ The requirement for protonation of the 3'-ketone to effect reduction by electron transfer from the disulfide radical anion²⁹ correctly predicted the buildup of this intermediate when the proton source (E441) was removed.

Use of 2'-halogenated-2'-deoxynucleotides has provided indirect evidence for a ketyl radical intermediate. Incubation of [3'-³H]-CIUDP with RNR resulted in the trapping of [2'-³H]-3'-keto-2'-deoxynucleotide.³⁰ The location of the label and its stereochemistry were established after its reduction with $NaBH_4$. Direct evidence for the 3'-ketodeoxynucleotide itself has remained elusive.

1.7 Scope of this thesis

The work described in this thesis makes use of two mechanism-based inhibitors, 2'-azido-2'-deoxyuridine-5'-diphosphate (N_3 UDP) and 2'-deoxy-2',2'-difluorocytidine-5'-diphos-

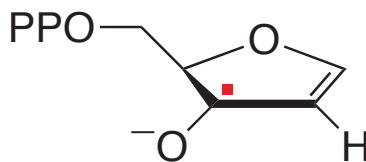


Figure 1.6: Proposed α,β -unsaturated ketyl radical anion formed in the active site of R1 during the reaction of E441Q-R1, wt-R2, TTP, DTT and CDP (Chapter 4)

phate (dFdCDP), and one active site mutant, E441Q-R1, to further our understanding of the catalytic capabilities of RNR. The results provide strong support for a 3'-ketodeoxynucleotide intermediate postulated to lie on the normal reduction pathway, as well as for the elimination of nitrogenous base in the active site of R1 during inhibition. The studies further show that under physiologically relevant reducing conditions, inhibition of RNR by the clinically important nucleotide analog dFdCDP is a result of covalent modification. An essential part of these studies was the development of a robust, high-yielding enzymatic method for the selective 5'-phosphorylation of cytidine, 2'-deoxycytidine, 2'-deoxyuridine and their analogs that are not amenable to standard chemical phosphorylation methods.

In Chapter 2 of this thesis, 9 GHz and 140 GHz EPR spectroscopic studies on the interaction of 2'-azido-2'-deoxy-[3'- ^{17}O]-uridine-5'-diphosphate³¹ ([3'- ^{17}O]- N_3UDP) with RNR are reported. The EPR studies, in conjunction with density functional theory (DFT) calculations in collaboration with Jörg Fritscher, reveal the structure of a nitrogen-centered radical ($\text{N}\cdot$) generated during the inactivation of RNR by N_3UDP . The results provide direct evidence for the trapping of a 3'-ketonucleotide in the reduction process.

As an extension of these studies, the amount of $\text{N}\cdot$ formed as a function of time in the reactions of N_3UDP and N_3CDP with wt-R1/wt-R2 and wt-R1/C268S-R2 is measured using 9 GHz EPR spectroscopy (Appendix A). Together with quantification of the ratio of $\text{N}\cdot$ to $\text{Y}\cdot$ as a function of time, the data represent an important step in the ability to measure the distance between $\text{N}\cdot$ in R1 and $\text{Y}\cdot$ in R2 using PELDOR spectroscopy in collaboration with Marina Bennati.

In Chapter 3, a high-yielding enzymatic procedure for the 5'-phosphorylation of cytidine, 2'-deoxycytidine, and 2'-deoxyuridine and their analogs is described. The procedure makes use of two recombinantly expressed human kinases: human deoxycytidine kinase³² (HdCK) and human UMP-CMP kinase.³³ For the first time it is possible to selectively phosphorylate in high yields analogs of cytidine, 2'-deoxycytidine, and 2'-deoxyuridine not amenable to chemical phosphorylation methods and to carry out the syntheses on nmol scale. Thus, the previously impractical phosphorylation of isotopically-labeled derivatives of these classes of compounds becomes feasible. Specifically, we have used this method to prepare 5'-nucleoside diphosphates of [5,6- ^2H]-cytidine, [1'- ^2H]-cytidine, [2'- ^2H]-cytidine, and [4'- ^2H]-cytidine for experiments described in Chapter 4; 5'-nucleoside diphosphates of dFdC, [5- ^3H]-dFdC, [1'- ^3H]-dFdC, and [1'- ^2H]-dFdC for experiments described in Chapter 5; and 2'-azido-

2'-deoxycytidine-5'-diphosphate and 2'-azido-2'-deoxyuridine-5'-diphosphate for experiments described in Appendix A.

In Chapter 4 of this thesis, experiments with isotopically labeled substrate and protein in conjunction with EPR and ENDOR spectroscopy are used to establish the structure of a radical formed on a minute timescale in the reaction of E441Q-R1/wt-R2 with CDP or GDP as substrate and TTP as the effector. It is proposed that the radical is an α,β -unsaturated ketyl radical anion (Figure 1.6). If confirmed, this structural assignment would constitute the first evidence for base elimination within the active site of R1, as opposed to in solution, during the course of mechanism-based inhibition. Furthermore, it would show that the disulfide radical anion is able to reduce a nucleotide-based intermediate in the active site of R1 when the redox potentials of the disulfide radical anion and the nucleotide-based intermediate are matched.

In Chapter 5, experiments on the inactivation of RNR by the diphosphate of the clinically important nucleoside analog 2'-deoxy-2',2'-difluorocytidine (gemcitabine, dFdC) are described. The first definitive evidence is presented that the new radical formed during inactivation in the absence of reductants is nucleotide-based. Furthermore, we show that under physiologically relevant reducing conditions, inhibition of RNR by dFdCDP is a result of covalent modification that requires C225. As with the inactivation of RNR by N_3 UDP described in Chapter 2, further studies on the inactivation by dFdCDP over the course of the next 5–10 years should allow a detailed understanding of the chemistry responsible for the inactivation, and provide insight into the mechanisms of dFdC resistance.

Bibliography

- [1] S. Licht and J. Stubbe, *Comprehensive Natural Products Chemistry*, vol. 5, ch. Mechanistic Investigations of Ribonucleotide Reductases, pp. 163–203. Elsevier, 1999.
- [2] B.-B. S. Zhou and S. J. Elledge, “The DNA damage response: putting checkpoints in perspective,” *Nature (London)*, vol. 408, no. 6811, pp. 433–439, 2000.
- [3] L. M. Kelly, J. Lisiewicz, and F. Lori, “Virostatics as a potential new class of HIV drugs,” *Current Pharmaceutical Design*, vol. 10, no. 32, pp. 4103–4120, 2004.
- [4] R. Rosell, L. Crino, K. Danenberg, G. Scagliotti, G. Bepler, M. Taron, V. Alberola, M. Provencio, C. Camps, F. De Marinis, J. J. Sanchez, and R. Penas, “Targeted therapy in combination with gemcitabine in non-small cell lung cancer,” *Seminars in Oncology*, vol. 30, no. 4, Suppl. 10, pp. 19–25, 2003.
- [5] J. Stubbe and W. A. Van der Donk, “Protein radicals in enzyme catalysis. [erratum],” *Chemical Reviews (Washington, D. C.)*, vol. 98, no. 7, p. 2661, 1998.
- [6] J. Stubbe, “Di-iron-tyrosyl radical ribonucleotide reductases,” *Current Opinion in Chemical Biology*, vol. 7, no. 2, pp. 183–188, 2003.
- [7] M. Högbom, P. Stenmark, N. Voevodskaya, G. McClarty, A. Gräslund, and P. Nordlund, “The radical site in chlamydial ribonucleotide reductase defines a new R2 subclass,” *Science (Washington, DC)*, vol. 305, no. 5681, pp. 245–248, 2004.

- [8] J. M. Bollinger, Jr, D. E. Edmondson, B.-H. Huynh, J. Filley, J. R. Norton, and J. Stubbe, "Mechanism of assembly of the tyrosyl radical-dinuclear iron cluster cofactor of ribonucleotide reductase," *Science (Washington, DC)*, vol. 253, no. 5017, pp. 292–298, 1991.
- [9] B. E. Sturgeon, D. Burdi, S. Chen, B.-H. Huynh, D. E. Edmondson, J. Stubbe, and B. M. Hoffman, "Reconsideration of X, the diiron intermediate formed during cofactor assembly in *E. coli* ribonucleotide reductase," *Journal of the American Chemical Society*, vol. 118, no. 32, pp. 7551–7557, 1996.
- [10] M. D. Sintchak, G. Arjara, B. A. Kellogg, J. Stubbe, and C. L. Drennan, "The crystal structure of class II ribonucleotide reductase reveals how an allosterically regulated monomer mimics a dimer," *Nature Structural Biology*, vol. 9, no. 4, pp. 293–300, 2002.
- [11] D. T. Logan, J. Andersson, B.-M. Sjöberg, and P. Nordlund, "A glycy radical site in the crystal structure of a class III ribonucleotide reductase," *Science (Washington, D. C.)*, vol. 283, no. 5407, pp. 1499–1504, 1999.
- [12] U. Uhlin and H. Eklund, "Structure of ribonucleotide reductase protein R1," *Nature (London)*, vol. 370, no. 6490, pp. 533–539, 1994.
- [13] N. C. Brown and P. Reichard, "Ribonucleoside diphosphate reductase; formation of active and inactive complexes of proteins B1 and B2," *Journal of Molecular Biology*, vol. 46, no. 1, pp. 25–38, 1969.
- [14] O. B. Kashlan and B. S. Cooperman, "Comprehensive model for allosteric regulation of mammalian ribonucleotide reductase: Refinements and consequences," *Biochemistry*, vol. 42, no. 6, pp. 1696–1706, 2003.
- [15] P. Nordlund and H. Eklund, "Structure and function of the *Escherichia coli* ribonucleotide reductase protein R2," *Journal of Molecular Biology*, vol. 232, no. 1, pp. 123–164, 1993.
- [16] B.-M. Sjöberg, P. Reichard, A. Graslund, and A. Ehrenberg, "The tyrosine free radical in ribonucleotide reductase from *Escherichia coli*," *Journal of Biological Chemistry*, vol. 253, no. 19, pp. 6863–6865, 1978.
- [17] L. Thelander and P. Reichard, "Reduction of ribonucleotides," *Annual Review of Biochemistry*, vol. 48, pp. 133–158, 1979.
- [18] M. Uppsten, M. Faernegardh, V. Domkin, and U. Uhlin, "The first holocomplex structure of ribonucleotide reductase gives new insight into its mechanism of action," *Journal of Molecular Biology*, vol. 359, no. 2, pp. 365–377, 2006.
- [19] J. Stubbe, D. G. Nocera, C. S. Yee, and M. C. Y. Chang, "Radical initiation in the class I ribonucleotide reductase: Long-range proton-coupled electron transfer?," *Chemical Reviews (Washington, DC)*, vol. 103, no. 6, pp. 2167–2201, 2003.
- [20] J. Ge, G. Yu, M. A. Ator, and J. Stubbe, "Pre-steady-state and steady-state kinetic analysis of *E. coli* class I ribonucleotide reductase," *Biochemistry*, vol. 42, no. 34, pp. 10071–10083, 2003.
- [21] H. K. Erickson, "Kinetics in the pre-steady state of the formation of cystines in ribonucleoside diphosphate reductase: Evidence for an asymmetric complex," *Biochemistry*, vol. 40, no. 32, pp. 9631–9637, 2001.
- [22] H. K. Erickson, "Formation of the cystine between cysteine 225 and cysteine 462 from ribonucleoside diphosphate reductase is kinetically competent," *Biochemistry*, vol. 39, no. 31, pp. 9241–9250, 2000.
- [23] L. Thelander and B. Larsson, "Active site of ribonucleoside diphosphate reductase from *Escherichia coli*. Inactivation of the enzyme by 2'-substituted ribonucleoside diphosphates," *Journal of Biological Chemistry*, vol. 251, no. 5, pp. 1398–1405, 1976.

- [24] G. J. Gerfen, W. A. van der Donk, G. Yu, J. R. McCarthy, E. T. Jarvi, D. P. Matthews, C. Farrar, R. G. Griffin, and J. Stubbe, "Characterization of a substrate-derived radical detected during the inactivation of ribonucleotide reductase from *Escherichia coli* by 2'-fluoromethylene-2'-deoxycytidine 5'-diphosphate," *Journal of the American Chemical Society*, vol. 120, no. 16, pp. 3823–3835, 1998.
- [25] W. A. van der Donk, G. J. Gerfen, and J. Stubbe, "Direct EPR spectroscopic evidence for an allylic radical generated from (E)-2'-fluoromethylene-2'-deoxycytidine 5'-diphosphate by *E. coli* ribonucleotide reductase," *Journal of the American Chemical Society*, vol. 120, no. 17, pp. 4252–4253, 1998.
- [26] J. Stubbe and D. Ackles, "On the mechanism of ribonucleoside diphosphate reductase from *Escherichia coli*. Evidence for 3'-carbon-hydrogen bond cleavage," *Journal of Biological Chemistry*, vol. 255, no. 17, pp. 8027–8030, 1980.
- [27] J. Stubbe, M. Ator, and T. Krenitsky, "Mechanism of ribonucleoside diphosphate reductase from *Escherichia coli*. Evidence for 3'-C-H bond cleavage," *Journal of Biological Chemistry*, vol. 258, no. 3, pp. 1625–1631, 1983.
- [28] C. C. Lawrence, M. Bennati, H. V. Obias, G. Bar, R. G. Griffin, and J. Stubbe, "High-field EPR detection of a disulfide radical anion in the reduction of cytidine 5'-diphosphate by the E441Q R1 mutant of *Escherichia coli* ribonucleotide reductase," *Proceedings of the National Academy of Sciences of the United States of America*, vol. 96, no. 16, pp. 8979–8984, 1999.
- [29] R. Lenz and B. Giese, "Studies on the mechanism of ribonucleotide reductases," *Journal of the American Chemical Society*, vol. 119, no. 12, pp. 2784–2794, 1997.
- [30] M. A. Ator and J. Stubbe, "Mechanism of inactivation of *Escherichia coli* ribonucleotide reductase by 2'-chloro-2'-deoxyuridine 5'-diphosphate: evidence for generation of a 2'-deoxy-3'-ketonucleotide via a net 1,2 hydrogen shift," *Biochemistry*, vol. 24, no. 25, pp. 7214–7221, 1985.
- [31] S. F. Wnuk, S. M. Chowdhury, P. I. Garcia, Jr., and M. J. Robins, "Stereo-defined synthesis of O3'-labeled uracil nucleosides. 3'-[¹⁷O]-2'-azido-2'-deoxyuridine 5'-diphosphate as a probe for the mechanism of inactivation of ribonucleotide reductases," *Journal of Organic Chemistry*, vol. 67, no. 6, pp. 1816–1819, 2002.
- [32] E. V. Usova and S. Eriksson, "The effects of high salt concentrations on the regulation of the substrate specificity of human recombinant deoxycytidine kinase," *European Journal of Biochemistry*, vol. 248, no. 3, pp. 762–766, 1997.
- [33] A. R. Van Rompay, M. Johansson, and A. Karlsson, "Phosphorylation of deoxycytidine analog monophosphates by UMP-CMP kinase: molecular characterization of the human enzyme," *Molecular Pharmacology*, vol. 56, no. 3, pp. 562–569, 1999.

Chapter 2

Structure of the nitrogen-centered radical formed during inactivation of Class I *Escherichia coli* ribonucleotide reductase by 2' - azido - 2' - deoxyuridine - 5' - diphosphate: Trapping of the 3' - ketonucleotide¹

2.1 Introduction

2' - Azido - 2' - deoxynucleoside - 5' - diphosphates (N_3 NDPs) have been studied in detail since their discovery as potent inhibitors of ribonucleotide reductases (RNRs) by the Eckstein and Thelander groups in 1976.² Together with 2' - chloro - 2' - deoxynucleoside - 5' - diphosphates, these inhibitors have played a pivotal role in understanding the catalytic capabilities of RNRs. Early studies revealed that incubation of RNRs with N_3 NDPs resulted in tyrosyl radical ($Y\cdot$) loss and formation of a new nitrogen-centered radical ($N\cdot$).^{3,4} These studies provided the first evidence for the involvement of nucleotide radicals in the reduction process.

A detailed understanding of the mechanism of inactivation of RNRs by these inhibitors has evolved since their discovery. In the reaction of N_3 UDP with RNR, it was shown that N_2 is lost prior to or upon $N\cdot$ formation.^{5,6} However, when C225S - R1 or oxidized - R1 was incubated with N_3 UDP, $Y\cdot$ loss occurred, but neither $N\cdot$ nor N_2 formed; instead azide (or hydrazoic acid) was released.⁶ These studies suggested that C225 is required for the generation of N_2 and $N\cdot$. Destruction of $N\cdot$ was shown to be a slow process ($t_{1/2}$ of 20 min), accompanied by the release of pyrophosphate, uracil, and 2 - methylene - 3 - furanone.^{2,5,6} In addition, reactions with [$3' - ^2H$] - N_3 UDP revealed an isotope effect on the loss of $Y\cdot$ and on the rate of inactivation of RNR.⁶ In both cases, kinetics were complex suggesting multiple modes of inactivation. Despite considerable mechanistic insight, structural assignment of

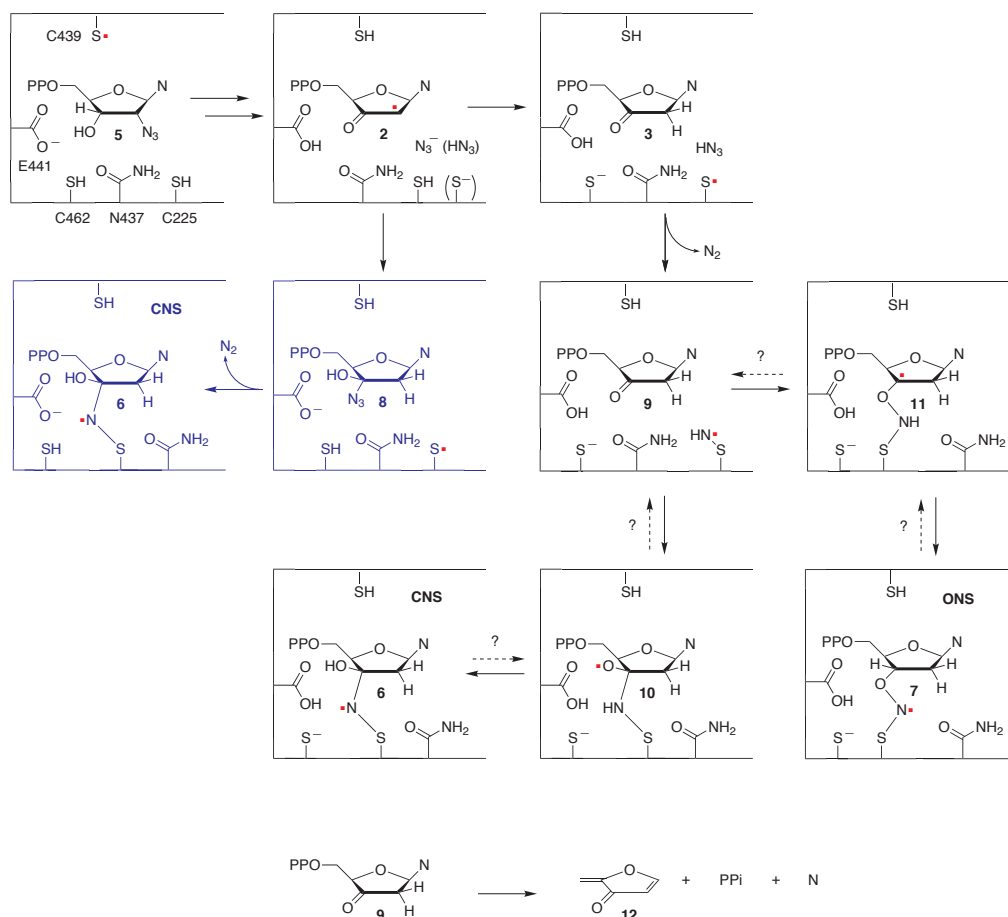


Figure 2.1: Pathways for the generation of two previously proposed structures for $N\cdot$. The blue pathway is proposed based on theoretical studies.⁷ The black pathways were proposed by van der Donk *et al.*⁸

$N\cdot$ has remained an unsolved problem.

Two structural models for $N\cdot$ (6 and 7, Figure 2.1) have been considered based on isotopic labeling experiments using $[\beta\text{-}^2\text{H}]$ -cysteine-R1, $[1'\text{-}^2\text{H}]$ -, $[2'\text{-}^2\text{H}]$ -, $[3'\text{-}^2\text{H}]$ -, $[4'\text{-}^2\text{H}]$ -, $[^{13}\text{C}]$ -, and $[^{15}\text{N}]$ -labeled N_3UDP and analysis of the resulting $N\cdot$ by EPR and ESEEM spectroscopies at 9 and 140 GHz.^{6,8} To distinguish between the proposed structures, inactivation was carried out with $46 \pm 2\%$ enriched $[3'\text{-}^{17}\text{O}]$ - N_3UDP ⁹, and $N\cdot$ examined by 9 and 140 GHz EPR spectroscopy. Broadening of the $N\cdot$ signal was detected, and the spectrum simulated to obtain the $[^{17}\text{O}]$ hyperfine tensor. Density functional theory (DFT) calculations were employed to determine which structures were in best agreement with the simulated hyperfine tensor and previous ESEEM data. These studies allow us to differentiate between the two models for $N\cdot$, and strongly support 6 as the structure.

Two mechanistic options were proposed to account for the formation of $N\cdot$, both involv-

ing the sulfinylimine radical (9, Figure 2.1) interacting with a 3'-keto-2'-deoxynucleotide. The sulfinylimine radical was proposed to be generated directly by reaction of a thiyl radical on C225 with HN_3 and to attack either the carbonyl carbon of the ketone (9 to 10, Figure 2.1) or the oxygen of the carbonyl group (9 to 11, Figure 2.1). The former mechanism was favored chemically, but the latter was more consistent with the ESEEM data. A recent theoretical study has proposed an alternative mechanism to generate 6 (blue pathway in Figure 2.1).⁷ In this mechanism, a released azide ion traps the ketyl radical 2 (Figure 2.1). This intermediate is then reduced by C225 to generate the corresponding thiyl radical. Finally, the thiyl radical attacks the internal N of the azide to liberate N_2 and generate 6 (Figure 2.1). Identification of the structure of $\text{N}\cdot$ as 6 has now provided direct evidence for the trapping of a 3'-ketone, through either a ketyl radical (2, Figure 2.1) or a 3'-keto-2'-deoxynucleotide (3, Figure 2.1), depending on the timing of N_2 release.

2.2 Materials and methods

2.2.1 Purchased materials and materials obtained as gifts

Triethylamine (99% pure) was purchased from Acros, N-(2-hydroxyethyl)piperazine-N'-(2-ethanesulfonic acid) (HEPES) from US Biochemicals, and 1,4-dithiothreitol (DTT) from Mallinckrodt. DEAE Sephadex A-25 was purchased from Pharmacia. All other chemicals were purchased from Sigma.

$[3' - ^{16}\text{O}] - \text{N}_3\text{UDP}$ was prepared from the nucleoside, 2'-azido-2'-deoxyuridine (Aldrich), as previously described.⁶ $[3' - ^{17}\text{O}] - \text{N}_3\text{UDP}$ was prepared as described by Wnuk *et al.*⁹ Mass spectra were recorded using the atmospheric pressure chemical ionization method in a positive mode using a Finnigan AQA Navigator. The percentage of $[^{17}\text{O}]$ incorporation into $[3' - ^{17}\text{O}] - \text{N}_3\text{UDP}$ was $46 \pm 2\%$.

2.2.2 Protein overexpression, purification, and activity assays

Wild type *E. coli* R1 protein was purified as previously described.⁶ It had specific activity (S.A.) of 2200–3000 $\text{nmol} \cdot \text{mg}^{-1} \cdot \text{min}^{-1}$ as measured by the standard spectrophotometric RDPR assay, and S.A. of 1799–2000 $\text{nmol} \cdot \text{mg}^{-1} \cdot \text{min}^{-1}$ as measured by the $[^{14}\text{C}]$ -CDP radioactive assay. R1 concentration was determined using $\epsilon_{280 \text{ nm}} = 189 \text{ mM}^{-1} \cdot \text{cm}^{-1}$. R1 was pre-reduced prior to each experiment as described in Section 5.2.2. All R1 concentrations are reported per dimer.

Wild type *E. coli* R2 was isolated as previously described¹⁰ and had S.A. of 6000–7000 $\text{nmol} \cdot \text{mg}^{-1} \cdot \text{min}^{-1}$. R2 concentration was determined using $\epsilon_{280 \text{ nm}} = 130.5 \text{ mM}^{-1} \cdot \text{cm}^{-1}$. Tyrosyl radical content was measured both by the drop-line correction method and by EPR spectroscopy as previously reported.¹¹ R2 contained 1.1–1.2 $\text{Y}\cdot$ per dimer based on both methods of quantification. All R2 concentrations are reported per dimer.

E. coli thioredoxin (TR) was isolated from strain pTrX BL21 (DE3) and had S.A. of 40 units · mg⁻¹.¹² *E. coli* thioredoxin reductase (TRR) was isolated from strain pMR14 K91 and had S.A. of 1600 units · mg⁻¹.¹³

2.2.3 Examination of the reaction of N₃UDP and RNR by 9 GHz EPR spectroscopy

In a final volume of 220 μL, the reactions contained 0.75 mM TTP, 0.8 mM either [3' - ¹⁶O]- or [3' - ¹⁷O]-N₃UDP, 90 μM R1 (pre-reduced), 80 μM R2, 50 mM HEPES pH 7.6, 15 mM MgSO₄, 1 mM EDTA, 0.75 mM NADPH, 20 μM TR, and 1 μM TRR. All components except for the inhibitor were combined and equilibrated at 25 °C for 5 min. The reaction was started by the addition of the inhibitor and then transferred to a 706 PQ EPR tube (quartz, OD 4 mm, ID 2.4 mm, from Wilmad LabGlass) where it was frozen in liquid nitrogen after 5 min incubation at 25 °C. A control sample with water replacing the inhibitor served as the standard for the amount of Y ·. EPR spectra at 9 GHz were acquired on a Bruker ESP-300 spectrometer equipped with a Bruker high-sensitivity 4419HS cylindrical cavity and an ER-041G microwave bridge containing an internal frequency counter. Spectra were acquired at 77 K using a liquid helium cooled ESR-900 cryostat and an Oxford LLT 650/1.0 transfer line. The parameters were: microwave frequency for the [3' - ¹⁶O]- and [3' - ¹⁷O]-N₃UDP samples was 9.389052 and 9.389072 GHz, respectively; microwave power 0.1 mW; modulation frequency 100 kHz; modulation amplitude 1 G; conversion time 20.48 ms; time constant 5.12 ms. For each sample, 100 scans were acquired with 2048 points per spectrum.

2.2.4 Examination of the reaction of N₃UDP and RNR by 140 GHz EPR spectroscopy

The reaction mixtures contained in a final volume of 25 μL: 300 μM R1 (pre-reduced), 300 μM R2, 1.0 mM TTP, 0.8 mM NADPH, 20 μM TR, 1 μM TRR, and 1.0 mM either [3' - ¹⁶O]- or [3' - ¹⁷O]-N₃UDP in 50 mM HEPES pH 7.6, 15 mM MgSO₄, and 1 mM EDTA. All components of the reaction mixture except for the inhibitor were combined and incubated at 25 °C for 5 min. The reaction was started by the addition of inhibitor, and the mixture was drawn into suprasil capillaries (silica, OD 0.55 mm, ID 0.4 mm, from Wilmad LabGlass) by capillary action and frozen in liquid nitrogen 5 min after initiation. Spectra were acquired at 70 K on a custom-designed pulsed spectrometer.¹⁴ The stimulated echo sequence¹⁵ was used with a pulse length of $t_{\pi/2} = 60$ ns and a pulse spacing of $\tau = 200$ ns. The pulsed method allowed the filtering out of the N · radical signal from the Y ·, as was previously demonstrated with the reaction of [3' - ¹⁶O]-N₃UDP.¹⁶ The external magnetic field was swept with the assistance of a field lock described elsewhere.¹⁷ The echo intensity at each field position was integrated, and an average of 1000 samples per point were taken. The number of scans and recycle delays were adjusted for different signal intensities and temperatures.

2.2.5 Simulations of the EPR spectra

The simulations were performed using the commercial software package SimFonia (Bruker). As a control, the $\text{N}\cdot$ spectrum observed in the reaction of $[3' - ^{16}\text{O}] - \text{N}_3\text{UDP}$ with RNR was first simulated using the parameters reported by van der Donk *et al.*,⁸ that is, $g_{xx} = 2.01557$, $g_{yy} = 2.00625$, $g_{zz} = 2.00209$, $A_{xx}(^{14}\text{N}) = 2 \text{ G}$, $A_{yy}(^{14}\text{N}) = 2 \text{ G}$, $A_{zz}(^{14}\text{N}) = 31 \text{ G}$, $A_{xx}(^1\text{H}) = A_{yy}(^1\text{H}) = A_{zz}(^1\text{H}) = 6.3 \text{ G}$, and a Gaussian line shape broadening of 4.9 G (data not shown). The spectrum of $\text{N}\cdot$ observed in the reaction of $[3' - ^{17}\text{O}] - \text{N}_3\text{UDP}$ with RNR was subsequently simulated by keeping the EPR parameters for the unlabeled species fixed and varying the values of the $[^{17}\text{O}]$ hyperfine tensor.

2.2.6 Computational methods

The calculations for all model compounds were performed using unrestricted Kohn-Sham density functional theory (DFT) methods as implemented in GAUSSIAN 03¹⁸ and TURBOMOLE.¹⁹ Spin contamination effects were generally insignificant in all calculations. All structure optimizations were carried out with TURBOMOLE employing Becke's exchange functional B²⁰ and Perdew's P86^{21,22} correlation functional together with the TZVP basis set²³ for all atoms and accelerated with the RI approximation using the standard TZVP auxiliary basis set from TURBOMOLE.^{24,25}

For the computation of the hyperfine coupling (HFC) tensors with GAUSSIAN 03, a combination of Becke's three-parameter hybrid exchange functional B3²⁶ with the Perdew/Wang correlation functional PW91^{27,28} was chosen. An ultrafine integration grid (58410 integration points per atom) and standard SCF=Tight convergence criteria were applied. For these calculations, the Huzinaga-Kutzelnigg-type IGLO-II basis sets²⁹ were used for all atoms: (5s,1p)/[3s,1p] for H, (11s,7p,2d)/[7s,6p,2d] for S, and (9s,5p,1d)/[5s,4p,1d] for C, N, and O.

Ab initio calculations of HFC tensors were carried out at the coupled cluster theory level with single and double excitations and a perturbative treatment of triple excitations CCSD(T). The calculations were performed with the ACES II program³⁰ using unrestricted Hartree-Fock (UHF) reference wave functions. Spin densities were evaluated analytically from the CC relaxed density matrix.³¹⁻³⁵ IGLO-III basis sets²⁹ were employed for all atoms: (6s,2p)/[4s,2p] for H, (12s,8p,3d)/[8s,7p,3d] for S, and (11s,7p,2d)/[7s,6p,2d] for C, N, and O. The small model systems for these calculations were created by cutting out the relevant parts of the larger structurally optimized models and adding hydrogen atoms with standard bond lengths and angles to satisfy the open valences. No further structure optimizations were performed for these substructures.

2.3 Results

Previous studies suggested two possible structures for $\text{N}\cdot$ observed during inactivation of *E. coli* RNR by N_3NDPs (6 and 7, Figure 2.1). To distinguish between them, $46 \pm 2\%$ enriched $[3' - ^{17}\text{O}] - \text{N}_3\text{UDP}$ was incubated with RNR in the presence of effector TTP for 5 min and

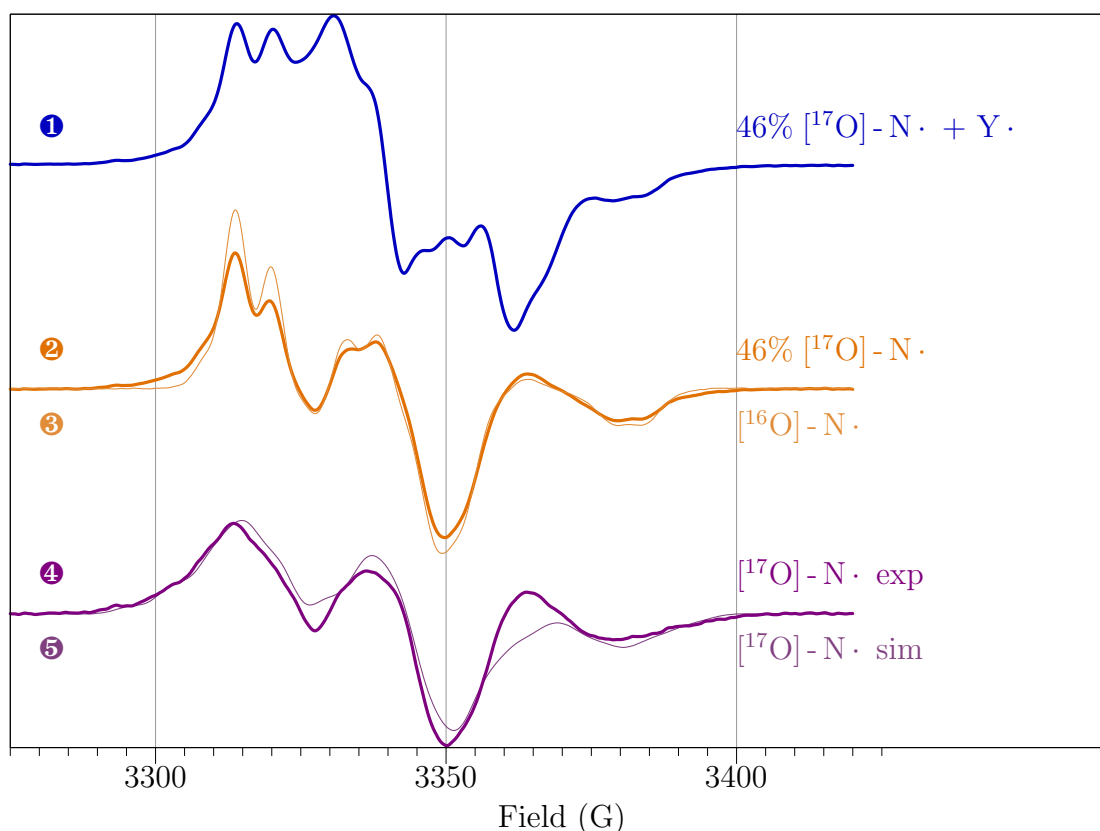


Figure 2.2: 9 GHz EPR spectra of $N\cdot$ formed during inactivation of RNR by $[3' - ^{16}\text{O}] - \text{N}_3\text{UDP}$ and $46 \pm 2\%$ enriched $[3' - ^{17}\text{O}] - \text{N}_3\text{UDP}$

the reactions were examined by 9 and 140 GHz EPR spectroscopy. DFT calculations were then employed to gain further insight into the structure of $N\cdot$ and into the mechanism of the $[^{17}\text{O}]$ hyperfine coupling. In a control experiment, $[3' - ^{17}\text{O}] - \text{N}_3\text{UDP}$ caused time-dependent inactivation of R1 and R2 that was identical to that observed with $[3' - ^{16}\text{O}] - \text{N}_3\text{UDP}$.

2.3.1 9 GHz EPR experiments

The 9 GHz CW EPR spectrum of the reaction of $46 \pm 2\%$ enriched $[3' - ^{17}\text{O}] - \text{N}_3\text{UDP}$ with RNR and effector TTP is shown in Figure 2.2, trace ❶. The spectrum is a composite of the $Y\cdot$ and the $N\cdot$ radicals. The contribution to the spectrum from the $Y\cdot$ (35.9% $Y\cdot$) was subtracted, giving the spectrum shown in Figure 2.2, trace ❷. This spectrum represents contributions from $[^{16}\text{O}] -$ and $[^{17}\text{O}] -$ labeled nucleotide in the ratio of 54:46. Subtraction of the contribution from the $[^{16}\text{O}] -$ labeled material (shown in Figure 2.2, trace ❸) resulted in the spectrum of $[^{17}\text{O}] - N\cdot$ shown in Figure 2.2, trace ❹. The observed spectrum exhibits considerable hyperfine broadening on its low-field features. Simulation of the spectrum

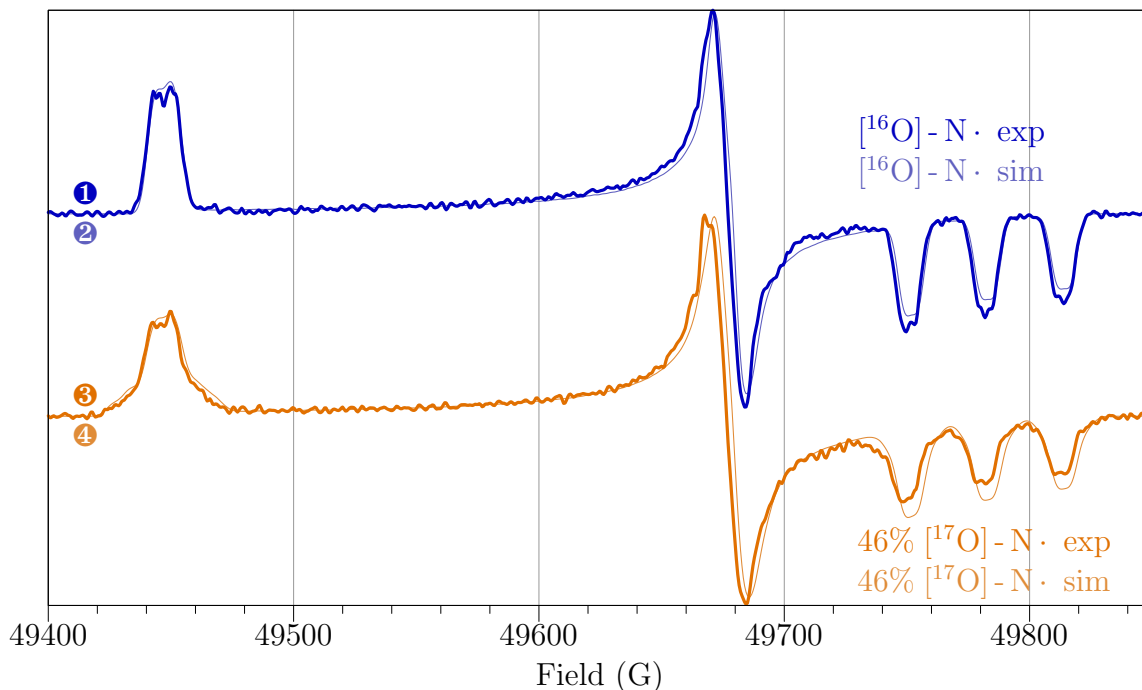


Figure 2.3: Derivative line shapes of the 140 GHz pulsed EPR spectra of $N\cdot$ formed during inactivation of RNR by $[3' - ^{16}\text{O}] - \text{N}_3\text{UDP}$ and $46 \pm 2\%$ enriched $[3' - ^{17}\text{O}] - \text{N}_3\text{UDP}$

(Figure 2.2, trace 5) reveals a $[^{17}\text{O}]$ hyperfine tensor with $A_{xx}(^{17}\text{O}) = 8.5$ G, $A_{yy}(^{17}\text{O}) = 1.5$ G, $A_{zz}(^{17}\text{O}) = 1.0$ G and Euler angles $\alpha = 0^\circ$, $\beta = 27^\circ$, and $\gamma = 0^\circ$ with respect to the g-tensor principal axes. From the principal HFC values, the isotropic (A_{iso}) and the anisotropic (T_{diag}) parts of the tensor can be separated. Since the signs of the tensor components are unknown, two cases are possible: one in which all tensor components have the same sign, and another in which the two smaller components, $A_{yy}(^{17}\text{O})$ and $A_{zz}(^{17}\text{O})$, which are almost equal, have an opposite sign from $A_{xx}(^{17}\text{O})$. With $A_{\text{iso}} = (A_{xx} + A_{yy} + A_{zz})/3$ and $T_{\text{diag}} = (A_{xx}, A_{yy}, A_{zz}) - A_{\text{iso}}$, in the first case $A_{\text{iso}} = -3.7$ G and $T_{\text{diag}} = (-4.8, 2.2, 2.7)$ G, and in the second case $A_{\text{iso}} = -2.0$ G and $T_{\text{diag}} = (-6.5, 3.5, 3.0)$ G. The signs of all the HFC constants are not absolute but relative to each other.

2.3.2 140 GHz EPR experiments

Reaction of $46 \pm 2\%$ enriched $[3' - ^{17}\text{O}] - \text{N}_3\text{UDP}$ with RNR and effector TTP was also examined by 140 GHz EPR spectroscopy. The derivatives of the echo-detected spectra are shown in Figure 2.3. Here, the spectra do not contain contributions from $Y\cdot$ because of the pulsed acquisition method employed. A comparison of the spectrum of $N\cdot$ derived from $[3' - ^{17}\text{O}] - \text{N}_3\text{UDP}$ (Figure 2.3, trace 3) with the spectrum derived from $[3' - ^{16}\text{O}] - \text{N}_3\text{UDP}$ (Figure 2.3, trace 1) reveals a visible broadening of the low-field portion of the spectrum relative to the

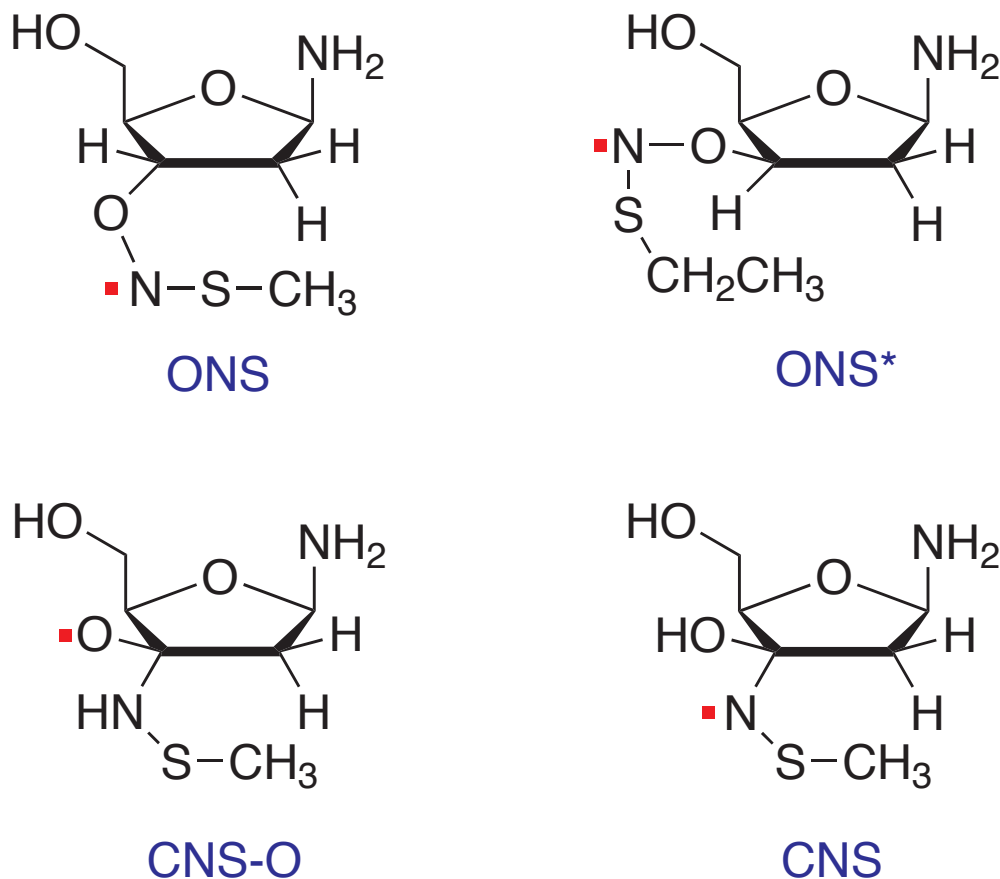


Figure 2.4: Structural models of $N\cdot$ used in DFT calculations

high-field portion. The $[3' - ^{16}\text{O}] - \text{N}_3\text{UDP}$ - and $[3' - ^{17}\text{O}] - \text{N}_3\text{UDP}$ -derived spectra could be simulated using the same parameters as those used for the simulation of the 9 GHz data and the simulations are shown as traces ② and ④ for $[3' - ^{16}\text{O}] - \text{N}_3\text{UDP}$ and $[3' - ^{17}\text{O}] - \text{N}_3\text{UDP}$ spectra, respectively.

2.3.3 Quantum chemical calculations to assign the structure of $N\cdot$

To allow the distinction between the two structural models of $N\cdot$, 6 and 7 Figure 2.1, and determine which of the two models is in best agreement with the simulated hyperfine tensor and previous ESEEM data, density functional theory (DFT) calculations were employed. To make the calculations tractable, models of $N\cdot$ were generated in which the 5'-diphosphate group was removed, uracil was replaced by an NH_2 group, and C225 in the active site of R1 was represented by either $-\text{S} - \text{CH}_3$ or $-\text{S} - \text{CH}_2\text{CH}_3$, Figure 2.4. These models were structurally optimized without constraints to obtain the equilibrium geometries.

Before calculating the EPR parameters of these model compounds, *ab initio* coupled

		ONS	ONS* ^a	CNS – O	CNS	exp ^b
¹⁴ N	A _{iso}	+8.90	+8.89	–0.61	+7.39	+9.0/+11.7
	A _{xx}	–3.99	–4.45	–3.27	–3.92	–/+2.0
	A _{yy}	–3.21	–3.44	–3.07	–3.70	–/+2.0
	A _{zz}	+33.90	+34.56	+4.51	+29.79	+/+31.0
¹⁷ O	A _{iso}	–6.64	–6.69	–5.67	–0.94	–2.0/–3.7
	A _{xx}	–25.63	–26.35	–48.55	–2.44	–/–8.5
	A _{yy}	+3.52	+3.93	+15.88	–0.26	+/–1.5
	A _{zz}	+2.20	+2.34	+15.67	–0.12	+/–1.0
r(N – H1')	4.07	5.17	4.54	3.33	3.0(2)	
r(N – H4')	3.72	4.51	2.53	2.36	2.7(3)	

^a The N – O – C3' – C4' dihedral angle was set to 180° and held constant for this model.

^b The error of the experimental HFC constants was estimated to be ±1 G. For the HFC tensors, two cases for the relative sign of the A_{ii} components are shown together with the two corresponding A_{iso} values.

Table 2.1: Calculated HFC tensors and selected N – H distances of structural models of N·.

cluster (CCSD(T)) calculations were carried out for two smaller substructures, HO – N· – SH and HO – CH₂ – N· – SH, to evaluate the validity of the DFT method in predicting the correct spin density distribution of radical structures such as 6 and 7. Results of the *ab initio* CCSD(T) study are presented in Appendix B. The results show that DFT calculations with an IGLO-II basis set yield satisfactory spin densities and HFC coupling constants for the systems under study.

After method validation, the EPR parameters for the larger freely geometry optimized model systems ONS, ONS*, CNS – O and CNS (Figure 2.4) were computed. For completeness, radical 11 in Figure 2.1 was included in the theoretical study. This radical was not stable during structure optimization, collapsing back to the starting material. Pereira *et al.* have also reported that the addition of the sulfinylimine (9, Figure 2.1) to the 3'-oxygen is energetically highly disfavored.⁷ The results for ONS, ONS*, CNS – O, and CNS structural models of N· are shown in Table 2.1 together with the experimental data for N·.

Based on the calculations, the CNS-O structural model can immediately be ruled out by comparison of the experimental with the calculated HFC tensors; the calculated HFC constants are much smaller for [¹⁴N] and much larger for [¹⁷O] than the experimentally observed ones. For all the other structural models (nitrogen-centered radicals ONS, ONS*, and CNS), the [¹⁴N] HFC tensors are in good agreement with experiment. Examination of

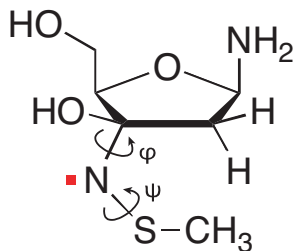


Figure 2.5: Definition of φ and ψ angles in the CNS structural model

the [^{17}O] HFC tensors shows that ONS-type structures (ONS or ONS*) should be excluded from consideration as structural models of $\text{N}\cdot$ because the direct bonding of the oxygen nucleus to the $\text{N}\cdot$ gives rise to [^{17}O] HFC tensors which are much larger than those observed experimentally. For the CNS model with free structure optimization, calculations gave [^{17}O] HFC constants that are smaller than the values found for $\text{N}\cdot$, but suggested that this structure should be considered for further geometrical refinement.

Additionally, to verify that the ONS-type structures should be excluded, further calculations on various systematic side chain conformers of ONS and ONS* structural models were performed (data not shown). In all cases, the [^{17}O] HFC tensors were similar to or even larger than those of the freely optimized ONS and ONS* structures (Table 2.1) and thus not in agreement with the experimental data. To find a better model for $\text{N}\cdot$, focus was turned to CNS-type structures in which the orientation of the $\text{N}-\text{S}-\text{CH}_3$ side chain relative to the sugar ring was altered. In these computations, the dihedral angle $\varphi = \angle(\text{S}-\text{N}-\text{C}3'-\text{C}4')$ (see Figure 2.5) was set to a specific value (100° , 120° , 140° , 160° , or 180°) and kept fixed during the structure optimizations, while all other degrees of freedom were allowed to fully relax. Freezing of the side chain orientation was done to mimic structural constraints imposed by the protein surroundings, in particular the positioning of the C225 side chain on the α face of the sugar ring.³⁶ The CNS-type structures in which $\varphi = \angle(\text{S}-\text{N}-\text{C}3'-\text{C}4')$ was set to 100° , 120° , 140° , 160° , or 180° are referred to as CNS_{100} , CNS_{120} , CNS_{140} , CNS_{160} , and CNS_{180} respectively. Geometry optimization of these structures in all cases yielded $\psi = \angle(\text{C}_{\text{CH}_3}-\text{S}-\text{N}-\text{C}3')$ close to 180° , Table 2.2. Also shown in Table 2.2 are [^{14}N] and [^{17}O] HFC tensors, selected distances, and molecular energies of the resulting conformers. For all structures in this series, the [^{14}N] HFC constants agree well with the experimental data, whereas the [^{17}O] HFC tensors and the $\text{N}-\text{H}1'$ distances strongly depend on the structural model. In those cases where the [^{17}O] HFC tensor is in reasonable accordance with the experiment (CNS_{160} , CNS_{140} , and CNS_{120}), the distance between N and the 1'-hydrogen appears too large compared to the experimental ESEEM values,⁶ that is, the sugar ring is in a different conformation. To create a model that addresses this discrepancy, a calculation with an additional $\text{N}-\text{H}1'$ distance constraint was performed (CNS_{140}^* in Table 2.2). Here, the sugar ring conformation and the $\text{N}-\text{H}1'$ distance were taken from the CNS equilibrium model (Table 2.1), and the side chain dihedral angle $\varphi = 140^\circ$ was taken from the model

	CNS ($\varphi = 203^\circ$) ($\psi = 186^\circ$)	CNS ₁₈₀ ($\varphi = 180^\circ$) ($\psi = 183^\circ$)	CNS ₁₆₀ ($\varphi = 160^\circ$) ($\psi = 176^\circ$)	CNS ₁₄₀ ($\varphi = 140^\circ$) ($\psi = 174^\circ$)	CNS ₁₂₀ ($\varphi = 120^\circ$) ($\psi = 182^\circ$)	CNS ₁₀₀ ($\varphi = 100^\circ$) ($\psi = 183^\circ$)	CNS* ₁₄₀ ^a ($\varphi = 140^\circ$) ($\psi = 173^\circ$)	exp ^b
¹⁴ N	A _{iso} +7.39	+7.12	+7.59	+7.90	+8.14	+8.22	+7.82	+9.0/+11.7
	A _{xx} -3.92	-4.01	-3.50	-3.40	-3.34	-3.29	-3.72	-/+2.0
	A _{yy} -3.70	-3.79	-3.32	-3.25	-3.24	-3.17	-3.57	-/+2.0
	A _{zz} 29.79	+29.16	+29.60	+30.35	+31.00	+31.12	+30.74	+/+31.0
¹⁷ O	A _{iso} -0.94	-0.91	-1.55	-2.56	-1.44	-0.43	-2.27	-2.0/-3.7
	A _{xx} -2.44	-4.69	-6.94	-8.63	-6.37	-3.14	-8.80	-/-8.5
	A _{yy} -0.26	+0.88	+1.04	+0.37	+0.94	+0.87	+0.88	+/-1.5
	A _{zz} -0.12	+1.08	+1.24	+0.58	+1.11	+0.98	+1.11	+/-1.0
r(N - H1')	3.33	3.59	4.55	4.58	3.97	3.87	3.33	3.0(2)
r(N - H4')	2.36	2.37	2.44	2.46	2.49	2.49	2.34	2.7(3)
energy	-969.64611	-969.64477	-969.64579	-969.64504	-969.64165	-969.64141	-969.64206	

^a The asterisk denotes that the N - H1' distance was set to a value of 3.33 Å and kept fixed during the structure optimization of this model.

^b The error of the experimental HFC constants was estimated to be ± 1 G. For the HFC tensors, two cases for the relative signs of the A_{ii} components are shown together with the two corresponding A_{iso} values.

Table 2.2: Hyperfine coupling tensors, molecular energies, and selected N - H distances for different conformers of the CNS model

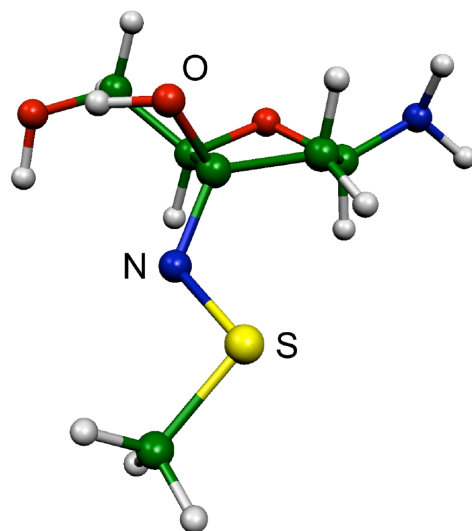


Figure 2.6: Structure of the $N\cdot$ radical with the CNS_{140}^* conformation

exhibiting the best agreement of the [^{17}O] HFC tensor (CNS_{140}). The fixed $N - \text{H}1'$ distance represents potential constraints imposed on the sugar conformation by the protein in the active site of RNR. Using these two structural constraints, the model displayed in Figure 2.6 was obtained in good agreement with experimental data. The model also accounts for the fact that the Cys225 residue is located below the sugar ring. Furthermore, the energy difference between the CNS_{140}^* model and the CNS equilibrium structure (CNS, Table 2.1) amounts to 2.5 kcal/mol, a value reasonably small to represent structural influences of the protein surroundings on the geometry of $N\cdot$. The CNS_{140}^* structure thus represents the best computational model for $N\cdot$, Figure 2.6. The model requires that the $\text{C}1' - \text{H}1'$ and $\text{C}3' - \text{N}$ bonds are oriented almost axially relative to the plane of the sugar ring defined by $\text{C}1'$, $\text{C}3'$, and $\text{C}4'$ and that the $\text{N} - \text{S} - \text{CH}_3$ side chain adopts a conformation that leads to an orientation of the p_z -type nitrogen orbital toward the 3'-oxygen.

2.4 Discussion

2.4.1 Structural assignment of $N\cdot$

Previous studies by van der Donk *et al.*⁸ suggested two possible structures for $N\cdot$ generated during inactivation of class I RNRs with N_3NDPs . The experimental data allowed 7 to be favored over 6, although generation of 7 and its decomposition to furanone 12 were mechanistically difficult to rationalize (Figure 2.1). Recently, pathways for generation of 6 and 7 (Figure 2.1) have been considered theoretically.⁷ Structure 6 was favored energetically and an alternative pathway for its production proposed. To distinguish between 6 and 7, $46 \pm 2\%$ enriched [$3' - ^{17}\text{O}$]- N_3UDP was synthesized,⁹ the resulting $N\cdot$ examined by

EPR spectroscopy, and quantum chemical calculations were carried out to reproduce the experimental HFC tensors.

The 9 and 140 GHz EPR spectra of the $N\cdot$ generated with $[3' - ^{17}\text{O}] - \text{N}_3\text{UDP}$ show substantial hyperfine broadening at the low-field side, indicating that the $[^{17}\text{O}]$ nucleus at the 3'-position is located close to the nitrogen-centered radical, as expected from the proposed structures 6 and 7. To our knowledge, there is no information in the literature on hyperfine couplings of $\text{R} - [^{17}\text{O}] - \text{N} - \text{S} - \text{R}$ - or $\text{H} - [^{17}\text{O}] - \text{C} - \text{N} - \text{S} - \text{R}$ -type radicals. Thus, it was not feasible to distinguish between 6 and 7 solely based on direct comparison of the observed $[^{17}\text{O}]$ hyperfine tensor ($A_{xx}(^{17}\text{O}) = 8.5 \text{ G}$, $A_{yy}(^{17}\text{O}) = 1.5 \text{ G}$, $A_{zz}(^{17}\text{O}) = 1.0 \text{ G}$) with literature data.

To get more insight into the structure of this unusual radical and into the mechanism of the $[^{17}\text{O}]$ hyperfine coupling, DFT calculations were employed. The DFT method was first validated by *ab initio* CCSD(T) calculations on small model systems and then applied to the radical structures 6 and 7. The DFT calculations clearly ruled out the ONS structure 7, as this structure requires a much larger $[^{17}\text{O}]$ hyperfine coupling than is observed experimentally.

The calculations for the CNS-type structures resulted in much smaller $[^{17}\text{O}]$ HFC tensor components than for ONS-type structures. A critical dependence of the $[^{17}\text{O}]$ HFC on the conformation of the side chain connecting the protein to the plane of the sugar ring determined by $\text{C}1'$, $\text{C}3'$, and $\text{C}4'$ could be observed. A rotation of this side chain into a position in which the $\text{S} - \text{CH}_3$ points below and almost perpendicular to the sugar ring plane (the CNS_{140}^* model) leads to $[^{17}\text{O}]$ HFC tensors in good agreement with the experimental data. These results have allowed us to qualitatively rationalize the mechanism of the $[^{17}\text{O}]$ HFC and the substantial value of A_{iso} . Since the main portion of spin density in $N\cdot$ is localized in the p_z -orbitals of the nitrogen and sulfur, rotation of the side chain can produce overlap between the nitrogen p_z -orbital and the p_z -orbital of the 3'-oxygen for some specific conformations, inducing spin density at the $[^{17}\text{O}]$ nucleus.

Additionally, we compared the geometry of the CNS_{140}^* structure with the distances between the nitrogen-centered radical and the protons at the 1'-, 2'-, and 4'-positions of the sugar ring determined from ESEEM studies.⁶ On the basis of these data, the distance between $N\cdot$ and the 1'- ^2H was determined to be 3.0 Å and the distance between $N\cdot$ and the 4'- ^2H was determined to be 2.7 Å. The interaction of $N\cdot$ with the 2'- ^2H in a selectively deuterated sample (^2H is on the β face) could not be detected by ESEEM. The DFT results reproduce these experimental distances reasonably well when the sugar ring assumes the conformation shown in Figure 2.6. The energy of the CNS_{140}^* structure was found to be only 2.5 kcal/mol above the equilibrium structure (CNS, Table 2.1), which can be reasonably attributed to constraints posed either by the large substituents of the sugar ring (not taken into account in the calculation) or by the active site. In the optimized structure of Figure 2.6, the distance to the 2'-hydrogen on the β face is 3.42 Å. The DFT calculations yield dipolar HFCs to the 1'-, 2'- (β face), and 4'-deuterons of $T_{\perp}(1' - ^2\text{H}) = -0.09 \text{ G}$, $T_{\perp}(2' - ^2\text{H}) = -0.07 \text{ G}$, and $T_{\perp}(4' - ^2\text{H}) = -0.23 \text{ G}$. The 2'- ^2H HFC constant is the smallest one among the couplings to the three deuterons. This may be the reason why the interaction with the 2'- ^2H has not been detected in the ESEEM experiment.

Another parameter that can be used to confirm the reliability and accuracy of the computational results is the HFC to the protons on the β -carbon of the C225 residue. Experimentally, a splitting of 6.3 G was found in the 9 GHz spectra that was assigned to a β -proton of C225.⁸ The fact that only one of the two β -protons can be observed is due to the different orientation of the protons with respect to the p-type SOMO on sulfur and nitrogen leading to a large (6.3 G) and a small (< 3 G) proton HFC. In the computational models, there is a methyl group instead of a methylene group at the position of the β -carbon of C225. For the CNS*₁₄₀ model, the calculations yield hyperfine couplings to the three protons of $A_{\text{iso}} = 6.7$ G and $T_{\text{diag}} = (-1.1, -0.7, +1.8)$ G, $A_{\text{iso}} = -0.6$ G and $T_{\text{diag}} = (-0.9, -0.7, +1.6)$ G, and $A_{\text{iso}} = 6.6$ G and $T_{\text{diag}} = (-1.1, -0.7, +1.9)$ G, as well as dihedral angles (H – C – S – N) of -64.7° , $+175.8^\circ$, and $+56.4^\circ$, respectively. In all cases, the anisotropy of the coupling tensors is sufficiently small not to be resolved in the EPR spectra. The size of the HFC is in agreement with the experimental findings; the coupling is either close to 6.3 G or much smaller. In the structure optimizations of CNS*₁₄₀, the methyl group was allowed to freely relax. It can be concluded that the favored model structure, CNS*₁₄₀, yields a spin density distribution which, together with the side chain orientation, is consistent with the β -proton HFC parameters of C225.

2.4.2 Mechanistic implications

The EPR results in conjunction with DFT calculations that reproduce the observed HFC tensors provide strong support for the $\text{N}\cdot$ structure being best represented by 6. The mechanism by which 6 is generated, however, is still not clear. Recent theoretical calculations suggested a mechanism that had not previously been considered, highlighted in blue in Figure 2.1.

Information collected over the past decade must be accounted for by any proposed mechanism. When N_3UDP is incubated with RNR, a stoichiometric amount of 2-methylene-3-furanone, inorganic pyrophosphate, and uracil are produced on a slow time scale (Figure 2.1) after $\text{N}\cdot$ breakdown. These products are proposed to result from nonenzymatic breakdown of the 3'-keto-2'-deoxynucleotide (9, Figure 2.1). Early in the time course of inactivation, the $\text{Y}\cdot$ on R2 is reduced. When [3'-²H]- N_3UDP is used in the reaction in place of the corresponding protonated material, there is an isotope effect on $\text{Y}\cdot$ loss, requiring hydrogen atom abstraction from C3'. The next step requires C2' – N bond cleavage based on isotopic labeling experiments using [2'-¹³C]- and [2'-¹⁵N]- N_3UDP .⁶ This process could occur either homolytically or heterolytically. We have favored the heterolytic mechanism based on studies with the normal substrate and 2'-halogenated-2'-deoxynucleotides.³⁷ In the original mechanistic proposal, prior to the structural information,³⁶ the role of E441-R1 was not appreciated. Studies of the inactivation of RNR when E441 mutants of R1 were incubated with N_3CDP revealed a greatly reduced rate of inactivation and slowed loss of $\text{Y}\cdot$.³⁸ These results are similar to those observed when E441Q-R1 is incubated with CDP and support the proposal that E441 acts as a general base catalyst in the generation of ketyl radical 2 (Figure 2.1). Theoretical studies about the role of E441 have been mixed in their

conclusions, but recently, a consensus has been reached which agrees with model studies. Conversion of 5 to 2 (Figure 2.1) is proposed to be identical to the first few steps in the normal reduction process (Figure 1.4).^{39–41}

The next step in the proposed N_3 NDP inhibition mechanism, reduction of the ketyl radical 2 by proton-coupled electron transfer to generate the 3'-keto-2'-deoxynucleotide 3 (Figure 2.1), is also analogous to the proposed mechanism of reduction for CDP. This process leaves a thiyl radical in the active site. Evidence in support of steps 2 and 3 has been provided by mutational studies on C225 in R1 and more recently on N437 and E441 in R1.^{42–46} Mutation of any of these residues results in rapid loss of $Y\cdot$, but no $N\cdot$ is detected except in the case of E441D. In the case of C225S-R1, azide was observed (a distinction between azide and HN_3 is not possible based on the experimental method). In the case of N437Q- and E441Q-R1, the fate of the azide was not monitored. Thus, when groups involved in catalysis or in the maintaining of the active site conformation required for efficient nucleotide reduction (Figure 1.4) are altered, azide ion (or potentially HN_3) is likely released instead of being trapped by the thiyl radical. Reaction of hydrazoic acid within the active site by the thiyl radical is proposed to generate N_2 , which is produced stoichiometrically, and a sulfinylimine radical (9, Figure 2.1) that has never been detected. It is unlikely that the thiyl radical would attack an azide ion. Thus, the protonated azide (pKa of 4.6) is essential for this mechanism.

The theoretical modeling study of Pereira *et al.*⁷ generated an alternative, attractive, mechanistic proposal. The released azide ion blocks reduction by C225, and it is proposed to add to the 2'-ketyl radical 2 (Figure 2.1) concomitant with protonation of the ketone oxygen by E441. The resulting radical is subsequently reduced at the 2'-position by C225 to generate the C225 thiyl radical (8, Figure 2.1). Addition of azide to ketones has chemical precedent,⁴⁷ but to our knowledge, there are no model systems where azide adds to ketyl radicals. The attachment of azide to C3' would move it out of the way sterically and hence facilitate the reduction process. In this case, the attack of the thiyl radical is on an alkyl azide (instead of HN_3), which has chemical precedence.^{48–50}

In our mechanism, the sulfinylimine radical attacks the 3'-keto-2'-deoxynucleotide, generating an alkoxy radical (10, Figure 2.1) which abstracts a hydrogen atom from the $-NH-$ to generate 6. These two steps are unprecedented and we propose could occur because of the steric constraints within the active site cavity. The resulting radical is very stable, and its breakdown ultimately regenerates the 3'-keto-2'-deoxynucleotide that is proposed to dissociate from the active site and generate the observed products, furanone, inorganic pyrophosphate, and uracil (Figure 2.1).

In the theoretical model, the loss of N_2 occurs through thiyl radical (C225)-mediated reaction on 8 with direct generation of 6 (Figure 2.1). No mechanism for this process is described. The theoretical model further suggests that the breakdown of 6 to the 3'-keto-2'-deoxynucleotide involves E441-assisted hydrogen atom migration. How E441 could carry out this chemistry is unclear. At present, it is unlikely that one can experimentally distinguish between these two mechanistic models.

Structure 6 is very far removed in chemical space from the initial 3'-nucleotide radical (1,

Figure 1.4). While N_3 NDPs are mechanism-based inhibitors of RNRs and thus the first few steps in the mechanism of reduction and inactivation are similar to the normal reduction reaction, after loss of water, the unique constellation of amino acid residues within the active site makes for unprecedented chemical transformations.

We have interpreted our results on the N_3 NDP inactivation of RNR to suggest that we have for the first time directly trapped the 3'-keto-2'-deoxynucleotide 3 (Figure 2.1) intermediate postulated to be involved in the normal reduction process or the 2'-ketyl radical 2 which is rapidly converted to 3 (Figure 2.1). The story of the mechanism of inactivation of RNR by N_3 NDP has been a long one, but has in the end given us a great deal of insight into the complex protein and substrate-based radical chemistry of ribonucleotide reduction.

2.5 Acknowledgments

I gratefully acknowledge Dr. Jörg Fritscher, Dr. Sylwia Kacprzak, and Dr. Martin Kaupp for performing DFT and *ab initio* coupled cluster calculations, and for their contributions to this manuscript. I thank the laboratory of Dr. Stanislaw Wnuk for the gift of [3'- ^{17}O]- N_3 UDP, Dr. Galit Bar for help with 140 GHz acquisition and simulations, Dr. John Robblee for excellent technical assistance with 9 GHz EPR spectroscopy and data analysis, and past and present members of the Stubbe laboratory for useful discussions. This work was supported by NIH grant 29595 to JoAnne Stubbe, NIH grants EB002804 and EB002026 to Robert Griffin, and DFG grants SPP 1071 and SFB 472 to Marina Bennati and Jörg Fritscher.

Bibliography

- [1] J. Fritscher, E. Artin, S. Wnuk, G. Bar, J. H. Robblee, S. Kacprzak, M. Kaupp, R. G. Griffin, M. Bennati, and J. Stubbe, "Structure of the nitrogen-centered radical formed during inactivation of *E. coli* ribonucleotide reductase by 2'-azido-2'-deoxyuridine-5'-diphosphate: Trapping of the 3'-ketonucleotide," *Journal of the American Chemical Society*, vol. 127, no. 21, pp. 7729–7738, 2005.
- [2] L. Thelander and B. Larsson, "Active site of ribonucleoside diphosphate reductase from *Escherichia coli*. Inactivation of the enzyme by 2'-substituted ribonucleoside diphosphates," *Journal of Biological Chemistry*, vol. 251, no. 5, pp. 1398–1405, 1976.
- [3] B.-M. Sjöberg, A. Graslund, and F. Eckstein, "A substrate radical intermediate in the reaction between ribonucleotide reductase from *Escherichia coli* and 2'-azido-2'-deoxynucleoside diphosphates," *Journal of Biological Chemistry*, vol. 258, no. 13, pp. 8060–8067, 1983.
- [4] M. Ator, S. P. Salowe, J. Stubbe, M. H. Emptage, and M. J. Robins, "2'-azido-2'-deoxynucleotide interaction with *E. coli* ribonucleotide reductase: generation of a new radical species," *Journal of the American Chemical Society*, vol. 106, no. 6, pp. 1886–1887, 1984.
- [5] S. P. Salowe, M. A. Ator, and J. Stubbe, "Products of the inactivation of ribonucleoside diphosphate reductase from *Escherichia coli* with 2'-azido-2'-deoxyuridine 5'-diphosphate," *Biochemistry*, vol. 26, no. 12, pp. 3408–3416, 1987.
- [6] S. Salowe, J. M. Bollinger, Jr., M. Ator, J. Stubbe, J. McCracken, J. Peisach, M. C. Samano, and M. J. Robins, "Alternative model for mechanism-based inhibition of *Escherichia coli* ribonucleotide reductase by 2'-azido-2'-deoxyuridine 5'-diphosphate," *Biochemistry*, vol. 32, no. 47, pp. 12749–12760, 1993.

- [7] S. Pereira, P. A. Fernandes, and M. J. Ramos, "Theoretical study of ribonucleotide reductase mechanism-based inhibition by 2'-azido-2'-deoxyribonucleoside 5'-diphosphates," *Journal of Computational Chemistry*, vol. 25, no. 2, pp. 227–237, 2004.
- [8] W. A. van der Donk, J. Stubbe, G. J. Gerfen, B. F. Bellew, and R. G. Griffin, "EPR investigations of the inactivation of *E. coli* ribonucleotide reductase with 2'-azido-2'-deoxyuridine 5'-diphosphate: Evidence for the involvement of the thiyl radical of C225-R1," *Journal of the American Chemical Society*, vol. 117, no. 35, pp. 8908–8916, 1995.
- [9] S. F. Wnuk, S. M. Chowdhury, P. I. Garcia, Jr., and M. J. Robins, "Stereo-defined synthesis of O3'-labeled uracil nucleosides. 3'-[¹⁷O]-2'-azido-2'-deoxyuridine 5'-diphosphate as a probe for the mechanism of inactivation of ribonucleotide reductases," *Journal of Organic Chemistry*, vol. 67, no. 6, pp. 1816–1819, 2002.
- [10] S. P. Salowe and J. Stubbe, "Cloning, overproduction, and purification of the B2 subunit of ribonucleoside-diphosphate reductase," *Journal of Bacteriology*, vol. 165, no. 2, pp. 363–366, 1986.
- [11] J. M. Bollinger, Jr, D. E. Edmondson, B.-H. Huynh, J. Filley, J. R. Norton, and J. Stubbe, "Mechanism of assembly of the tyrosyl radical-dinuclear iron cluster cofactor of ribonucleotide reductase," *Science (Washington, DC)*, vol. 253, no. 5017, pp. 292–298, 1991.
- [12] P. T. Chivers, K. E. Prehoda, B. F. Volkman, B.-M. Kim, J. L. Markley, and R. T. Raines, "Microscopic pK_a values of *Escherichia coli* thioredoxin," *Biochemistry*, vol. 36, no. 48, pp. 14985–14991, 1997.
- [13] M. Russel and P. Model, "Direct cloning of the *trx*B gene that encodes thioredoxin reductase," *Journal of Bacteriology*, vol. 163, no. 1, pp. 238–242, 1985.
- [14] M. Bennati, C. T. Farrar, J. A. Bryant, S. J. Inati, V. Weis, G. J. Gerfen, P. Riggs-Gelasco, J. Stubbe, and R. G. Griffin, "Pulsed electron-nuclear double resonance (ENDOR) at 140 GHz," *Journal of Magnetic Resonance*, vol. 138, no. 2, pp. 232–243, 1999.
- [15] E. L. Hahn, "Spin echoes," *Physical Review*, vol. 80, no. 4, pp. 580–594, 1950.
- [16] M. Bennati, J. Stubbe, and R. G. Griffin, "High-frequency EPR and ENDOR: time-domain spectroscopy of ribonucleotide reductase," *Applied Magnetic Resonance*, vol. 21, no. 3-4, pp. 389–410, 2001.
- [17] S. Un, J. Bryant, and R. G. Griffin, "Precision field-sweep system for superconducting solenoids and its application to high-frequency EPR spectroscopy," *Journal of Magnetic Resonance, Series A*, vol. 101, no. 1, pp. 92–94, 1993.
- [18] M. J. Frisch, G. W. Trucks, H. B. Schlegel, G. E. Scuseria, M. A. Robb, J. R. Cheeseman, J. Montgomery, J. A., T. Vreven, K. N. Kudin, J. C. Burant, J. M. Millam, S. S. Iyengar, J. Tomasi, V. Barone, B. Mennucci, M. Cossi, G. Scalmani, N. Rega, G. A. Petersson, H. Nakatsuji, M. Hada, M. Ehara, K. Toyota, R. Fukuda, J. Hasegawa, M. Ishida, T. Nakajima, Y. Honda, O. Kitao, H. Nakai, M. Klene, X. Li, J. E. Knox, H. P. Hratchian, J. B. Cross, V. Bakken, C. Adamo, J. Jaramillo, R. Gomperts, R. E. Stratmann, O. Yazyev, A. J. Austin, R. Cammi, C. Pomelli, J. W. Ochterski, P. Y. Ayala, K. Morokuma, G. A. Voth, P. Salvador, J. J. Dannenberg, V. G. Zakrzewski, S. Dapprich, A. D. Daniels, M. C. Strain, O. Farkas, D. K. Malick, A. D. Rabuck, K. Raghavachari, J. B. Foresman, J. V. Ortiz, Q. Cui, A. G. Baboul, S. Clifford, J. Cioslowski, B. B. Stefanov, G. Liu, A. Liashenko, P. Piskorz, I. Komaromi, R. L. Martin, D. J. Fox, T. Keith, M. A. Al-Laham, C. Y. Peng, A. Nanayakkara, M. Challacombe, P. M. W. Gill, B. Johnson, W. Chen, M. W. Wong, C. Gonzalez, and J. A. Pople, *Gaussian 03*. Gaussian, Inc., Pittsburgh, PA, revision b.03 ed., 2003.
- [19] R. Ahlrichs, M. Bär, H.-P. Baron, R. Bauernschmitt, S. Böcker, P. Deglmann, M. Ehrig, K. Eichkorn, S. Elliott, F. Furche, F. Haase, M. Häser, H. Horn, C. Hättig, C. Huber, U. Huniar, M. Kattannek, A. Köhn, C. Kölmel, M. Kollwitz, K. May, C. Ochsenfeld, H. Öhm, A. Schäfer, U. Schneider, M. Sierka, O. Treutler, B. Unterreiner, M. von Arnim, F. Weigend, P. Weis, and H. Weiss, *TURBOMOLE*. Quantum Chemistry Group, University of Karlsruhe, Karlsruhe, Germany, version 5.6 ed., 2002.

- [20] A. D. Becke, "Density-functional exchange-energy approximation with correct asymptotic behavior," *Physical Review A: Atomic, Molecular, and Optical Physics*, vol. 38, no. 6, pp. 3098–3100, 1988.
- [21] J. P. Perdew, "Density-functional approximation for the correlation energy of the inhomogeneous electron gas," *Physical Review B*, vol. 33, no. 12, pp. 8822–8824, 1986.
- [22] J. P. Perdew, "Erratum: Density-functional approximation for the correlation energy of the inhomogeneous electron gas," *Physical Review B*, vol. 34, no. 10, p. 7406, 1986.
- [23] A. Schaefer, C. Huber, and R. Ahlrichs, "Fully optimized contracted Gaussian basis sets of triple zeta valence quality for atoms Li to Kr," *Journal of Chemical Physics*, vol. 100, no. 8, pp. 5829–5835, 1994.
- [24] K. Eichkorn, O. Treutler, H. Oehm, M. Haeser, and R. Ahlrichs, "Auxiliary basis sets to approximate Coulomb potentials. [Erratum]," *Chemical Physics Letters*, vol. 242, no. 6, pp. 652–660, 1995.
- [25] K. Eichkorn, F. Weigend, O. Treutler, and R. Ahlrichs, "Auxiliary basis sets for main row atoms and transition metals and their use to approximate Coulomb potentials," *Theoretical Chemistry Accounts*, vol. 97, no. 1-4, pp. 119–124, 1997.
- [26] A. D. Becke, "Density-functional thermochemistry. III. The role of exact exchange," *Journal of Chemical Physics*, vol. 98, no. 7, pp. 5648–5652, 1993.
- [27] J. P. Perdew and Y. Wang, "Accurate and simple analytic representation of the electron-gas correlation energy," *Physical Review B: Condensed Matter and Materials Physics*, vol. 45, no. 23, pp. 13244–13249, 1992.
- [28] J. P. Perdew, "Generalized gradient approximations for exchange and correlation: A look backward and forward," *Physica B*, vol. 172, no. 1-2, pp. 1–6, 1992.
- [29] W. Kutzelnigg, U. Fleisher, and M. Schindler, *NMR*, vol. 23, p. 165ff. Heidelberg, Germany: Springer-Verlag, 1990. Basic principles and progress.
- [30] J. F. Stanton, G. J., J. D. Watts, M. Nooijen, N. Oliphant, P. S. A., P. Szalay, W. J. Lauderdale, S. A. Kucharski, S. R. Gwaltney, S. Beck, A. Balkova, D. E. Bernholdt, K. K. Baeck, P. Rozyczko, H. Sekino, C. Huber, J. Pittner, and R. J. Bartlett. ACES II is a program product of the Quantum Theory Project, University of Florida. Integral packages included are VMOL (Almlöf, J.; Taylor, P. R.), VPROPS (Taylor, P. R.), and ABACUS (Helgaker, T.; Jensen, H. J. A.; Jørgensen, P.; Olsen, J.; Taylor, P. R.).
- [31] J. Gauss, J. F. Stanton, and R. J. Bartlett, "Analytic evaluation of energy gradients at the coupled-cluster singles and doubles level using quasirestricted Hartree-Fock open-shell reference functions," *Journal of Chemical Physics*, vol. 95, no. 4, pp. 2639–2645, 1991.
- [32] J. Gauss, W. J. Lauderdale, J. F. Stanton, J. D. Watts, and R. J. Bartlett, "Analytic energy gradients for open-shell coupled-cluster singles and doubles (CCSD) calculations using restricted open-shell Hartree-Fock (ROHF) reference functions," *Chemical Physics Letters*, vol. 182, no. 3-4, pp. 207–215, 1991.
- [33] J. D. Watts, J. Gauss, and R. J. Bartlett, "Open-shell analytical energy gradients for triple excitation many-body, coupled-cluster methods: MBPT(4), CCSD+T(CCSD), CCSD(T), and QCISD(T)," *Chemical Physics Letters*, vol. 200, no. 1-2, pp. 1–7, 1992.
- [34] J. D. Watts, J. Gauss, and R. J. Bartlett, "Coupled-cluster methods with noniterative triple excitations for restricted-open-shell-Hartree-Fock and other general single-determinant reference functions. Energies and analytical gradients," *Journal of Chemical Physics*, vol. 98, no. 11, pp. 8718–8733, 1993.
- [35] S. A. Perera, J. D. Watts, and R. J. Bartlett, "A theoretical study of hyperfine coupling constants," *Journal of Chemical Physics*, vol. 100, no. 2, pp. 1425–1434, 1994.
- [36] U. Uhlin and H. Eklund, "Structure of ribonucleotide reductase protein R1," *Nature (London)*, vol. 370, no. 6490, pp. 533–539, 1994.

- [37] S. Licht and J. Stubbe, *Comprehensive Natural Products Chemistry*, vol. 5, ch. Mechanistic Investigations of Ribonucleotide Reductases, pp. 163–203. Elsevier, 1999.
- [38] A. L. Persson, M. Eriksson, B. Katterle, S. Potsch, M. Sahlin, and B.-M. Sjöberg, “A new mechanism-based radical intermediate in a mutant R1 protein affecting the catalytically essential Glu441 in *Escherichia coli* ribonucleotide reductase,” *Journal of Biological Chemistry*, vol. 272, no. 50, pp. 31533–31541, 1997.
- [39] P. E. M. Siegbahn, “Theoretical study of the substrate mechanism of ribonucleotide reductase,” *Journal of the American Chemical Society*, vol. 120, no. 33, pp. 8417–8429, 1998.
- [40] F. Himmo and P. E. M. Siegbahn, “Very stable ribonucleotide substrate radical relevant for class I ribonucleotide reductase,” *Journal of Physical Chemistry B*, vol. 104, no. 31, pp. 7502–7509, 2000.
- [41] V. Pelmenschikov, K.-B. Cho, and P. E. M. Siegbahn, “Class I ribonucleotide reductase revisited: the effect of removing a proton on Glu441,” *Journal of computational chemistry*, vol. 25, no. 3, pp. 311–321, 2004.
- [42] A. Aberg, S. Hahne, M. Karlsson, A. Larsson, M. Ormo, A. Ahgren, and B.-M. Sjöberg, “Evidence for two different classes of redox-active cysteines in ribonucleotide reductase of *Escherichia coli*,” *The Journal of Biological Chemistry*, vol. 264, no. 21, pp. 12249–12252, 1989.
- [43] S. S. Mao, M. I. Johnston, J. M. Bollinger, and J. Stubbe, “Mechanism-based inhibition of a mutant *Escherichia coli* ribonucleotide reductase (cysteine-225 → serine) by its substrate CDP,” *Proceedings of the National Academy of Sciences of the United States of America*, vol. 86, no. 5, pp. 1485–1489, 1989.
- [44] S. S. Mao, T. P. Holler, J. M. Bollinger, Jr., G. X. Yu, M. I. Johnston, and J. Stubbe, “Interaction of C225S-R1 mutant subunit of ribonucleotide reductase with R2 and nucleoside diphosphates: tales of a suicidal enzyme,” *Biochemistry*, vol. 31, no. 40, pp. 9744–9751, 1992.
- [45] W. A. van der Donk, C. Zeng, K. Biemann, J. Stubbe, A. Hanlon, and J. E. Kyte, “Identification of an active site residue of the R1 subunit of ribonucleotide reductase from *Escherichia coli*: Characterization of substrate-induced polypeptide cleavage by C225S-R1,” *Biochemistry*, vol. 35, no. 31, pp. 10058–10067, 1996.
- [46] A. Kasrayan, A. L. Persson, M. Sahlin, and B.-M. Sjöberg, “The conserved active site asparagine in class I ribonucleotide reductase is essential for catalysis,” *Journal of Biological Chemistry*, vol. 277, no. 8, pp. 5749–5755, 2002.
- [47] P. A. S. Smith, “Schmidt reaction: experimental conditions and mechanism,” *Journal of the American Chemical Society*, vol. 70, pp. 320–323, 1948.
- [48] S. Kim, G. H. Joe, and J. Y. Do, “Novel radical cyclizations of alkyl azides. A new route to N-heterocycles,” *Journal of the American Chemical Society*, vol. 116, no. 12, pp. 5521–5522, 1994.
- [49] I. L. Cartwright, D. W. Hutchinson, and V. W. Armstrong, “The reaction between thiols and 8-azidoadenosine derivatives,” *Nucleic Acids Research*, vol. 3, no. 9, pp. 2331–2339, 1976.
- [50] J. V. Staros, H. Bayley, D. N. Strandring, and J. R. Knowles, “Reduction of aryl azides by thiols: implications for the use of photoaffinity reagents,” *Biochemical and Biophysical Research Communications*, vol. 80, no. 3, pp. 568–572, 1978.

Chapter 3

Development of a high-yielding enzymatic method for the 5'-phosphorylation of C, dC, dU and their 2'-analogs

3.1 Introduction

Nucleoside di- and tri-phosphates and their analogs have important therapeutic roles in diagnostic applications and in the treatment of viral and malignant diseases; however, no general and high-yielding route for the phosphorylation of nucleosides and their analogs to di- and tri-phosphates currently exists.¹

Currently used chemical phosphorylation methods

During the 1950s, pioneering work on nucleoside phosphorylation using phosphorus oxytrichloride was impeded by a lack of regioselectivity. Yoshikawa *et al.* made a key discovery that the rate of phosphorylation of nucleosides was accelerated if trimethylphosphate or triethylphosphate were used as the solvent.² Although early studies by Yoshikawa *et al.* made use of 2',3'-O-isopropylidene-protected nucleosides, it was subsequently reported that selective reaction at the 5'-hydroxyl was possible with unprotected nucleosides and deoxynucleosides. An advantageous aspect of the Yoshikawa method is that the chlorophosphate intermediate can be used directly in reactions with phosphate or pyrophosphate ion to generate corresponding di- and tri-phosphates in one-pot reactions.^{3,4}

Despite clear advantages of the Yoshikawa method, it is not ideal. Careful analyses have shown that the reaction times are highly variable depending on the type of nucleoside used, and modern analytical techniques have revealed that the selectivity of the reaction for the 5'-hydroxyl is seldom perfect.^{4,5}

More recently, Ludwig and Eckstein have reported a procedure in which nucleoside derivatives were activated with 2-chloro-4H-1,3,2-benzodioxaphosphorin-4-one,⁶ a reagent that had previously been used to form nucleoside H-phosphonates. This reaction gave an activated phosphite that was allowed to react with pyrophosphate and then hydrolyzed/oxidized to give the corresponding triphosphate. Protection of nucleobase functionality for A, T, G, and C was not required, but selectivity for the 5'-hydroxyl was low if the 2'- and 3'-hydroxyl groups were not protected.

Similarly, conditions for activation of nucleoside monophosphates for reaction with phosphate or pyrophosphates ions took considerable effort to develop. Early studies focused on the use of dicyclohexylcarbodiimide (DCC) in pyridine for activation, but mono-, di-, and poly-phosphates were formed.^{7,8} Furthermore, alkylamines with differing basicity and reactivity were studied for the formation of a variety of nucleoside phosphoramidates. In 1961 Moffat and Khorana introduced nucleoside phosphomorpholidate derivatives that made possible the syntheses of nucleoside di- and tri-phosphates as well as nucleoside coenzyme analogs.⁹

Phosphoimidazolidate was another form of activated phosphate that was introduced in 1957 by Staab through activation of either phosphoric acid or organophosphate analogs with carbonyldiimidazole.¹⁰ Goldman *et al.* were first to report the synthesis of ADP from AMP using imidazole activation of the monophosphate.¹¹ This procedure was subsequently improved by Cramer *et al.*, Hoard and Ott, and Kozarich *et al.* and featured syntheses of deoxynucleoside triphosphates from deoxynucleoside monophosphates with yields in the range between 20% and 70%.¹²⁻¹⁴ The method became known as the Hoard and Ott procedure. Complications with this procedure have been reported when nucleoside monophosphates are used in place of deoxynucleoside monophosphates. It was shown that in these cases 1,1'-carbonyldiimidazole forms cyclic carbonate byproducts with the nucleotide cis diol functionality.¹⁵

Finally, direct nucleophilic substitution of 5'-leaving-groups with diphosphate and triphosphate ions has been explored. Reaction of tetrabasic triphosphate with 5'-O-tosyladenosine in acetonitrile at RT has been used to synthesize ATP.¹⁶ Unfortunately, this method to prepare nucleoside di- and tri-phosphates requires protection of the 2'- and 3'-hydroxyl groups prior to the tosylation step.¹⁷

Thus despite several key developments, chemical phosphorylation of nucleosides in a specific position without reversible protection of other functional groups remains a challenge.

Enzymatic phosphorylation methods In enzyme-catalyzed synthesis of nucleoside phosphates, ATP has received the most attention because of its utility as a phosphorylating agent. Little effort has been spent on the development of methods to generate nucleotides other than ATP.

Enzymatic conversion of nucleosides, deoxynucleosides, and their analogs to triphosphates requires the action of three kinases, one each for the synthesis of the corresponding mono-, di-, and tri-phosphate. For the conversion of diphosphates to triphosphates, three kinases are available that convert all four of the NDPs (ADP, CDP, GDP, and UDP) to the correspond-

ing NTPs: pyruvate kinase (PK), which uses phosphoenolpyruvate (PEP) as the phosphoryl donor, acetate kinase which uses acetylphosphate, and nucleosidediphosphate kinase which uses ATP. Pyruvate kinase has also been shown to phosphorylate dNDPs including dTDP to the corresponding dNTPs.¹⁸ The preparation of NDPs and dNDPs from NMPs and dNMPs is more difficult, and no single enzyme is known that can convert all (d)NMPs to (d)NDPs. Until recently, this was also true for the conversion of nucleosides and deoxynucleosides to the corresponding monophosphates. However, a broadly specific deoxynucleoside kinase has been identified in *Drosophila melanogaster* and in tomato.^{19,20} Both have been shown to phosphorylate all natural nucleosides and deoxynucleosides to corresponding monophosphates, and have considerable potential to become general nucleoside and deoxynucleoside phosphorylating reagents.

Specifically in the Stubbe laboratory, a long-standing interest has existed for the development of a high-yielding method for the selective 5'-phosphorylation of isotopically labeled cytidine for use in ribonucleotide reductase (RNR) activity assays, and for the selective 5'-phosphorylation of cytidine- and uridine-derived 2'-deoxy-2'-nucleoside analogs. Studies with one such analog, 2'-deoxy-2',2'-difluorocytidine (dFdC), have been hampered for many years by the inability to reproducibly make dFdCDP and dFdCTP in significant yields using the known chemical phosphorylation methods reviewed above. Due to the presence of two fluorines at the 2'-position of the ribose ring, the pKa of the 3'-hydroxyl group of dFdC is lowered. This altered pKa has caused complications during monophosphate syntheses by both compromising the selectivity of the reaction for the 5'-hydroxyl and by causing the formation of 3',5'-cyclic phosphates.²¹

Based on preliminary reports in the literature by Usova and Eriksson²² and by van Rompay *et al.*²³ that human deoxycytidine kinase (HdCK) and human UMP-CMP kinase phosphorylate C, dC, U, dU and several nucleoside analogs including dFdC, a high-yielding enzymatic procedure for the 5'-phosphorylation of cytidine, 2'-deoxycytidine, and 2'-deoxyuridine and their analogs was developed. For the first time it is possible to selectively phosphorylate in high yields analogs of cytidine, 2'-deoxycytidine, and 2'-deoxyuridine not amenable to chemical phosphorylation methods and to carry out the syntheses on nmol scale. Thus, the previously impractical phosphorylation of isotopically-labeled derivatives of these classes of compounds now becomes feasible. Specifically, we have used this method to prepare 5'-nucleoside diphosphates of [5,6-²H]-cytidine, [1'-²H]-cytidine, [2'-²H]-cytidine, and [4'-²H]-cytidine for experiments described in Chapter 4; 5'-nucleoside diphosphates of dFdC, [5-³H]-dFdC, [1'-³H]-dFdC, and [1'-²H]-dFdC for experiments described in Chapter 5; and 2'-azido-2'-deoxycytidine-5'-diphosphate and 2'-azido-2'-deoxyuridine-5'-diphosphate for experiments described in Appendix A.

3.2 Materials and methods

3.2.1 Purchased materials and materials obtained as gifts

Triethylamine (99% pure) was purchased from Acros, and 1,4-dithiothreitol (DTT) from Mallinckrodt. $[\gamma\text{-}^{32}\text{P}]\text{-ATP}$ (3000 Ci/mmol) was obtained from Amersham Pharmacia Biotech. DEAE Sephadex A-25 and Glutathione Sepharose were purchased from Pharmacia. Ni-NTA Agarose was obtained from Qiagen. All other materials were purchased from Sigma.

The pET-9d expression vector for human 6xHis-deoxycytidine kinase (6xHis-HdCK) was obtained in *E. coli* BL21 (DE3) pLysS strain as a gift from Dr. Staffan Eriksson.²² The pGEX expression vector for human GST-UMP-CMP kinase was a gift from Dr. Anna Karlsson.²³

3.2.2 Growth and induction of 6xHis-HdCK expression strain

All cultures were grown in LB at 37 °C in the presence of 50 µg/mL kanamycin and 50 µg/mL chloramphenicol.

Growth and induction study of *E. coli* BL21 (DE3) pLysS 6xHis-HdCK

pET-9d vector coding for the 6xHis-HdCK was used in a fresh transformation of *E. coli* BL21 (DE3) pLysS cell line according to standard transformation procedure.²⁴ In an initial growth, 3 × 5 mL cultures were seeded from single colonies and their growth monitored by absorption at 600 nm (OD_{600}) to determine the doubling time and saturation point for the strain. A 5 mL culture was then seeded from a single colony and grown to saturation overnight. From the overnight culture, six 50 mL cultures were inoculated at a 1 : 500 dilution (100 µL of the overnight culture per 50 mL culture). Two of the 50 mL cultures were induced at $\text{OD}_{600} = 0.5$, one with IPTG at a final concentration of 0.5 mM and the other with IPTG at a final concentration of 1.0 mM. Of the four remaining 50 mL cultures, two were induced at $\text{OD}_{600} = 1.0$ and two at $\text{OD}_{600} = 1.5$. Once again, in each set, one of the cultures was induced with IPTG at a final concentration of 0.5 mM while the other culture was induced with IPTG at a final concentration of 1.0 mM. One mL aliquots of the cultures were collected before induction and at 1, 2, and 3 h after induction.

All culture aliquots were centrifuged at 14000 rpm and the cell pellets resuspended in 10 µL of lysozyme cracking buffer (50 mM TRIS pH 8.0, 1 mM EDTA, 100 mM NaCl). One µL of 10 mg/mL lysozyme solution was added to each aliquot. The suspensions were incubated on ice with occasional vortexing for 20 min. One µL of a 13 mg/mL deoxycholic acid solution was added to each aliquot followed by 1 unit of DNase I (Sigma). After 10 min at room temperature, the suspensions were centrifuged at 14000 rpm for 10 min. The supernatants and pellets were separated by pipetting. To each supernatant ($V_f = 10$ µL), 10 µL of 2X Laemmli gel loading buffer²⁴ were added. To each pellet, 10 µL of dH₂O and

10 μ L of 2X Laemmli gel loading buffer²⁴ were added. The samples were analyzed by 12% SDS-PAGE.

Large-scale growth and induction of of *E. coli* BL21 (DE3) pLysS 6xHis - HdCK

For each large-scale growth, a fresh transformation of *E. coli* BL21 (DE3) pLysS strain with the pET-9d vector coding for 6xHis - HdCK was carried out as described above. Typically, two 100 mL starter cultures were seeded from single colonies and grown to saturation overnight while shaking at 200 rpm.

A 100 mL culture was spun down at 3000 rpm for 0.5 h and the pellet resuspended in 100 mL of LB. Two mL of the resuspension were used to inoculate 1 L cultures in 4 L shaker flasks at a 1 : 500 dilution. One L cultures were grown to an $OD_{600} = 1.0$ at which time 1 mM IPTG was added. Cells were grown for 4 additional hours and harvested by centrifugation at 14000 rpm.

Alternatively, a 100 mL overnight culture was spun down at 3000 rpm for 0.5 h, the pellet resuspended in 10 mL of LB, and the resuspension used to inoculate 10 L of LB in a New Brunswick Scientific 10 L fermentor, model MF-118 at a 1 : 200 dilution by adding 5 mL of the suspension. The culture was grown with constant stirring at 500 rpm and with an air flow of 15000 cm^3/min . When OD_{600} reached 1, IPTG was added to a final concentration of 1 mM. Cells were harvested 4 h after induction by centrifugation at 14000 rpm.

3.2.3 Purification of 6xHis - HdCK

Purification of 6xHis - HdCK was carried out by a modified procedure of Usova *et al.*²² In place of freeze-thawing and sonication reported by Usova *et al.*, the cells were lysed in a French Pressure Cell. Twenty mM imidazole was added to the column wash buffer, and imidazole concentration in the column elution buffer was lowered from 0.5–0.2 M. Additionally, phenylmethylsulfonyl fluoride (PMSF) was not used in the column elution buffer, and a Sephadex G-25 size-exclusion column was run to remove imidazole after elution of the protein from the Ni-NTA affinity column.

All steps were performed at 4 °C. Cell paste (15 g) was resuspended in 75 mL of cracking buffer (20 mM Tris pH 7.9, 0.5 M NaCl, 1 mM PMSF) and the suspension lysed at 14000 psi by two passes through the French Pressure Cell. Twenty units of DNase I (Sigma) were added to the lysate and the suspension stirred for 15 min. After centrifugation at 14000 rpm for 30 min, the supernatant was loaded onto a 30 mL Ni-NTA column pre-equilibrated in 10 column volumes (CVs) of cracking buffer. Loading was done at a flow rate of 20 mL/min. The column was washed overnight with 40 CV of cracking buffer containing 20 mM imidazole and eluted with 20 mM Tris pH 7.9, 0.5 M NaCl buffer containing 0.2 M imidazole and collecting 20 mL fractions. Protein-containing fractions as judged by $A_{280\text{ nm}}$ were concentrated in an Amicon device with a YM10 membrane to a final volume of 10 mL and loaded onto a 100 mL G-25 column (2 \times 32 cm) equilibrated in 20 mM Tris pH 7.9, 0.5 M NaCl, 10 mM DTT, 20% glycerol buffer. After elution, the fractions containing protein were concentrated

in an Amicon device with a YM10 membrane to a final concentration of 6 mg/mL. 6xHis-HdCK concentration was determined using $A_{280\text{nm}} = 0.55 \text{ mg/mL}$.

3.2.4 Spectrophotometric and radioactive assays of 6xHis - HdCK

$[\gamma\text{-}^{32}\text{P}]\text{-ATP}$ 6xHis - HdCK phosphate transfer assay Typical assay mixture in a final volume of 100 μL contained 10 $\mu\text{g/mL}$ 6xHis - HdCK, 100 μM $[\gamma\text{-}^{32}\text{P}]\text{-ATP}$ (S.A. $4\text{--}5 \cdot 10^3 \text{ cpm/nmol}$), 100 μM dCyt, 2 mM DTT, and 0.5 mg/mL BSA all in 50 mM TRIS pH 7.6, 100 mM KCl, 5 mM MgCl_2 . All reaction components except for 6xHis-HdCK were combined and equilibrated at 37 °C for 5 min. Reactions were initiated by the addition of 6xHis - HdCK and incubated at 37 °C. At 5, 10, 15, 20, and 25 min into the reaction, 10 μL aliquots of the assay mixture were removed and quenched by immersion into a boiling water bath for a period of 2 min. The aliquots were briefly spun, and 5 μL of each were spotted onto a 10 \times 10 cm PEI plate (Merck & Co., Inc.) prewashed by brief immersion in methanol. The plate was developed in 0.6 M LiCl (R_f values: ATP 0.1, dCMP 0.53). Based on the R_f value of a control spot of 20 nmol dCMP, the product bearing regions were excised in 2 \times 3 cm rectangles and immersed into 20 mL vials containing 1 mL of a 0.1 M HCl / 0.2 M KCl solution for 5 min. Nine ml of Scint-A XF scintillation fluid were added to the vials and the mixtures analyzed for radioactivity on a Beckman LS 6500 Scintillation Counter.

Spectrophotometric assay for 6xHis - HdCK using pyruvate kinase and lactate dehydrogenase Typical reactions in a final volume of 450 μL contained 54 $\mu\text{g/mL}$ 6xHis - HdCK, 5 mM ATP, 1 mM PEP, 1 mM dCyt, 2 mM DTT, 0.5 mg/mL BSA, 0.2 mM NADH, 5 U/ml LDH (one unit oxidizes one μmol of NADH per min at 25 °C, pH 7.3), and 10 U/ml PK (one unit of activity causes the oxidation of one μmol of NADH per minute at 25 °C, pH 7.6) all in 50 mM TRIS pH 7.6, 100 mM KCl, 5 mM MgCl_2 . All reaction components except for dCyt were mixed and equilibrated at 37 °C for 5 min. Reactions were initiated by the addition of dCyt. Rate of NADH consumption was monitored at 340 nm in a spectrophotometric cell equilibrated at 37 °C. The assay was run using 6xHis - HdCK for which S.A. of 150 $\text{nmol} \cdot \text{mg}^{-1} \cdot \text{min}^{-1}$ had previously been determined by the $[\gamma\text{-}^{32}\text{P}]\text{-ATP}$ phosphate transfer assay.

3.2.5 Growth and induction of human GST - UMP - CMP kinase

pGEX plasmid coding for the human GST - UMP - CMP kinase was transformed into *E. coli* Turner (DE3) pLysS strain (Novagen) using standard procedure.²⁴ Typically, two 100 mL starter cultures in LB were seeded from single colonies and grown to saturation overnight. One of the cultures was spun at 3000 rpm for 0.5 h to collect the cells, and the pellet resuspended in 10 mL of LB. The resuspension was used to inoculate 1 L cultures in 4 L shaker flasks at a 1 : 150 dilution by adding 0.7 mL of the resuspension to each flask. The flasks were incubated at 37 °C with 200 rpm agitation until $\text{OD}_{600} = 0.8$. The temperature was then lowered to 27 °C over a period of 1 hr by changing the temperature setting. At this time

IPTG (1 mM) was added. Cells were grown at 27 °C for 12 additional hours and harvested by centrifugation at 10000 rpm.

3.2.6 Purification of human GST - UMP - CMP kinase

Frozen cell paste (11 g) was suspended in 55 mL of phosphate-buffered saline (PBS) pH 7.3 containing 0.5 mM PMSF. The suspension was lysed at 14000 psi by two passes through the French Pressure Cell. The lysate was centrifuged at 12000 rpm for 20 min and the supernatant loaded onto a pre-equilibrated 10 mL Glutathione Sepharose column at a flow rate 1 mL/min (maximum binding capacity 5 mg GST per mL of resin based on manufacturer's specifications). Flow-through was collected and passed through the column once again. The column was then washed with 40 CV of PBS buffer containing 0.5 mM PMSF (2.5 mL/min flow rate). The protein was eluted with 50 mM TRIS pH 8.0 containing 10 mM reduced glutathione. The fractions (3 mL) were examined for protein content by $A_{280\text{ nm}}$.

Throughout the purification, protein concentration was measured using the Bradford assay with BSA as the standard. Protein purity was judged by SDS-PAGE.

3.2.7 Assay of human GST - UMP - CMP kinase

Typical assay mixture in a final volume of 100 μL contained 1 $\mu\text{g}/\text{mL}$ human GST - UMP - CMP kinase, 4 mM $[\gamma\text{-}^{32}\text{P}]\text{-ATP}$ (S.A. $4\text{--}5 \cdot 10^3$ cpm/nmol), 1 mM CMP, and 2 mM DTT all in 50 mM TRIS pH 8.0, 5 mM MgCl_2 . Reactions were initiated by the addition of human GST - UMP - CMP kinase. At 2, 4, 6 and 8 min into the reaction, 10 μL aliquots of the assay mixture were removed and quenched by immersion into a boiling water bath for a period of 2 min. The aliquots were briefly spun, and 5 μL of each were spotted onto a 10×10 cm PEI plate (Merck & Co., Inc.) prewashed by brief immersion in methanol. The plate was developed in 0.6 M LiCl (R_f values: ATP 0.1, CDP 0.36). Based on the R_f value of a control spot of 20 nmol CDP, the product bearing regions were excised in 2×3 cm rectangles and immersed into 20 mL vials containing 1 mL of a 0.1 M HCl / 0.2 M KCl solution for 5 min. Nine ml of Scint-A XF scintillation fluid were added to the vials and the mixtures analyzed for radioactivity on a Beckman LS 6500 Scintillation Counter.

3.2.8 Formation of nucleoside monophosphates

Phosphorylation of C, dC, dU and their 2'-analogs was achieved in the presence of 6xHis-HdCK with S.A. of $150\text{--}170$ nmol \cdot mg $^{-1}$ \cdot min $^{-1}$ using ATP as the phosphate donor. Typical reactions were carried out on 5–10 μmol of nucleoside. Under conditions optimized for the conversion of nucleosides to the corresponding monophosphates reactions contained 1 mM C, (d)C, (d)U or their 2'-analogs, 1.33 mg/mL 6xHis-HdCK, 2 mM ATP, 2 mM DTT, and 0.5 mg/mL BSA, all in 50 mM TRIS pH 7.6, 100 mM KCl, 5 mM MgCl_2 in a final volume of 5–10 mL.

Reactions were initiated by the addition of 6xHis-HdCK and incubated at 37 °C for 10 min. At the end of this time period, the reaction mixture was loaded onto a DEAE Sephadex A-25 column (10 mL, 1 × 12.5 cm for a 5 μmol synthesis). The (d)NMP was eluted with a linear gradient of 0.005–0.4 M triethylammonium bicarbonate (TEAB) pH 7.5 in dH₂O (90 × 90 mL for a 5 μmol synthesis). The fractions (4.5 mL) were assayed by A_{260nm} and A_{280nm}. Fractions eluting at 0.2 M TEAB, which is characteristic of nucleoside monophosphates, were pooled. Excess TEAB was removed by repeated cycles of dilution and concentration *in vacuo* from a 1:1 mixture of water and ethanol.¹⁴ Yield was assessed by UV/Vis absorption.

3.2.9 Formation of nucleoside diphosphates

Phosphorylation of CMP, dCMP, dUMP and their 2'-analogs was carried out in the presence of human GST-UMP-CMP kinase with S.A. of 2.1–4.8 μmol · mg⁻¹ · min⁻¹ using ATP as the phosphate donor. Typical reactions were carried out on 5–10 μmol of monophosphate and contained 1 mM CMP, (d)CMP, (d)UMP or their 2'-analogs, 65 μg/mL human GST-UMP-CMP kinase, 4 mM ATP, and 2 mM DTT all in 50 mM TRIS pH 8.0, 5 mM MgCl₂ in a final volume of 5–10 mL.

Reactions were initiated by the addition of human GST-UMP-CMP kinase and incubated at 37 °C for 30 min.

3.2.10 Purification of dCDP, dUDP, and their 2'-analogs after enzymatic diphosphorylation

In the case of 2'-deoxynucleoside diphosphates or their 2'-analogs, products from the reaction mixture above were loaded onto a DEAE Sephadex A-25 column (15 mL, 1.5 × 11.5 cm for a 5 μmol synthesis). The product was eluted using a linear gradient of 0.005–0.6 M TEAB pH 7.5 in dH₂O (120 × 120 mL for a 5 μmol synthesis). The fractions (5 mL) were assayed by A_{260nm} and A_{280nm}. Fractions eluting at 0.4 M TEAB, which is characteristic of nucleoside diphosphates, were pooled. Excess TEAB was removed by 6 cycles of dilution and concentration *in vacuo* from a 1:1 mixture of water and ethanol¹⁴ and then dissolved in 1 mL of dH₂O.

To the aqueous solution of nucleotides/deoxynucleotides, 0.5 M freshly prepared sodium periodate (Sigma) solution in water was added to a final concentration of 20 mM (4 equivalents relative to starting dNMP). The mixture was incubated at 37 °C for 10 minutes. After this time period, 4 M methyl amine solution was added to a final concentration of 100 mM, and the mixture incubated at 37 °C for additional 20 minutes. The 4 M methyl amine stock solution was freshly prepared from a commercially available 40% aqueous solution and brought to pH 7.3 by the dropwise addition of 85% phosphoric acid while stirring on ice. The oxidative cleavage was quenched by the addition of L-rhamnose to a final concentration of 40 mM (8 equivalents relative to starting dNMP, 4 equivalents relative to starting periodate) and incubation at 37 °C for 10 additional minutes. To remove liberated pyrophosphate, the

reaction was brought to 33 mM TRIS pH 7.2 by addition of 0.33 volumes of 100 mM TRIS pH 7.2 and incubated with 5U / 1.5 mL inorganic pyrophosphatase from Baker's yeast (E.C. 3.6.1.1, Sigma) in the presence of 1.6 mM MgCl₂. The reaction was incubated at 25 °C for 30 minutes. Before and after treatment with inorganic pyrophosphatase, the amount of contaminating pyrophosphate was measured by the method of O'Brien.²⁵ In a typical 5 μmol scale synthesis, final product was purified over an 11 mL DEAE Sephadex A-25 column (1 × 14 cm) running a 100 × 100 mL linear gradient of 0.005 M to 0.6 M TEAB pH 7.5 in dH₂O collecting 5 mL fractions. Fractions eluting at 0.4 M TEAB, which is characteristic of nucleoside diphosphates, were pooled. Excess TEAB was removed by 6 cycles of dilution and concentration *in vacuo* from a 1:1 mixture of water and ethanol.¹⁴ Yield was assessed by UV/Vis absorption.

3.2.11 Purification of CDP after enzymatic diphosphorylation

After enzymatic diphosphorylation, CDP was purified from ADP by two anion exchange chromatographic steps. For a 5 μmol synthesis, an 11 mL (1 × 14 cm) DEAE Sephadex A-25 column was eluted with a linear gradient of 0.005–0.6 M TEAB pH 7.5 in dH₂O, 120 × 120 mL. This larger than normal gradient allowed the removal of ~90% of ADP. Fractions (~ 3 mL) were assayed by UV/Vis absorption. Those with an A_{260 nm}/A_{280 nm} ratio which is characteristic of cytidine-derived nucleoside diphosphates were pooled. Excess TEAB was removed by 6 cycles of dilution and concentration *in vacuo* from a 1 : 1 mixture of water and ethanol.¹⁴ The material was then purified over a second anion exchange column exactly as described above to remove residual ADP. Yield was assessed by UV/Vis absorption.

3.3 Results

3.3.1 Growth and induction of 6xHis - HdCK expression strain

The doubling time of the *E. coli* BL21 (DE3) pLysS 6xHis - HdCK strain was 20 min. Based on the saturation point of OD₆₀₀ = 2.1 in 5 mL cultures, an induction study was carried out as described in Section 3.2. The lysed aliquots of the cultures were examined for protein content and for the partitioning of the protein between the soluble and insoluble fraction at various intervals after induction.

The expression level of soluble 6xHis - HdCK 3 h after induction was high. A very slight difference in the level of over-expression between cultures induced with 0.5 mM IPTG and cultures induced with 1.0 mM IPTG was detectable. The highest level of overexpression 3 h post-induction was achieved in cultures induced at OD₆₀₀ = 1.0 corresponding to the mid-log phase of the growth curve. Thus, induction with 1 mM IPTG at OD₆₀₀ = 1.0 was employed in all subsequent growths of this strain.

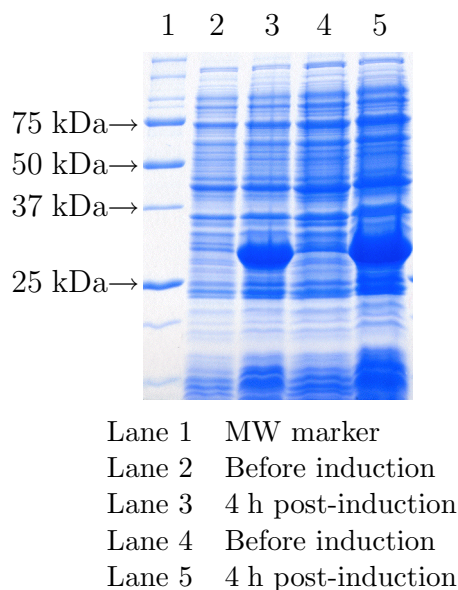


Figure 3.1: 6xHis-HdCK induction gel

Large-scale growth and induction of BL21 (DE3) pLysS 6xHis-HdCK strain was carried out either in shaker flasks or in a 10 L fermentor. Typical yield from shaker flask cultures was 3.5 g of wet cell paste per L of culture. From the fermentor growths, typically 4.4 g of wet cell paste per L of culture were obtained. A gel comparing total cell protein before induction and 4 h after induction during a representative fermentor growth is shown in Figure 3.1.

3.3.2 Purification and activity assays of 6xHis-HdCK

Initial purification carried out as reported by Usova *et al.*²² yielded protein of < 80% purity as shown in Figure 3.2. The purification scheme was changed to include a Ni-NTA column wash containing 20 mM imidazole. Furthermore, imidazole concentration in the elution buffer was lowered to 200 mM and imidazole was removed by size-exclusion chromatography after elution from the Ni-NTA column. Using this modified procedure, protein of > 95% purity was routinely obtained with a yield of 11 mg per g of cell paste. A representative purification gel is shown in Figure 3.3.

Based on the $[\gamma\text{-}^{32}\text{P}]\text{-ATP}$ phosphate transfer assay described in Section 3.2, the activity of the protein isolated by the modified procedure of Usova *et al.* was $150\text{--}170\text{ nmol}\cdot\text{mg}^{-1}\cdot\text{min}^{-1}$. This is up to 30% higher than the published range of $130\text{--}150\text{ nmol}\cdot\text{mg}^{-1}\cdot\text{min}^{-1}$.²²

To facilitate S.A. determination during protein isolation, a spectrophotometric, coupled activity assay for 6xHis-HdCK was developed using PK/LDH. In the test reactions, 6xHis-HdCK with S.A. of $150\text{ nmol}\cdot\text{mg}^{-1}\cdot\text{min}^{-1}$ measured by the $[\gamma\text{-}^{32}\text{P}]\text{-ATP}$ phosphate transfer assay was used. By the spectrophotometric assay, S.A. for this protein was determined to be $146 \pm 5\text{ nmol}\cdot\text{mg}^{-1}\cdot\text{min}^{-1}$ (three trials, values are presented as mean \pm SD). Thus, the

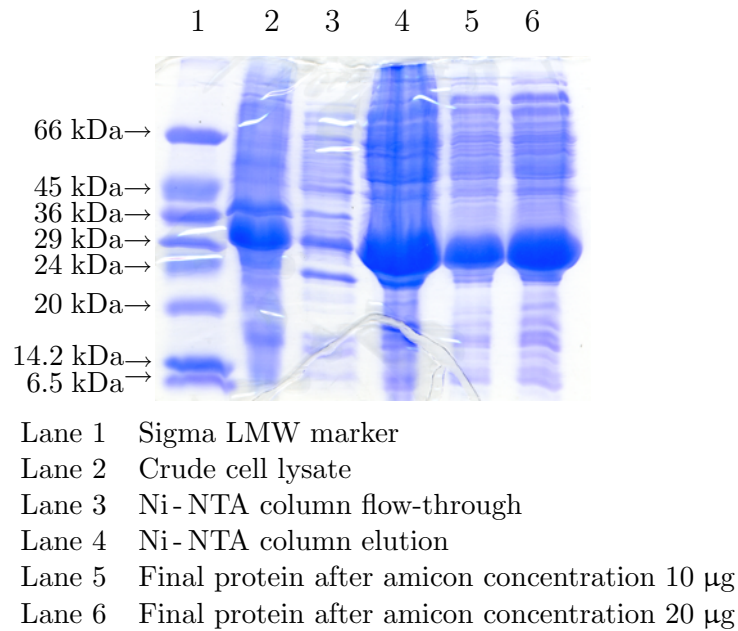


Figure 3.2: 6xHis-HdCK purification gel by the procedure of Usova *et al.*

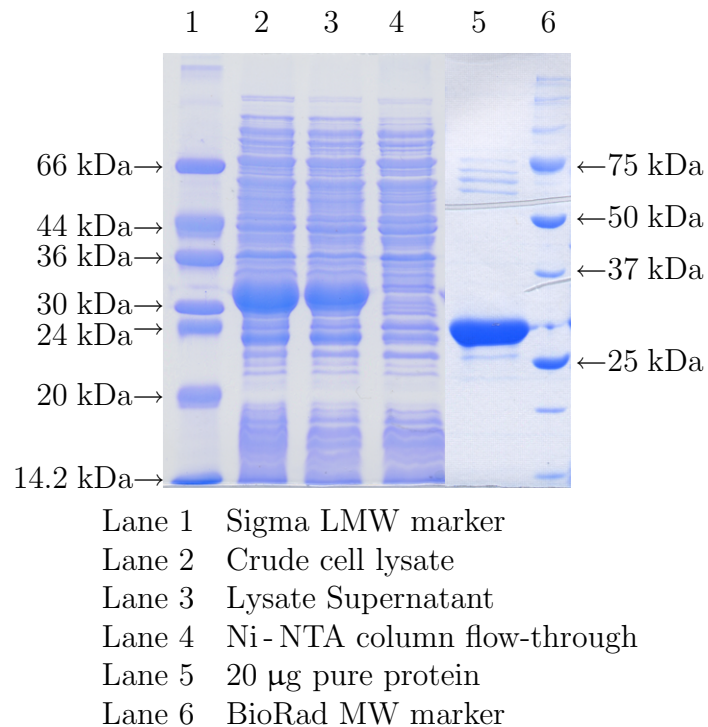


Figure 3.3: 6xHis-HdCK purification gel by the optimized procedure

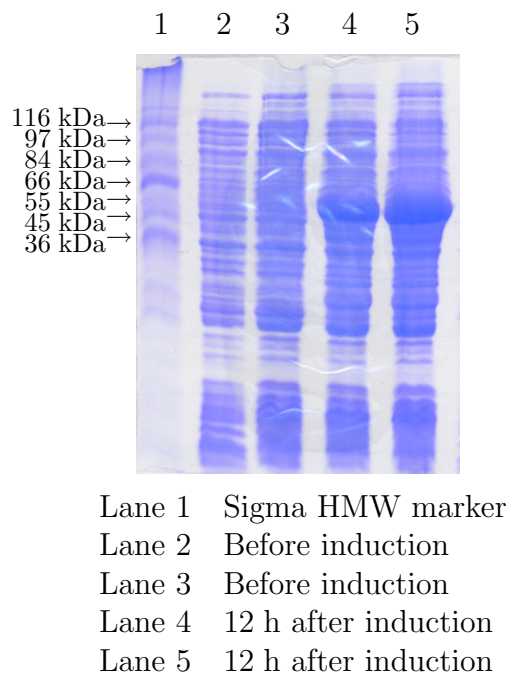


Figure 3.4: Human GST - UMP - CMP kinase induction gel

spectrophotometric assay is in good agreement with the $[\gamma\text{-}^{32}\text{P}]\text{-ATP}$ phosphate transfer assay. The spectrophotometric assay was subsequently used for all 6xHis-HdCK activity determinations.

3.3.3 Growth and induction of human GST - UMP - CMP kinase

Induction level of human GST - UMP - CMP kinase in *E. coli* Turner (DE3) pLysS strain was assessed by SDS-PAGE. A representative gel comparing total cell protein before induction and 12 h after induction is shown in Figure 3.4 and reveals an induced band of 47 kDa. Average yield was 3.4 g of wet cell paste per L of culture.

3.3.4 Purification and activity assays of human GST - UMP - CMP kinase

Although the induction of human GST - UMP - CMP kinase in *E. coli* Turner (DE3) pLysS strain is good, the amount of protein isolated was typically 10 mg per 10 g of cell paste. A typical purification gel for human GST - UMP - CMP kinases is shown in Figure 3.5. As seen in Lane 3, a significant amount of the desired protein (MW 47 kDa) is present in the flow-through of the column. Several approaches were tested for their effectiveness to enhance binding of human GST - UMP - CMP kinase to Glutathione Sepharose. Supernatant from 5 g of induced, cracked cells was prepared as described in Section 3.2 and incubated with 5 mL

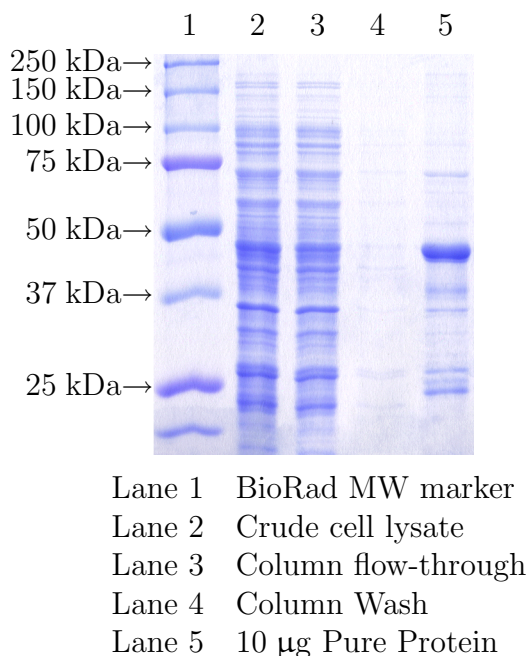


Figure 3.5: Human GST - UMP - CMP kinase purification gel

of Glutathione Sepharose at 4 °C for 45 min with continuous agitation. The flow-through was examined for human GST - UMP - CMP kinase content by SDS-PAGE. No improvement in binding was achieved as judged by SDS-PAGE. Similarly, addition of 10 mM DTT to the purification buffer or the increase in purification buffer pH from 7.3 to 8.0 resulted in no detectable improvement in binding as judged by SDS-PAGE. The final protein is ~85% pure, and is shown in Figure 3.5 Lane 5. The original report of van Rompay *et al.*²³ does not discuss any difficulties with binding, and no SDS-PAGE analysis of the purified protein is reported. The S.A. of protein shown in Figure 3.5 Lane 5 was measured to be $4.8 \mu\text{mol} \cdot \text{mg}^{-1} \cdot \text{min}^{-1}$ by the $[\gamma\text{-}^{32}\text{P}]\text{-ATP}$ phosphate transfer assay. This value is on the high end of the published range of $2.1\text{--}4.8 \mu\text{mol} \cdot \text{mg}^{-1} \cdot \text{min}^{-1}$.²³

3.3.5 Formation of nucleoside monophosphates

Reaction conditions described in Section 3.2.8 resulted in quantitative conversion of nucleosides to the corresponding monophosphates as assessed by UV/Vis absorption after anion exchange purification. A typical column elution profile is shown in Figure 3.6. In this particular case, fractions 2 through 5 contain $\alpha\text{-}[1'\text{-}^2\text{H}]\text{-dFdC}$ which is not phosphorylated by HdCK. Fractions 41 through 50 contain ADP. Fractions 31 through 36 eluted at 0.2 M TEAB concentration, which is characteristic of nucleoside monophosphates, and exhibited an $A_{260\text{ nm}}/A_{280\text{ nm}}$ ratio characteristic of cytidine-derived nucleotides. They correspond to $\beta\text{-}[1'\text{-}^2\text{H}]\text{-dFdCMP}$.

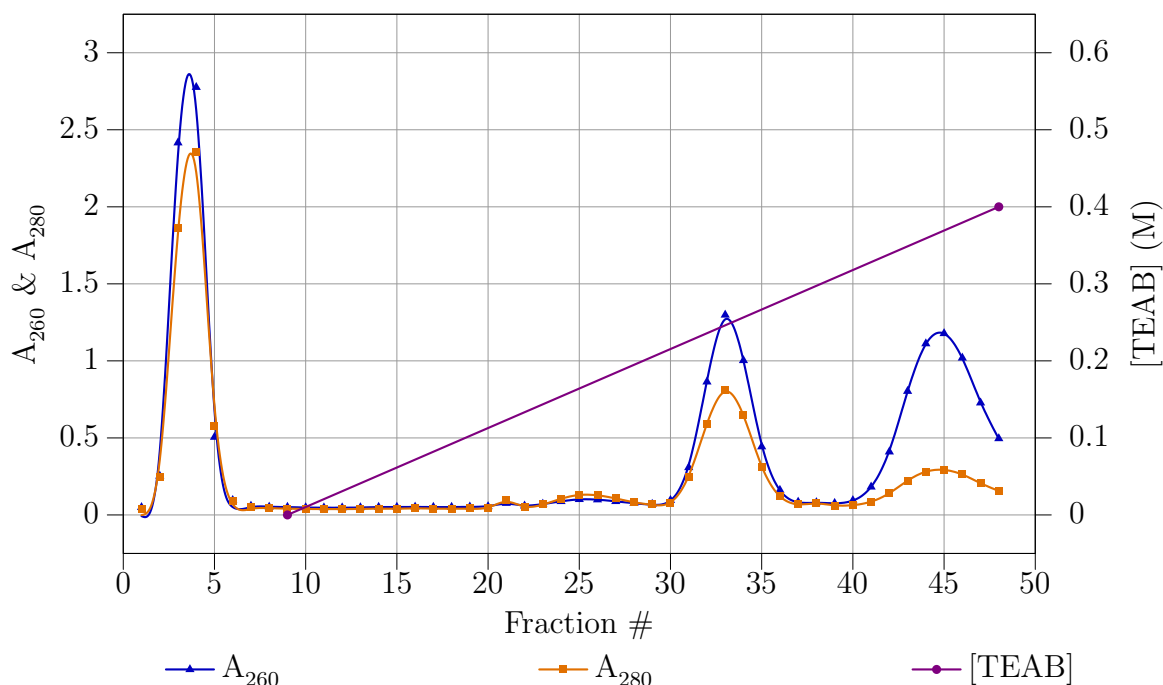


Figure 3.6: Purification of dFdCMP

3.3.6 Formation of nucleoside diphosphates

The conversion of monophosphates to diphosphates in the presence of human GST-UMP-CMP kinase was achieved in 75–85% yield under condition described in Section 3.2.9. Purification of CDP was straightforward, and was achieved with two successive anion exchange chromatographic steps as described below. In the particular case of dFdCDP, anion exchange methods proved ineffective. dFdCDP co-eluted with ADP at pH 7.0 to pH 7.5 regardless of the size of the column and gradient used. Furthermore, FPLC chromatography on POROS HQ resin using a gradient of TEAB also resulted in the co-elution of the two compounds. Therefore, an alternative procedure for isolating deoxynucleoside diphosphates and deoxynucleoside analog diphosphates was developed.

3.3.7 Purification of dCDP, dUDP, and their 2'-analogs after enzymatic diphosphorylation

After enzymatic diphosphorylation, a mixture of the desired deoxynucleotide diphosphate and ADP was isolated by gravity anion exchange chromatography. A typical column elution profile is shown in Figure 3.7. In this particular case, fractions 23 through 27 contained a mixture of AMP and unphosphorylated [1'-²H]-dFdCMP. Fractions 39 through 47 contained ATP. Fractions 31 through 38 eluted at 0.4 M TEAB concentration characteristic of

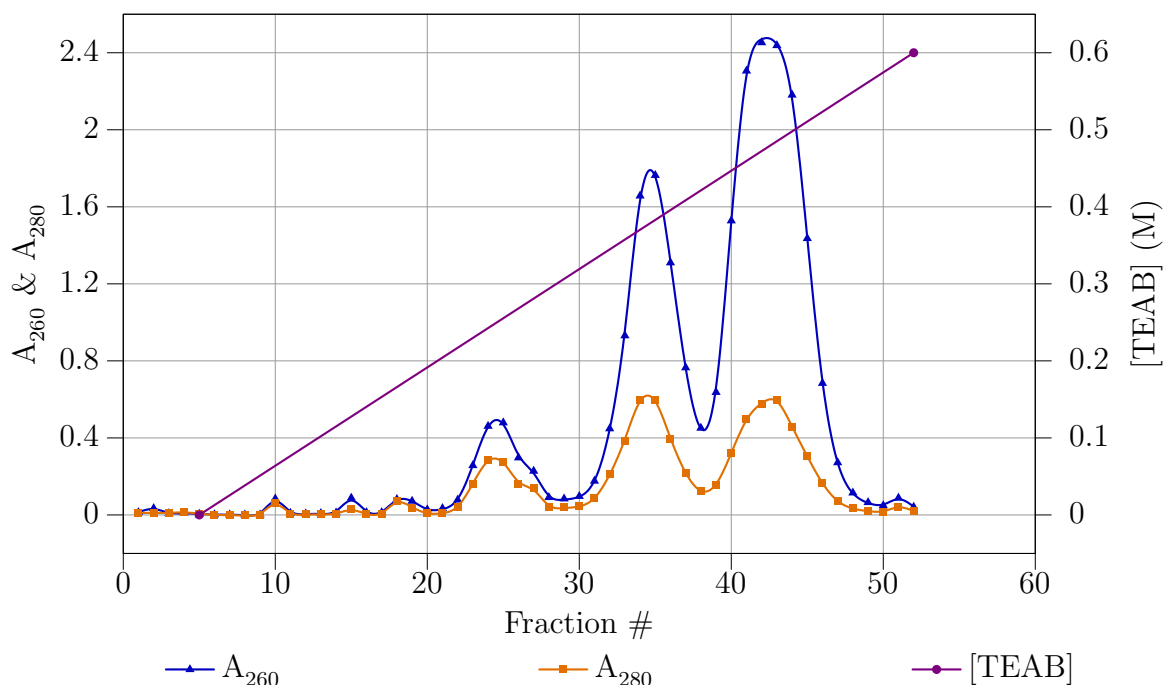


Figure 3.7: First purification of dFdCDP

diphosphate species. They correspond to a mixture of $[1' - ^2\text{H}]$ -dFdCDP and ADP.

Deoxynucleoside diphosphates were purified from the mixture with ADP by oxidative cleavage of ADP with periodate followed by pyrophosphatase treatment to convert liberated pyrophosphate into inorganic phosphate. A final anion exchange column was then run to isolate the desired deoxynucleoside diphosphate. A typical column elution profile is shown in Figure 3.8. In this specific case, eluting in fractions 40 through 46 at 0.4 M TEAB concentration is $[1' - ^2\text{H}]$ -dFdCDP with an $A_{260 \text{ nm}}/A_{280 \text{ nm}}$ ratio characteristic of cytidine-derived nucleotides. Eluting in fractions 4 through 9 is adenine, a byproduct of oxidative cleavage. Fractions 40 through 46 were pooled and excess TEAB was removed as described above. The product was obtained in 83% yield as judged by UV/Vis absorption (λ_{max} 271 nm, λ_{min} 249 nm). It was not characterized further.

3.3.8 Purification of CDP after enzymatic diphosphorylation

Purification of CDP from ADP was achieved by two successive anion exchange chromatographic steps. For a 5 μmol synthesis, a typical first DEAE column (20 mL, 1.5 \times 11.5 cm) was run using a 220 \times 220 mL linear gradient of 5 mM to 0.6 M TEAB. The first chromatographic step allowed the removal of 90% of ADP. Specifically in Figure 3.9, fractions 31 through 36 contained residual $[4' - ^2\text{H}]$ -CMP; fractions 47 through 53 contained $[4' - ^2\text{H}]$ -CDP; while fractions 54 through 62 contained ADP and fractions 65 through 80 contained

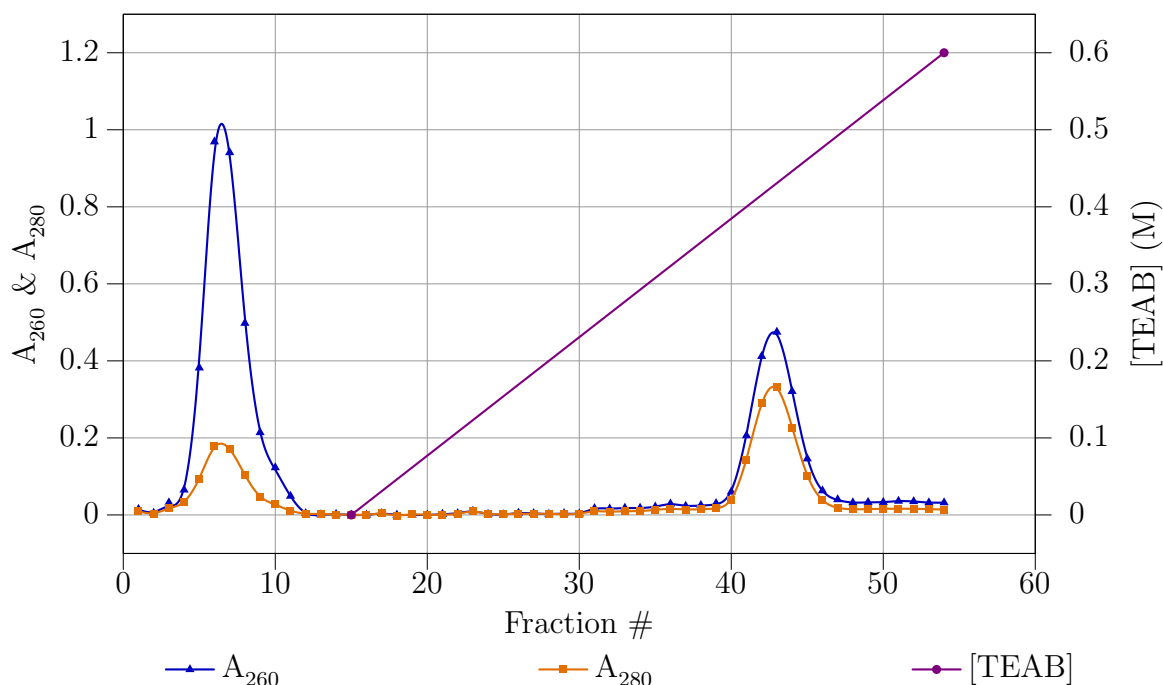


Figure 3.8: Second purification of dFdCDP

ATP. Fractions 47 through 53 were pooled and concentrated *in vacuo* from a mixture of ethanol and water 6 times to remove excess TEAB. A second DEAE column was then run exactly as above to remove residual ADP. The elution profile of the second column is shown in Figure 3.10. Trace ATP eluted in fractions 56 through 64. Fractions 48 through 55 had an $A_{260\text{ nm}}/A_{280\text{ nm}}$ ratio characteristic of cytidine-derived nucleotides and correspond to $[4' - ^2\text{H}] - \text{CDP}$. These fractions were pooled and concentrated *in vacuo*. Excess TEAB was removed under reduced pressure by rotovapping 6 times from a mixture of water and ethanol.

3.4 Discussion

Chemical phosphorylation of nucleosides in a specific position without reversible protection of other functional groups remains a challenge. Using human dCK (HdCK) and human UMP-CMP kinase, a high-yielding enzymatic method for the 5'-phosphorylation of cytidine, 2'-deoxycytidine, 2'-deoxyuridine and their analogs was developed. For this purpose, overexpression and purification of 6xHis-HdCK were optimized.²² The enzyme can now be purified to ~95% homogeneity in high yields. A spectrophotometric assay for determining its activity was developed. It represents a significant improvement over the previously utilized $[\gamma - ^{32}\text{P}] - \text{ATP}$ phosphate transfer assay in the ease of handling and time required to

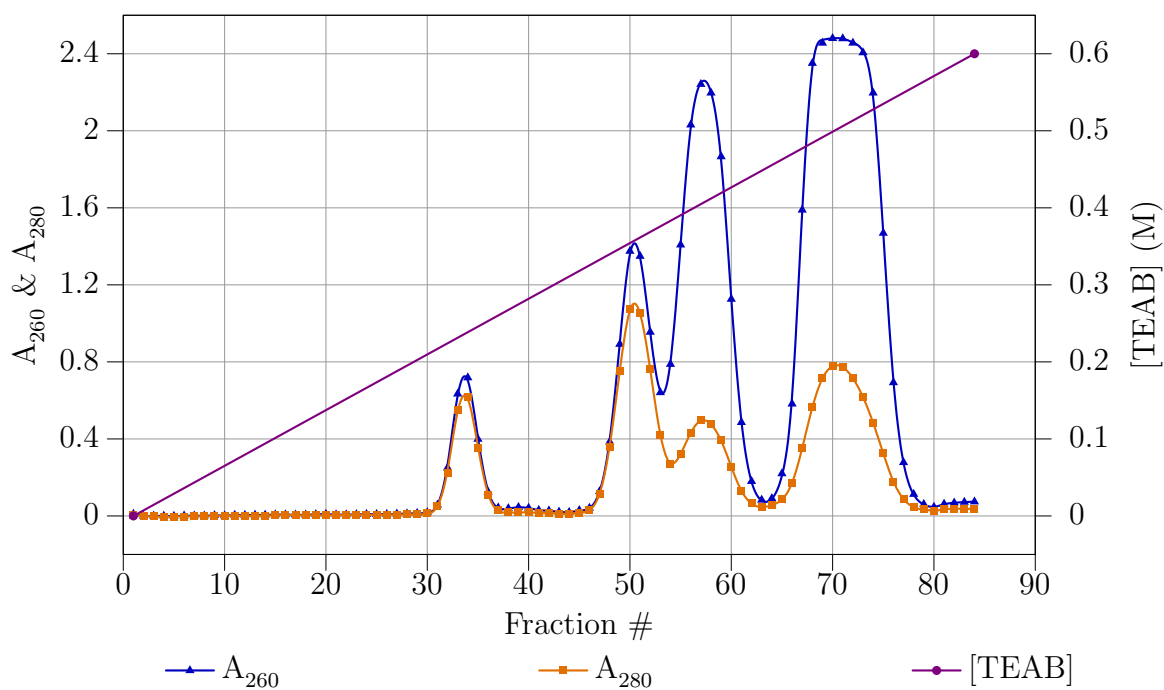


Figure 3.9: First purification of CDP

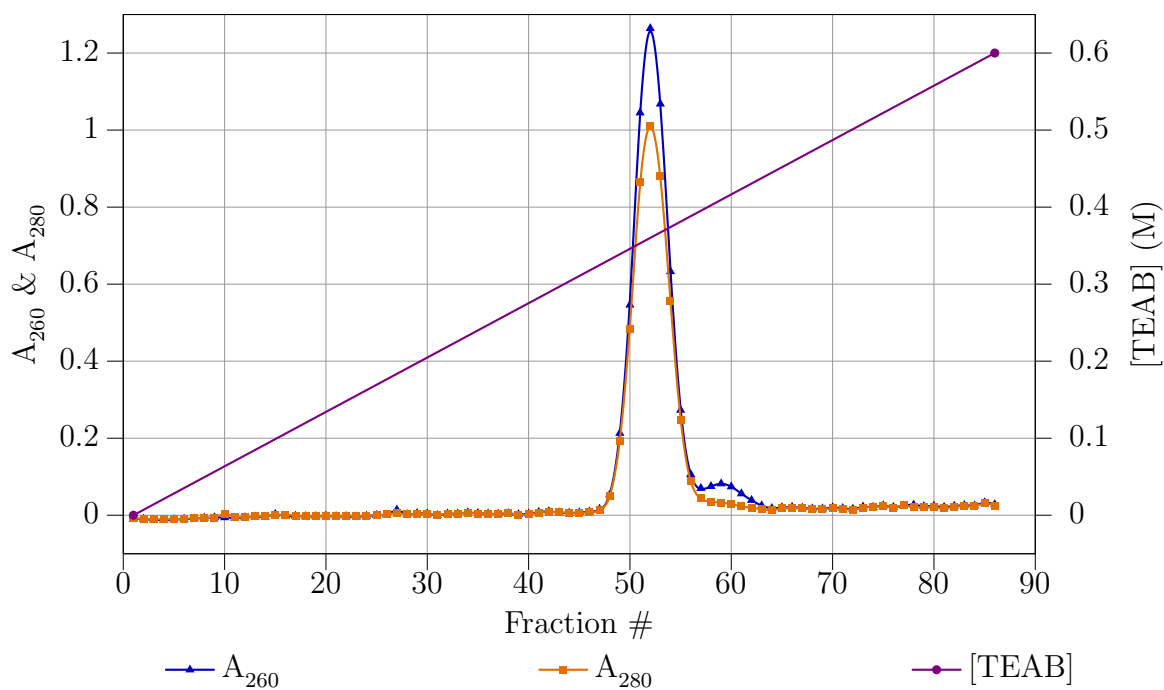


Figure 3.10: Second purification of CDP

<i>Starting Material</i>	<i>Product</i>	<i>Yield</i>	<i>Characterization</i>
dFdC (dC)	dFdCDP	78%	Section 5.2.6
C	CDP	83%	Section 4.2.6
N ₃ C (dC)	N ₃ CDP	83%	Appendix A
N ₃ U (dU)	N ₃ UDP	75%	Appendix A

Table 3.1: Summary of yields and characterization of compounds made by the enzymatic method

perform an assay, making activity assessment during purification feasible. Under optimized conditions, 5'-monophosphates of C, dC, dU, dFdC and 2'-azido-2'-deoxycytidine were obtained in quantitative yield as determined by UV/Vis absorption after anion exchange purification.

For the conversion of monophosphates of C, dC analogs (such as dFdC and 2'-azido-2'-deoxycytidine) and dU analogs (such as 2'-azido-2'-deoxyuridine) to the corresponding diphosphates, GST-tagged human UMP-CMP kinase was employed.²³ Problems with binding of this enzyme to Glutathione Sepharose resin were encountered. Batch absorption technique, addition of DTT to the purification buffer, or the increase in purification buffer pH from 7.3 to 8.0 did not result in detectable improvements in binding as judged by SDS-PAGE. Recently, Liou *et al.* have cloned human UMP-CMP kinase as a his-tagged fusion protein and measured its *in vitro* S.A. with CMP as substrate to be $350 \mu\text{mol} \cdot \text{mg}^{-1} \cdot \text{min}^{-1}$.²⁶ This activity is much higher than the V_{max} reported by van Rompay *et al.*²³ The considerable difference may be attributable to the fact that the protein used by van Rompay *et al.* was fused to the large GST protein. Removal of the GST tag and recloning of the UMP-CMP kinase into a vector for expression with an N-terminal hexa-histidine tag is recommended. By this procedure, diphosphates could be obtained in high yield as summarized in Table 3.1.

Using human GST-UMP-CMP kinase, CDP was obtained in 83–85% yield after two anion exchange chromatographic steps. For the purification of deoxynucleoside diphosphates, a method which makes use of periodate to remove ADP was developed. dCDP, dUDP, dFdCDP and N₃CDP were obtained in 75–80% yield. The method is amenable to nmol scale reactions and thus makes feasible the phosphorylation of small amounts of isotopically-labeled derivatives.

Bibliography

- [1] M. Vaghefi, ed., *Nucleoside Triphosphates and their Analogs*. CRC Press, Taylor and Francis Group, 2005.
- [2] M. Yoshikawa, T. Kato, and T. Takenishi, "A novel method for phosphorylation of nucleosides to 5'-nucleotides," *Tetrahedron Letters*, no. 50, pp. 5065–5068, 1967.
- [3] J. Ludwig, "A new route to nucleoside 5'-triphosphates," *Acta Biochimica et Biophysica Academiae Scientiarum Hungaricae*, vol. 16, no. 3-4, pp. 131–133, 1981.

- [4] J. L. Ruth and Y. C. Cheng, "Nucleoside analogs with clinical potential in antiviral chemotherapy. The effect of several thymidine and 2'-deoxycytidine analog 5'-triphosphates on purified human (a, b) and herpes simplex virus (types 1, 2) DNA polymerases," *Molecular Pharmacology*, vol. 20, no. 2, pp. 415–422, 1981.
- [5] W. H. Dawson, R. L. Cargill, and R. B. Dunlap, "The phosphorylation of unprotected nucleosides. Nonselectivity of phosphorus oxychloride in trialkylphosphate," *Journal of Carbohydrates, Nucleosides, Nucleotides*, vol. 4, no. 6, pp. 363–375, 1977.
- [6] J. Ludwig and F. Eckstein, "Rapid and efficient synthesis of nucleoside 5'-O-(1-thiotriphosphates), 5'-triphosphates and 2',3'-cyclophosphorothioates using 2-chloro-4H-1,3,2-benzodioxaphosphorin-4-one," *Journal of Organic Chemistry*, vol. 54, no. 3, pp. 631–635, 1989.
- [7] M. Smith and H. G. Khorana, "Nucleoside polyphosphates. VI. An improved and general method for the synthesis of ribo- and deoxyribonucleoside 5'-triphosphates," *Journal of the American Chemical Society*, vol. 80, pp. 1141–1145, 1958.
- [8] G. Weimann and H. G. Khorana, "Polynucleotides. XVII. The mechanism of internucleotide bond synthesis by the carbodiimide method," *Journal of the American Chemical Society*, vol. 84, pp. 4329–4341, 1962.
- [9] J. G. Moffatt and H. G. Khorana, "Nucleoside polyphosphates. X. The synthesis and some reactions of nucleoside 5'-phosphoromorpholidates and related compounds. Improved methods for the preparation of nucleoside 5'-polyphosphates," *Journal of the American Chemical Society*, vol. 83, pp. 649–658, 1961.
- [10] H. A. Staab, "Reactive N-carboxylic acid esters and N-carboxamides of imidazole and triazole," *Liebigs Annalen der Chemie*, vol. 609, pp. 83–88, 1957.
- [11] L. Goldman, J. W. Marsico, and G. W. Anderson, "The preparation of adenosine-5' imidazol-1-ylphosphonate and its reactions with nucleophiles. A novel synthesis of nucleotide coenzymes," *Journal of the American Chemical Society*, vol. 82, pp. 2969–2970, 1960.
- [12] F. Cramer and H. Neunhoeffer, "Chemistry of high-energy phosphates. XV. Reactions of adenosine 5'-phosphoric acid imidazolide – a new synthesis of adenosine diphosphate and flavine adenine dinucleotide," *Chemische Berichte*, vol. 95, pp. 1664–1669, 1962.
- [13] D. E. Hoard and D. G. Ott, "Conversion of mono- and oligodeoxyribonucleotides to 5'-triphosphates," *Journal of the American Chemical Society*, vol. 87, no. 8, pp. 1785–1788, 1965.
- [14] J. W. Kozarich, A. C. Chinault, and S. M. Hecht, "Ribonucleoside phosphates via phosphorimidazolide intermediates. Synthesis of pseudoadenosine 5'-triphosphate," *Biochemistry*, vol. 12, no. 22, pp. 4458–4463, 1973.
- [15] M. Maeda, A. D. Patel, and A. Hampton, "Formation of ribonucleotide 2',3'-cyclic carbonates during conversion of ribonucleoside 5'-phosphates to diphosphates and triphosphates by the phosphorimidazolide procedure," *Nucleic Acids Research*, vol. 4, no. 8, pp. 2843–2853, 1977.
- [16] V. M. Dixit and C. D. Poulter, "Convenient syntheses of adenosine 5'-diphosphate, adenosine 5'-methylenediphosphonate, and adenosine 5'-triphosphate," *Tetrahedron Letters*, vol. 25, no. 37, pp. 4055–4058, 1984.
- [17] V. J. Davisson, D. R. Davis, V. M. Dixit, and C. D. Poulter, "Synthesis of nucleotide 5'-diphosphates from 5'-O-tosyl nucleosides," *Journal of Organic Chemistry*, vol. 52, no. 9, pp. 1794–1801, 1987.
- [18] J. Bao, G. A. Bruque, and D. D. Y. Ryu, "Biosynthesis of deoxynucleoside triphosphates, dCTP and dTTP: reaction mechanism and kinetics," *Enzyme and Microbial Technology*, vol. 36, no. 2-3, pp. 350–356, 2005.

-
- [19] B. Munch-Petersen, J. Piskur, and L. Sondergaard, "Four deoxynucleoside kinase activities from *Drosophila melanogaster* are contained within a single monomeric enzyme, a new multifunctional deoxynucleoside kinase," *Journal of Biological Chemistry*, vol. 273, no. 7, pp. 3926–3931, 1998.
- [20] S. Eriksson, B. Munch-Petersen, K. Johansson, and H. Eklund, "Structure and function of cellular deoxyribonucleoside kinases," *Cellular and Molecular Life Sciences*, vol. 59, no. 8, pp. 1327–1346, 2002.
- [21] A. Loos. Unpublished results.
- [22] E. V. Usova and S. Eriksson, "The effects of high salt concentrations on the regulation of the substrate specificity of human recombinant deoxycytidine kinase," *European Journal of Biochemistry*, vol. 248, no. 3, pp. 762–766, 1997.
- [23] A. R. Van Rompay, M. Johansson, and A. Karlsson, "Phosphorylation of deoxycytidine analog monophosphates by UMP-CMP kinase: molecular characterization of the human enzyme," *Molecular Pharmacology*, vol. 56, no. 3, pp. 562–569, 1999.
- [24] J. Sambrook, E. F. Fritsch, and T. Maniatis, *Molecular Cloning: A Laboratory Manual*. Cold Spring Harbor Laboratory Press, 1989.
- [25] W. E. O'Brien, "A continuous spectrophotometric assay for argininosuccinate synthetase based on pyrophosphate formation," *Analytical Biochemistry*, vol. 76, no. 2, pp. 423–430, 1976.
- [26] J.-Y. Liou, G. E. Dutschman, W. Lam, Z. Jiang, and Y.-C. Cheng, "Characterization of human UMP/CMP kinase and its phosphorylation of D- and L-form deoxycytidine analogue monophosphate," *Cancer Research*, vol. 62, no. 6, pp. 1624–1631, 2002.

Chapter 4

Effect of removing the general acid/base catalyst E441 from the RNR reaction: evidence for the formation of an α,β -unsaturated 2'-ketyl radical anion

4.1 Introduction

The mechanism of ribonucleotide reduction catalyzed by ribonucleotide reductases (RNRs) has been studied for more than two decades using biochemical, chemical, and structural probes. These studies have led to the mechanistic model shown in Figure 4.1, in which the role of E441 is to act as a general acid-base catalyst.

E441 is proposed to act as a general base catalyst that removes the proton from the 3'-hydroxyl group concomitantly with the formation of a putative 2'-ketyl radical and loss of the 2'-hydroxyl group as water (Figure 4.1, conversion of 1 to 2).¹ Formation of the 2'-ketyl radical (Figure 4.1, 2) was proposed by Stubbe based on model studies on rearrangements occurring during ethylene glycol oxidation.² Chemical precedent, along with evidence accumulated over the years for the steps surrounding the generation of the putative 2'-ketyl radical, strongly suggest that this species is an intermediate on the nucleotide reduction pathway. However, direct evidence for this radical has never been obtained. Depending on the timing of water loss from the 2'-position relative to the deprotonation of the 3'-hydroxyl by E441, the putative 2'-ketyl radical can be generated from a radical anion, a radical cation, or through a concerted process. The mechanism of its generation remains an unresolved issue.

E441 is proposed to act as a general acid catalyst in the reduction of the 2'-deoxy-3'-ketonucleotide by the disulfide radical anion (Figure 4.1, conversion of 3 to 4). This is thermodynamically the most difficult step in the nucleotide reduction process, and requires

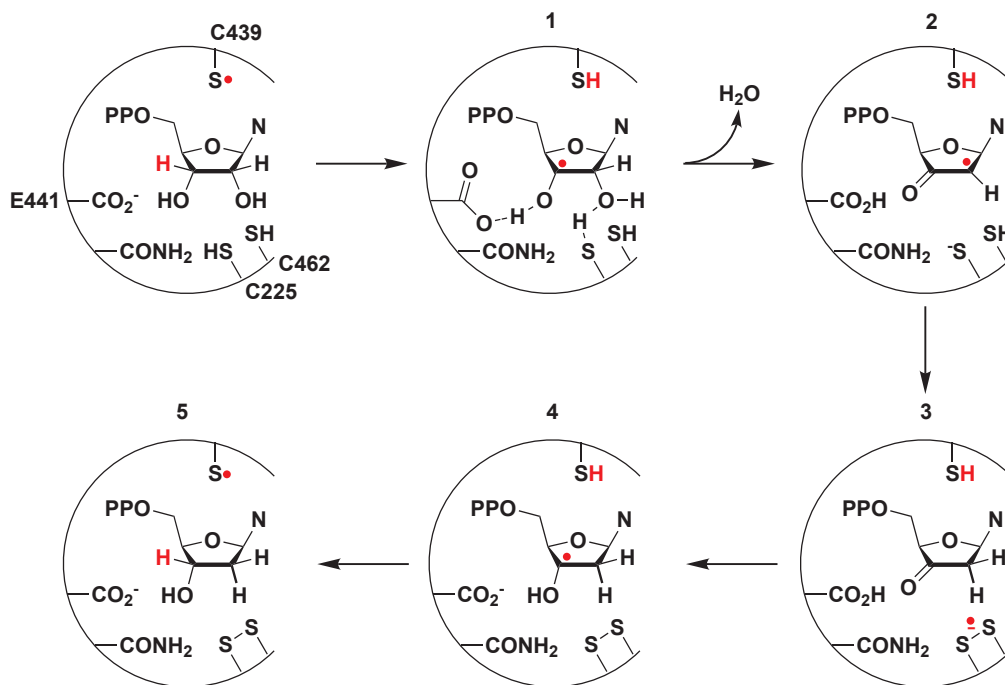


Figure 4.1: Mechanistic model for the reaction catalyzed by RNR

that the ketone is protonated concomitantly with electron transfer.¹

The potential roles of the E441 residue in both the chemistry of water loss and ketone reduction provided the impetus for our laboratory and the laboratory of Britt-Marie Sjöberg to make and investigate a glutamate to glutamine mutation of residue 441 in the catalytic subunit of *E. coli* RNR, E441Q-R1. Since the slow chemical step in the conversion of NDPs to dNDPs was proposed to be the reduction of the 2'-deoxy-3'-ketonucleotide by the disulfide radical anion,³⁷ mutation of the glutamate to glutamine was expected to allow buildup of the disulfide radical anion intermediate.

Preliminary studies from the Sjöberg laboratory by Persson *et al.* allowed the detection of two transient intermediates by EPR in the reactions in which E441Q-R1 and wild type R2 were incubated with CDP as substrate, TTP as the effector, and DTT as reductant.³ The first intermediate was detected on a second time-scale (called the 10 s radical). The second intermediate was detected on a minute time-scale (called the 3 min radical). Studies which made use of E441Q-R1 in which all cysteine residues were di-deuterated at the β -position ($[\beta\text{-}^2\text{H}]$ -cysteine E441Q-R1) to generate the radicals and the examination of these radicals by 9 GHz EPR showed a change in the hyperfine structure of the 10 s radical and no change in the hyperfine structure of the 3 min radical, implying that the 10 s radical was cysteine-based.⁴ Based on this result, Persson *et al.* suggested that the 10 s radical was a thyl radical derived from C439 in the active site of R1. Further 9 GHz EPR experiments published by Persson *et al.* in which CDP uniformly labeled with ^{13}C and ^{15}N ($[\text{U-}^{13}\text{C},^{15}\text{N}]$ -CDP)

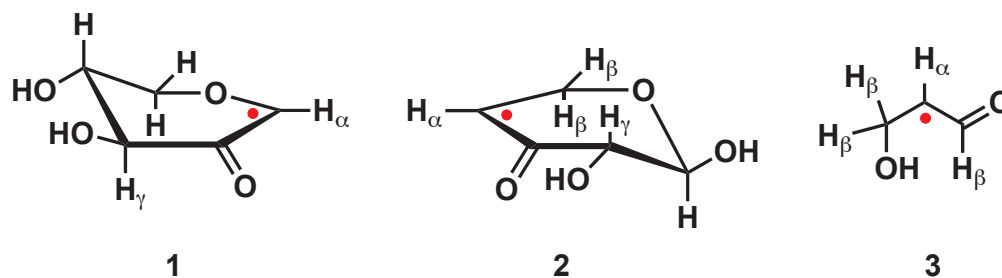


Figure 4.2: Structures of model ketyl radicals

Model	g_{av}	H_{α}	H_{β}	H_{γ}
1	2.0049	13.7	–	2.3
2	2.0044	17.7	36.5 & 29.4	2.8
3	2.0043	18.1	25.6(2) 1.4(1)	–

Table 4.1: g_{av} and hyperfine coupling constant in G for model ketyl radicals in Figure 4.2^{6,7}

was used revealed a broadening of the 3 min radical EPR spectrum and no change in the spectrum of the 10 s radical. These results suggested that the 3 min radical was nucleotide-based. Persson *et al.* proposed that this radical is a 3'-nucleotide radical (1 in Figure 4.1).

In addition, Persson *et al.* analyzed the end products of the reaction of E441Q-R1 with R2, CDP, TTP, and DTT.³ The analysis revealed that cytosine was released in the reaction, and that R1 was alkylated by 2-methylene-3-2*H*-furanone. These results strongly suggest that 2'-deoxy-3'-ketonucleotide (3, Figure 4.1) is formed in the reaction, and that it decomposes to lose base and inorganic pyrophosphate as discussed in Chapter 1 (Figure 1.5).

Subsequent studies by Lawrence *et al.*⁵ which made use of pulsed, high-field EPR techniques facilitated deconvolution of the spectra of the three radicals. The studies revealed that the cysteine based radical was a disulfide radical anion. The assignment was based on the comparison of the observed g -values with well-characterized model systems and by stopped-flow UV/Vis spectroscopy. Identification of this species gave the first supporting evidence for the proposed mechanism of the one-electron reduction of the putative 2'-ketyl radical (Figure 4.1, 2) and subsequent one-electron reduction of the 3'-keto-2'-deoxynucleotide (Figure 4.1, 3).

Lawrence *et al.*⁵ also reported the first 140 GHz EPR spectrum of the 3 min radical. These measurements revealed unusual g -values characteristic of ketyl radicals, namely, $g_1 = 2.0072$, $g_2 = 2.0061$, $g_3 = 2.0021$. Based on the magnitude of hyperfine interactions with two

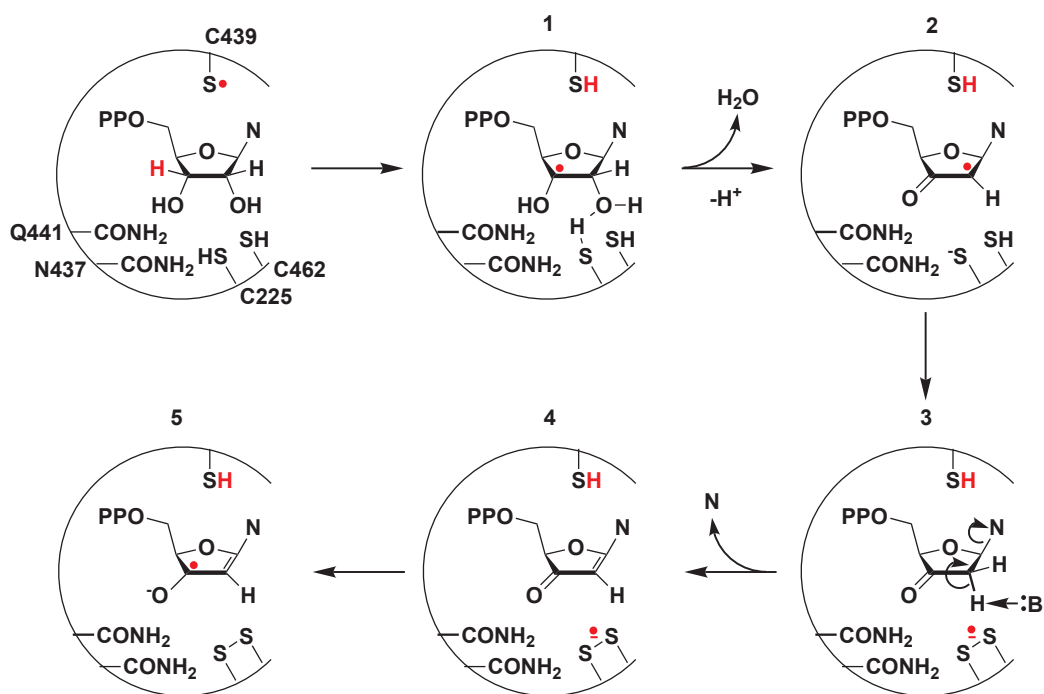


Figure 4.3: Proposed mechanism for the formation of α,β -unsaturated ketyl radical anion in the active site of R1

spin 1/2 nuclei (one of 8.5 G and the other 11.4 G)⁴ and g -values reported in the literature for model ketyl radicals in solution (see Figure 4.2 and Table 4.1), Lawrence *et al.* suggested that the 3 min radical species was a 4'-ketyl radical.

Here we report efforts using isotopically labeled substrate and protein analogs in conjunction with EPR and ENDOR spectroscopy to establish the structure of the 3 min radical. I propose that the 3 min radical is an α,β -unsaturated ketyl radical anion formed by the reduction of enone 4, Figure 4.3 by the disulfide radical anion. If confirmed, this structural assignment would constitute the first evidence for base elimination within the active site of R1, as opposed to in solution, during the course of mechanism-based inhibition. Furthermore, it would show that the disulfide radical anion is able to reduce a nucleotide-based intermediate bound in the active site of R1 when the redox potentials of the disulfide radical anion and the nucleotide-based intermediate are matched.

4.2 Materials and methods

4.2.1 Purchased materials and materials obtained as gifts

Triethylamine (99% pure) was purchased from Acros, N-(2-hydroxyethyl)piperazine-N'-(2-ethanesulfonic acid) (HEPES) from US Biochemicals, and 1,4-dithiothreitol (DTT) from Mallinckrodt. DEAE Sephadex A-25 was purchased from Pharmacia, and Dowex AG 1 × 8 from Bio-Rad. Tyrosine 99% dideuterated at the C-β position was obtained from Cambridge Isotope Laboratories; analysis of this material by ¹H-NMR revealed the absence of resonances due to β-protons. All other materials were purchased from Sigma.

[1'-²H]-cytidine was available from the Stubbe laboratory freezer stock (¹H NMR (²H₂O) δ 3.74–3.92 (dd × dd, *J* = 3.05, 12.66, 4.27, 12.81 Hz, 2H), 4.09 (m, 1H), 4.16 (t, *J* = 4.70 Hz, 1H), 4.26 (d, *J* = 5.8 Hz, 1H), 5.85 (d, *J* = 3.7 Hz, 0.15H), 6.00 (d, *J* = 7.63 Hz, 1H), 7.79 (d, *J* = 7.63 Hz, 1H); 85% ²H-atom incorporation at the 1'-position by NMR integration). [4'-²H]-cytidine (¹H NMR (DMSO-*d*₆) δ 3.52 (dd, *J* = 5.2, 12.1 Hz, 1H), 3.64 (dd, *J* = 5.2, 12.1 Hz, 1H), 3.92–3.94 (m, 2H), 4.96 (d, *J* = 4.5 Hz, 1H), 5.03 (t, *J* = 5.1 Hz, 1H), 5.27 (d, *J* = 4.7 Hz, 1H), 5.70 (d, *J* = 7.4 Hz, 1H), 5.76 (d, *J* = 3.7 Hz, 1H), 7.12 (br d, *J* = 6.2 Hz, 2H), 7.84 (d, *J* = 7.4 Hz, 1H; < 97% ²H-atom incorporation at the 4'-position by NMR integration) and [5'-²H]-CDP (¹H NMR (²H₂O) δ 4.02 (dd, *J* = 2.6, 5.5 Hz, 0.5H), 4.07–4.12 (m, 1.5H), 4.16 (t, *J* = 4.7 Hz, 1H), 4.21 (t, *J* = 5.0 Hz, 1H), 5.82 (d, *J* = 4.2 Hz, 1H), 6.00 (d, *J* = 7.6 Hz, 1H), 7.88 (d, *J* = 7.6 Hz, 1H); ³¹P NMR (²H₂O) δ -10.18 (d, *J* = 20.4 Hz, 1P), -9.44 (d, *J* = 20.0 Hz, 1P); < 97% ²H-atom incorporation nonstereospecifically at the 5'-position by NMR integration) were gifts from Stanislaw Wnuk's laboratory at the Florida International University. [U-¹⁵N]-CDP and [U-¹³C, U-¹⁵N]-CDP were gifts from the Schwalbe laboratory at MIT.

4.2.2 Protein overexpression, purification, and activity assays

Overexpression of unlabeled *E. coli* E441Q-R1

All cultures were grown in the presence of 50 μg/mL kanamycin and 50 μg/mL ampicillin. *E. coli* K38 pGP1-2 pMJ1 strain⁸ was plated from a glycerol stock onto LB plates and grown overnight at 30 °C. Single colonies were used the next day to inoculate two 100 mL overnight starter cultures in LB. The overnight cultures were spun down at 3000 rpm for 0.5 h and the pellet resuspended in 10 mL of LB. The entire resuspension was used to inoculate 6 L of LB in the New Brunswick Scientific 10 L fermentor, model MF-118 at 30 °C. Temperature of the culture was monitored by a thermocouple built into the fermentor unit, and independently, by a separate temperature probe to verify the readout from the fermentor. The culture was grown with constant stirring at 500 rpm and with an air flow of 15000 cc per min. When OD₆₀₀ reached 1, 2.4 L of 90 °C LB were added to the fermentor over a period of 5 min. The temperature was adjusted to 42 °C, and the culture incubated at this temperature for 0.5 h. The temperature was then lowered to 37 °C for 3 additional h. Cells were harvested by centrifugation at 10000 rpm, frozen in liquid N₂, and stored at -80 °C overnight.

<i>Amino Acid</i>	g/L	<i>Amino Acid</i>	g/L
Ala	0.5	Lys	0.4
Arg	0.5	Met	0.25
Cys	0.1	Phe	0.15
Glu	0.7	Pro	0.15
Gly	0.6	Ser	2.1
His	0.15	Thr	0.25
Ile	0.25	Val	0.3
Leu	0.25		

Table 4.2: Amino acid composition of the minimal medium

Overexpression of *E. coli* E441Q-R1 in the presence of [β - ^2H] - tyrosine

Expression of E441Q-R1 deuterium labeled at C- β of tyrosine residues ([β, β' - ^2H] - Y E441Q-R1) was achieved in minimal media using a protocol designed by Dr. Hiep-Hoa Nguyen of Stubbe laboratory for overexpression of R2 on tyrosine derivatives. In a control experiment, growth and induction of *E. coli* K38 pGP1-2 pMJ1 stain were assessed in this media using unlabeled tyrosine.

Initial growth of the *E. coli* K38 pGP1-2 pMJ1 stain was carried out from a glycerol stock as described above for unlabeled E441Q-R1. The pellet from an overnight 100 mL culture was resuspended in 50 mL of minimal medium (see below for composition) and 12 mL of the suspension were used to inoculate a 1 L minimal medium culture in a 6 L flask at 30 °C.

The culture was grown until OD_{600} reached 1.4 at which point 1 g of tyrosine dissolved in a minimal volume of saturated NaCO_3 was added. After a period of 15 min, the flask was transferred to a floor shaker and 400 mL of 90 °C minimal medium were added over the course of 5 min while maintaining constant stirring. When the temperature of the culture reached 42 °C as measured by a thermometer sterilized in ethanol, the flask was moved to a 42 °C shaker and incubated at this temperature for 0.5 h. The temperature was then lowered to 37 °C, and the culture grown for 4 additional h. Doubling time in this medium was 1 h and 40 min. Cells were harvested at 10000 rpm, frozen in liquid N_2 , and stored at -80 °C. Final yield was 4.5 g of cell paste per L of culture.

Components of the minimal medium and their final concentrations are listed in Table 4.2, Table 4.3, and Table 4.4. A solution of salt free amino acids was prepared at a 4x concentration and sterilized by filtration through a 0.22 μm filter. Solutions of other salts and nitrogenous bases were prepared at a 4x concentration and sterilized by autoclaving. MgSO_4 solution was prepared separately at a 4x concentration to avoid precipitation of MgHPO_4 . Thiamine and biotin were added directly to the medium as solids. Additionally, 1 mL of Vogel-Bonner salt solution was added per L of culture. Vogel-Bonner solution contains 3.3 g of $\text{FeCl}_3 \times 6\text{H}_2\text{O}$, 18 mg of $\text{ZnSO}_4 \times 7\text{H}_2\text{O}$, 16 mg of $\text{CuSO}_4 \times 6\text{H}_2\text{O}$, 18 mg of $\text{CoCl}_2 \times 6\text{H}_2\text{O}$, and 3.8 g of $\text{Na}_2\text{EDTA} \times 2\text{H}_2\text{O}$ per 100 mL of dH_2O .

<i>Base</i>	g/L
Adenine	0.5
Guanine	0.3
Cytosine	0.7
Uracil	0.5
Thymine	0.3

Table 4.3: Nitrogenous base composition of the minimal medium

<i>Component</i>	<i>per L</i>	<i>Component</i>	<i>per L</i>
(NH ₄)SO ₄	2.0 g	Glycerol	40 g
KH ₂ PO ₄	1.6 g	Sodium Citrate	0.5 g
MgSO ₄ × 7H ₂ O	1.0 g	Na ₂ PO ₄ × 7H ₂ O	10 g
Thiamine	25 mg	Biotin	5 mg

Table 4.4: Other components of the minimal medium

Purification of E441Q-R1 and wild type R2

Unlabeled *E. coli* E441Q-R1 and [β -²H]-Y *E. coli* E441Q-R1 were purified as previously described for wild type R1⁹ except that fractions collected from the DEAE column were assayed for E441Q-R1 content by 10% SDS-PAGE. With E441Q-R1, it is not possible to use the standard RNR spectrophotometric coupled assay because of the inability of this mutant to support turnover. E441Q-R1 concentration was determined using $\epsilon_{280nm} = 189 \text{ mM}^{-1}\text{cm}^{-1}$. The protein was characterized by SDS-PAGE. All R1 concentrations are reported per dimer.

Wild type *E. coli* R2 was isolated as previously described¹⁰ and had specific activity (S.A.) of 6000–7000 nmol · mg⁻¹ · min⁻¹. R2 concentration was determined using $\epsilon_{280nm} = 130.5 \text{ mM}^{-1} \cdot \text{cm}^{-1}$. Tyrosyl radical content was assessed both by the drop-line correction method and by EPR as previously reported.¹¹ R2 contained 1.1–1.2 Y · per dimer based on both methods of quantification. All R2 concentrations are reported per dimer.

Tryptic digest of *E. coli* E441Q-R1

The procedure was performed on 15 nmol of unlabeled or [β -²H]-Y E441Q-R1. The protein (typically 215–250 μL of a 60–70 μM solution) was mixed with 5 volumes of denaturing buffer (0.4 M TRIS pH 8.0, 6M GuHCl, 15 mM MgSO₄, 1 mM EDTA). DTT solution (1 M, prepared in denaturing buffer) was added to a final concentration of 10 mM and the mixture was degassed on a Schlenk line. The mixture was allowed to stand at RT for 30 min. Iodoacetamide dissolved in a minimal volume of denaturing buffer was added to a final concentration of 0.1 M and the mixture allowed to stand in the dark at RT for 3 h. β -ME was then added at a final concentration of 0.2 M (two equivalents relative to iodoacetamide),

the solution incubated at RT for 10 min, and then dialyzed against $2 \times 2\text{L}$ of water over a period of 17 h. The dialyzed mixture was lyophilized over 24 h.

Protein powder obtained by lyophilization was dissolved in 460 μL of 0.1 M ammonium carbonate pH 8.0, and 43 μg of TPCK treated trypsin (Sigma) were added (1:60 mass ratio of trypsin to $[\beta\text{-}^2\text{H}]\text{-Y E441Q-R1}$). The mixture was placed at 37 $^\circ\text{C}$ for 30 h and subsequently lyophilized overnight.¹²

Analysis of the tryptic digest was performed by HPLC. The peptides were partially resolved using a Jupiter C-18 column from Phenomenex ($150 \times 4.6\text{ mm}$, 5 micron, 300 \AA pore size) at 1 mL/min flow rate with the following gradient:

- 0–5 min 100% dH_2O , 0.1% TFA
- 5–7 min 0→10% MeCN, 0.1% TFA
- 7–75 min 10→50% MeCN, 0.1% TFA

Fractions of 450 μL were collected during the runs and lyophilized or placed on the speed-vac overnight. Fractions corresponding to elution times with high $A_{280\text{ nm}}$ were analyzed by MALDI-TOF at the Chemistry Department Instrumentation Facility and by ESI mass spectrometry at the Harvard Microchemistry and Proteomics Facility.

4.2.3 Tyrosyl radical loss on R2

In the reaction of E441Q-R1 and wild type R2 with substrate and effector, tyrosyl radical loss was monitored as a function of time at 410 nm on a Cary 3 spectrophotometer in a 1 cm path length quartz cuvette equilibrated at 25 $^\circ\text{C}$. The reaction mixtures contained in a final volume of 450 μL 0.75 mM TTP, 15 μM pre-reduced E441Q-R1, 15 μM R2, 1 mM CDP, and either 5 mM DTT or no DTT, all in 50 mM HEPES pH 7.6, 15 mM MgSO_4 , 1 mM EDTA. E441Q-R1 was pre-reduced as described previously.¹³

All components of the reaction mixture except for the substrate were equilibrated at 25 $^\circ\text{C}$ for 5 min. The tyrosyl radical spectrum was recorded in the 350–550 nm range before reaction initiation. Reaction was initiated by the addition of CDP followed by rapid mixing by inversion of the cuvette. Loss of $A_{410\text{ nm}}$ was monitored until no further change in $A_{410\text{ nm}}$ was observed (~ 15 min). Another spectrum was then recorded by rescanning the 350–550 nm range.

4.2.4 Synthesis of 5,6-dideuteriocytidine

5,6-dideuteriocytidine was synthesized based on a modified procedure of Rabi *et al.*¹⁴ In this reaction, exchange of the 5 and 6 protons of cytidine is promoted by a reversible addition of base across the 5,6 double bond at elevated temperature.

Cytidine (2 mmol) was exchanged into $^2\text{H}_2\text{O}$ by three evaporations from 5 mL of $^2\text{H}_2\text{O}$. It was then evaporated three times from 5 mL of $\text{DMSO-}d_6$ and the residue was dissolved

in 4.5 mL of DMSO- d_6 . A 2.5 M solution of MeONa in MeOD was prepared by dissolving a small piece of elemental sodium, which was washed with hexane and weighed on an analytical balance, in an appropriate amount of MeOD under argon. The exchange reaction was initiated by the addition of 2.2 mmol of MeONa in MeOD. The mixture was stirred for 17 h at 60 °C and quenched by the addition of dilute hydrochloric acid until the pH dropped to 7.0. Product formation was assessed by ^1H NMR as described by Rabi *et al.*¹⁴ (^1H NMR (DMSO- d_6) δ 3.40–3.70 (m, 2H), 3.80–4.00 (m, 3H), 5.00 (d, $J = 4.5$ Hz, 1H), 5.05 (t, $J = 5.1$ Hz, 1H), 5.30 (d, $J = 4.7$ Hz, 1H), 5.70 (s, 0.17H), 5.75 (d, $J = 7.60$ Hz, 1H), 7.00–7.20 (br d, 2H), 7.82 (s, 0.04H); 83% ^2H incorporation at position 5 and 96% ^2H incorporation at position 6 by NMR integration.)

4.2.5 Synthesis of [2' - ^2H] - cytidine

[2' - ^2H] - cytidine was synthesized based on a procedure of Cook and Greenberg¹⁵ with the following modifications: workup after the synthesis of α -D-1,3,5-tri-O-benzoyl-2-ketoribofuranose was modified to include an extraction step with $\text{Na}_2\text{S}_2\text{O}_3 \times 5 \text{H}_2\text{O}$ in 1 M phosphate pH 7.0 (12.5 g per 100 mL) to destroy unreacted Dess-Martin periodinane (Sigma) since it was shown by NMR that extraction with $\text{Na}_2\text{S}_2\text{O}_3 \times 5 \text{H}_2\text{O}$ in saturated NaHCO_3 resulted in decomposition of the ketone due to the acidity of α -protons (see also page 4704 of the Cook and Greenberg paper); α -D-1,3,5-tri-O-benzoyl-2-ketoribofuranose was not purified by crystallization but instead used directly in the next step; workup procedure after the synthesis of α -D-1,3,5-tri-O-benzoylribofuranose was modified to include a neutralization step to prevent acetic acid-catalyzed migration of benzoyl groups; cytosine was silylated by refluxing in a 1:10 mixture of chlorotrimethyl silane (TMSCl, redistilled from Aldrich) and 1, 1, 1, 3, 3, 3-hexamethyldisilazane (Aldrich) as opposed to using bis(trimethylsilyl)acetamide; final deprotection step was carried out using sodium methoxide in methanol at the ratio of 0.2 eq of sodium methoxide per benzoyl group in place of saturated methanolic ammonia. (^1H NMR ($^2\text{H}_2\text{O}$) δ 3.74–3.92 (dd \times dd, $J = 3.05, 12.66, 4.27, 12.81$ Hz, 2H), 4.09 (m, 1H), 4.16 (d, $J = 5.80$ Hz, 1H), 4.26 (t, $J = 4.73$ Hz, 0.22H), 5.85 (s, 1H), 6.00 (d, $J = 7.63$ Hz, 1H), 7.79 (d, $J = 7.63$ Hz, 1H); 78% ^2H incorporation at the 2'-position by NMR integration.)

4.2.6 Enzymatic phosphorylation of specifically deuterated cytidine analogs

Specifically deuterated cytidine analogs were phosphorylated to the mono- and di-phosphate forms using the enzymatic procedure described in Chapter 3.

Phosphorylation of [1' - ^2H] - cytidine to form [1' - ^2H] - CMP

[1' - ^2H] - CMP was synthesized from [1' - ^2H] - cytidine on a 5 μmol scale. The reaction contained in a final volume of 5 mL 1 mM [1' - ^2H] - cytidine, 1.33 mg/mL 6xHis-HdCK (S.A. 170 nmol \cdot mg $^{-1}$ \cdot min $^{-1}$), 2 mM ATP, 2 mM DTT, and 0.5 mg/mL BSA, all in 50 mM TRIS

pH 7.6, 100 mM KCl, 5 mM MgCl₂. Reaction was initiated by the addition of 6xHis-HdCK and incubated in a 37 °C circulating water bath for 10 min. At the end of this time period, the reaction mixture was loaded onto a DEAE Sephadex A-25 column (11 mL, 1 × 14 cm). [1'-²H]-CMP was eluted with a 100 × 100 mL linear gradient of 0.005–0.4 M TEAB pH 7.5 in dH₂O. The fractions (5.5 mL) were assayed by absorption at 260 and 280 nm. Fractions 21 through 27, which eluted at 0.2 M TEAB and had an A_{260 nm}/A_{280 nm} ratio that was characteristic of cytidine-derived nucleotides, were pooled. Excess TEAB was removed by repeated cycles of dilution and concentration *in vacuo* from a 1:1 mixture of water and ethanol.¹⁶ The product was obtained in quantitative yield as judged by UV/Vis absorption (λ_{max} 271 nm, λ_{min} 249 nm).

Phosphorylation of [1'-²H]-CMP to form [1'-²H]-CDP

[1'-²H]-CDP was prepared on a 5 μmol scale from [1'-²H]-CMP. The reaction contained in a final volume of 5 mL 1 mM [1'-²H]-CMP, 65 μg/mL GST-UMP-CMP kinase (S.A. 4.8 μmol · mg⁻¹, 4 mM ATP, and 2 mM DTT all in 50 mM TRIS pH 8.0, 5 mM MgCl₂. Reactions were initiated by the addition of GST-UMP-CMP kinase and incubated in a 37 °C circulating water bath for 30 min. The diphosphate material was purified over a DEAE column (11 mL, 1 × 14 cm) using a 120 × 120 mL linear gradient of 5 mM to 0.6 M TEAB pH 7.5 in dH₂O collecting 5.3 mL fractions. Fractions 29 through 32 were pooled. Excess TEAB was removed by repeated evaporations from a 1:1 mixture of ethanol and dH₂O under reduced pressure.¹⁶ A second DEAE column (11 mL, 1 × 14 cm) was then run using a 120 × 120 mL linear gradient of 5 mM to 0.6 M TEAB pH 7.5 in dH₂O to remove residual ADP. Fractions of 5.3 mL were collected. Fractions 29, 30, and 31, whose A_{260 nm}/A_{280 nm} ratio that was characteristic of cytidine-derived nucleotides, were pooled and mixed with an equal volume of ethanol. Excess TEAB was removed under reduced pressure by repeated evaporation from a 1:1 mixture of ethanol and dH₂O.¹⁶ The product was obtained in 83% yield as judged by UV/Vis absorption (λ_{max} 271 nm, λ_{min} 249 nm). It was not characterized further.

Phosphorylation of [2'-²H]-cytidine to form [2'-²H]-CMP

[2'-²H]-CMP was synthesized from [2'-²H]-cytidine on a 10 μmol scale as described above for [1'-²H]-CMP except in final volume of 10 mL. The monophosphate was purified over a DEAE column (26.5 mL, 1.5 × 15 cm) using a 200 × 200 mL linear gradient of 5 mM to 0.4 M TEAB pH 7.5 in dH₂O. Fractions of 6.7 mL were collected. Fractions 34 through 41, which eluted at 0.2 M TEAB and had an A_{260 nm}/A_{280 nm} ratio that was characteristic of cytidine-derived nucleotides, were pooled. Excess TEAB was removed under reduced pressure by 4 evaporations from a 1:1 mixture of ethanol and dH₂O.¹⁶ The product was obtained in quantitative yield as judged by UV/Vis absorption (λ_{max} 271 nm, λ_{min} 249 nm).

Phosphorylation of [2' - ²H] - CMP to form [2' - ²H] - CDP

[2' - ²H] - CDP was prepared on a 10 μmol scale from [2' - ²H] - CMP as described above for [1' - ²H] - CDP except in final volume of 10 mL. The diphosphate material was purified over a DEAE column (10 mL, 1 × 13 cm) using a 140 × 140 mL linear gradient of 5 mM to 0.6 M TEAB pH 7.5 in dH₂O collecting 4.7 mL fractions. Fractions 35 through 41 were pooled. Excess TEAB was removed under reduced pressure by 6 evaporations from a 1:1 mixture of ethanol and dH₂O.¹⁶ A second DEAE column (10 mL, 1 × 13 cm) was then run using a 120 × 120 mL linear gradient of 5 mM to 0.6 M TEAB pH 7.5 in dH₂O to remove residual ADP. Fractions of 2.8 mL were collected. Fractions 37 through 58 were pooled and excess TEAB was removed under reduced pressure by several evaporations from a 1:1 mixture of ethanol and dH₂O.¹⁶ The product was obtained in 84% yield as judged by UV/Vis absorption (λ_{max} 271 nm, λ_{min} 249 nm). It was not further characterized.

Phosphorylation of [4' - ²H] - cytidine to form [4' - ²H] - CMP

[4' - ²H] - CMP was synthesized from [4' - ²H] - cytidine on a 5 μmol scale as described above for [1' - ²H] - CMP. The monophosphate was purified over a DEAE column (15 mL, 1 × 20 cm) using a 100 × 100 mL linear gradient of 5 mM to 0.4 M TEAB pH 7.5 in dH₂O collecting 5 mL fractions. Fractions 27 through 32 were pooled and excess TEAB was removed under reduced pressure by rotovapping 4 times from a 1:1 mixture of ethanol and dH₂O.¹⁶ The product was obtained in quantitative yield as judged by UV/Vis absorption (λ_{max} 271 nm, λ_{min} 249 nm).

Phosphorylation of [4' - ²H] - CMP to form [4' - ²H] - CDP

[4' - ²H] - CDP was prepared on a 5 μmol scale from [4' - ²H] - CMP as described above for [1' - ²H] - CDP. The diphosphate material was purified over a DEAE column (20 mL, 1.5 × 11.5 cm) using a 220 × 220 mL linear gradient of 5 mM to 0.6 M TEAB pH 7.5 in dH₂O collecting 5.2 mL fractions. Fractions 47 through 53 were pooled and concentrated *in vacuo* from a 1:1 mixture of ethanol and dH₂O 6 times to remove excess TEAB.¹⁶ A second DEAE column (20 mL, 1.5 × 11.5 cm) was then run using a 220 × 220 mL linear gradient of 5 mM to 0.6 M TEAB pH 7.5 in dH₂O to remove residual ADP. Fractions of 5.2 mL were collected. Fractions 48 through 55 with an $A_{260\text{ nm}}/A_{280\text{ nm}}$ ratio characteristic of cytidine-derived nucleotides were pooled. Excess TEAB was removed under reduced pressure by rotovapping 6 times from a mixture of water and ethanol.¹⁶ The product was obtained in 80% yield as judged by UV/Vis absorption (λ_{max} 271 nm, λ_{min} 249 nm).

4.2.7 9 GHz EPR experiments and simulations

Reactions contained in a final volume of 230 μL 45 μM E441Q-R1, 45 μM R2, 1 mM CDP, 0.8 mM TTP, and 5 mM DTT, all in 50 mM HEPES pH 7.6, 15 mM MgSO₄, 1 mM EDTA.

All reaction components except for the substrate were combined and incubated at 25 °C for 5 min. The reaction was then initiated by the addition of substrate and transferred into a calibrated 706 PQ EPR tube (quartz, OD 4 mm, ID 2.4 mm, from Wilmad LabGlass) where it was frozen in liquid N₂ 1–4 min after initiation.

EPR spectra at 9 GHz were acquired on a Bruker ESP-300 spectrometer equipped with a Bruker high sensitivity 4119HS cylindrical cavity and an ER-041G microwave bridge containing an internal frequency counter. Measurements were carried out at 77 K using a liquid-helium cooled ESR-900 cryostat and an Oxford LLT 650/1.0 transfer line. Spectra were acquired at 20 μW with 100 kHz modulation frequency, 1 G modulation amplitude, conversion time of 20.48 ms, and time constant of 5.12 ms. The sweep width was 150 G, and 2048 points were acquired per spectrum. The microwave frequency was 9.380774 GHz for the [1' - ²H] - CDP reaction, 9.381503 GHz for the [2' - ²H] - CDP reaction, 9.382075 GHz for the [4' - ²H] - CDP reaction, and 9.383792 GHz for the [5' - ²H] - CDP reaction.

Simulations of 9 GHz EPR spectra were performed with the commercial software package SimFonia. The g-values determined from 140 GHz measurements were used: $g_{xx} = 2.00738$, $g_{yy} = 2.00592$, $g_{zz} = 2.00230$. All spectra were simulated with a Lorentzian to Gaussian line-shape broadening ratio of 1. Parameters for line-width and the components of the hyperfine coupling tensor, namely A_{xx} , A_{yy} , A_{zz} , were varied to obtain the best fit.

4.2.8 140 EPR experiments

In a final volume of 15 μL, reactions contained 300 μM E441Q-R1, 300 μM R2, 1 mM CDP or 0.3 mM GDP, 0.8 mM TTP, and 5 mM DTT, all in 50 mM HEPES pH 7.6, 15 mM MgSO₄, 1 mM EDTA.

All reaction components except for the substrate were combined and incubated at 25 °C for 5 min. The reaction was then initiated by the addition of substrate and aliquots were drawn into suprasil capillaries (silica, OD 0.55 mm, ID 0.4 mm, from Wilmad LabGlass) by capillary action. The samples were frozen in liquid N₂ 10 s to 3 min after initiation.

²H₂O-exchanged reaction To twenty μL of 50 mM HEPES pH 7.6, 15 mM MgSO₄, 1 mM EDTA were added 500 μL ²H₂O and the mixture was frozen in liquid nitrogen and evaporated to dryness on the speed-vac. The procedure was repeated three times, and the resulting powder redissolved in 20 μL ²H₂O. The pD of the buffer was adjusted to 7.6.

To 10 μL of 180 mM CDP were added 500 μL ²H₂O and the mixture was frozen in liquid nitrogen and evaporated to dryness on the speed-vac. The procedure was repeated three times, and the resulting powder redissolved in 10 μL ²H₂O.

To 10 μL of 22.67 mM TTP solution were added 500 μL ²H₂O and the mixture was frozen in liquid nitrogen and evaporated to dryness on the speed-vac. The procedure was repeated three times, and the resulting powder redissolved in 10 μL ²H₂O.

To 150 μL of 250 mM DTT solution were added 500 μL ²H₂O and the mixture was frozen in liquid nitrogen and evaporated to dryness on the speed-vac. The procedure was repeated three times, and the resulting powder redissolved in 150 μL ²H₂O.

E441Q-R1 was pre-reduced as described previously.¹³ A 480 μM 1:1 mixture of E441Q-R1/wt-R2 was prepared by concentration in a minicon device with a YM-30 membrane from Millipore. Protein concentration was determined as previously described.^{9,10} Twenty μL of 480 μM pre-reduced E441Q-R1/wt-R2 mixture were mixed with 480 μL of $^2\text{H}_2\text{O}$ and concentrated using a microcon device with a YM-30 membrane from Millipore to a final volume of 20 μL . The dilution/concentration with $^2\text{H}_2\text{O}$ procedure was repeated two times.

The final concentrations of the E441Q-R1/wt-R2 mixture, CDP, and TTP were determined by UV/Vis absorption.

EPR analysis Spectra were acquired at 60 K on a custom-designed pulsed spectrometer.¹⁷ The stimulated echo sequence¹⁸ was used with a pulse length of $t_{\pi/2} = 72$ ns and a pulse spacing of $\tau = 230$ ns for spectra shown in Figure 4.10 or a pulse length of $t_{\pi/2} = 65$ ns and a pulse spacing of $\tau = 200$ ns for spectra shown in Figure 4.15. The external magnetic field was swept with the assistance of a field lock described elsewhere.¹⁹ The echo intensity at each field position was integrated, and an average of 1000 samples per point were taken. The number of scans and recycle delays were adjusted for different signal intensities and temperatures.

Previous studies have shown that $\text{Y}\cdot$ on R2 has enhanced spin-lattice relaxation time (T1) due to magnetic dipolar and exchange interactions with the adjacent diferric cluster.²⁰ Furthermore, T1 of $\text{Y}\cdot$ is strongly temperature-dependent, ranging from 3 ms at 12 K to <1 μs at 55 K.²¹ The latter time approaches the length of the stimulated echo pulse sequence;¹⁸ above 60 K, the stimulated echo detected signal of the $\text{Y}\cdot$ is no longer detectable because of its fast magnetization decay after the first microwave pulse. The stimulated echo detected signals of other radicals with longer relaxation times (such as the 10 s radical and the 3 min radical) remain detectable.

4.2.9 35 GHz ENDOR experiments

Reactions were prepared as described above for 140 GHz EPR experiments except that the final reaction volume was 60 μL . Custom made tubes prepared in the Hoffman laboratory at Northwestern University were used. Reaction mixtures were frozen in a liquid N_2 / isopentane bath instead of a liquid N_2 bath. All reactions were frozen 3 min after initiation.

35 GHz ENDOR spectra were acquired at 2 K on a custom-designed pulsed spectrometer²² using previously published mims ($[2' - ^2\text{H}]$ -CDP sample and unlabeled sample) and remims ($[1' - ^2\text{H}]$ -CDP and $[5' - ^2\text{H}]$ -CDP sample) pulse sequences.²³ Parameters for the $[1' - ^2\text{H}]$ -CDP reaction were as follows: magnetic field 12260 G, microwave frequency 34.823 GHz, number of pulses 3, pulse widths 32, 32, 32 ns, pulse spacing 144 and 73332 ns, scan range 4.11–12.11 MHz, number of scans 8, power 12 dB 3445, and gain 200 mV. Parameters for the $[5' - ^2\text{H}]$ -CDP reaction were as follows: magnetic field 12255 G, microwave frequency 34.815 GHz, number of pulses 3, pulse widths 32, 32, 32 ns, pulse spacing 200 and 73332 ns, scan range 5.11–11.11 MHz, number of scans 10, power 16 dB 3445, and gain 100 mV. Parameters for the $[2' - ^2\text{H}]$ -CDP reaction were as follows: magnetic field 12265 G, microwave

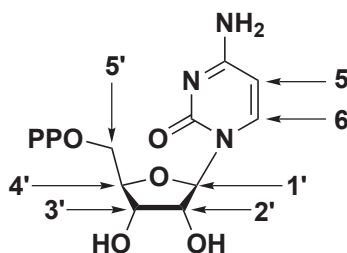


Figure 4.4: Nucleotide nomenclature

frequency 34.839 GHz, number of pulses 3, pulse widths 52, 52, 52 ns, pulse spacing 500 and 73352 ns, scan range 7.12–9.12 MHz, number of scans 5, power 12 dB 3445, and gain 500 mV. Parameters for the unlabeled reaction were as follows: magnetic field 12265 G, microwave frequency 34.839 GHz, number of pulses 3, pulse widths 52, 52, 52 ns, pulse spacing 500 and 73352 ns, scan range 7.12–9.12 MHz, number of scans 14, power 12 dB 3445, and gain 200 mV.

4.3 Results

To test the hypothesis originally proposed by Lawrence *et al.*⁵ that the 3 min radical species is a 4' - ketyl radical, 9 GHz and 140 GHz EPR experiments with [5' - ²H] - CDP (see Figure 4.4 for nucleotide nomenclature) were performed. The synthesis of [5' - ²H] - cytidine was carried out by reducing the 5' - aldehyde of cytidine with NaBD₄ which resulted in the incorporation of one ²H non-stereospecifically at C5'. After phosphorylation, the nucleotide was incubated with E441Q-R1, R2, TTP, and DTT, and reactions examined by 9 GHz CW and 140 GHz pulsed EPR spectroscopy.

Results of 9 GHz EPR measurements are shown in Figure 4.5. The 3 min trace represents the spectrum of the reaction mixture as acquired, while the Y· trace is a scaled spectrum of the tyrosyl radical. Scaling of the tyrosyl radical spectrum was done so as to match the intensity of the right shoulder of the reaction spectrum as acquired. The 3 min – Y· trace is the result of subtraction of the scaled tyrosyl radical spectrum (Y· trace, 38% of starting tyrosyl radical) from the reaction spectrum as acquired (3 min trace, 52% of starting tyrosyl radical). The resulting spectrum (3 min – Y· trace, 14% of starting tyrosyl radical) is a triplet spectrum identical to the one obtained with unlabeled CDP.⁴ Similarly, the spectrum obtained by pulsed 140 GHz EPR measurements (trace ⑤ in Figure 4.10) was identical to the one obtained with unlabeled CDP (trace ① in Figure 4.10). Because there was no change in the hyperfine structure of the 3 min radical signal, the results indicate that the 3 min radical cannot be the 4' - ketyl radical as originally proposed.

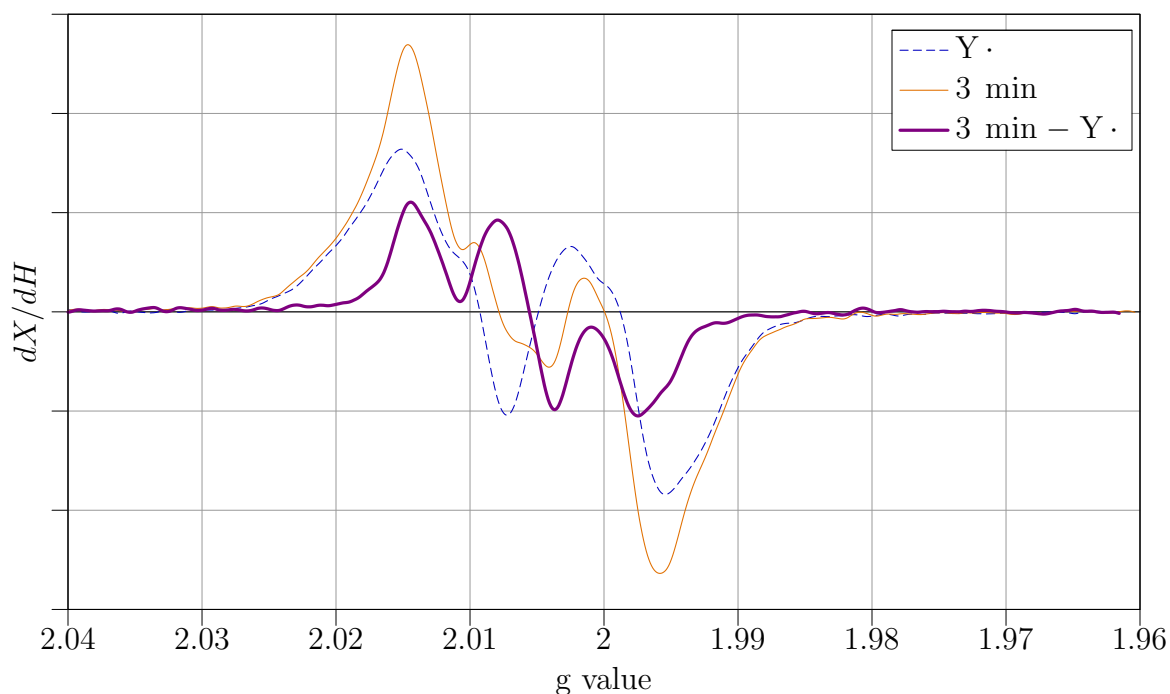


Figure 4.5: 9 GHz EPR spectra of the E441Q-R1, R2, [5'-²H]-CDP, TTP and DTT reaction (blue), scaled tyrosyl radical (red), and the result of subtraction as explained in the text (purple)

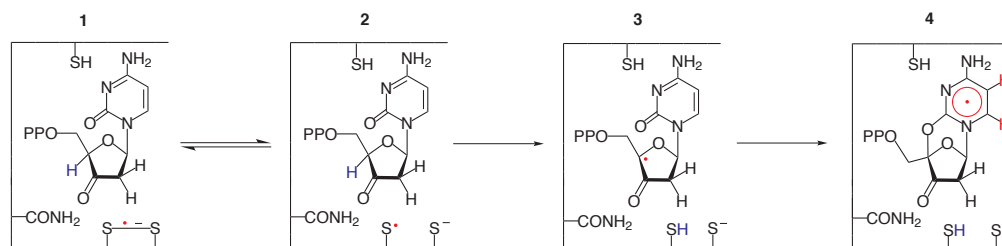


Figure 4.6: Formation and base-trapping of the 4'-ketyl radical (hydrogens shown in red are at position 5 and 6 of the base)

We further reasoned that the 4'-ketyl radical (3, Figure 4.6) can be trapped by the reaction with the nucleotide base to generate a base-delocalized radical (4, Figure 4.6). In this case, the hyperfine interaction would arise from the 5 and 6 protons on the nitrogenous base (protons shown in red in structure 4, Figure 4.6). 9 GHz CW EPR studies by Persson *et al.*⁴ suggested that in reactions of either GDP or CDP with E441Q-R1, R2, TTP, and DTT similar radicals were generated seemingly implying that the 3 min radical is not delocalized to the base since a radical localized on guanine would have a different EPR spectrum from the radical delocalized on cytosine. However, the complexity of the spectra due to the fact

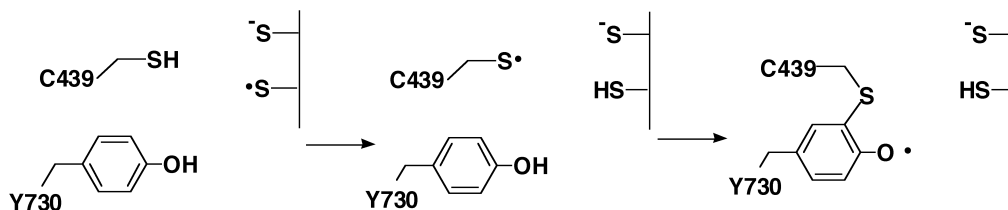


Figure 4.7: Formation of the thioether crosslink between C439 and Y730 of E441Q-R1

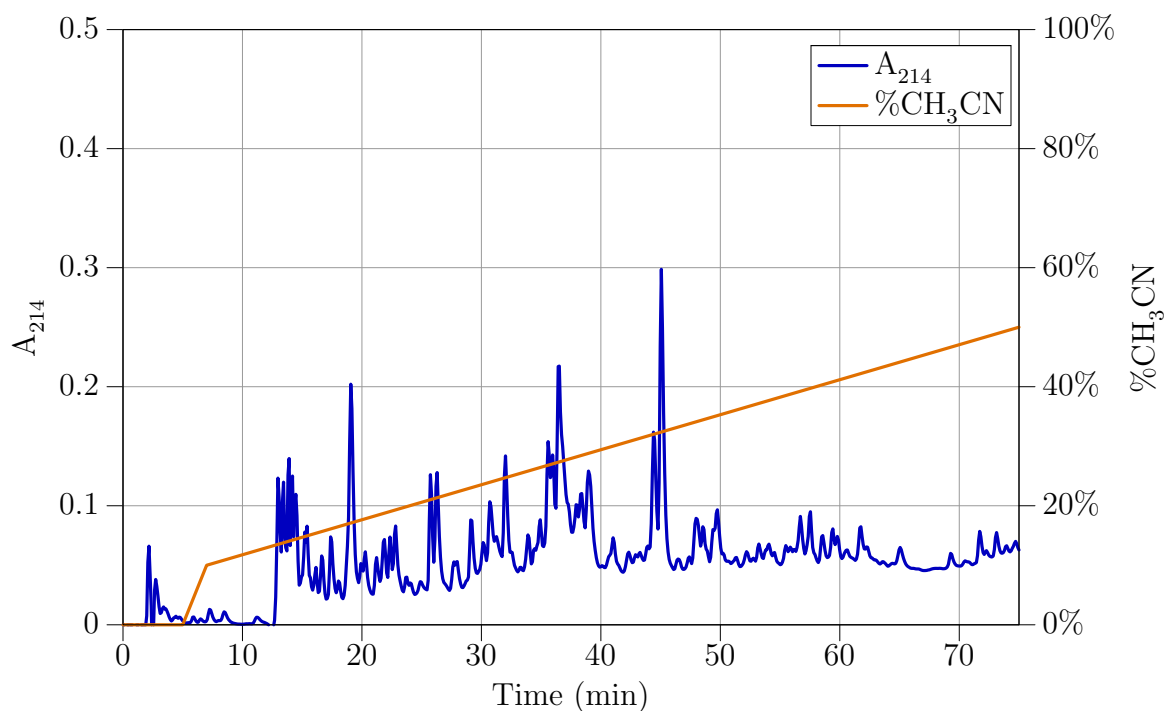


Figure 4.8: HPLC separation of peptides from the tryptic digest of [β -²H]-tyrosine E441Q-R1

that a minimum of three different signals are superimposed, as well as the necessity of using subtractions to obtain the spectra of each radical, prompted the experiments to directly test the possibility that the unpaired spin is delocalized onto the nucleotide base. [5, 6-²H]-CDP and [U-¹⁵N]-CDP were synthesized and their reaction with E441Q-R1, R2, TTP, and DTT examined by 140 GHz pulsed EPR spectroscopy. Both the spectrum obtained in the presence of [5, 6-²H]-CDP as substrate (trace ③ in Figure 4.10) and the spectrum obtained with [U-¹⁵N]-CDP as substrate (trace ⑥ in Figure 4.10) proved identical to that observed with unlabeled CDP as substrate (trace ① in Figure 4.10). Because there was no change in the hyperfine structure of the 3 min radical signal, these results confirm that the radical is not delocalized onto the nucleotide base.

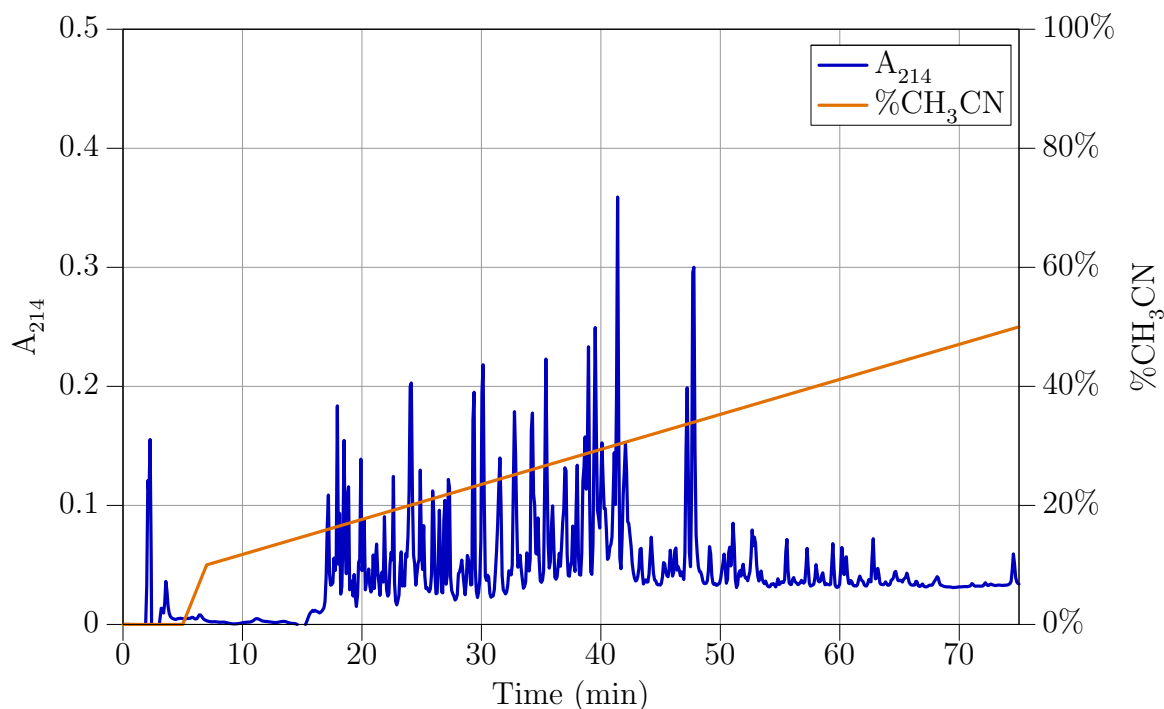


Figure 4.9: HPLC separation of peptides from the tryptic digest of wt *E. coli* R1

Peptide	Expected mass	+2 ion	+3 ion	Measured mass
$[\beta\text{-}^2\text{H}]$ -Y F688-R703	1829.86	915.41	610.36	1829.89
unlabeled F688-R703	1827.85	914.37	609.95	1827.85

Table 4.5: Analysis by ESI mass spectrometry of the F688-R703 peptide

We also observed that the spectrum of the 3 min radical looked strikingly similar to the spectrum reported for the thiomethyl ether radical of apo-galactose oxidase.²⁴ It was proposed that the disulfide radical anion in equilibrium with a thiolate and a thiyl radical could generate a thiyl radical on C439 by hydrogen atom transfer (first step in Figure 4.7). The radical on C439 could then react with Y730 shown crystallographically to be within 3.3 Å of C439 (second step in Figure 4.7). Y730 is thought to be a major player in the initiation by the PCET pathway and is in fact proposed to generate the thiyl radical on C439 by direct hydrogen atom abstraction. Previous studies of Whittaker *et al.*²⁵ demonstrated that when galactose oxidase was isolated from overproducing bacteria grown in media containing $[\beta\text{-}^2\text{H}]$ -tyrosine, the EPR spectrum of the $[\beta\text{-}^2\text{H}]$ -tyrosine containing protein was dramatically altered relative to that of the unlabeled protein, presumably due to the removal of the hyperfine interactions with a β -hydrogen of tyrosine. Thus, E441Q-R1 was expressed in media that allowed quantitative incorporation of $[\beta\text{-}^2\text{H}]$ -tyrosine as determined by trypsin digestion of the protein, HPLC isolation of F688-R703 peptide containing Y699 (fraction eluting at 38.5 min), and mass spectrometry (Figure 4.8, Figure 4.9, and Table 4.5).

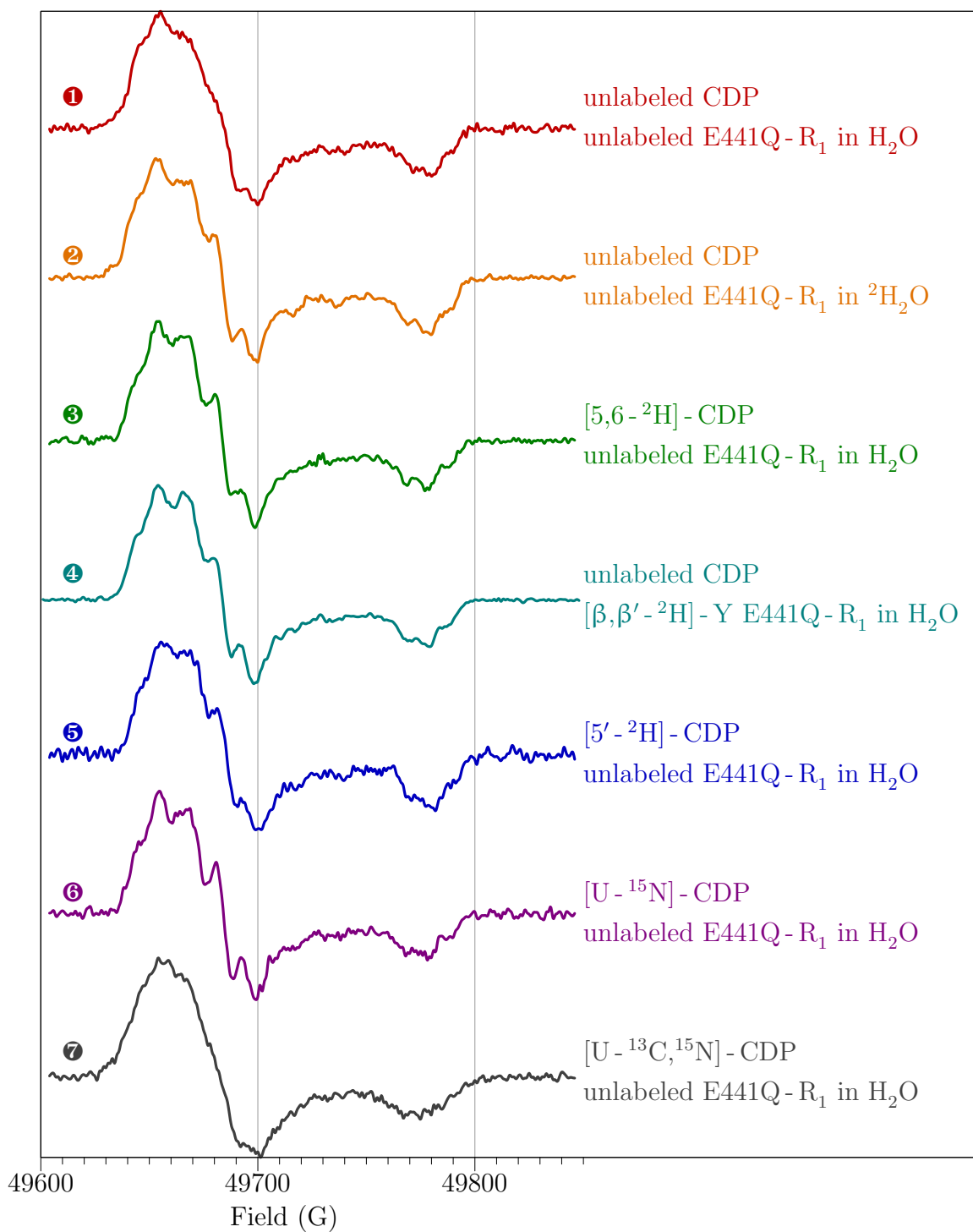


Figure 4.10: 140 GHz EPR spectra of unlabeled or deuterated reactions of E441Q-R1, R2, CDP, TTP, and DTT

The labeled E441Q-R1 was used to generate the 3 min radical and its 140 GHz pulsed EPR spectrum was recorded (trace ④ in Figure 4.10); in contrast to the results obtained in the galactose oxidase system, no alteration in the high-field EPR spectrum was observed in the presence of [β - ^2H]-tyrosine E441Q-R1 as compared to that observed with the unlabeled protein (trace ① in Figure 4.10). The results demonstrate that thiomethyltyrosyl radical is not a structural option.

Two control experiments were carried out in order to gain further insight into the structure of the 3 min radical. In one experiment, all reaction components were exchanged into $^2\text{H}_2\text{O}$ and the reaction run in $^2\text{H}_2\text{O}$ buffer. Examination by pulsed 140 GHz EPR spectroscopy revealed no change in the EPR spectrum (trace ② in Figure 4.10) relative to the reaction run in dH_2O (trace ① in Figure 4.10) indicating that coupled nuclei are not derived from solvent. The second experiment was a repetition of an experiment first published by Persson *et al.*⁴ in which [U- ^{13}C , U- ^{15}N]-CDP was used as substrate. While the initial experiments of Persson *et al.* employed 9 GHz CW EPR spectroscopy, our analysis was carried out using the pulsed EPR method at 140 GHz. As in the previous studies, a broadening of the entire spectrum was observed (trace ⑦ in Figure 4.10). The magnitude of this broadening indicated that the unpaired electron cannot be localized on any one carbon, but instead must be delocalized.²⁶ This result further demonstrates that the 3 min radical cannot be the 3'-nucleotide radical intermediate (1 in Figure 1.4) as originally proposed by Persson *et al.*⁴

We further reasoned that, if the 10 s radical gave rise to the 3 min radical, the disulfide radical anion in equilibrium with the thiyl radical/thiolate had limited reactivity options. One option is electron transfer to the putative 3'-keto-2'-deoxynucleotide. However, in the absence of E441 general acid, electron transfer cannot occur because it requires concomitant protonation of the ketone to make the reaction thermodynamically feasible.¹ Another option is that the thiyl radical adds to the carbonyl of the putative 3'-keto-2'-deoxynucleotide. Such an adduct would be expected to have g-values inconsistent with those observed for the 3 min E441Q radical, thus being an unlikely structural candidate. Finally, thiyl radical could mediate hydrogen atom abstraction as initially proposed by Lawrence *et al.*⁵ to occur at C4' of the 3'-keto-2'-deoxynucleotide to affect formation of the 4'-ketyl radical.

Initially, 2'-ketyl radical was dismissed as a structural option due to the fact that hyperfine coupling constants of model ketyl radicals in solution were several fold greater in magnitude than those observed for the 3 min radical. However, the lack of any change in hyperfine structure of this radical with isotopic substitutions shown in Figure 4.10, the structural constraints imposed by the g-values, and our reasoning about the reactivity of the disulfide radical anion compelled us to consider the possibility that the 3 min radical is a 2'-ketyl radical with altered hyperfine interactions due to the protein environment. Such a species could result from an equilibrium between the disulfide radical anion and the 3'-keto-2'-deoxynucleotide through hydrogen atom abstraction at C2' (Figure 4.11). In this structural model, the unpaired electron density would be delocalized over the 2'-carbon, 3'-carbon, and the 3'-oxygen atoms with possible hyperfine interactions arising from the 1'- and 4'-protons through hyperconjugation and the 2'-proton through spin polarization.

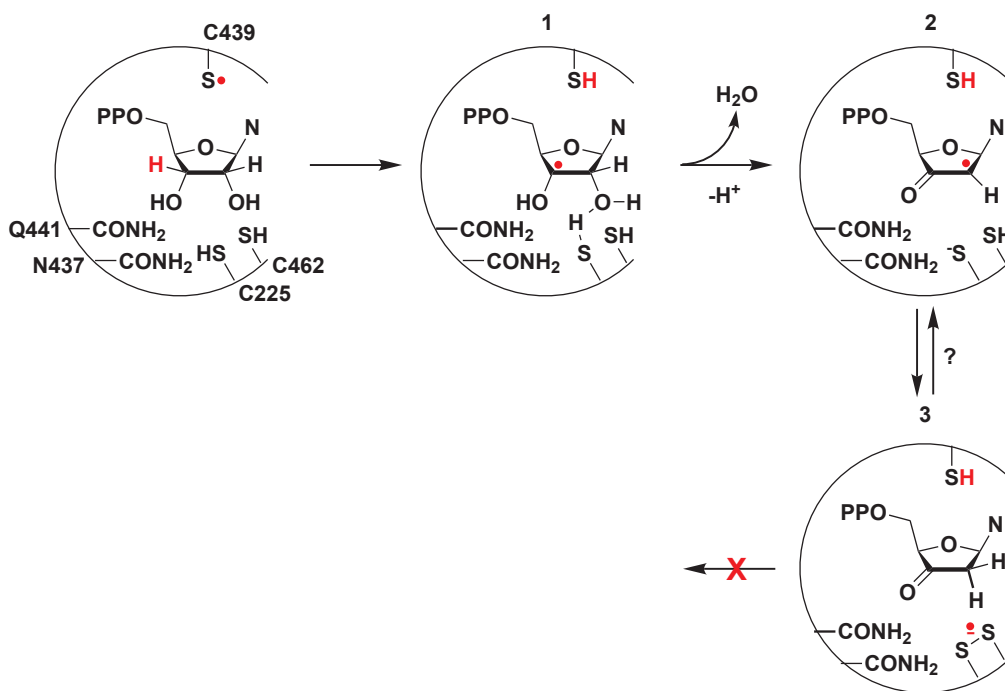


Figure 4.11: Formation of the 2'-ketyl radical

To test the hypothesis that the 3 min radical is a 2'-ketyl radical, $[1' - ^2\text{H}]$ -CDP, $[2' - ^2\text{H}]$ -CDP, and $[4' - ^2\text{H}]$ -CDP were synthesized, and their reactions with E441Q-R1, R2, TTP, and DTT examined by 9 GHz CW EPR spectroscopy, 140 GHz pulsed EPR spectroscopy, and 35 GHz deuterium ENDOR spectroscopy.

Results of 9 GHz CW EPR measurements on the reaction of $[1' - ^2\text{H}]$ -CDP with E441Q-R1, R2, TTP, and DTT are shown in Figure 4.12. The 3 min trace represents the spectrum of the reaction mixture as acquired, while the $\text{Y}\cdot$ trace is a scaled spectrum of the tyrosyl radical. As for the $[5' - ^2\text{H}]$ -CDP reaction, scaling of the tyrosyl radical spectrum was done so as to match the intensity of the right shoulder of the reaction spectrum as acquired. The 3 min - $\text{Y}\cdot$ trace is the result of subtraction of the scaled tyrosyl radical spectrum ($\text{Y}\cdot$ trace, 30% of starting tyrosyl radical) from the reaction spectrum as acquired (3 min trace, 46% of starting tyrosyl radical). The resulting spectrum (3 min - $\text{Y}\cdot$ trace, 16% of starting tyrosyl radical) is a doublet, in contrast to the triplet spectra obtained in the presence of unlabeled CDP⁴ or $[5' - ^2\text{H}]$ -CDP, Figure 4.5. A comparison of the doublet spectrum resulting from the $[1' - ^2\text{H}]$ -CDP reaction and the triplet spectrum resulting from the $[5' - ^2\text{H}]$ -CDP reaction is shown in Figure 4.14 traces ① and trace ⑥, respectively. Very clearly, substitution of the 1'-hydrogen by a deuterium resulted in the collapse of the hyperfine structure. The spectrum could be simulated using g-values published by Lawrence *et al.*⁵, an isotropic coupling of 11.8 G, a line-width of 8 G, and a Lorentzian to Gaussian line-shape broadening ratio of 1 (trace ② in Figure 4.14). The data set provides first definitive evidence that the 3 min

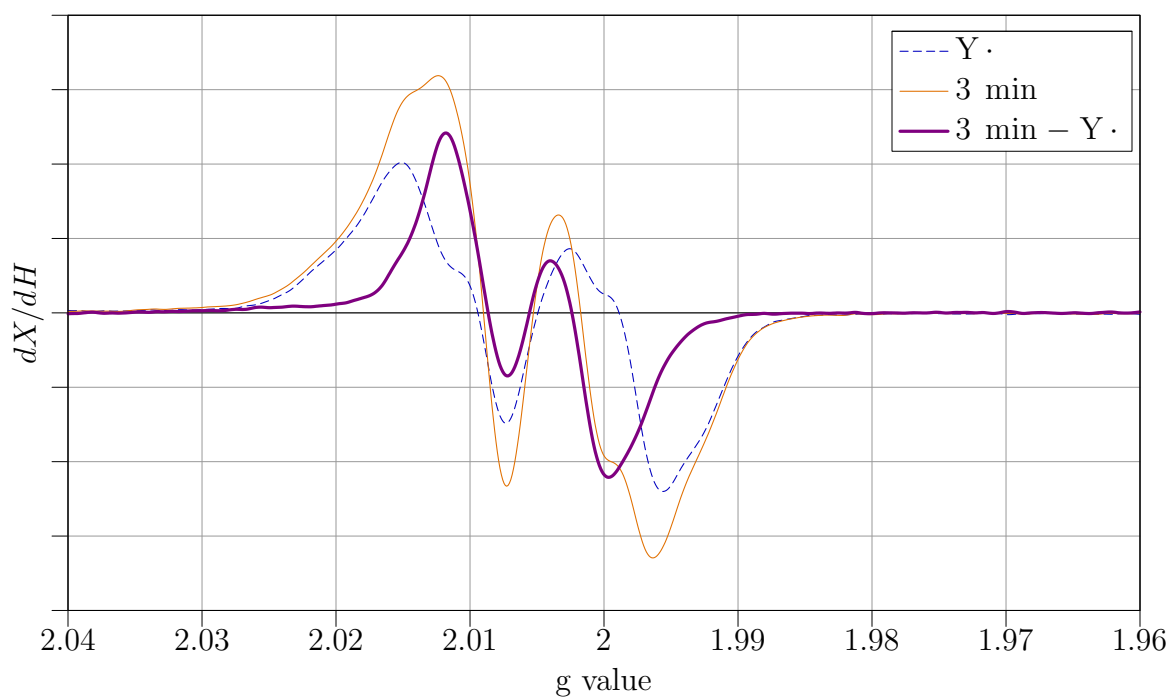


Figure 4.12: 9 GHz EPR spectra of the E441Q-R1, R2, [$1'$ - ^2H]-CDP, TTP and DTT reaction, scaled tyrosyl radical, and results of subtraction

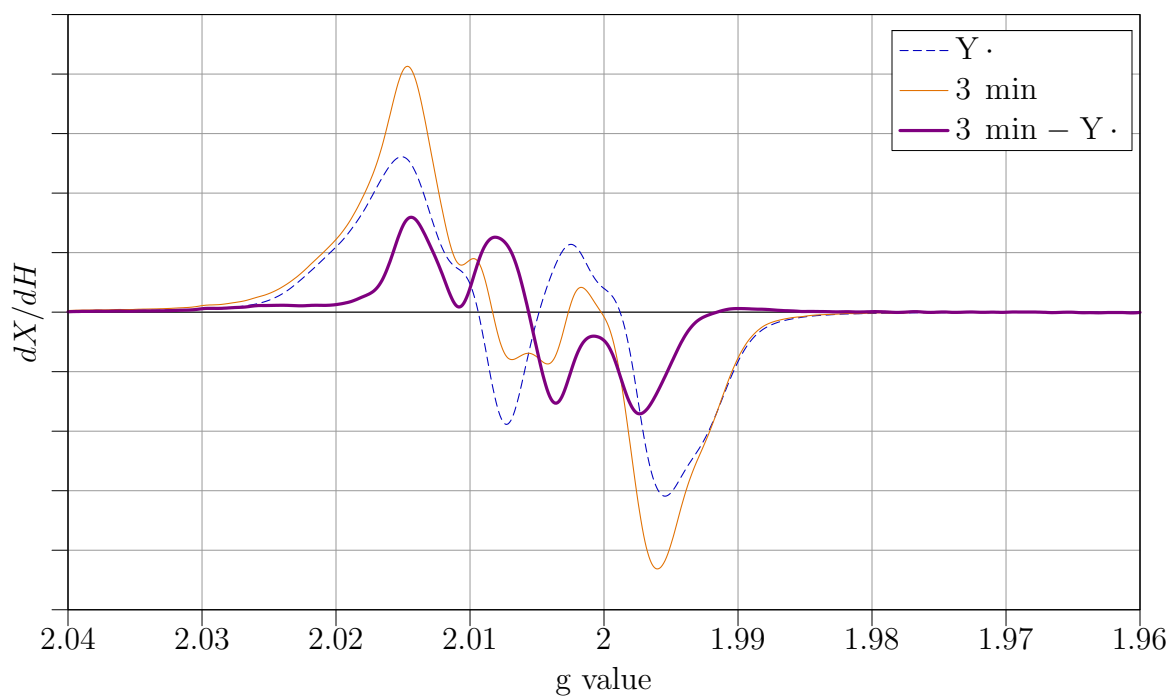


Figure 4.13: 9 GHz EPR spectra of the E441Q-R1, R2, [$2'$ - ^2H]-CDP, TTP and DTT reaction, scaled tyrosyl radical, and results of subtraction

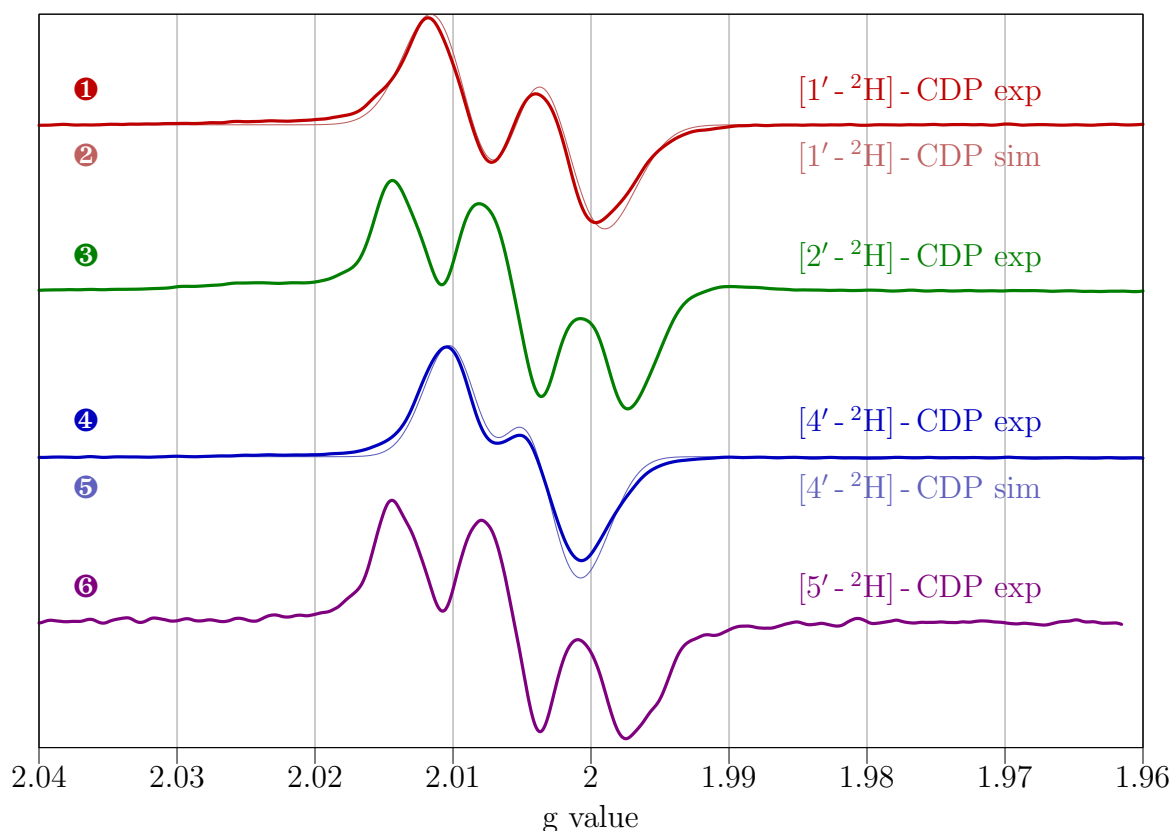


Figure 4.14: 9 GHz EPR spectra of the E441Q-R1, R2, TTP, DTT and CDP reactions after $Y\cdot$ subtraction

radical is substrate-based.

Examination of the reaction of $[1'-^2\text{H}]\text{-CDP}$ with E441Q-R1, R2, TTP, and DTT by 140 GHz pulsed EPR spectroscopy similarly showed a change in the hyperfine structure, most prominently in the high field feature centered around 49775 G which collapsed from a triplet observed in the reaction with unlabeled CDP (trace **1** in Figure 4.15) to a doublet when $[1'-^2\text{H}]\text{-CDP}$ was used as substrate (trace **2** in Figure 4.15).

Our further prediction was that the second hyperfine interaction in the 3 min radical is derived from the 2'-proton. Thus, $[2'-^2\text{H}]\text{-CDP}$ was synthesized and its reaction with E441Q-R1, R2, TTP, and DTT was examined. Results of 9 GHz CW EPR measurements are shown in Figure 4.13. The 3 min trace represents the spectrum of the reaction mixture as acquired, while the $Y\cdot$ trace is a scaled spectrum of the tyrosyl radical. As before, scaling of the tyrosyl radical spectrum was done so as to match the intensity of the right shoulder of the reaction spectrum as acquired. The 3 min - $Y\cdot$ trace is the result of subtraction of the scaled tyrosyl radical spectrum ($Y\cdot$ trace, 30% of starting tyrosyl radical) from the reaction spectrum as acquired (3 min trace, 44% of starting tyrosyl radical). The resulting spectrum (3 min - $Y\cdot$ trace, 14% of starting tyrosyl radical) is a triplet very similar to that observed

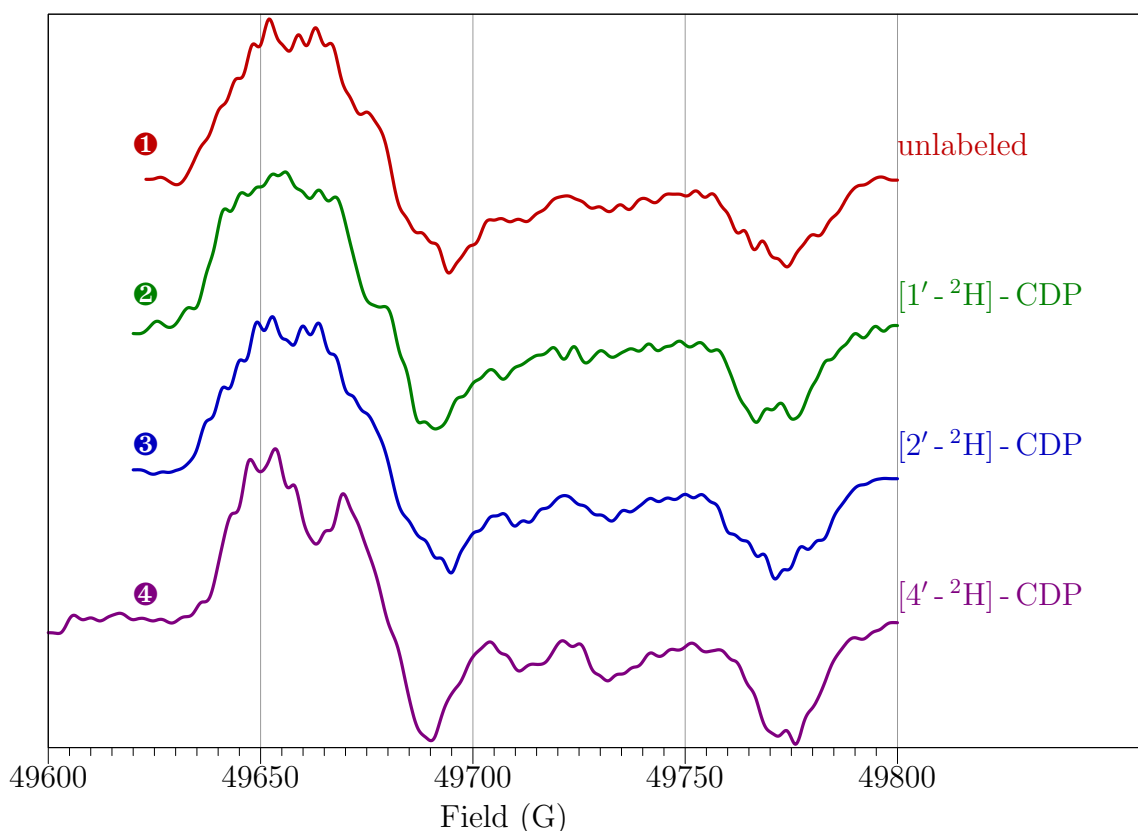


Figure 4.15: 140 GHz EPR spectra of unlabeled or deuterated reactions of E441Q-R1, R2, CDP, TTP, and DTT

in the reaction of unlabeled CDP⁴ or [5' - ²H] - CDP (Figure 4.5). A comparison of the triplet spectrum resulting from the [2' - ²H] - CDP reaction and the triplet spectrum resulting from the [5' - ²H] - CDP reaction is shown in Figure 4.14 traces ③ and ⑥, respectively. No collapse of the hyperfine features is observed indicating that the 8.5 G hyperfine interaction is not derived from the 2' - proton.

Further examination of the reaction of [2' - ²H] - CDP with E441Q-R1, R2, TTP, and DTT by 140 GHz pulsed EPR spectroscopy (trace ③ in Figure 4.15) revealed no change in the structure of the high field feature centered around 49775 G relative to the reaction carried out in the presence of CDP (trace ① in Figure 4.15). The results confirmed the observations made by 9 GHz CW EPR measurements which showed no change in the hyperfine structure of the 3 min radical when [2' - ²H] - CDP was used as substrate.

The remaining candidate for the origin of the second hyperfine interaction in the 2' - ketyl radical species was the 4' - proton. Thus, [4' - ²H] - CDP was synthesized and its reaction with E441Q-R1, R2, TTP, and DTT examined by 9 GHz CW EPR spectroscopy. Results are shown in Figure 4.16. The 3 min trace represents the spectrum of the reaction mixture as

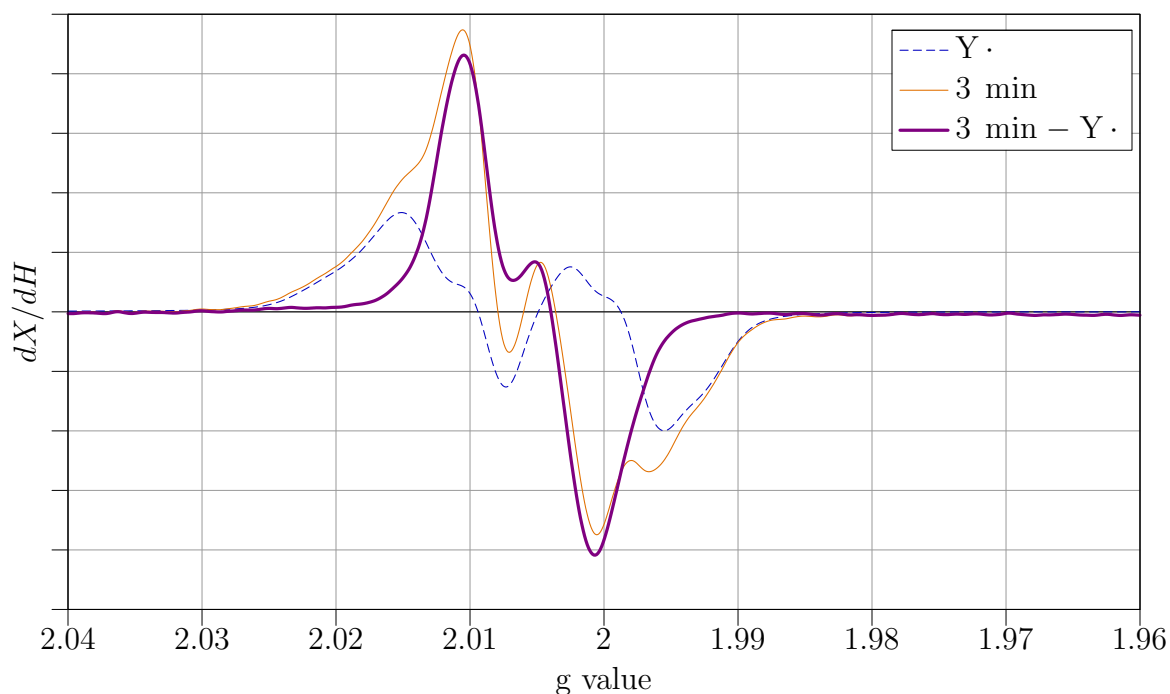


Figure 4.16: 9 GHz EPR spectra of the E441Q-R1, R2, $[4' - ^2\text{H}]$ -CDP, TTP and DTT reaction, scaled tyrosyl radical, and results of subtraction

acquired, while the $\text{Y}\cdot$ trace is a scaled spectrum of the tyrosyl radical. Once again, scaling of the tyrosyl radical spectrum was done so as to match the intensity of the right shoulder of the reaction spectrum as acquired. The 3 min - $\text{Y}\cdot$ trace is the result of subtraction of the scaled tyrosyl radical spectrum ($\text{Y}\cdot$ trace, 22% of starting tyrosyl radical) from the reaction spectrum as acquired (3 min trace, 43% of starting tyrosyl radical). The resulting spectrum (3 min - $\text{Y}\cdot$ trace, 21% of starting tyrosyl radical) is a doublet, in contrast to the triplet spectra obtained in the presence of unlabeled CDP,⁴ $[5' - ^2\text{H}]$ -CDP (Figure 4.5) or $[2' - ^2\text{H}]$ -CDP (Figure 4.13).

A comparison of the doublet spectrum resulting from the $[4' - ^2\text{H}]$ -CDP reaction and the triplet spectrum resulting from the $[5' - ^2\text{H}]$ -CDP reaction is shown in Figure 4.14 traces ④ and ⑥, respectively. Substitution of the 4'-hydrogen by a deuterium caused an unambiguous collapse of the hyperfine structure. The remaining hyperfine interaction is due to the 1'-proton, as shown by experiments with $[1' - ^2\text{H}]$ -CDP. Thus, the remaining splitting in the spectrum shown as trace ④ in Figure 4.14 is due to the 1'-proton. This spectrum could be simulated using g-values published by Lawrence *et al.*⁵, an axially symmetric coupling of $A_{xx} = 9.8$ G, $A_{yy} = A_{zz} = 7.5$ G, a line-width of 6.5 G, and a Lorentzian to Gaussian line-shape broadening ratio of 1 (trace ⑤ in Figure 4.14). This data set demonstrates that the smaller of the two hyperfine interaction (A_{iso} of 8.5 G) is derived from the 1'-proton, and that the remaining coupling in the radical formed with $[1' - ^2\text{H}]$ -CDP is derived from the 4'-proton.

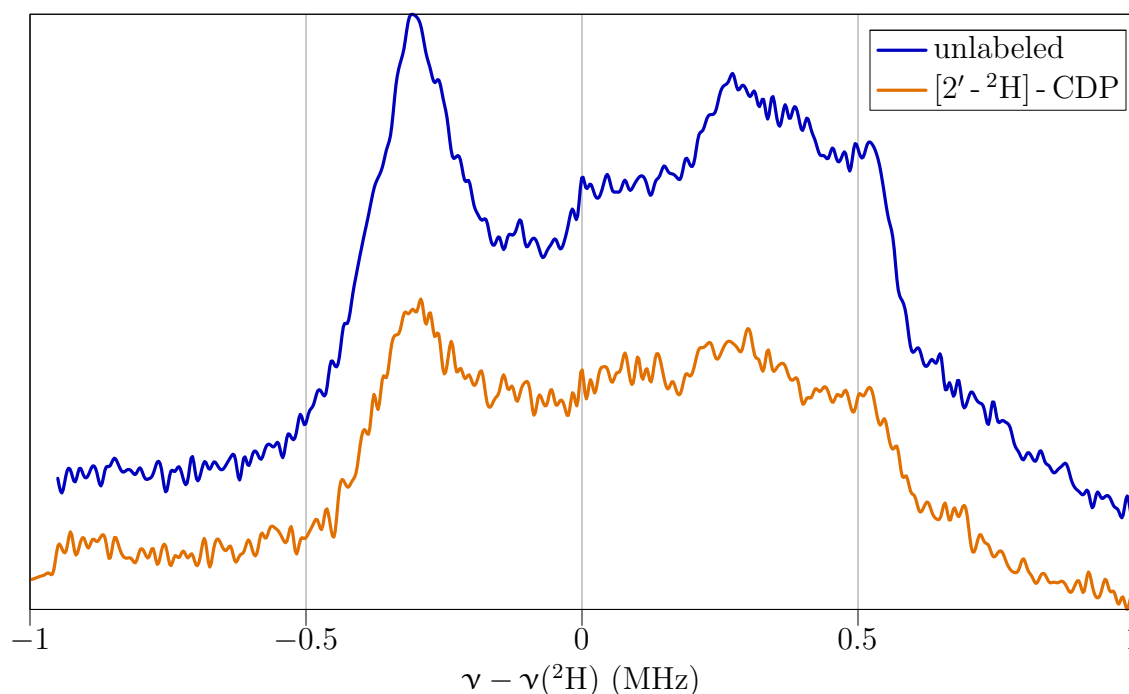


Figure 4.17: Deuterium ENDOR spectra of reactions of E441Q-R1, R2, TTP, and DTT with unlabeled or $[2' - ^2\text{H}]$ -CDP

Examination of the reaction of $[4' - ^2\text{H}]$ -CDP with E441Q-R1, R2, TTP, and DTT by 140 GHz pulsed EPR spectroscopy similarly showed a change in the hyperfine structure. In addition to the change in the high field feature centered around 49775 G which, as in the case of the $[1' - ^2\text{H}]$ -CDP reaction, collapsed from a triplet observed with unlabeled CDP (trace **1** in Figure 4.15) to a doublet when $[4' - ^2\text{H}]$ -CDP was used (trace **4** in Figure 4.15), a clear change in hyperfine features in the low field region of the spectrum was also observed.

To probe the possibility that the coupling of the $2'$ -nucleus in the 3 min radical was present but smaller than 5 G and thus lost in the line-width of the EPR spectra, reaction of $[2' - ^2\text{H}]$ -CDP with E441Q-R1, R2, TTP, and DTT was examined by 35 GHz deuterium ENDOR spectroscopy. No difference compared to the unlabeled CDP reaction was detected (Figure 4.17). Thus, no detectable deuterium coupling was observed from the $2'$ -nucleus. In addition, reactions of $[1' - ^2\text{H}]$ -CDP and $[5' - ^2\text{H}]$ -CDP were examined by ENDOR spectroscopy (Figure 4.18). A deuterium ENDOR effect consistent with an isotropic coupling constant of 3.6 MHz (1.3 G) was detected from the $1'$ -deuteron (equivalent to an 8.5 G proton coupling), consistent with 9 GHz EPR measurements. No evidence for the coupling of $5'$ -deuterons was found (Figure 4.18).

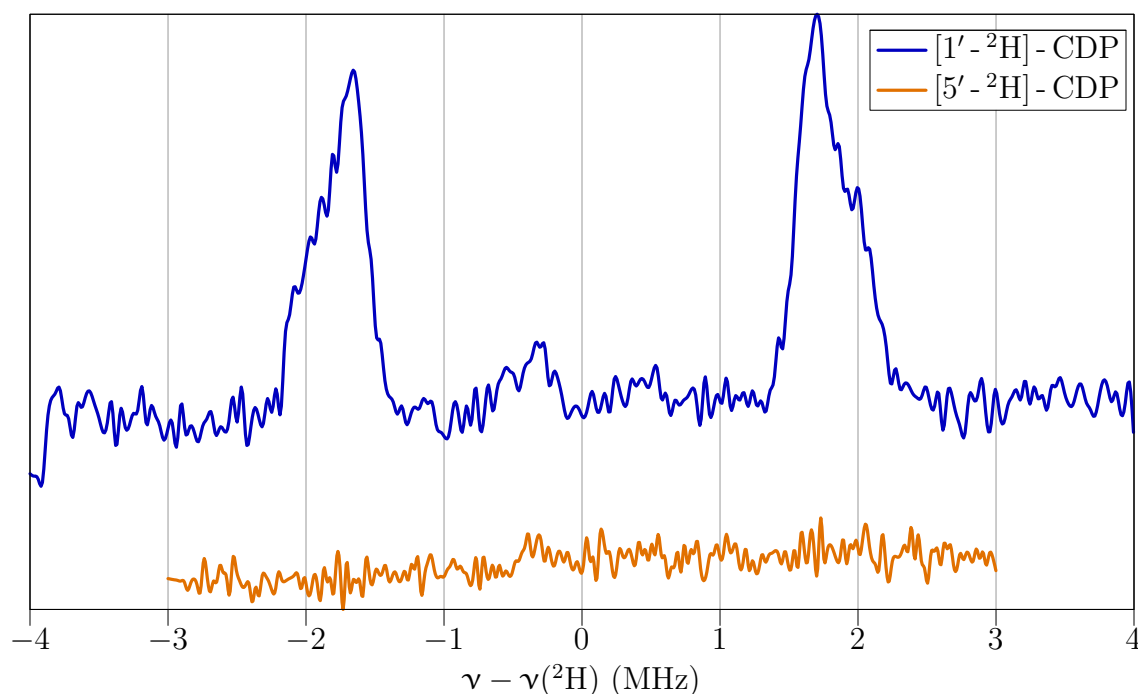


Figure 4.18: Deuterium ENDOR spectra of reactions of E441Q-R1, R2, TTP, and DTT with $[1' - ^2\text{H}] - \text{CDP}$ or $[5' - ^2\text{H}] - \text{CDP}$

4.4 Discussion

The initial isotope labeling experiments and EPR measurements (Figure 4.10) on the 3 min radical formed in the reaction of E441Q-R1 with R2, CDP, TTP and DTT revealed no change in the hyperfine structure of the 3 min radical and hence eliminated the 4'-ketyl radical as a structural option, demonstrated that the radical is not delocalized onto the nucleotide base, and that it is not structurally related to the thiomethyl ether radical species observed in apo-galactose oxidase. Based on these results, our chemical reasoning on the reactivity of the disulfide radical anion, and the structural constraints imposed by the g -values, we formulated a hypothesis that the 3 min radical is related to the 2'-ketyl radical, structure 2 in Figure 4.3. Although in model systems the coupling constants for α and β protons (the equivalent of the 1'- and 2'-protons in structure 2, Figure 4.3) are two- to three-fold greater than the coupling constants observed in the 3 min radical, we reasoned that the hyperfine interactions in the 3 min radical could be altered due to the fact that the radical is bound in an unusual geometry in the active site and not free in solution. To test this hypothesis, we synthesized $[1' - ^2\text{H}] - \text{CDP}$, $[2' - ^2\text{H}] - \text{CDP}$, and $[4' - ^2\text{H}] - \text{CDP}$ and examined their reactions with E441Q-R1, R2, TTP, and DTT by 9 GHz CW EPR spectroscopy, 140 GHz pulsed EPR spectroscopy, and 35 GHz deuterium ENDOR spectroscopy.

Results of the 9 GHz CW EPR, 140 GHz pulsed EPR, and 35 GHz ENDOR experiments all show that an 11.8 G hyperfine coupling in the 3 min radical is derived from the 4'-proton

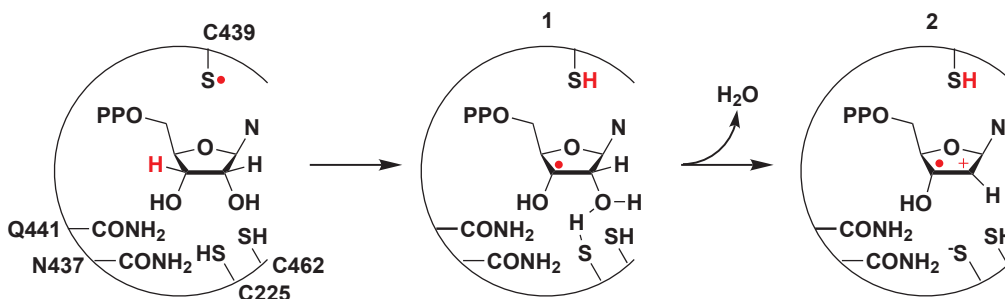


Figure 4.19: Formation of the radical cation in the absence of general base

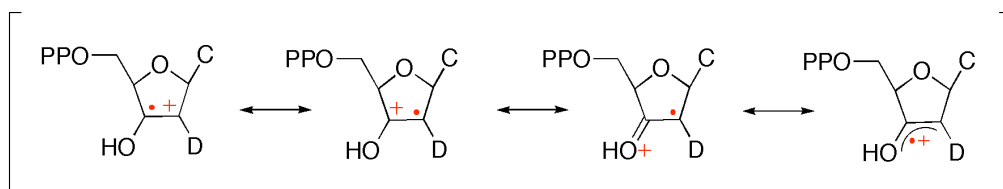


Figure 4.20: Resonance structures for the radical cation formed in Figure 4.19

and that an axially symmetric coupling of $A_{xx} = 9.8$ G, $A_{yy} = A_{zz} = 7.5$ G is derived from the 1'-proton. Furthermore, neither spectra at 9 GHz nor spectra at 140 GHz reveal changes in the hyperfine structure of the signal when $[2' - ^2\text{H}]$ -CDP is used as substrate. More significantly, 35 GHz deuterium ENDOR experiments with $[2' - ^2\text{H}]$ -CDP as substrate revealed no obvious coupling of the unpaired spin density with the deuterium nucleus at the 2'-position.

Results of $[2' - ^2\text{H}]$ -CDP experiments are difficult to reconcile with the 2'-ketyl radical hypothesis. The hyperfine interaction of a proton such as that on an sp^2 hybridized carbon of a ketyl radical is one of the best understood couplings. It seems beyond doubt that the coupling from such a proton would have an effect on the EPR signal. Yet, the fact that the radical eventually collapses to release cytosine and furanone and the observed g -values strongly suggest the presence of a ketone at C3'.

We have thus considered alternative models which are structurally related to the 2'-ketyl radical, but have reduced electron density at the 2'-position. In one model, the absence of the general base catalyst could lead to the formation of the ketyl radical cation 4, Figure 4.19 within the active site. The resonance structures for this radical are shown in Figure 4.20. However, it is unlikely that such a species would have a long lifetime, as the loss of proton from the 3'-oxygen to the residual solvent within the active site would be rapid.

Alternatively, we envisioned that in the absence of the E441 general acid, the electron transfer from the disulfide radical anion to the 2'-deoxy-3'-ketoribonucleotide (3, Figure 4.3) is too slow to compete with base elimination to generate enone 5, Figure 4.3.¹ The

resulting enone could then be reduced by the disulfide radical anion to generate an α , β -unsaturated ketyl radical anion 5, Figure 4.3. The H-abstraction from C439 which occurs in the normal reduction process would be slowed down in the case of radical 5, Figure 4.3 because of the stabilization of this radical by the alkene and by the oxygen anion. Structure 5 would account for the magnitude of the hyperfine coupling constant observed from the 1'-proton and would be expected to give rise to a small coupling of 0.5–3 G for the nucleus at the 2'-position.^{27–32} A deuterium ENDOR effect from such a coupling is below the detection limit of our methods.

The experiments with E441Q-R1 have been mechanistically informative about the normal mechanism of ribonucleotide reduction. The mechanistic model suggested that the removal of the proton source by replacement of the E441 with a glutamine would prevent the reduction of the 3'-keto-2'-deoxynucleotide to the 3'-(2'-deoxy)nucleotide radical, Figure 4.1. Thus, the model predicted the buildup of a disulfide radical anion and a 3'-keto-2'-deoxynucleotide. Previous studies by Lawrence *et al.*⁵ provided evidence for a disulfide radical anion in the E441Q-R1 reaction. We now interpret the results of our present study as evidence for the concomitant generation of a 3'-keto-2'-deoxynucleotide which rapidly loses base to generate an α , β -unsaturated enone (4, Figure 4.3). The enone can then be reduced by the disulfide radical anion to generate an α , β -unsaturated ketyl radical anion 5, Figure 4.3.

No direct evidence for the mechanism of conversion of the 3'-keto-2'-deoxynucleotide to the 3'-(2'-deoxy)nucleotide radical is currently available (Chapter 1). Although several other mechanistic options have been proposed,^{33–35} direct electron transfer from the disulfide radical anion to the 3'-ketone concomitantly with the protonation of the 3'-oxygen by E441 has been favored.^{1,37} Confirmation of the structure of the 3 min E441Q-R1 radical as 5, Figure 4.3, would provide evidence for the lack of reactivity of the disulfide radical anion except in direct electron transfer and show that the disulfide radical anion is able to reduce a nucleotide-based intermediate bound in the active site of R1 when the redox potentials of the disulfide radical anion and the nucleotide-based intermediate are matched.

To gain further support for this hypothesis, solution phase model of α , β -unsaturated 2'-ketyl radical anion will be generated by Dr. Alexandre Ferrand at the University of Basel, and the models will be examined by EPR spectroscopy to determine if the g-values and hyperfine coupling constants match those of the 3 min radical. Additionally, Dr. Hendrik Zipse at the Ludwig-Maximilians-Universität München will carry out DFT calculations in an attempt to computationally reproduce the hyperfine coupling constants and g-values.

The hypothesis makes a prediction that the disulfide radical anion and the α , β -unsaturated 2'-ketyl radical anion are kinetically coupled, and that formation of the disulfide radical anion precedes that of the α , β -unsaturated 2'-ketyl radical. The difficulty of CW EPR analysis due to spectral overlap requires the use of pulsed methods to deconvolute the radicals in any type of kinetic analysis. At the same time, the rate of the reaction requires rapid freeze quench methods. A device for performing rapid freeze quench experiments at high field is currently being developed by Dr. Debora Martino in the Griffin laboratory at MIT who will examine the kinetic relationship between the disulfide radical anion and the

proposed α , β -unsaturated 2'-ketyl radical anion.

4.5 Acknowledgments

I gratefully acknowledge Dr. Stanislaw Wnuk of Florida International University and Dr. Dierk Blechschmidt of the Schwalbe laboratory at MIT for providing several isotopically enriched compounds as described in Section 4.2. Dr. Galit Bar and Dr. Debora Martino of the Griffin laboratory at MIT acquired the 140 GHz EPR spectra in Figure 4.10 and Figure 4.15, respectively. All ENDOR measurements were carried out by Dr. Nicholas Lees of the Hoffman laboratory at Northwestern University. I thank Professor Bernd Giese of the University of Basel for inspiring discussions from which the α , β -unsaturated 2'-ketyl radical anion hypothesis arose, and for his enthusiasm to carry this project forward. This work was supported by NIH grant 29595 to Dr. JoAnne Stubbe, NIH grants EB002804 and EB002026 to Dr. Robert Griffin, and NIH grant HL13531 to Dr. Brian Hoffman.

Bibliography

- [1] R. Lenz and B. Giese, "Studies on the mechanism of ribonucleotide reductases," *Journal of the American Chemical Society*, vol. 119, no. 12, pp. 2784–2794, 1997.
- [2] C. Walling and R. A. Johnson, "Fenton's reagent. VI. Rearrangements during glycol oxidations," *Journal of the American Chemical Society*, vol. 97, no. 9, pp. 2405–2407, 1975.
- [3] A. L. Persson, M. Eriksson, B. Katterle, S. Potsch, M. Sahlin, and B.-M. Sjöberg, "A new mechanism-based radical intermediate in a mutant R1 protein affecting the catalytically essential Glu441 in *Escherichia coli* ribonucleotide reductase," *Journal of Biological Chemistry*, vol. 272, no. 50, pp. 31533–31541, 1997.
- [4] A. L. Persson, M. Sahlin, and B.-M. Sjöberg, "Cysteinylyl and substrate radical formation in active site mutant E441Q of *Escherichia coli* class I ribonucleotide reductase," *The Journal of Biological Chemistry*, vol. 273, no. 47, pp. 31016–31020, 1998.
- [5] C. C. Lawrence, M. Bennati, H. V. Obias, G. Bar, R. G. Griffin, and J. Stubbe, "High-field EPR detection of a disulfide radical anion in the reduction of cytidine 5'-diphosphate by the E441Q R1 mutant of *Escherichia coli* ribonucleotide reductase," *Proceedings of the National Academy of Sciences of the United States of America*, vol. 96, no. 16, pp. 8979–8984, 1999.
- [6] A. L. Buley, R. O. C. Norman, and R. J. Pritchett, "Electron spin resonance studies of oxidation. VIII. Elimination reactions of some hydroxyalkyl radicals," *Journal of the Chemical Society B: Physical Organic*, no. 9, pp. 849–852, 1966.
- [7] B. C. Gilbert, D. M. King, and C. B. Thomas, "Radical reactions of carbohydrates. Part 4. Electron spin resonance studies of radical-induced oxidation of some aldopentoses, sucrose, and compounds containing furanose rings," *Journal of the Chemical Society, Perkin Transactions 2: Physical Organic Chemistry*, no. 5, pp. 675–683, 1983.
- [8] W. A. van der Donk, G. Yu, D. J. Silva, J. Stubbe, J. R. McCarthy, E. T. Jarvi, D. P. Matthews, R. J. Resvick, and E. Wagner, "Inactivation of ribonucleotide reductase by (E)-2'-fluoromethylene-2'-deoxycytidine 5'-diphosphate: A paradigm for nucleotide mechanism-based inhibitors," *Biochemistry*, vol. 35, no. 25, pp. 8381–8391, 1996.

- [9] S. Salowe, J. M. Bollinger, Jr., M. Ator, J. Stubbe, J. McCracken, J. Peisach, M. C. Samano, and M. J. Robins, "Alternative model for mechanism-based inhibition of *Escherichia coli* ribonucleotide reductase by 2'-azido-2'-deoxyuridine 5'-diphosphate," *Biochemistry*, vol. 32, no. 47, pp. 12749–12760, 1993.
- [10] S. P. Salowe and J. Stubbe, "Cloning, overproduction, and purification of the B2 subunit of ribonucleoside-diphosphate reductase," *Journal of Bacteriology*, vol. 165, no. 2, pp. 363–366, 1986.
- [11] J. M. Bollinger, Jr, D. E. Edmondson, B.-H. Huynh, J. Filley, J. R. Norton, and J. Stubbe, "Mechanism of assembly of the tyrosyl radical-dinuclear iron cluster cofactor of ribonucleotide reductase," *Science (Washington, DC)*, vol. 253, no. 5017, pp. 292–298, 1991.
- [12] A. N. I. Lin, G. W. Ashley, and J. Stubbe, "Location of the redox-active thiols of ribonucleotide reductase: sequence similarity between the *Escherichia coli* and *Lactobacillus leichmannii* enzymes," *Biochemistry*, vol. 26, no. 22, pp. 6905–6909, 1987.
- [13] J. Ge, G. Yu, M. A. Ator, and J. Stubbe, "Pre-steady-state and steady-state kinetic analysis of *E. coli* class I ribonucleotide reductase," *Biochemistry*, vol. 42, no. 34, pp. 10071–10083, 2003.
- [14] J. A. Rabi and J. J. Fox, "Nucleosides. LXXIX. Facile base-catalyzed hydrogen isotope labeling at position 6 of pyrimidine nucleosides," *Journal of the American Chemical Society*, vol. 95, no. 5, pp. 1628–1632, 1973.
- [15] G. P. Cook and M. M. Greenberg, "A general synthesis of C2'-deuterated ribonucleosides," *Journal of Organic Chemistry*, vol. 59, no. 16, pp. 4704–4706, 1994.
- [16] J. W. Kozarich, A. C. Chinault, and S. M. Hecht, "Ribonucleoside phosphates via phosphorimidazolidate intermediates. Synthesis of pseudoadenosine 5'-triphosphate," *Biochemistry*, vol. 12, no. 22, pp. 4458–4463, 1973.
- [17] M. Bennati, C. T. Farrar, J. A. Bryant, S. J. Inati, V. Weis, G. J. Gerfen, P. Riggs-Gelasco, J. Stubbe, and R. G. Griffin, "Pulsed electron-nuclear double resonance (ENDOR) at 140 GHz," *Journal of Magnetic Resonance*, vol. 138, no. 2, pp. 232–243, 1999.
- [18] E. L. Hahn, "Spin echoes," *Physical Review*, vol. 80, no. 4, pp. 580–594, 1950.
- [19] S. Un, J. Bryant, and R. G. Griffin, "Precision field-sweep system for superconducting solenoids and its application to high-frequency EPR spectroscopy," *Journal of Magnetic Resonance, Series A*, vol. 101, no. 1, pp. 92–94, 1993.
- [20] M. Sahlin, L. Petersson, A. Gräslund, A. Ehrenberg, B. M. Sjöberg, and L. Thelander, "Magnetic interaction between the tyrosyl free radical and the antiferromagnetically coupled iron center in ribonucleotide reductase," *Biochemistry*, vol. 26, no. 17, pp. 5541–8, 1987.
- [21] M. Bennati, J. Stubbe, and R. G. Griffin, "High-frequency EPR and ENDOR: time-domain spectroscopy of ribonucleotide reductase," *Applied Magnetic Resonance*, vol. 21, no. 3-4, pp. 389–410, 2001.
- [22] V. J. DeRose and B. M. Hoffman, "Protein structure and mechanism studied by electron nuclear double resonance spectroscopy," *Methods in Enzymology*, vol. 246, pp. 554–589, 1995.
- [23] C. E. Davoust, P. E. Doan, and B. M. Hoffman, "Q-band pulsed electron spin-echo spectrometer and its application to ENDOR and ESEEM," *Journal of Magnetic Resonance, Series A*, vol. 119, no. 1, pp. 38–44, 1996.
- [24] G. J. Gerfen, B. F. Bellew, R. G. Griffin, D. J. Singel, C. A. Ekberg, and J. W. Whittaker, "High-frequency electron paramagnetic resonance spectroscopy of the apogalactose oxidase radical," *Journal of Physical Chemistry*, vol. 100, no. 41, pp. 16739–16748, 1996.
- [25] M. M. Whittaker and J. W. Whittaker, "A tyrosine-derived free radical in apogalactose oxidase," *Journal of Biological Chemistry*, vol. 265, no. 17, pp. 9610–9613, 1990.

- [26] F. Himo and P. E. M. Siegbahn, "Very stable ribonucleotide substrate radical relevant for class I ribonucleotide reductase," *Journal of Physical Chemistry B*, vol. 104, no. 31, pp. 7502–7509, 2000.
- [27] G. A. Russell, T. Takano, and Y. Kosugi, "Application of ESR spectroscopy to problems of structure and conformation. 32. Aliphatic semidiones. 38. Conversion of polymeric peroxides and hydroperoxides to 1,2- and 1,4-semidiones in basic solution," *Journal of the American Chemical Society*, vol. 101, no. 6, pp. 1491–1495, 1979.
- [28] G. A. Russell, V. Malatesta, T. Morita, C. Osuch, R. L. Blankespoor, K. D. Trahanovsky, and E. Goertert, "Ketyls of cyclic α,β -unsaturated ketones. 2. Formation of radical anions by electron transfer using trimethylsilylsodium or dimethyl sulfoxide-potassium tert-butoxide," *Journal of the American Chemical Society*, vol. 101, no. 8, pp. 2112–2116, 1979.
- [29] K. S. Chen and J. K. S. Wan, "Photolytic generation of radical anions and dianions and group IV-A organometallic adducts of β -diketones. An electron-spin-resonance study on the effects of fluorine substitution and crown ethers," *Journal of the Chemical Society, Perkin Transactions 2: Physical Organic Chemistry*, no. 4, pp. 419–423, 1982.
- [30] H. G. Korth, P. Lommès, and R. Sustmann, "Rotational barrier in 1-cyano-1-methoxyallyl radical: a contribution to the problem of captodative radical stabilization," *Journal of the American Chemical Society*, vol. 106, no. 3, pp. 663–668, 1984.
- [31] H. M. Novais and S. Steenken, "ESR studies of electron and hydrogen adducts of thymine and uracil and their derivatives and of 4,6-dihydropyrimidines in aqueous solution. Comparison with data from solid state. The protonation at carbon of the electron adducts," *Journal of the American Chemical Society*, vol. 108, no. 1, pp. 1–6, 1986.
- [32] M. Okubo, "Ketyl radicals formed in the Grignard reaction. IV. Sterically hindered ketyl radicals in nuclear replacement and conjugate addition," *Bulletin of the Chemical Society of Japan*, vol. 50, no. 9, pp. 2379–2384, 1977.
- [33] N. M. F. S. A. Cerqueira, P. A. Fernandes, L. A. Eriksson, and M. J. Ramos, "Ribonucleotide activation by enzyme ribonucleotide reductase: Understanding the role of the enzyme," *Journal of Computational Chemistry*, vol. 25, no. 16, pp. 2031–2037, 2004.
- [34] P. A. Fernandes and M. J. Ramos, "Theoretical insights into the mechanism for thiol/disulfide exchange," *Chemistry—A European Journal*, vol. 10, no. 1, pp. 257–266, 2004.
- [35] V. Pelmenschikov, K.-B. Cho, and P. E. M. Siegbahn, "Class I ribonucleotide reductase revisited: the effect of removing a proton on Glu441," *Journal of computational chemistry*, vol. 25, no. 3, pp. 311–321, 2004.

Chapter 5

Inactivation of aerobic *Escherichia coli* ribonucleotide reductase by 2',2'-difluoro - 2' - deoxycytidine - 5' - diphosphate: studies on the structure of a substrate-based radical and evidence for covalent modification

5.1 Introduction

2',2'-difluorodeoxycytidine (dFdC or gemcitabine) is a dC analog used clinically in the treatment of non-small cell lung and pancreatic cancers.¹ Biological activity of dFdC has been demonstrated to arise from its inhibitory actions directed at DNA metabolism.^{2,3} As a nucleoside analog, gemcitabine is a pro-drug and must be metabolized in the cell to the active nucleotide forms. dFdC is transported across the cell membrane by nucleoside transporters (equilibrative nucleoside transporter 1 (ENT1), equilibrative nucleoside transporter 2 (ENT2), concentrative nucleoside transporter 1 (CNT1)). Once inside the cell, it is phosphorylated by human deoxycytidine kinase (HdCK) to its 5'-monophosphate (dFdCMP).⁴ Human UMP - CMP kinase is thought to convert dFdCMP to the 5'-diphosphate (dFdCDP) *in vivo*.^{5,6} Conversion of dFdCDP to the 5'-triphosphate (dFdCTP) has not been studied extensively. Intracellularly, this reaction is most likely carried out by nucleoside diphosphate kinases.⁷ We have shown that dFdCTP can be generated *in vitro* by the action of pyruvate kinase on dFdCDP in the presence of phosphoenolpyruvate (PEP).⁸

dFdCTP is believed to be the major causative agent of apoptosis in malignant cells.² It exerts its action by incorporating into DNA where it causes stalling of DNA synthesis and DNA chain termination.⁹ This mode of action is potentiated by the ability of dFdCDP to inhibit human ribonucleotide reductase (RNR).¹⁰⁻¹³ Inhibition of RNR results in depleted

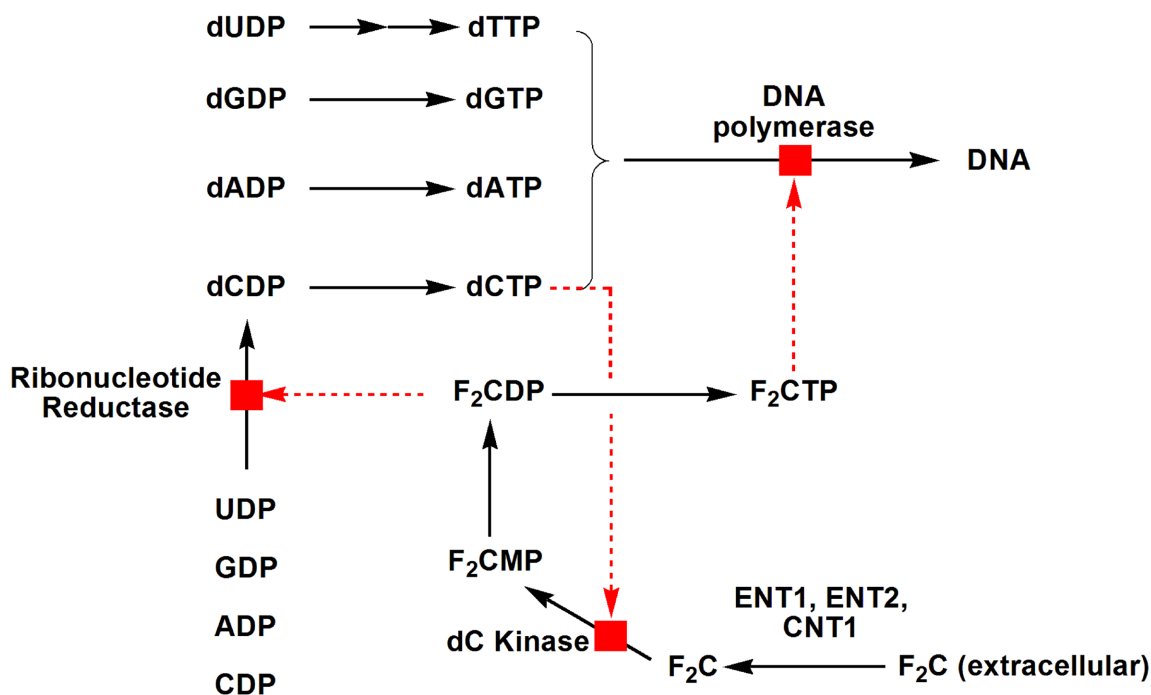


Figure 5.1: Gemcitabine metabolism

levels of deoxyribonucleotides in the cell and allows dFdCTP to successfully compete with dCTP for incorporation into DNA. Further downstream effects of depleted dNTP levels include the release of tight feedback inhibition of HdCK by dCTP and the decrease in activity of dCMP deaminase.¹⁴ As a result, dFdC is more efficiently processed to dFdCMP and subsequently to the diphosphate and triphosphate forms. This ability of dFdC-derived nucleotides to affect their own metabolism has been termed “self-potential” and has made dFdC unique among nucleoside analogs (Figure 5.1).

Although the major mechanism by which dFdC metabolites cause cell death involves stalling of DNA replication through DNA chain termination with concomitant induction of apoptosis, the efficiency of this process is directly related to the altered dNTP pools in the cell, and therefore relies on the inhibition of RNR by dFdCDP. Several recent reports in the literature have shown that dFdC resistance in malignant cell lines is coupled to elevated levels of RNR subunits. Precisely which subunit is up-regulated and to what extent is tissue specific.^{15,16} The detailed understanding of the mechanism of inhibition of RNR by dFdCDP and the role of tissue-specific RNR subunit overexpression in dFdC resistance remain unresolved issues.

E. coli RNR has been used as the prototype of the human enzyme (Chapter 1). Preliminary studies in our laboratory on the inactivation of *E. coli* RNR by dFdCDP revealed that the mode of inhibition is reductant-dependent.¹³ In the presence of a reducing system, such as thioredoxin/thioredoxin reductase/reduced nicotinamide adenine dinucleotide phosphate

(TR/TRR/NADPH) or 1,4-dithiothreitol (DTT), inhibition results from the inactivation of the catalytic subunit (R1) of RNR. In the absence of reductants, inhibition results from the loss of the essential tyrosyl radical ($Y\cdot$) located on the R2 subunit of RNR. R2 inactivation is also observed with the C-terminal tail cysteine double mutant of R1 (C754S/C759S-R1) in the presence of TR/TRR/NADPH. In both cases, $Y\cdot$ loss is accompanied by formation of a new stable radical whose 9 GHz EPR spectrum shows hyperfine interactions with two spin 1/2 nuclei with coupling constants of ~ 12 G. EPR studies in $^2\text{H}_2\text{O}$ and with perdeuterated-R1 ([U- ^2H]-R1) revealed that the hyperfine interactions are not derived from solvent or from R1. Furthermore, examination of the microwave power saturation of the observed signal indicated that its spin-lattice relaxation time (T1) is not enhanced due to magnetic dipolar and exchange interactions with the diferric cluster on R2, and that therefore, the radical is not adjacent to the di-iron cluster on R2. In addition, initial quantification of the products of inactivation by non-labeled dFdCDP suggested that two equivalents of fluoride and one equivalent of cytosine were released per R1 both in the presence and in the absence of reductants.¹³

All initial time-dependent inactivation experiments of *E. coli* RNR by dFdCDP were carried out at 15 μM enzyme concentration.¹³ Recently, Ge *et al.* have reported a threefold decrease in the k_{cat} value of R1 at 15 μM enzyme concentration relative to the k_{cat} value at 3 μM enzyme concentration.¹⁷ Ge *et al.* suggested that the decline in turnover numbers may be associated with a change in the rate-limiting step at high protein concentrations, or possibly with altered aggregation states of R1. Here, time-dependent inactivation of R1 and R2 subunits of *E. coli* RNR in the presence and in the absence of reductants at 3 μM enzyme concentration is reported. We find that two equivalents of dFdCDP are necessary for complete loss of R1 activity in the presence of reductants, as well as that two equivalents of dFdCDP are necessary for complete loss of R2 activity in the absence of reductants. Stoichiometry of cytosine release in the presence and in the absence of reductants is obtained with [5- ^3H]-dFdCDP. Additionally, we show that under physiologically relevant reducing conditions, inhibition of RNR by dFdCDP is a result of covalent modification that requires C225. The first 140 GHz EPR analysis of the radical formed in the absence of reductants is reported and the principal g-values of the radical are determined. We show that one of the hyperfine interactions is derived from the 1'-proton. The implications of these findings on the mechanism of RNR inactivation by dFdCDP are discussed.

5.2 Materials and methods

5.2.1 Purchased materials and materials obtained as gifts

Triethylamine (99% pure) was purchased from Acros, and 1,4-dithiothreitol (DTT) from Mallinckrodt. DEAE Sephadex A-25 was obtained from Pharmacia. [5- ^3H]-2',2'-difluoro-2'-deoxycytidine (1 mCi, 14 Ci/mmol) was purchased from Moravek Biochemicals. Bio-Express medium for growth of perdeuterated R2 was obtained from Cambridge Isotope Laboratories. All other materials were purchased from Sigma.

2',2'-difluoro-2'-deoxycytidine was a gift from Eli Lilly and Company. [1' - ^2H] - 2',2'-difluoro-2'-deoxycytidine and [1' - ^3H] - 2',2'-difluoro-2'-deoxycytidine-5'-diphosphate (S.A. 8261 cpm/nmol) were gifts from Gregory Lohman.

5.2.2 Protein overexpression, purification, and activity assays

Wild type *E. coli* R1 protein was purified as previously described¹⁸ and had specific activity (S.A.) of 2200–3000 nmol · mg⁻¹ · min⁻¹ by the spectrophotometric RNR assay, and S.A. of 1799–2000 nmol · mg⁻¹ · min⁻¹ by the [^{14}C] - CDP radioactive assay. R1 concentration was determined using $\varepsilon_{280\text{nm}} = 189 \text{ mM}^{-1} \cdot \text{cm}^{-1}$. R1 was pre-reduced prior to each experiment as described below.

Wild type *E. coli* R2 was isolated as previously described¹⁹ and had S.A. of 6000–7000 nmol · mg⁻¹ · min⁻¹. R2 concentration was determined using $\varepsilon_{280\text{nm}} = 130.5 \text{ mM}^{-1} \cdot \text{cm}^{-1}$. Tyrosyl radical content was measured both by the drop-line correction method and by EPR spectroscopy as previously reported.²⁰ R2 contained 1.1–1.2 Y · per dimer based on both methods of quantification. All R2 concentrations are reported per dimer.

E. coli thioredoxin (TR) was isolated from strain pTrX BL21 (DE3) and had S.A. of 40 units · mg⁻¹.¹² *E. coli* thioredoxin reductase (TRR) was isolated from strain pMR14 K91 and had S.A. of 1600 units · mg⁻¹.²¹

Prereduction of R1

Prereduced R1 was prepared either on a small scale prior to each experiment using the spin column protocol described below, or on a 10 mg scale using the gravity G-25 column protocol described below.

Prereduction by the spin column protocol In a typical pre-reduction experiment, 40–60 μM R1 was incubated with 35 mM DTT at 25 °C for 20 min in a final volume of 50–60 μL .

Prior to each experiment, pre-packed Bio-Spin columns (1 mL of G-25 resin in 10 mM TRIS pH 7.4 from BioRad) were pre-equilibrated in RNR assay buffer (50 mM HEPES pH 7.6, 15 mM MgSO₄, 1 mM EDTA) by the addition of 500 μL of assay buffer to the top of the column and centrifugation of the column at 1000 × g for 1 min. The procedure was repeated three additional times.

The mixture of R1 and DTT was loaded onto a pre-equilibrated Bio-Spin G-25 column (1 mL, BioRad) and the column spun at 1000 × g for 4 min. The flow-through of the column was collected (typically 60–70 μL) and loaded onto a second pre-equilibrated Bio-Spin column. The flow-through from the second column was directly used in the experiments without freezing.

To ensure that complete DTT removal was achieved, a control experiment was performed in which 50 μL of a 35 mM DTT solution were loaded onto a pre-equilibrated Bio-Spin column and the column centrifuged at 1000 × g for 4 min. The flow-through

of the column (60 μL) was collected, and 50 μL were assayed for DTT content by the 5, 5'-dithio-bis(2-nitrobenzoic acid) (DTNB) assay.²² A second experiment was performed in which the flow-through from a Bio-Spin column as above (60 μL) was loaded onto a second pre-equilibrated Bio-Spin column. The second column was then centrifuged at $1000 \times g$ for 4 min and 50 μL of the flow-through were assayed for DTT content by the DTNB assay. Use of the first column resulted in the removal of $\sim 90\%$ of DTT. After the second column, no DTT was detected under the conditions of the DTNB assay.

Prereduction by the sephadex G-25 column protocol R1 (10.3 mg) in a final volume of 1 mL (60 μM final concentration) was incubated with 30 mM DTT for 30 min at 25 $^{\circ}\text{C}$ in 50 mM HEPES pH 7.6, 15 mM MgSO_4 , 1 mM EDTA. The mixture was loaded onto a 20 mL G-25 column (1 \times 25.5 cm) pre-equilibrated in the same buffer. Fractions of 1 mL were collected and assayed for protein content by $A_{280\text{nm}}$. Fractions 10 through 15 were collected. The protein was concentrated in a centricon device fitted with a 30000 MW cutoff YM membrane to a final concentration of 36 μM . One hour elapsed between the time the protein was loaded onto the G-25 column and frozen in aliquots. The protein thus obtained was either used in experiments directly, or frozen in liquid N_2 and kept at -80°C for up to ten days. Single turnover experiments were carried out periodically over the storage period of 10 days in order to assess if oxidation of thiols took place under these conditions.

Single turnover experiments to assess oxidation of R1 at -80°C

Experiments were carried out immediately after prereduction of the enzyme and following 5 and 10 days of storage at -80°C . In a final volume of 110 μL , the reaction mixtures contained 3 μM R1, 3 μM R2 (S.A. $7000 \text{ nmol} \cdot \text{mg}^{-1} \cdot \text{min}^{-1}$, 1.2 Y per dimer), 1 mM [^{14}C]-CDP (S.A. 12630 cpm/nmol), and 1.6 mM ATP in 50 mM HEPES pH 7.6, 15 mM MgSO_4 , 1 mM EDTA buffer.

Before addition of R1, a 46 μL aliquot of the reaction mixture was withdrawn. The reaction was initiated by the addition of R1 and incubated at 25 $^{\circ}\text{C}$ for 25 min. At this time, a 50 μL aliquot was withdrawn. Both the aliquot withdrawn before addition of R1 (0 min) and the aliquot withdrawn after 25 min (25 min) were then placed in a boiling water bath for 2 min. The aliquots were chilled on ice for 3 min and the precipitated protein removed by centrifugation. To each aliquot, 12.5 μL of 0.5 M TRIS pH 8.5, 1 mM EDTA buffer and 20 units of calf intestine alkaline phosphatase (Boehringer-Mannheim, one unit is defined as the amount of enzyme required to catalyze the hydrolysis of 1 μmol 4-nitrophenyl phosphate per min at 37 $^{\circ}\text{C}$ in 1 M diethanolamine, 10.9 mM 4-nitrophenyl phosphate, 0.5 mM MgCl_2 , pH 9.8) were added. The mixtures were then incubated at 37 $^{\circ}\text{C}$ for 2 h.

dC and cytidine from a 65 μL aliquot of each mixture were separated on Dowex-1 borate columns by the procedure of Steeper and Steuart²³ using 200–400 mesh resin. The columns were eluted with 10 mL of dH_2O . One mL of eluent was mixed with 9 mL of Emulsifier-Safe scintillation fluid from Packard and analyzed for radioactivity on a Beckman LS 6500 Scintillation Counter.

Purification of C225S - R1

E. coli C225S-R1^{24,25} was purified as previously described for wild type R1¹⁸ except that fractions collected from the DEAE column were assayed for C225S-R1 content by 10% SDS-PAGE.

Overexpression of R2 in deuterated media

BL21 (DE3) pTB2 strain was acclimated to growth in LB containing ²H₂O through five successive growth phases starting in LB prepared in 25% ²H₂O, switching to LB prepared in 50% ²H₂O, LB prepared in 75% ²H₂O, LB prepared in 90% ²H₂O, and finally LB prepared in 100% ²H₂O. Each culture was grown to OD₆₀₀ of 0.7 at 37 °C and subsequently reinoculated to an OD₆₀₀ of 0.1 in the medium with higher ²H₂O content. The acclimated strain was then grown on a 5 mL scale in BioExpress medium (Cambridge Isotope Laboratories) prepared in ²H₂O according to manufacturer's instructions. R2 overexpression was induced at OD₆₀₀ = 0.74 with 1 mM IPTG dissolved in ²H₂O. Cell yield was determined, and induction was assessed by SDS-PAGE.

Purification of [U - ²H] - R2

All steps were carried out at 4 °C. Cell paste (250 mg) was resuspended in 3 mL of purification buffer (50 mM TRIS pH 7.6, 5% v/v glycerol, 1.0 mM PMSF) and 150 µL of Sigma protease inhibitor cocktail. Resuspended cells were lysed by two passes through the French pressure cell at 14000 psi. The resulting cell lysate was cleared by centrifugation at 14000 rpm for 10 min. The supernatant was brought to 1% streptomycin sulfate by the dropwise addition of 1/9 volumes of 10% streptomycin sulfate in standard buffer over the course of 20 min. The solution was then stirred for 20 additional min. The lysate was cleared by centrifugation at 14000 rpm for 20 min. The resulting supernatant was brought to 60% ammonium sulfate saturation over 20 min, and then stirred for 30 additional min. Precipitated protein was collected by centrifugation at 14000 rpm for 20 min. The protein pellet was redissolved in 800 µL of purification buffer and loaded onto a 10 mL (1 × 12.5 cm) Sephadex G-25 column. Protein containing fractions as judged by brown color and A_{280 nm} were pooled and loaded onto a 6.7 mL DEAE Sepharose Fast Flow column (1 × 8.5 cm) which was then washed with three column volumes of purification buffer, followed by four column volumes of purification buffer containing 110 mM NaCl. R2 was eluted with 140 mM NaCl in purification buffer. R2 containing fractions were pooled based on A_{410 nm}, diluted to 70 mM NaCl, and loaded onto a 5 mL Q-Sepharose column pre-equilibrated with purification buffer containing 70 mM NaCl. The column was washed with three column volumes of purification buffer containing 225 mM NaCl and then eluted with purification buffer containing 300 mM NaCl. Fractions containing R2 as judged by A_{410 nm} were pooled and concentrated in an Amicon device fitted with a YM-30 membrane.

Overexpression, purification, and reconstitution of apo-6xHis-R2 for characterization in time-dependent inactivation experiments with dFdCDP

Overexpression of apo-6xHis-R2 Wt-apo-6xHis-R2 was overexpressed from the pHISR2 plasmid constructed and sequenced by Yongting Wang. Growth was carried out in the presence of 50 $\mu\text{g}/\text{mL}$ kanamycin at 37 °C. *E. coli* BL21 (DE3) competent cells from Novagen were transformed with pHISR2 using the standard protocol²⁴ and grown on LB-agar plates overnight. Single colonies were used to seed 100 mL LB cultures which were grown overnight for 12 h. Cells from an overnight culture were collected at 3000 rpm and resuspended in 10 mL of fresh LB. The entire resuspension was then used to inoculate 10 L of LB in a New Brunswick Scientific 10 L fermenter, model MF-118. The culture was grown with 500 rpm agitation and 15000 cm^3/min air flow until OD_{600} reached 0.85. At this time, 100 mM 1,10-phenanthroline (Sigma) in 0.1 M HCl was added to a final concentration of 100 μM . The culture was incubated in the presence of 1,10-phenanthroline for 15 min before addition of IPTG to a final concentration of 1 mM. Cells were harvested 5 h after induction by centrifugation at 4 °C, 8000 rpm.

Purification of apo-6xHis-R2 All steps were performed at 4 °C. Cell paste (21.2 g) was resuspended in 100 mL of purification buffer (50 mM TRIS pH 7.6, 500 mM NaCl, 10 mM imidazole, 0.5 mM PMSF) and 5 mL of Sigma protease inhibitor cocktail were added. Partially suspended cells were homogenized in a glass homogenizer, and the crude cell suspension was passed through the French pressure cell at 14000 psi. The suspension was incubated with 100 units of DNase I (Sigma) for 20 min with stirring. The cells were then passed once again through the French pressure cell at 14000 psi. Crude cell lysate was spun for 20 min at 12000 rpm to pellet the insoluble cellular debris. The resulting supernatant was loaded onto a 60 mL (2.5×12 cm) Ni-NTA column (Qiagen) pre-equilibrated in purification buffer. Loading was done at a flow rate of 1 mL/min. The column was washed with 27 column volumes (CVs) of purification buffer at a flow rate of 2 mL/min. Protein was eluted in purification buffer containing 250 mM imidazole and no protease inhibitors at a flow rate of 6 mL/min. Column fractions (9 mL) were examined for protein by $A_{280 \text{ nm}}$. Fractions 7 through 9 were pooled and loaded directly onto a 1 L G-25 column (4.5×52 cm) equilibrated in 50 mM TRIS pH 7.6, 5% (v/v) glycerol. Protein-containing fraction as judged by $A_{280 \text{ nm}}$ were pooled and concentrated in an Amicon filtration device fitted with a YM-30 membrane to a final concentration of 12 mg per mL (137.8 μM). Protein purity was judged by SDS-PAGE analysis and UV/Vis absorption.

Reconstitution of apo-6xHis-R2 Apo-6xHis-R2 was reconstituted as described for wt-R2.²⁰ Following reconstitution, 2×36 mg of apo-6xHis-R2 (8 mL of a 114 μM solution from two reconstitution reactions) were incubated with 10 mM ascorbate at RT for 5 min. Ascorbate stock solution was prepared in degassed buffer. The mixture was loaded onto a 200 mL (2.5×40 cm) G-25 column equilibrated in 50 mM TRIS pH 7.6, 5% v/v glycerol to remove excess iron as well as ascorbate. Visibly green fractions (7 through 10, 4.3 mL each)

were pooled. The fractions were concentrated in an Amicon 50 device from Millipore, and the protein analyzed by SDS-PAGE. Measurements of radical content for the reconstituted protein were carried out spectrophotometrically using the published dropline correction method ($A_{412 \text{ nm}} - (2 \times A_{406 \text{ nm}} + 3 \times A_{416 \text{ nm}})/5$) and an extinction coefficient of $1.78 \text{ mM}^{-1} \cdot \text{cm}^{-1}$.²⁰

5.2.3 Time-dependent inactivation of R1 and R2 by dFdCDP in the presence and absence of reductants

In a final volume of 110 μL , a typical inactivation mixture contained 1.6 mM ATP, 3 μM pre-reduced R1 (wt or mutant, all R1 concentrations are reported per dimer), 3 μM R2 (wt or perdeuterated, all R2 concentrations are reported per dimer), 3, 6, or 15 μM dFdCDP, and no reductants, or 5 mM DTT, or 20 μM TR, 0.5 μM TRR, 1.0 mM NADPH, all in 50 mM HEPES pH 7.6, 15 mM MgSO_4 , 1 mM EDTA. All reactions were carried out at 25 $^\circ\text{C}$. Inhibition was initiated by the addition of dFdCDP. Before initiation, an aliquot of the reaction mixture was assayed as described below to determine activity at time zero.

R1 inactivation measurements During the inactivation, 15 μL aliquots of the inhibition mixture were removed at predetermined timepoints (0.5, 2.0, 4.0, 6.5, 10.5, 15, and 23 min) and diluted with 435 μL of the assay mixture at final concentrations of 1.6 mM ATP, 0.1 μM R1, 0.5 μM R2, 1 mM CDP, 20 μM TR, 0.5 μM TRR, and 0.2 mM NADPH, all in 50 mM HEPES pH 7.6, 15 mM MgSO_4 , 1 mM EDTA. Deoxynucleotide was quantified based on decrease in $A_{340 \text{ nm}}$ over the course of 1 min ($6.22 \text{ mM}^{-1} \cdot \text{cm}^{-1}$) as previously described.²⁶

Alternatively, for the radioactive assay, 5 μL aliquots of the inhibition mixture were removed and incubated with 95 μL of the assay mixture at final concentrations of 1.6 mM ATP, 0.1 μM R1, 0.5 μM R2, 1 mM [^{14}C]-CDP (S.A. 3200–5000 cpm/nmol), 20 μM TR, 0.5 μM TRR, and 1.0 mM NADPH, all in 50 mM HEPES pH 7.6, 15 mM MgSO_4 , 1 mM EDTA. The resulting solution was incubated at 25 $^\circ\text{C}$ for 5 min, at which point it was quenched with 50 μL of 2% (v/v) perchloric acid and placed on ice. After all time points were collected (typically ~ 25 min, time points as above for the spectrophotometric assays), the quenched reaction mixture aliquots were neutralized with 50 μL 0.4 M KOH (aliquot pH = 7.45 after base addition). Precipitated protein was removed by centrifugation. To each aliquot, 50 μL of 0.5 M TRIS pH 8.6, 1 mM EDTA and 20 units of calf intestine alkaline phosphatase (Boehringer-Mannheim) were added and the mixtures incubated at 37 $^\circ\text{C}$ for 2 h. To all mixtures, 100 nmol of dC carrier were added, and dC and cytidine were separated on Dowex-1 borate columns by the procedure of Steeper and Steuart using 200–400 mesh resin.²³ The columns were eluted with 10 mL of dH_2O . One mL of eluent was mixed with 9 mL of Emulsifier-Safe scintillation fluid from Packard and analyzed for radioactivity on a Beckman LS 6500 Scintillation Counter.

R2 inactivation measurements R2 activity was measured as described above except that final R1 concentration in assay mixtures was 0.5 μM , final R2 concentration in assay mixtures was 0.1 μM , and the timepoints were 1.0, 3.0, 5.0, 7.5, 11.0, 17.0, and 24.0 min.

5.2.4 Tyrosyl radical loss on R2 in the presence of dFdCDP

In a final volume of 450 μL , the inhibition mixtures contained 1.6 mM ATP or 0.75 mM TTP or no effector, 15 μM pre-reduced wt-R1, 15 μM wt-R2, and 75 μM dFdCDP, all in 50 mM HEPES pH 7.6, 15 mM MgSO_4 , 1 mM EDTA. All components except for dFdCDP were mixed and equilibrated at 25 $^\circ\text{C}$ for 10 min. Prior to initiation, the spectrum of the reaction mixture from 350–550 nm was recorded. Reactions were initiated by the addition of dFdCDP. Loss of $A_{410\text{ nm}}$ was monitored until no further change was observed (~ 15 min) at which point the spectrum of the reaction mixture from 350–550 nm was recorded.

5.2.5 Phosphorylation of [5- ^3H] - dFdC to form [5- ^3H] - dFdCMP

The synthesis of [5- ^3H] - dFdCMP was carried out by the enzymatic method described in Section 3.2 with 50 μCi of radioactivity using a total of 5 μmol of [5- ^3H] - dFdC (Moravek) with S.A. of 22958 ± 345 cpm/nmol. In a final volume of 5 mL, the reaction contained 1 mM [5- ^3H] - dFdC, 1.33 mg/mL 6xHis-HdCK (S.A. $170\text{ nmol} \cdot \text{mg}^{-1} \cdot \text{min}^{-1}$), 2 mM ATP, 2 mM DTT, and 0.5 mg/mL BSA, all in 50 mM TRIS pH 7.6, 100 mM KCl, 5 mM MgCl_2 . The reaction was initiated by the addition of 6xHis-HdCK and incubated in a 37 $^\circ\text{C}$ circulating water bath for 10 min.

Anion-exchange purification of the monophosphate was carried out on a 15 mL DEAE A-25 Sephadex column (1×19 cm) with a linear gradient of 90×90 mL of 0.005–0.4 M TEAB pH 7.5 in dH_2O as the mobile phase. Fractions of 9 mL (300 drops) were collected. Five μL of each fraction were mixed with 10 mL of Emulsifier-Safe scintillation fluid from Packard and analyzed for radioactivity on a Beckman LS 6500 Scintillation Counter. Fractions 18 through 24 were pooled and concentrated *in vacuo* seven times from a mixture of ethanol and water to remove excess TEAB. The product was obtained in 93% yield as judged by UV/Vis absorption (λ_{max} 271 nm, λ_{min} 249 nm) and recovery of radioactivity.

5.2.6 Phosphorylation of [5- ^3H] - dFdCMP to form [5- ^3H] - dFdCDP

[5- ^3H] - dFdCDP was prepared on a 4.65 μmol scale from [5- ^3H] - dFdCMP. The reaction contained in a final volume of 4.65 mL 1 mM [5- ^3H] - dFdCMP, 65 $\mu\text{g/mL}$ human GST-UMP-CMP kinase (S.A. $4.8\text{ } \mu\text{mol} \cdot \text{mg}^{-1} \cdot \text{min}^{-1}$), 4 mM ATP, and 2 mM DTT all in 50 mM TRIS pH 8.0, 5 mM MgCl_2 . Reactions were initiated by the addition of human GST-UMP-CMP kinase and incubated at 37 $^\circ\text{C}$ for 30 min. The diphosphate material was purified over a DEAE column (15 mL, 1×19 cm) using a 120×120 mL linear gradient of 5 mM to 0.6 M TEAB pH 7.5 in dH_2O collecting 6 mL fractions. Fractions were assayed by scintillation counting as described above for [5- ^3H] - dFdCMP synthesis. Fractions 28 through 36 eluting at 0.4 M TEAB and containing the diphosphates [5- ^3H] - dFdCDP and ADP were pooled and concentrated *in vacuo* six times from a mixture of ethanol and water to remove excess TEAB²⁷ and then dissolved in 1 mL of dH_2O .

To the aqueous solution of [5-³H]-dFdCDP and ADP, 0.5 M freshly prepared sodium periodate (Sigma) solution in water was added to a final concentration of 18.6 mM (4 equivalents relative to starting [5-³H]-dFdCMP). The mixture was incubated at 37 °C for 10 min. After this time period, 4 M methyl amine solution was added to a final concentration of 100 mM, and the mixture incubated at 37 °C for 20 additional min. The 4 M methyl amine stock solution was freshly prepared from a commercially available 40% aqueous solution and brought to pH 7.3 by the dropwise addition of 85% phosphoric acid while stirring on ice. The oxidative cleavage was quenched by the addition of L-rhamnose to a final concentration of 37.5 mM (8 equivalents relative to starting [5-³H]-dFdCMP, 4 equivalents relative to starting periodate) followed by incubation at 37 °C for 10 additional min. To remove liberated pyrophosphate, the reaction was brought to 33 mM TRIS pH 7.2 by addition of 0.33 volumes of 100 mM TRIS pH 7.2 and incubated with 5U / 1.5 mL inorganic pyrophosphatase from Baker's yeast (E.C. 3.6.1.1, Sigma) in the presence of 1.6 mM MgCl₂. The reaction was incubated at 25 °C for 30 minutes. Before and after treatment with inorganic pyrophosphatase, the amount of contaminating pyrophosphate was measured by the method of O'Brien.²⁸ [5-³H]-dFdCDP was purified over a 15 mL DEAE Sephadex A-25 column (1 × 19 cm) running a 120 × 120 mL linear gradient of 0.005 M to 0.6 M TEAB pH 7.5 in dH₂O collecting 6 mL fractions. Fractions were assayed by scintillation counting as described above for [5-³H]-dFdCMP synthesis. Fractions 28 through 36 eluting at 0.4 M TEAB and containing [5-³H]-dFdCDP were pooled and concentrated *in vacuo* six times from a 1:1 mixture of ethanol and water to remove excess TEAB²⁷. The product was obtained in 78% final yield as judged by UV/Vis absorption (λ_{max} 271 nm, λ_{min} 249 nm) and recovery of radioactivity.

The ³¹P and ¹H NMR analyses of [5-³H]-dFdCDP were carried out in ²H₂O at pH 5.6. The ¹H NMR spectrum was acquired on a 500 MHz INOVA spectrometer from Varian. No internal standard was used for the proton NMR, and the spectrum was referenced based on the residual solvent peak: ¹H NMR (²H₂O) δ 4.13 (m, 1H), 4.30 (m, 2H), 4.56 (m, 1H), 6.10 (d, J = 7.6 Hz, 1H), 6.20 (t, J = 7.0 Hz, 1H), 7.85 (d, J = 7.6 Hz, 1H). The ³¹P NMR was acquired on a 300 MHz MERCURY spectrometer from Varian using 85% H₃PO₄ in water as the external standard: ³¹P NMR (²H₂O) δ -10.08 (d, J = 20.4 Hz, 1P), -5.95 (d, J = 20.0 Hz, 1P).

5.2.7 Phosphorylation of [1' - ²H] - dFdC to form [1' - ²H] - dFdCMP

[1' - ²H] - dFdCMP was synthesized on a 5 μ mol scale from a ~60:40 mixture of α : β anomers of [1' - ²H] - dFdC (~90% D atom incorporation as determined by ¹H NMR integration).²⁹ Since HdCK selectively converts the β nucleoside to the monophosphate,⁴ the α : β anomer mixture of [1' - ²H] - dFdC was phosphorylated directly in the presence of ATP as the phosphate donor using the enzymatic method described in Section 3.2. In a final volume of 5 mL, the reaction contained 1 mM [1' - ²H] - dFdC, 1.33 mg/mL 6xHis-HdCK (S.A. 170 nmol · mg⁻¹ · min⁻¹), 2 mM ATP, 2 mM DTT, and 0.5 mg/mL BSA, all in 50 mM TRIS pH 7.6, 100 mM KCl, 5 mM MgCl₂. The reaction was initiated by the addition of 6xHis-HdCK and incubated at 37 °C for 10 min.

Anion-exchange purification of the monophosphate was carried out on a 10 mL DEAE A-25 Sephadex column (1 × 13 cm) with a linear gradient of 100 × 100 mL of 0.005–0.4 M TEAB pH 7.5 in dH₂O as the mobile phase. Fractions of ~ 5 mL (175 drops) were collected. The fractions were assayed by UV/Vis absorption. Fractions 31 through 36, which eluted at 0.2 M TEAB and had an $A_{260\text{ nm}}/A_{280\text{ nm}}$ ratio characteristic of cytidine-derived nucleotides were pooled. Excess TEAB was removed by repeated cycles of dilution and concentration *in vacuo* from a 1:1 mixture of water and ethanol.²⁷ The product was obtained in quantitative yield as judged by UV/Vis absorption (λ_{max} 271 nm, λ_{min} 249 nm).

5.2.8 Phosphorylation of [1' - ²H] - dFdCMP to form [1' - ²H] - dFdCDP

[1' - ²H] - dFdCDP was synthesized on a 5 μmol scale from [1' - ²H] - dFdCMP. In a final volume of 5 mL, the reaction contained 1 mM [1' - ²H] - dFdCMP, 65 μg/mL human GST-UMP-CMP kinase (S.A. 4.8 μmol · mg⁻¹), 4 mM ATP, and 2 mM DTT all in 50 mM TRIS pH 8.0, 5 mM MgCl₂. Reactions were initiated by the addition of human GST-UMP-CMP kinase and incubated at 37 °C for 30 min. The diphosphate material was purified over a 10 mL DEAE A-25 Sephadex column (1 × 13 cm) using a linear gradient of 120 × 120 mL of 0.005–0.6 M TEAB pH 7.5 in dH₂O as the mobile phase. Fractions of ~ 5 mL (175 drops) were collected. Fractions were assayed by UV/Vis absorption. Fractions 31 through 39 were pooled. The material was concentrated *in vacuo* six times from a mixture of ethanol and water to remove excess TEAB and then dissolved in 1 mL of dH₂O.

To the above mixture of [1' - ²H] - dFdCDP and ADP in water, 0.5 M freshly prepared sodium periodate (Sigma) solution in water was added to a final concentration of 20 mM (4 equivalents relative to starting [1' - ²H] - dFdCMP). The mixture was incubated at 37 °C for 10 min. After this time period, 4 M methyl amine solution was added to a final concentration of 100 mM, and the mixture incubated at 37 °C for additional 20 min. The 4 M methyl amine stock solution was freshly prepared from a commercially available 40% aqueous solution and brought to pH 7.3 by the dropwise addition of 85% phosphoric acid while stirring on ice. The oxidative cleavage was quenched by the addition of L-rhamnose to a final concentration of 37.5 mM (8 equivalents relative to starting [5 - ³H] - dFdCMP, 4 equivalents relative to starting periodate) followed by incubation at 37 °C for 10 additional min. To remove liberated pyrophosphate, the reaction was brought to 33 mM TRIS pH 7.2 by addition of 0.33 volumes of 100 mM TRIS pH 7.2 and incubated with 5U / 1.5 mL inorganic pyrophosphatase from Baker's yeast (E.C. 3.6.1.1, Sigma) in the presence of 1.6 mM MgCl₂. The reaction was incubated at 25 °C for 30 minutes. Before and after treatment with inorganic pyrophosphatase, the amount of contaminating pyrophosphate was measured by the method of O'Brien.²⁸ [1' - ²H] - dFdCDP was purified over an 11 mL DEAE A-25 Sephadex column (1 × 14 cm) using a 100 × 100 mL linear gradient of 0.005–0.6 M TEAB pH 7.5 in dH₂O collecting 5 mL fractions. Fractions 40 through 46 eluting at 0.4 M TEAB concentration and with an $A_{260\text{ nm}}/A_{280\text{ nm}}$ ratio characteristic of cytidine-derived nucleotides were pooled. Excess TEAB was removed under reduced pressure by 6 cycles of dilution and

concentration from a 1:1 mixture of water and ethanol.²⁷ The product was obtained in 83% yield as judged by UV/Vis absorption (λ_{max} 271 nm, λ_{min} 249 nm). It was not characterized further.

5.2.9 Size-exclusion experiments with radio-labeled dFdCDP to look for evidence of covalent modification

In a final volume of 210 μ L, reactions in the absence of reductants external to RNR contained 3 μ M R1 (wt or mutant), 3 μ M R2 (wt or 6xHis), 6 μ M or 15 μ M [5-³H]-dFdCDP or [1'-³H]-dFdCDP, and 1.6 mM ATP, all in 50 mM HEPES pH 7.6, 15 mM MgSO₄, 1 mM EDTA. Reactions in the presence of reductants external to RNR were identical except that they contained either 5 mM DTT or 20 μ M TR, 0.5 μ M TRR, and 1.0 mM NADPH.

All reaction components except for the inhibitor were mixed and equilibrated at 25 °C for 5 min. A 15 μ L aliquot of the reaction mixture was removed to determine activity at time zero by the RNR spectrophotometric assay.²⁶ The inactivation was initiated by the addition of radio-labeled dFdCDP. After initiation, a second 15 μ L aliquot was removed and incubated for 30 min at 25 °C. The second aliquot was used to determine remaining activity after 30 min of inactivation. The inhibition mixtures were incubated at 25 °C either for 3 min or for 20 min. A 200 μ L aliquot of the reaction mixture was then removed. In the non-denaturing case, the 200 μ L aliquot was loaded directly onto a G-50 Sephadex column as described below. In the denaturing case, the 200 μ L aliquot was diluted with 600 μ L of 8 M guanidinium hydrochloride. The 20 mL G-50 columns (1 \times 25.5 cm) were equilibrated and run either in 50 mM HEPES pH 7.6, or 50 mM HEPES pH 7.6 containing 2 M guanidinium hydrochloride. Fractions of \sim 1 mL were collected. Aliquots of each fraction (500 μ L) were assayed by scintillation counting as described in Section 5.2.2. The protein content of the fractions was then determined by A_{280 nm} in the non-denaturing case.

5.2.10 Identification of non-covalent products generated during inactivation of RNR by dFdCDP

In a final volume of 1.1 mL, the reactions contained 1.6 mM ATP, 3 μ M pre-reduced wt-R1, 3 μ M wt-R2, 6 μ M [5-³H]-dFdCDP (S.A. 1.5–3 \cdot 10³ cpm per nmol), and either no reductants or 20 μ M TR, 0.5 μ M TRR, 1.0 mM NADPH, all in 50 mM HEPES pH 7.6, 15 mM MgSO₄, 1 mM EDTA. All components of the reaction were pre-equilibrated at 25 °C for 5 min and the reaction was then initiated by the addition of [5-³H]-dFdCDP. Before initiation, a 15 μ L aliquot of the reaction mixture was taken to measure activity at time zero by the RNR spectrophotometric assay.²⁶ The reaction was incubated at 25 °C for 30 min. A 15 μ L aliquot was then removed to assay remaining activity by the spectrophotometric assay.

Quantification of fluoride during inactivation of RNR by dFdCDP

After inactivation was confirmed as in the above paragraph, 1 mL of the above reaction mixture was transferred into an Amicon centrifugation device with a 5000 MW cutoff YM membrane in order to separate the protein from the low MW components of the reaction mixture. The flow-through was analyzed for fluoride content directly using the 96-09 Orion combination electrode and Orion digital pH/mV meter model 611. The electrode was filled with Optimum Results A reference electrode filling solution from Orion.

Fluoride standard curves in the 4–15 μM range were derived before each measurement from fluoride standards prepared in 50 mM HEPES pH 7.6, 15 mM MgSO_4 , 1 mM EDTA by dilution of the Orion 0.1 M fluoride solution. The standards were prepared in 2059 Falcon tubes (Fisher) in a final volume of 1 mL by pipetting. All measurements were carried out with the test-tube and the electrode equilibrated at 25 ± 0.1 °C for 10 min with the help of a custom-designed water jacket made by the MIT glassblowing shop. The jacket was connected to a circulating water bath. Temperature of the water jacket was monitored with an external thermocouple. All solutions were stirred at a constant speed.

Quantification of cytosine during inactivation of RNR by dFdCDP

Following fluoride measurements, 700 μL of the above solution were mixed with 175 μL of 0.5 M TRIS pH 8.5, 1 mM EDTA and 20 units of calf intestine alkaline phosphatase (Boehringer-Mannheim) and incubated at 37 °C for 2 h. The reaction was then transferred into an Amicon centrifugal device with a 5000 MW cutoff YM membrane in order to separate alkaline phosphatase from the small molecular weight components. The flow-through (750 μL) was combined with 120 nmol cytosine, 80 nmol dFdC, and 80 nmol dC and analyzed by reverse phase HPLC.

Reverse phase HPLC analysis was carried out on an Econosil C-18 RP column (4.5×250 mm, Alltech) at a flow rate of 1.0 mL/min using isocratic elution with 5 mM potassium phosphate buffer (pH 6.8) for 10 min, followed by a linear gradient to 30% methanol/70% phosphate buffer over the course of 30 min (retention times using this flow program were cytosine, 5 min; dC, 20 min; dFdC, 25 min). Alternatively, Adsorbosphere Nucleotide Nucleoside column from Alltech (250×4.6 mm) was used at a flow rate of 1.0 mL/min with an isocratic elution in 50 mM ammonium acetate (pH 6.8) for 10 min, followed by a linear gradient to 50% methanol/50% ammonium acetate over 30 min (retention times using this flow program were cytosine, 6 min; dC, 19 min; gemcitabine, 24 min). One minute fractions were collected. A 200 μL aliquot of each was mixed with 10 mL of Emulsifier-Safe scintillation fluid from Packard and analyzed for radioactivity on a Beckman LS 6500 Scintillation Counter.

5.2.11 Tryptic digest of wt-RNR inhibited by [1' - ³H] - dFdCDP in the presence of DTT

Labeling procedure

Labeling of RNR with [1' - ³H] - dFdCDP was carried out in a final volume of 510 or 1010 μ L. The reactions contained 15 μ M R1, 15 μ M R2, 30 μ M [1' - ³H] - dFdCDP S.A. 8261 cpm / nmol, 1.6 mM ATP, and 5 mM DTT, all in 50 mM HEPES pH 7.6, 15 mM MgSO₄, 1 mM EDTA. Reactions were initiated by the addition of [1' - ³H] - dFdCDP. R1 activity was measured prior to initiation and after 20 min of inactivation by the RNR spectrophotometric assay.²⁶ Following inactivation, 5 volumes of 0.4 M TRIS pH 8.0, 8 M GuHCl and DTT at a final concentration of 10 mM were added to the reactions. The mixtures were deoxygenated on a Schlenk line and incubated at RT for 0.5 h with stirring. Iodoacetamide was then added to a final concentration of 0.1 M in a minimum volume of 0.4 M TRIS pH 8.0, 8 M GuHCl. The mixtures were deoxygenated on a Schlenk line, and incubated in the dark at RT for 3 h with stirring.

Test of stability of the label formed during RNR inhibition by [1' - ³H] - dFdCDP in the presence of DTT

Stability of the covalent label on RNR formed in the presence of [1' - ³H] - dFdCDP and ATP under reducing conditions was assessed in the presence of 0.1% trifluoroacetic acid (TFA). An inactivation mixture was prepared as above in a final volume of 510 μ L. After the labeling with iodoacetamide was complete, two equivalents of β -mercaptoethanol relative to iodoacetamide were added and the mixture dialyzed against 12 L (3 \times 4 L) of dH₂O over a period of 12 h. The precipitated protein was then transferred to two siliconized pear-shaped flasks and lyophilized over 24 h. Following lyophilization, the protein was dissolved in 2 mL of 0.4 M TRIS pH 8.0, 6 M GuHCl denaturing buffer. One mL was dialyzed at RT against 80 mL of dH₂O containing 0.1% TFA for 4 h.

Digestion of RNR inhibited by [1' - ³H] - dFdCDP in the presence of DTT

Following labeling as described above, iodoacetamide and other small molecular weight components of the reaction were removed over a 40 mL G-50 column (1.5 \times 23 cm) equilibrated and run in NH₄HCO₃ pH 8.0, 2 M urea. Fractions were assayed by scintillation counting as described in Section 5.2.2. Fractions 10 through 14 constituting the sharp peak of radioactivity associated with the protein were pooled. Protein recovery was calculated based on a 1.05 labels per RNR ratio and the recovered radioactivity. TPCK treated trypsin was then added in a 1 to 60 ratio to R1. Concentration of trypsin was determined by A_{280 nm} using 1.21 AU \cdot mg⁻¹ \cdot mL⁻¹ as the extinction coefficient. The mixture was incubated at 37 $^{\circ}$ C and aliquots were taken at 10 and 20 h. Following digestion, the reaction aliquots were either lyophilized and then dissolved in dH₂O containing 0.1% v/v TFA or directly injected onto the HPLC system after the addition of TFA to a final concentration of 0.1% v/v. Analysis of the

tryptic digest was performed using a Jupiter C-18 column from Phenomenex (150 × 4.6 mm, 5 μm, 300 Å pore size) with a 0–45% gradient of MeCN 0.1% TFA in dH₂O 0.1% TFA over 45 min. Fractions were collected every minute. A 200 μL aliquot of each was assayed for radioactivity as described in Section 5.2.2.

5.2.12 9 GHz EPR experiments and simulations of the reaction of RNR with dFdCDP

Reaction composition

All reactions using wt, mutant, or deuterated proteins and non-labeled or specifically deuterated dFdCDP were carried out in a final volume of 230 μL. Final concentrations of reaction components were 15 μM R1, 15 μM R2, 75 μM dFdCDP, and 1.6 mM ATP, all in 50 mM HEPES pH 7.6, 15 mM MgSO₄, 1 mM EDTA.

Reactions in the presence of reductants external to RNR were carried out as described above with the addition of 20 μM TR, 0.5 μM TRR, 1.0 mM NADPH or 5 mM DTT to the inhibition reaction.

All reaction components except for the inhibitor were combined and incubated at 25 °C for 5 min. A 5 μL aliquot was then assayed spectrophotometrically²⁶ to determine initial R2 activity. The reaction was initiated by the addition of dFdCDP. An aliquot of the reaction was removed and incubated at 25 °C for 30 min. The remaining reaction mixture was transferred into a calibrated 706 PQ EPR tube and frozen in liquid N₂ at 0.5–4 min after initiation. The aliquot incubated at 25 °C for 30 min was assayed spectrophotometrically to confirm R2 inactivation.

Acquisition parameters

EPR spectra at 9 GHz were acquired on a Bruker ESP-300 spectrometer equipped with a Bruker high sensitivity 4119HS cylindrical cavity and an ER-041G microwave bridge containing an internal frequency counter. Measurements were carried out at 77 K using a liquid-helium cooled ESR-900 cryostat and an Oxford LLT 650/1.0 transfer line. Spectra were acquired at 20 μW with 100 kHz modulation frequency, 1 G modulation amplitude, conversion time of 20.48 ms, and time constant of 5.12 ms. Typically, the sweep width was 150 G and 2048 points were acquired per spectrum.

9 GHz EPR experiments with wide sweep-width and high modulation amplitude

The spectra were collected at 77 K under conditions described above, except that a sweep width of 700 G was used and 8192 points per spectrum were collected. Alternatively, the spectra were collected at 77 K as above, except that the modulation amplitude was set to 30 G.

9 GHz simulations

Simulations of 9 GHz EPR spectra were performed with the commercial software package SimFonia. The g -values determined from 140 GHz measurements were used: $g_{xx} = 2.00738$, $g_{yy} = 2.00592$, $g_{zz} = 2.00230$. All spectra were simulated with a Lorentzian to Gaussian line-shape broadening ratio of 1. Parameters for line-width and the components of the hyperfine coupling tensor, namely A_{xx} , A_{yy} , A_{zz} , were varied to obtain the best fit.

5.2.13 140 GHz EPR experiments of the reaction of RNR with dFdCDP

140 GHz experiments were carried out on reaction mixtures prepared in a final volume of 15 μ L containing 1.6 mM ATP, 75 μ M wt-R1, 75 μ M R2, and 300 μ M dFdCDP, all in 50 mM HEPES pH 7.6, 15 mM $MgSO_4$, 1 mM EDTA. All reaction components except for the substrate were combined and incubated at 25 $^{\circ}C$ for 5 min. The reaction was then initiated by the addition of dFdCDP and aliquots were drawn into suprasil capillaries (silica, OD 0.55 mm, ID 0.4 mm, from Wilmad LabGlass) by capillary action. The samples were frozen in liquid N_2 30 s to 3 min after initiation.

Acquisition parameters

Spectra were acquired at 60 K on a custom-designed pulsed spectrometer.³⁰ The stimulated echo sequence¹⁸ was used with a pulse length of $t_{\pi/2} = 72$ ns and a pulse spacing of $\tau = 230$ ns for spectra shown in Figure 4.10 or a pulse length of $t_{\pi/2} = 65$ ns and a pulse spacing of $\tau = 200$ ns for spectra shown in Figure 4.15. The external magnetic field was swept with the assistance of a field lock described elsewhere.³¹ The echo intensity at each field position was integrated, and an average of 1000 samples per point were taken. The number of scans and recycle delays were adjusted for different signal intensities and temperatures.

5.3 Results

5.3.1 Protein purification and assays

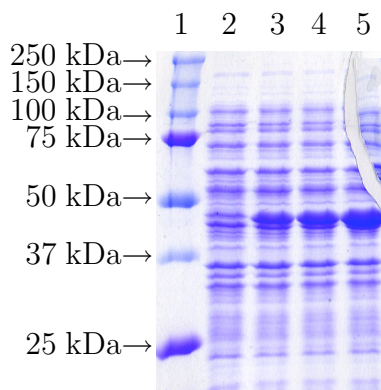
Single turnover experiments on prereduced R1

All experiments described in this chapter were carried out with prereduced R1. In some cases, prereduced R1 was stored at -80 $^{\circ}C$ for a maximum of 10 days before use. Single turnover experiments were first performed to establish if oxidation of R1 thiols to disulfides occurs at -80 $^{\circ}C$ over a period of 10 days.

Results are shown in Table 5.1. Experiment 1 was carried out immediately after prereduction, Experiment 2 after 5 days of storage at -80 $^{\circ}C$, and Experiment 3 after 10 days of storage at -80 $^{\circ}C$. The number of equivalents of dCDP formed per R1 decreased by 0.1 over the course of 10 days at -80 $^{\circ}C$. Thus, approximately 3% of R1 was oxidized.

<i>Experiment</i>	<i>Background cpm</i>	1 mL <i>Borate wash</i>	<i>Equivalents/R1</i>
Experiment 1	55	680	3.7
Experiment 2	53	671	3.6
Experiment 3	55	660	3.6

Table 5.1: Results of single turnover experiments



Lane 1 Bio-Rad marker Lane 4 8 h after induction
 Lane 2 Uninduced lysate Lane 5 15 h after induction
 Lane 3 4 h after induction

Figure 5.2: Induction of R2 in deuterated media

Overexpression and purification of perdeuterated R2

Overexpression of perdeuterated R2 was achieved using BioExpress medium from Cambridge Isotope Laboratories. The doubling time of *E. coli* BL21 (DE3) pTB2 in the BioExpress medium was ~ 6 h. From a 100 mL culture, 250 mg of cell paste were obtained. Overexpression was very good as evidenced by the induction gel shown in Figure 5.2 where a band of 43.5 kDa grows in after induction as a function of time.

Purification was carried out by the procedure described in Section 5.2.2. The gel of the final protein is shown in Figure 5.3. The protein is $\sim 90\%$ pure. A total of 1.5 mg of perdeuterated R2 were obtained from 250 mg of cell paste.

The radical content was determined to be 0.8 radicals per dimer using the published drop-line correction method.²⁰ The activity was measured to be $4010 \text{ nmol} \cdot \text{mg}^{-1} \cdot \text{min}^{-1}$ by the spectrophotometric RNR assay.²⁶

Time-dependent inactivation of perdeuterated R2 by dFdcDP was examined in the presence of wt-R1 and ATP with no reductants present as described in Section 5.2.3. The experiment revealed complete loss of R2 activity over the course of 15 min.

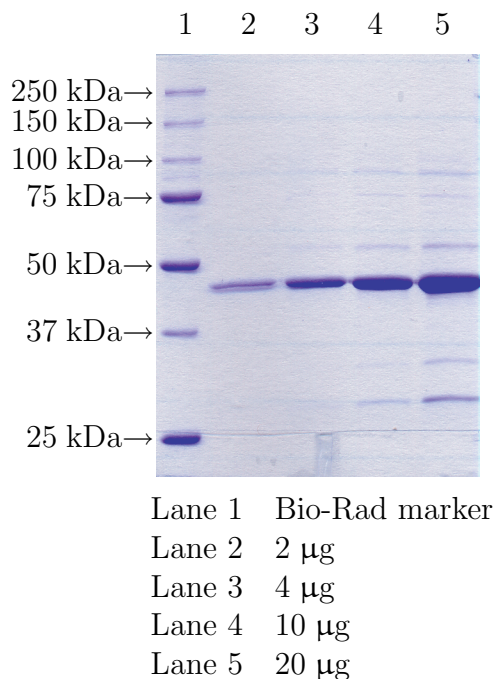


Figure 5.3: SDS-PAGE of purified perdeuterated R2

Overexpression, purification, and reconstitution of apo-6xHis-R2

Overexpression of apo-6xHis-R2 carried out in the New Brunswick 10 L fermentor resulted in very good cell yield of 2.2 g/L of culture. Average yield of cell paste in growths of apo-6xHis-R2 carried out in shaker flasks in the presence of 1,10-phenanthroline is 1.7 g/L of culture. The gel comparing total soluble cell protein before and after induction is shown in Figure 5.4. It reveals excellent induction of apo-6xHis-R2 (MW 43.5 kDa). Therefore, fermentor growth and induction of apo-6xHis-R2 offers improved yields over cultures grown in shaker flasks.

The purification gel of apo-6xHis-R2 is shown in Figure 5.5. The yield of apo-6xHis-R2 protein was 1.112 g from 22 g of cell paste. The protein is ~95% pure. The major contaminant is a band of approximate MW of 26 kDa. This band is present on denaturing gels of all apo-6xHis-R2 proteins that have been purified in the Stubbe laboratory thus far, and has been identified as an N-terminal apo-6xHis-R2 proteolytic fragment.³²

Following reconstitution, ascorbate treatment, and the final size-exclusion chromatographic step, the radical content of the reconstituted holo-6xHis-R2 (referred to as 6xHis-R2) protein was typically 1.2–1.3 tyrosyl radicals per dimer measured by the published drop-line correction method.²⁰ The activity was determined to be $6010 \text{ nmol} \cdot \text{mg}^{-1} \cdot \text{min}^{-1}$ by the spectrophotometric RNR assay.²⁶ The reconstituted protein was concentrated over a YM-50 membrane in an effort to separate the 26 kDa fragment from the full length protein. However, after the concentration step, the contaminant band of 26 kDa was still present. Possibly, this proteolytic fragment is forming multimers with itself or full length protein and

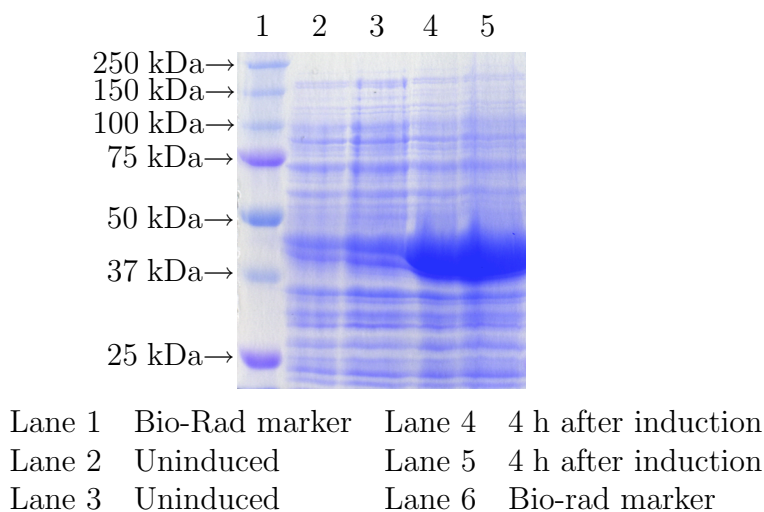


Figure 5.4: 6xHis - R2 induction gel

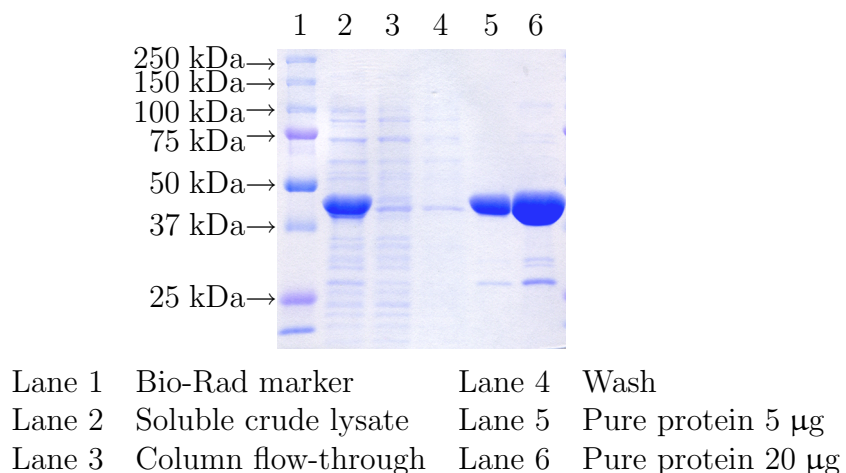


Figure 5.5: 6xHis - R2 purification gel

is thus retained in filtrations employing a 50 kDa MW cutoff membrane.

Time-dependent inactivation experiments of 6xHis-R2 in the presence of wt-R1, dFd-CDP, and DTT under conditions described in Section 5.2.3 revealed the expected complete loss of R1 activity and ~40% loss of 6xHis-R2 activity over the course of 15 min. Thus, in the presence of reductants, 6xHis-R2 behaves the same as wt-R2.

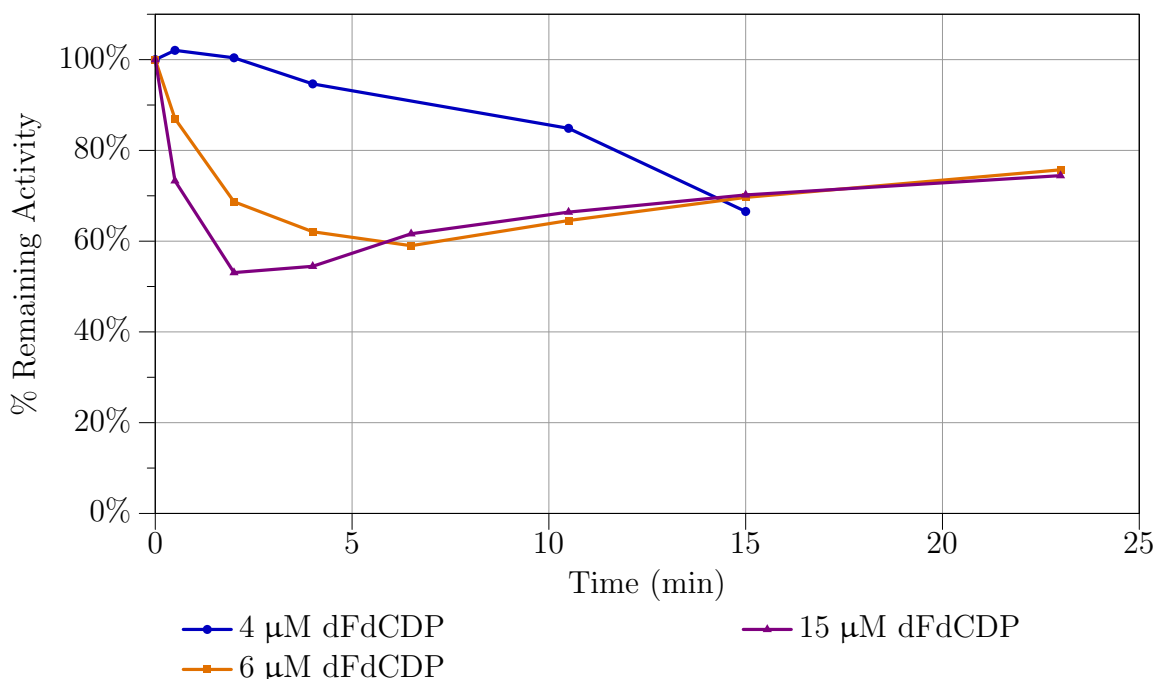


Figure 5.6: Time-dependent inactivation of R1 in the absence of reductants

5.3.2 Time-dependent inactivation of RNR subunits by dFdCDP at 3 μM enzyme concentration

As discussed in Section 5.1, all of the initial time-dependent inactivation experiments of *E. coli* R1 and R2 subunits by dFdCDP were carried out at 15 μM enzyme concentration using a fivefold molar excess of dFdCDP relative to R1 (all R1 and R2 concentrations are reported per dimer).¹³ Recently, Ge *et al.* have reported a threefold decrease in the k_{cat} value of R1 at 15 μM enzyme concentration relative to the k_{cat} value measured at 3 μM enzyme concentration.¹⁷ Thus, time-dependent inactivation of R1 and R2 by dFdCDP was reexamined at 3 μM enzyme concentration in the presence and in the absence of reductants using one, two, or five molar equivalents of the inhibitor relative to R1.

The results of inactivations carried out in the absence of reductants are shown in Figure 5.6 for R1 inactivation and Figure 5.7 for inactivation of R2. The experiments reveal that, in the absence of reductants, two equivalents of dFdCDP are needed for complete loss of R2 activity. Under those conditions, fast loss of 50% of the R1 activity was observed, followed by a recovery to about 70% of the original activity. A similar recovery of R1 activity has previously been observed with 2'-azido-2'-deoxyuridine-5'-diphosphate (N_3UDP),¹⁸ and may result from the dissociation of inactive R2 and nucleotide fragments from R1 which liberate R1 for additional turnover.

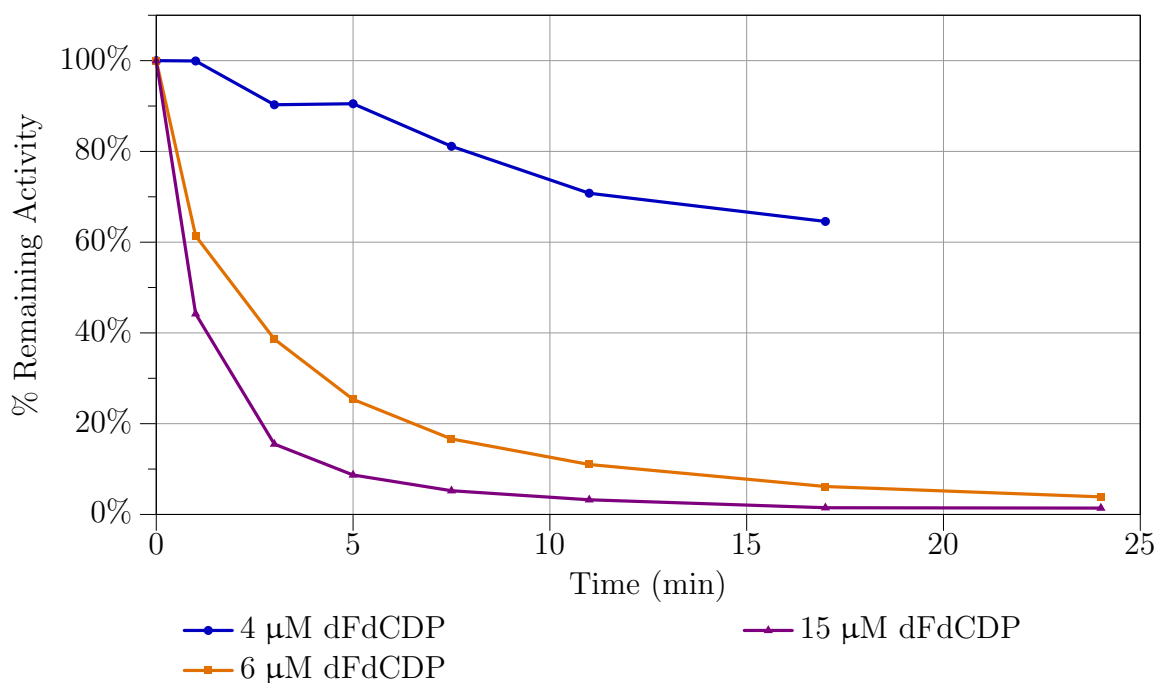


Figure 5.7: Time-dependent inactivation of R2 in the absence of reductants

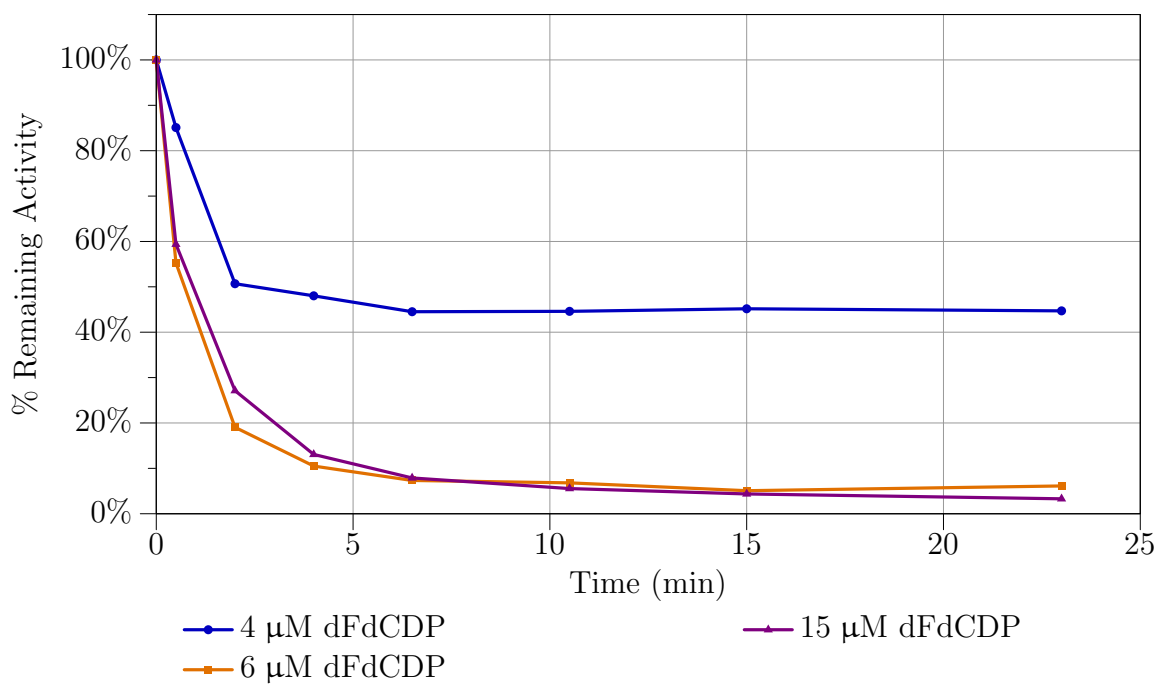


Figure 5.8: Time-dependent inactivation of R1 in the presence of reductants

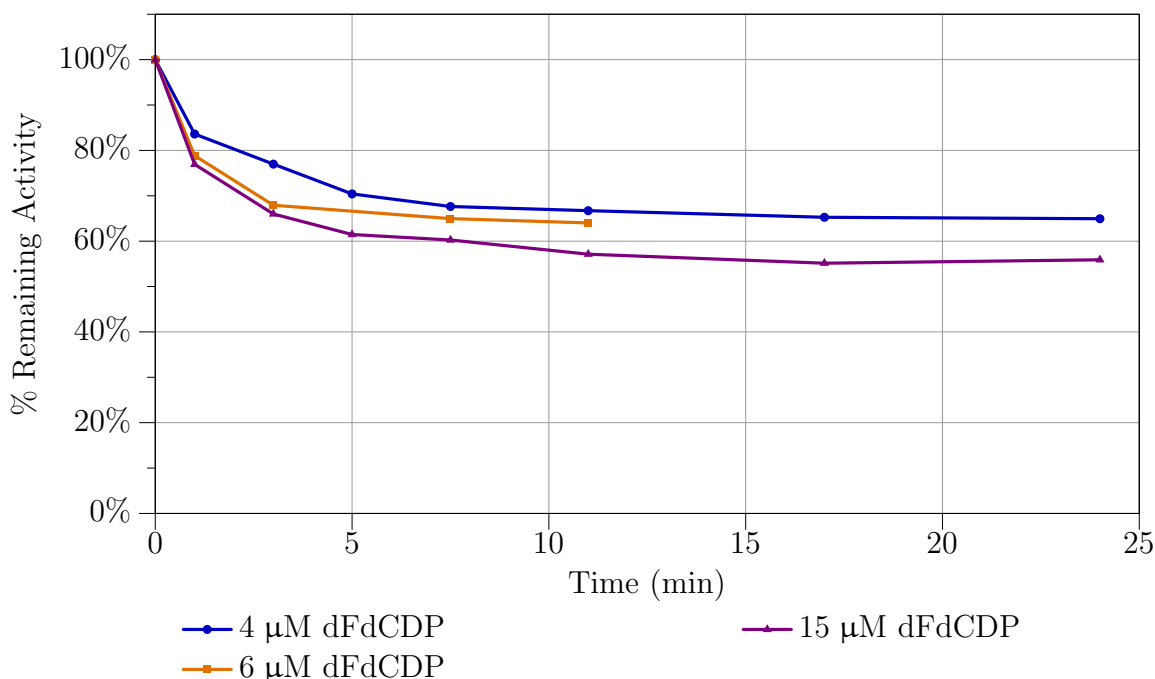


Figure 5.9: Time-dependent inactivation of R2 in the presence of reductants

In experiments carried out in the presence of reductants, two equivalents of dFdCDP were necessary for complete loss of R1 activity as shown in Figure 5.8. Simultaneously, these conditions resulted in the loss of approximately 35% of R2 activity as shown in Figure 5.9.

5.3.3 Quantification of end products of inactivation and size-exclusion experiments with radiolabeled dFdCDP

In order to obtain precise numbers for the amount of released cytosine during inactivations of RNR by dFdCDP, $[5-^3\text{H}]\text{-dFdCDP}$ was prepared from $[5-^3\text{H}]\text{-dFdC}$ by the enzymatic method described in Chapter 3. The material was characterised by ^1H NMR and ^{31}P NMR and by its ability to cause timed-dependent loss of tyrosyl radical on R2. When incubated with wt-R1, wt-R2, and ATP, the material caused a biphasic loss of tyrosyl radical on R2 (Figure 5.10) that could be fit with a double exponential curve of the form $y = m1 + m2 \cdot e^{(m3 \cdot t)} + m4 \cdot e^{(m5 \cdot t)}$ where y is $A_{410\text{ nm}}$, t is elapsed time, and $m3$ and $m5$ have values of -1.9544 min^{-1} and -0.32083 min^{-1} , respectively. These values are similar to the values measured with unlabeled dFdCDP (-1.4431 min^{-1} and -0.29456 min^{-1}).³³ The diphosphate was obtained in 78% yield.

The amounts of released cytosine and fluoride were measured both in the presence and in the absence of reductants using two equivalents of dFdCDP per RNR. From three separate measurements in the presence of reductants, the amount of fluoride released was measured

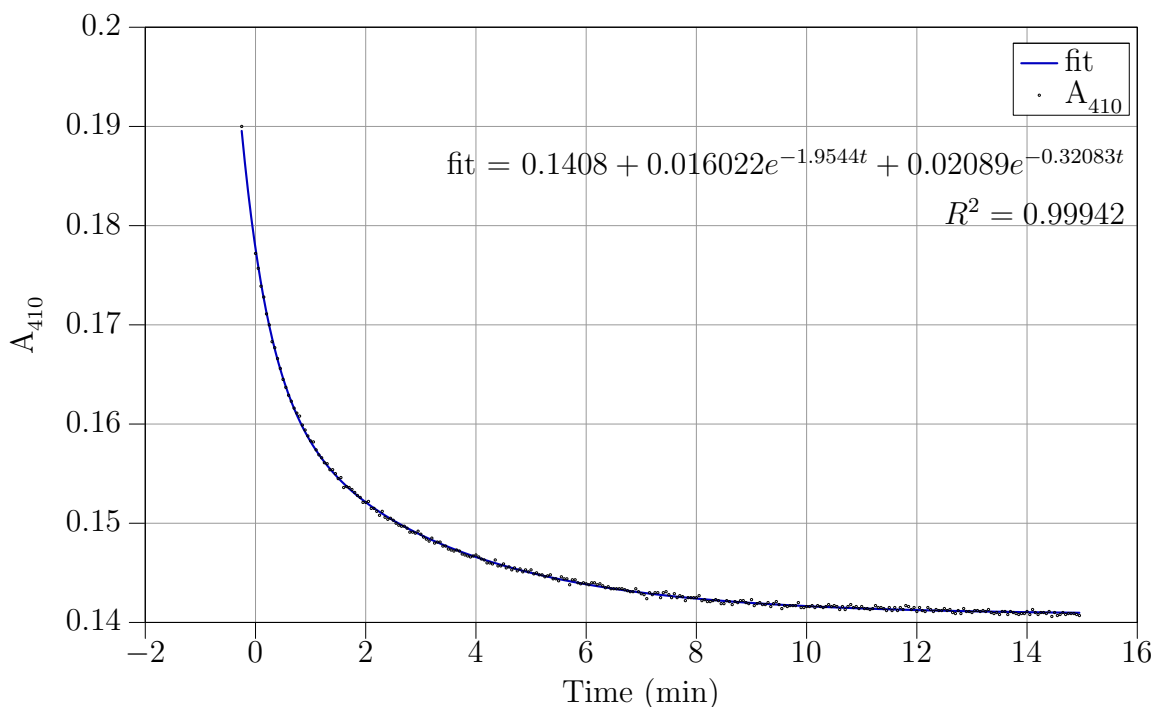


Figure 5.10: Loss of $A_{410\text{ nm}}$ in the presence of $[5\text{-}^3\text{H}]\text{-dFdCDP}$

to be 4, 3.7, and 3.7 equivalents per R1 or an average of 3.8 equivalents. From two separate measurements, the amount of cytosine released was 5.23 nmol and 5.20 nmol or 1.74 and 1.73 equivalents of cytosine released per R1. The amount of radioactivity recovered as gemcitabine corresponded to 0.47 nmol and 0.53 nmol or 0.16 and 0.17 equivalents per R1 (corresponds to $\sim 8\%$ of the starting nucleotide). Since $\sim 8\%$ of remaining R1 activity was detected at the end of the 30 min inactivation period, the recovered gemcitabine corresponds to unreacted material. Total recovery of radioactivity from the HPLC runs was between 90 and 95%.

In reactions carried out in the absence of reductants, the amount of cytosine measured on twelve separate occasions was between 0.2 and 0.3 equivalents per R1 with an average of 0.26 equivalents per R1. Additionally, a broad region of radioactivity was detected in fractions eluting between 10 min and 20 min. Low counts in these fractions make difficult the assessment of recovered radioactivity. These experiments should be repeated in the presence of NaBH_4 in an effort to trap any unstable intermediate(s) whose decomposition products may be associated with the broad radioactivity region. For the same experiments, the amount of fluoride measured ranged between 1.4 and 1.7 equivalents per R1 with an average of 1.56 equivalents per R1. The uncertainty in the meter reading is ± 1.0 mV which corresponds to an uncertainty in fluoride concentration of ± 0.4 μM in the 4–12 μM range. If one assumes an additional 10% error from pipetting and handling, the uncertainty in fluoride numbers is between 0.2 and 0.4 equivalents. One way to improve the fluoride analysis is to

Condition	[5- ³ H]-dFdCDP ^a	[1'- ³ H]-dFdCDP ^a	Fluoride ^b	Cytosine ^b
With reductants	0.15	1.0	3.8	1.73
No reductants	0.15	0.12	1.6	0.26

^a Number of equivalents of radioactivity associated with the protein in size exclusion experiments

^b Average number of equivalents per R1

Table 5.2: Results of product identification studies with dFdCDP

obtain a meter with accuracy of ± 0.1 mV.

Size-exclusion experiments to determine if covalent labeling of RNR occurred in the course of inactivation by dFdCDP were carried out with [5-³H]-dFdCDP and [1'-³H]-dFdCDP in the presence and in the absence of reductants as described in Section 5.2.9. In three separate experiments with [5-³H]-dFdCDP under non-denaturing conditions, between 0.1 and 0.21 equivalents of the inhibitor were associated with the protein both in the presence and in the absence of reductants.

With [1'-³H]-dFdCDP, experiments were analyzed under denaturing conditions and quantitative protein recovery was assumed. In the presence of reductants, between 1 and 1.08 equivalents of the inhibitor were associated with the protein in three separate runs. In an experiment carried out in the absence of reductants, 0.12 equivalents of the inhibitor were associated with the protein.

The results of studies on the products of inactivation during RNR inhibition by dFdCDP are summarized in Table 5.2.

5.3.4 Tryptic digest of wt - RNR inhibited by [1'-³H]-dFdCDP in the presence of DTT

Partial resolution of RNR peptides labeled with [1'-³H]-dFdCDP in the presence of DTT was achieved by reverse phase HPLC under acidic conditions in the presence of 0.1% v/v trifluoroacetic acid (TFA). In a test of the stability of the RNR-associated label under acidic conditions described in Section 5.2.11, a total of 27400 cpm were dialyzed against 80 mL of dH₂O containing 0.1% v/v TFA. After 4 h of dialysis at RT, only background radioactivity (26.6 cpm) was detected in the dialysis chamber suggesting that the label is stable in the presence of 0.1% v/v TFA. Results of HPLC analysis after 10 h of digestion are shown in Figure 5.11 and Figure 5.12. The elution of radioactivity at $\sim 35\%$ MeCN concentration was reproducible in three separate runs; however, the radioactivity elutes in at least 3 separate peaks. Interestingly, Lin *et al.*³⁴ have previously reported that Q221-K246 peptide containing the catalytically essential C225 elutes at the same MeCN concentration under acidic conditions.

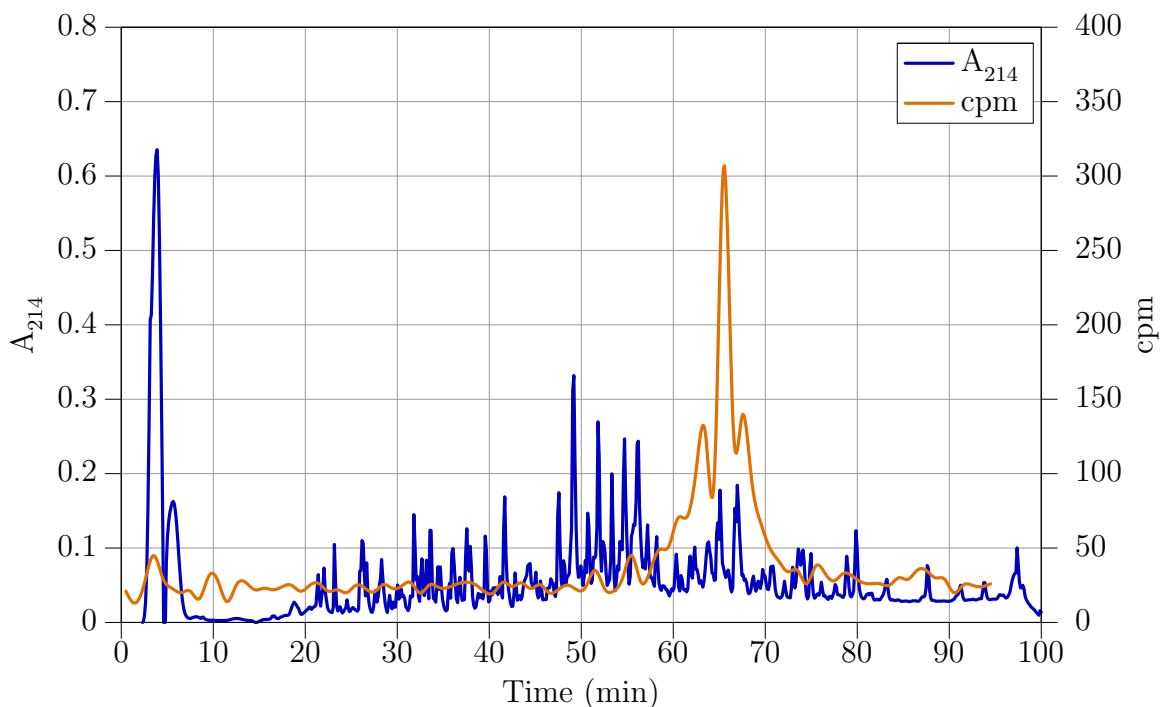


Figure 5.11: Tryptic digest of RNR labeled with $[1'-^3\text{H}]$ -dFdCDP in the presence of DTT and radioactivity profile

<i>System</i>	g_x	g_y	g_z
dFdCDP+wt - RNR	2.00738	2.00592	2.00230
E441Q- R1/R2+CDP	2.00730	2.00604	2.00225

Table 5.3: Comparison of g-values for wt - RNR plus dFdCDP, and 3 min E441Q- R1/wt - R2 plus CDP radicals

5.3.5 Studies on the structure of the radical formed in the absence of reductants

140 GHz EPR experiments

The first 140 GHz EPR spectrum of the radical formed in the reaction of *E. coli* RNR with dFdCDP in the absence of reductants was acquired in collaboration with Dr. Galit Bar from the Griffin Laboratory. These measurements allowed the precise determination of the g-values for the new radical. Both the high-field spectrum and the g-values of the new radical are strikingly similar to those obtained for the 3 min radical in the reaction of E441Q- R1 with R2, CDP, TTP and DTT described in Chapter 4. The g-values for the two radicals are compared in Table 5.3. Given the similarities between the two radicals and the fact that one

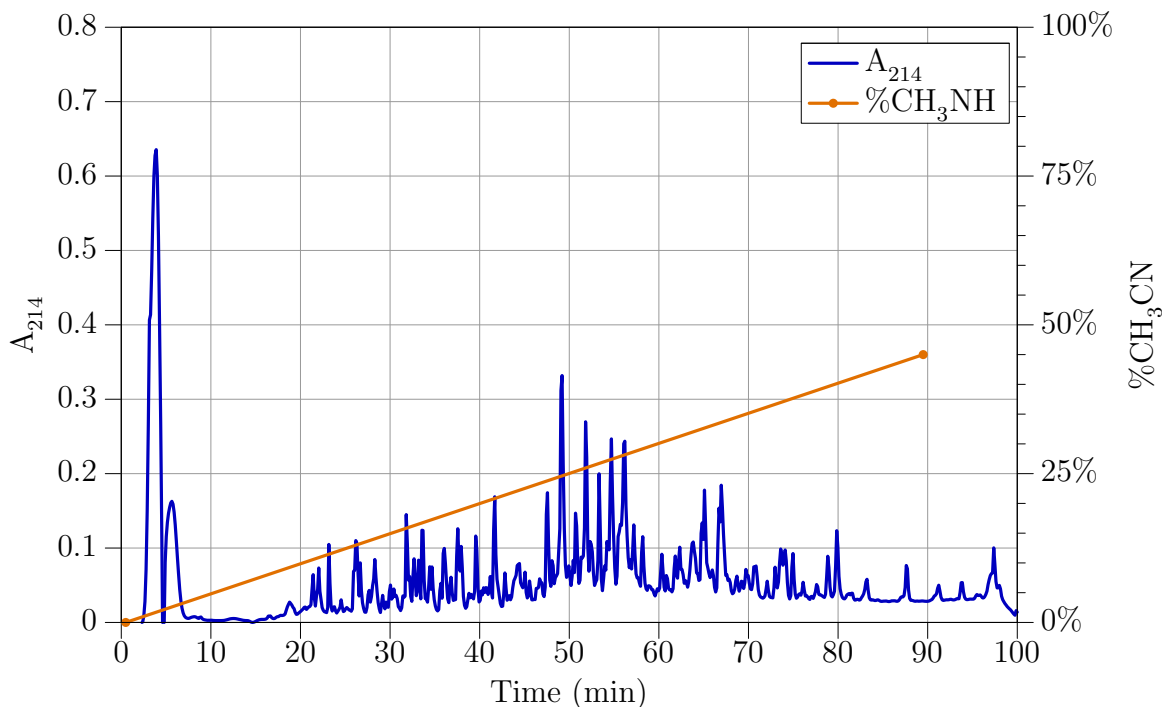


Figure 5.12: Tryptic digest of RNR labeled with $[1' - ^3\text{H}]$ -dFdCDP in the presence of DTT and $[\text{CH}_3\text{CN}]$

of the hyperfine interactions in the 3 min E441Q radical is derived from the $1' - \text{H}$, reactions of RNR with $[1' - ^2\text{H}]$ -dFdCDP were examined by 9 GHz CW EPR spectroscopy.

9 GHz EPR experiments

Figure 5.13 shows the results of 9 GHz EPR measurements on the reaction of wt-R1, wt-R2, dFdCDP, and ATP. The 45 s trace represents the spectrum of the reaction mixture as acquired. The $\text{Y}\cdot$ trace is a scaled spectrum of the tyrosyl radical. The 45 s - $\text{Y}\cdot$ trace is the result of subtraction of the scaled tyrosyl radical ($\text{Y}\cdot$ trace) from the reaction spectrum as acquired (45 s). Scaling of the tyrosyl radical spectrum was done so as to match the intensities of the left and right shoulders of the reaction spectrum as acquired. The shoulders are entirely due to the unreacted tyrosyl radical in the reaction. The resulting spectrum is a triplet as previously reported.¹³

The results of 9 GHz EPR measurements on the reaction of wt-R1, wt-R2, ATP and $[1' - ^2\text{H}]$ -dFdCDP are shown in Figure 5.14. The 45 s trace represents the spectrum of the reaction mixture as acquired. The $\text{Y}\cdot$ trace is a scaled spectrum of the tyrosyl radical (scaling was done as described above). The 45 s - $\text{Y}\cdot$ trace is the result of subtraction of the scaled tyrosyl radical ($\text{Y}\cdot$ trace) from the reaction spectrum as acquired (45 s trace). The data clearly shows that substitution of the $1'$ -hydrogen by a deuterium results in the

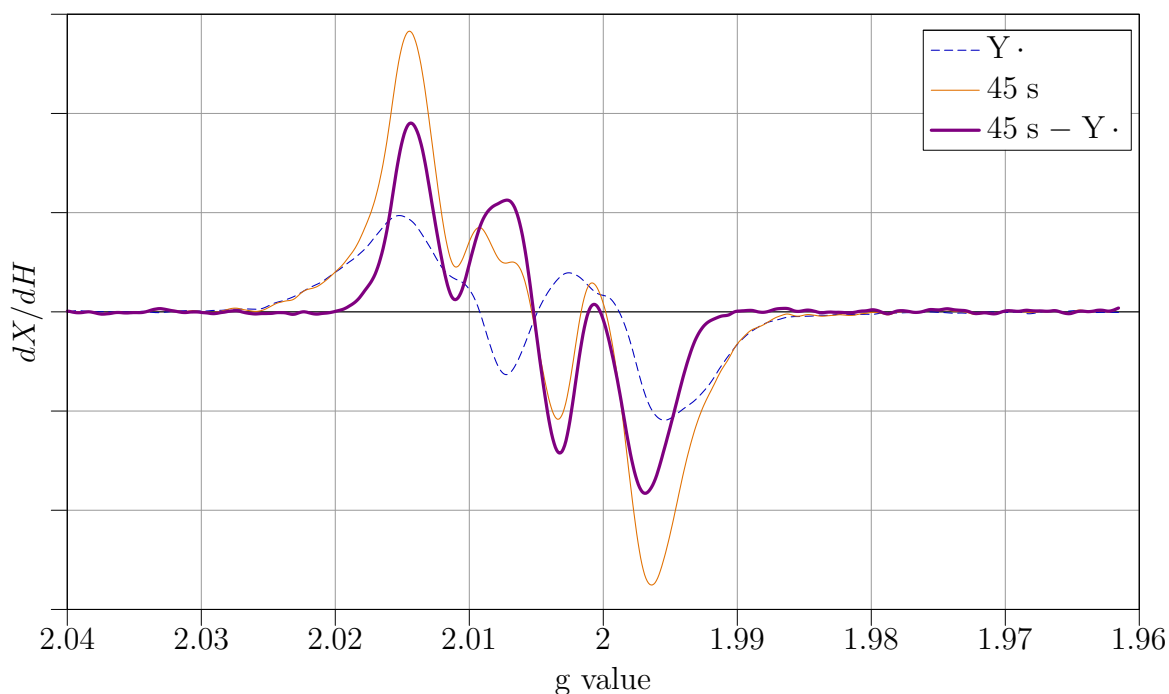


Figure 5.13: 9 GHz EPR spectra of the reaction of wt - R1, wt - R2, and ATP with dFdCDP, scaled $Y\cdot$, and the result of subtraction

collapse of the hyperfine structure in the EPR signal from a triplet to a doublet. Figure 5.15 shows the comparison of the new radical formed in the reactions of wt - R1, wt - R2 and ATP with dFdCDP or $[1' - ^2\text{H}] - \text{dFdCDP}$.

Experiments in which perdeuterated R2 was used in place of wt - R2 did not result in the change of the hyperfine structure of the EPR signal. The spectrum was a triplet such as the one shown in Figure 5.13 and as published previously.¹³

5.3.6 C225 is necessary for the mode of inactivation observed in the presence of reductants

As noted in Section 5.1, initial experiments on the inhibition of C754S/C759S - R1/R2 showed that in the presence of TR/TRR/NADPH this enzyme behaved the same as the wt - R1/wt - R2 enzyme in the absence of reductants as judged by time-dependent inactivation and 9 GHz EPR experiments. However, in the presence of DTT, C754S/C759S - R1/R2 behaved as wt - R1/wt - R2 in the presence of reductants (either TR/TRR/NADPH or DTT) as revealed by time-dependent inactivation and 9 GHz EPR experiments.¹³

These results indicate that the mode of inactivation observed in the presence of reductants requires the delivery of reducing equivalents to the active site. The reducing equivalents can be delivered directly by DTT or indirectly by transfer to the active site redox cysteines,

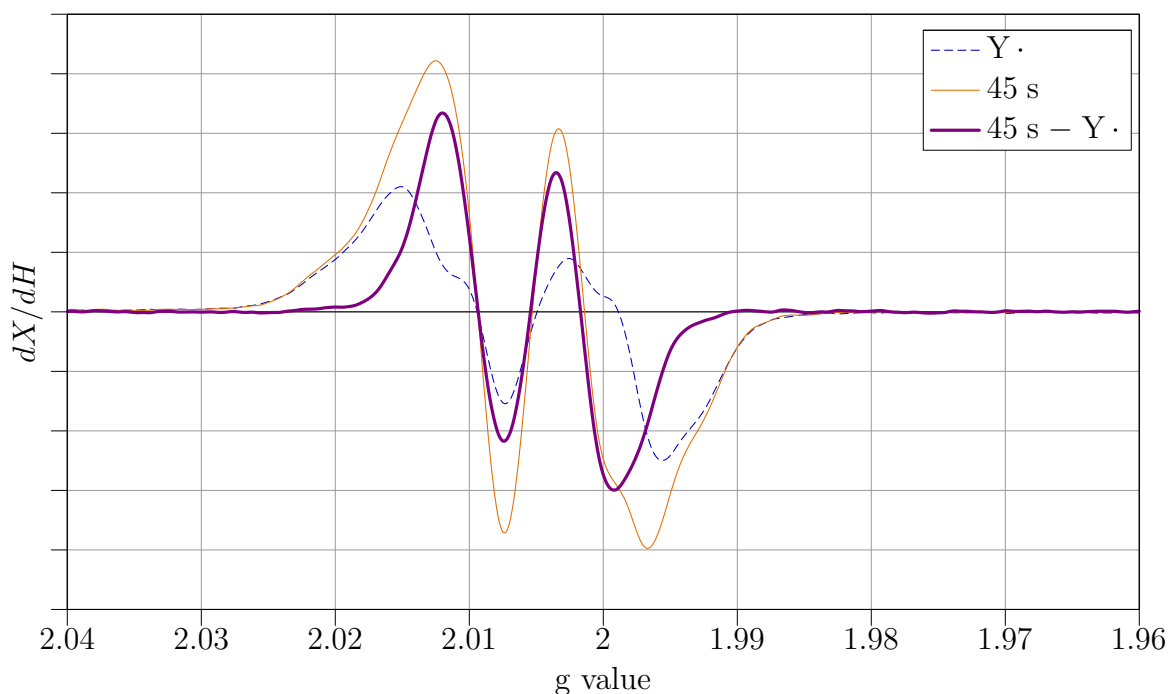


Figure 5.14: 9 GHz EPR spectra of the reaction of wt-R1, wt-R2, and ATP with $[1'-^2\text{H}]$ -dFdCDP, scaled $Y\cdot$, and the result of subtraction

C225 and C462. Thus, a hypothesis was made that C225 and C462 may be necessary for the inactivation mode observed in the presence of reductants. Previously in the Stubbe laboratory, inhibition of C225S-R1/wt-R2 and C462S-R1/wt-R2 by dFdCDP was characterized spectrophotometrically in the absence of reductants by monitoring $Y\cdot$ loss at 410 nm.³³ In the case of C225S-R1/wt-R2, the experiments revealed complete $Y\cdot$ loss at 15 μM enzyme concentration with kinetic parameters very similar to those observed for wt-R1/wt-R2 at the same enzyme concentration in the absence of reductants. In the case of C462S-R1/wt-R2, slow loss of $\sim 40\%$ of $Y\cdot$ was observed. However, no time-dependent inactivation experiments or 9 GHz EPR experiments on C225S-R1/wt-R2 or C462S-R1/wt-R2 in the absence of reductants were performed. Most importantly, no examination of either mutant in the presence of TR/TRR/NADPH and in the presence of DTT was carried out by either time-dependent inactivation or 9 GHz EPR.

Time-dependent inactivation of wt-R2 in the presence of C225S-R1

Given the hypothesis that C225 may be necessary for the mode of inactivation observed in the presence of reductants, time-dependent inactivation of C225S-R1/wt-R2 by dFdCDP was monitored in the presence of TR/TRR/NADPH or DTT. If C225 and C462 were not necessary for the mode of inactivation observed in the presence of reductants, then DTT

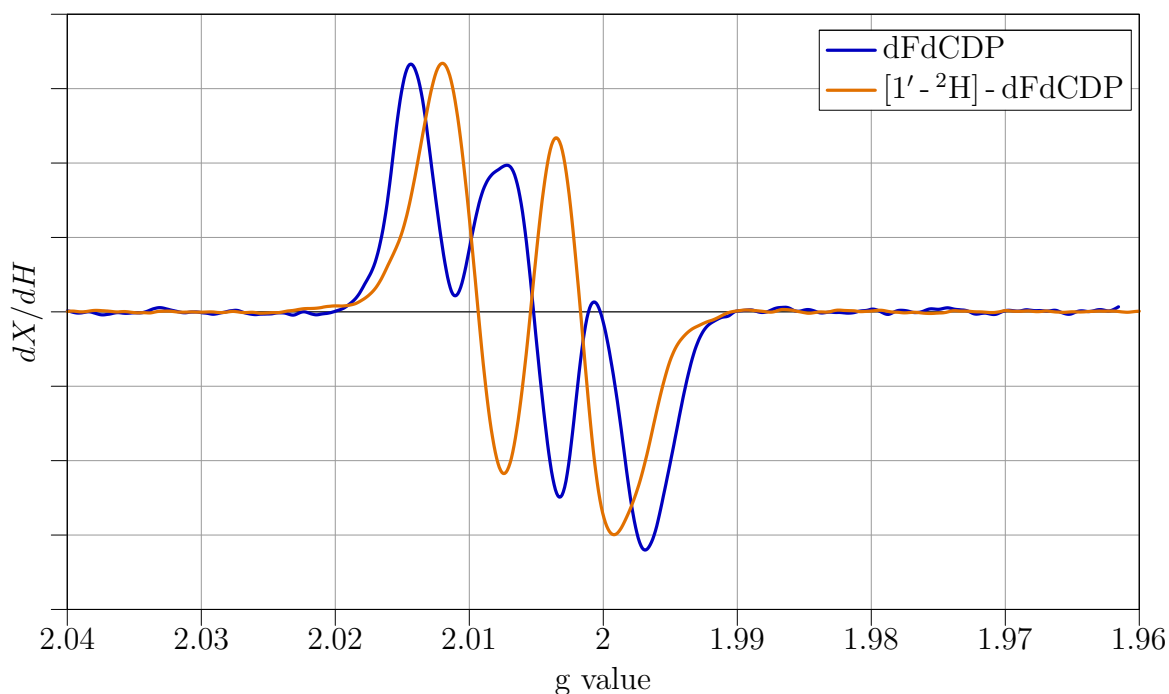


Figure 5.15: Comparison of the new radical from the reaction of wt-R1, wt-R2, and ATP with dFdCDP and [1' - ^2H]-dFdCDP

could possibly deliver the required reducing equivalents to the active site. Thus, one may be able to observe a difference in the reactions in the presence of TR/TRR/NADPH, which depend on C225 and C462 for the channeling of reducing equivalents, and those in the presence of DTT.

Time-dependent inactivation of R2 in the presence of C225S-R1, dFdCDP, and ATP was carried out either in the absence of reductants, or in the presence of TR/TRR/NADPH or DTT. The data sets are presented in Figure 5.17. Under all conditions, the C225S-R1/wt-R2 enzyme exhibits a pattern of R2 inactivation that is characteristic of the wt reaction in the absence of reductants shown in Figure 5.16 for comparison.

Size-exclusion experiments on the reaction of C225S-R1/wt-R2 with dFdCDP

The behavior of C225S-R1 in the presence of reductants was further characterized by size exclusion experiments after inactivation by [1' - ^3H]-dFdCDP. As shown in Table 5.2, wt enzyme is labeled with 1.0 equivalent of radioactivity when incubated with [1' - ^3H]-dFdCDP in the presence of reductants and with 0.12 equivalents of radioactivity when incubated with [1' - ^3H]-dFdCDP in the absence of reductants (analysis performed under denaturing conditions in both cases). When C225S-R1/wt-R2 was incubated with [1' - ^3H]-dFdCDP in the presence of TR/TRR/NADPH and ATP as the effector, 0.14 of the inhibitor were

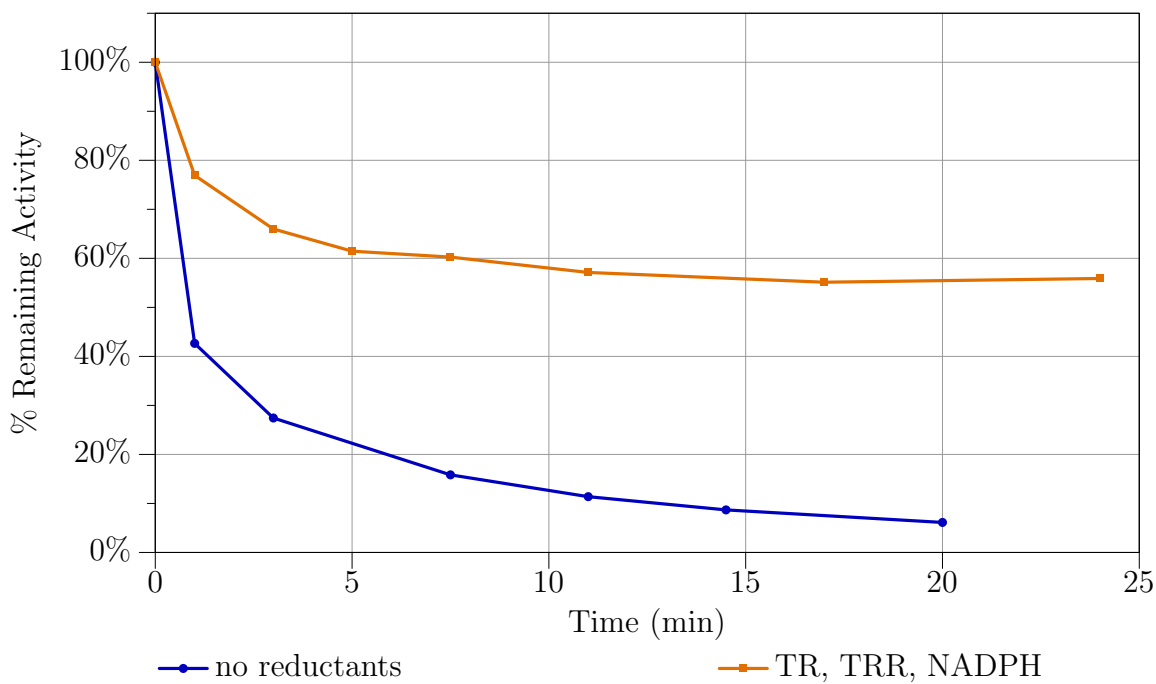


Figure 5.16: R2 activity loss with wt-R1

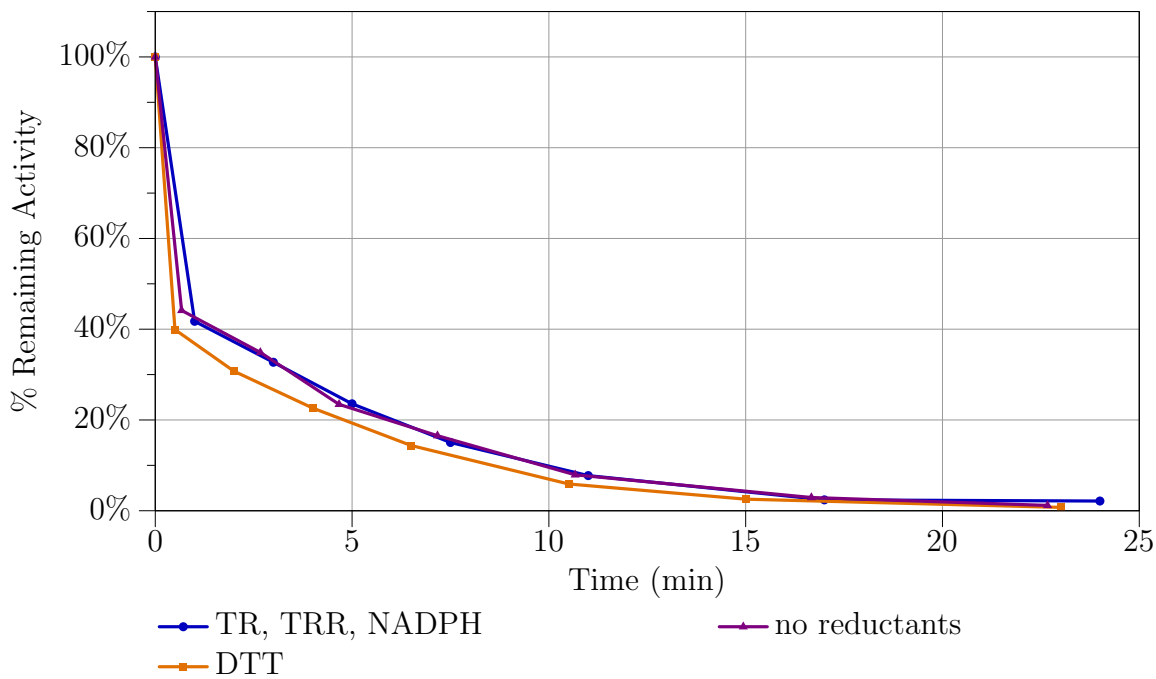


Figure 5.17: R2 activity loss with C225S-R1

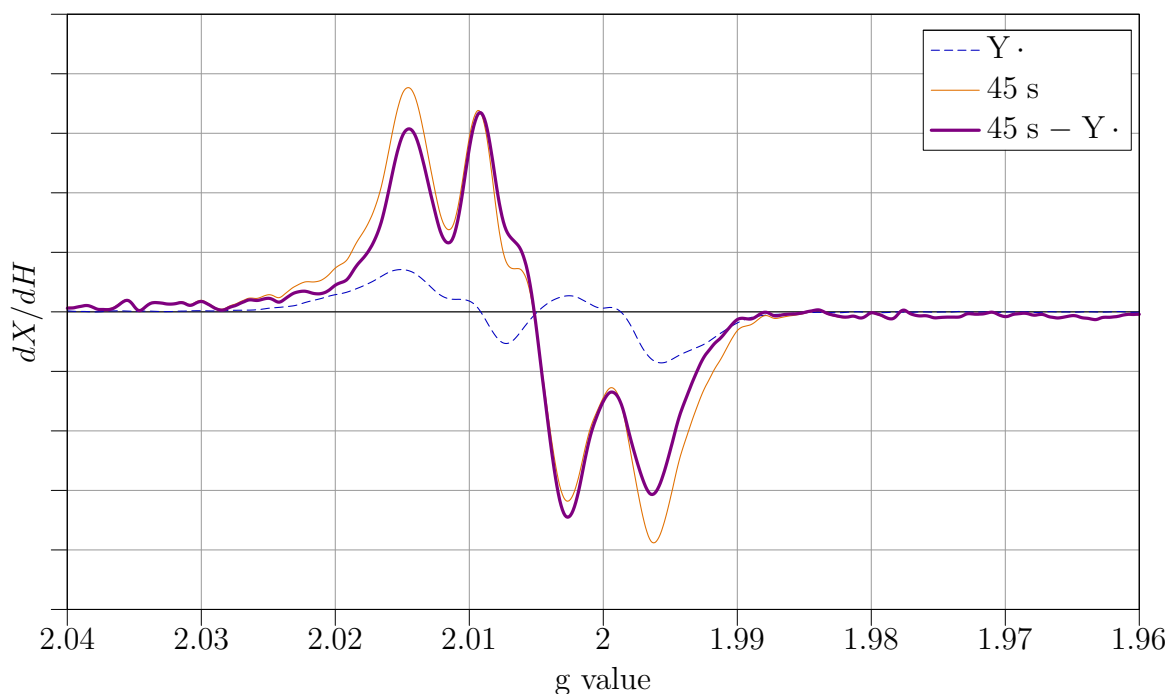


Figure 5.18: 9 GHz EPR spectra of the reaction of C225S-R1, wt-R2, and ATP with dFdCDP, scaled $Y\cdot$, and the result of subtraction

associated with the protein under native conditions (average of two runs) and 0.15 equivalents of the inhibitor were associated with the protein under denaturing conditions. This data clearly shows that C225S is required for the majority of labeling that occurs in the wt reaction in the presence of reductants.

9 GHz experiments on the reaction of C225S-R1 with wt R2, dFdCDP and ATP

9 GHz EPR measurements on the mixtures of C225S-R1, wt-R2, dFdCDP and ATP were prepared either in the absence of reductants or in the presence of TR/TRR/NADPH or DTT. Under all conditions, the measurements revealed formation of the new triplet radical shown in Figure 5.18 which is similar to the triplet radical observed in the reaction of wt-R1, wt-R2, dFdCDP and ATP in the absence of reductants shown in Figure 5.13.

Furthermore, incubation of C225S-R1, wt-R2, $[1'-^2\text{H}]$ -dFdCDP, and ATP and examination of the reaction by 9 GHz EPR revealed a similar collapse in the hyperfine structure of the new radical as when wt-RNR was incubated with $[1'-^2\text{H}]$ -dFdCDP. In Figure 5.18 and Figure 5.19, the 45 s trace represents the spectrum of the reaction mixture as acquired. The $Y\cdot$ trace is a scaled spectrum of the tyrosyl radical (scaling was done as described in Section 5.3.5). The 45 s - $Y\cdot$ trace is the result of subtraction of the scaled tyrosyl radical ($Y\cdot$ trace) from the reaction spectrum as acquired (45 s trace).

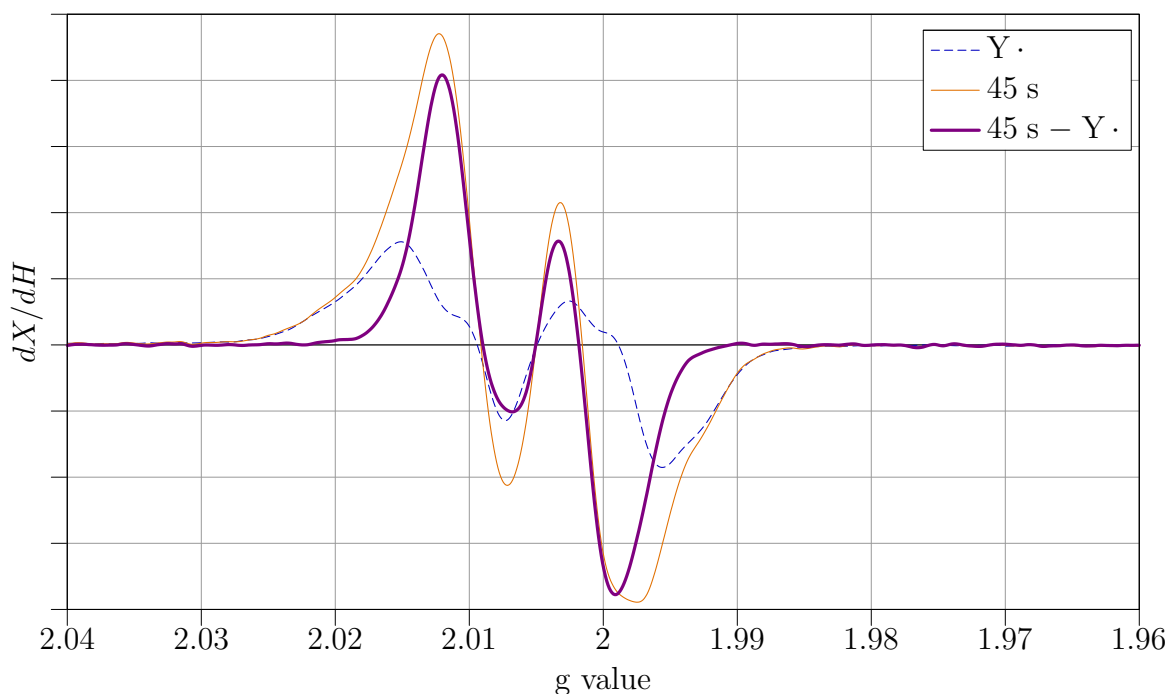


Figure 5.19: 9 GHz EPR spectra of the reaction of C225S-R1, wt-R2, and ATP with $[1' - ^2\text{H}] - \text{dFdCDP}$, scaled $\text{Y}\cdot$, and the result of subtraction

5.3.7 9 GHz EPR measurements aimed at looking for fluorine hyperfine interactions

Examination of the literature on α -fluorine coupling constants revealed that couplings are highly anisotropic with g_{\perp} in the range of 12–25 G and g_{\parallel} in the range of 180–300 G.^{35,36} Because the original experiments used a sweep-width of only 150 G, the reactions of both wt-R1/wt-R2 and C225S-R1/wt-R2 with either dFdCDP or $[1' - ^2\text{H}] - \text{dFdCDP}$ were examined using a sweep-width of 700 G. No additional wing peaks were observed under any circumstances.

Furthermore, since literature examples show that the wing peaks due α -fluorine couplings are broad and low in intensity compared to the center-field peaks,^{35,36} the reactions described above were examined with a high modulation amplitude of 30 G. Again, no difference in the spectra was detected at the wings.

5.3.8 9 GHz simulations

Simulations of the 9 GHz spectra of the reaction of wt-R1/wt-R2 and C225S-R1/wt-R2 with $[1' - ^2\text{H}] - \text{dFdCDP}$ and ATP were performed as described in Section 5.2.12. For the wt reaction, the best fit was obtained with a line-width of 7 G and an isotropic coupling

constant of 13.2 G. In the case of the C225S-R1, wt-R2 reaction, the best fit was obtained with a line-width of 8 G and an isotropic coupling constant of 12.2 G.

5.4 Discussion

Two key contributions were made toward understanding the mechanism of inhibition of *E. coli* RNR by dFdCDP. We demonstrated that under physiologically relevant reducing conditions, inhibition of RNR by dFdCDP is a result of covalent modification that requires C225. Furthermore, we showed that one of the hyperfine interactions in the new radical formed in the absence of reductants is derived from the 1'-proton of dFdCDP.

In addition, size-exclusion experiments carried out with [5-³H]-dFdCDP and [1'-³H]-dFdCDP in the absence of reductants revealed that only 0.15 labels are covalently bound to RNR. In the presence of reductants, use of [5-³H]-dFdCDP and [1'-³H]-dFdCDP revealed that 0.15 and 1.2 labels, respectively, are covalently bound to RNR. These results strongly suggest that RNR inactivation in the presence of reductants is a result of covalent modification. The molecular weight of RNR is 280 kDa ($\alpha_2\beta_2$), making the peptide mapping to identify the site of labeling challenging, as revealed by preliminary protease digestion experiments and partial peptide resolution. Separation of R1 and R2 subunits using affinity chromatography on dATP-Sepharose or Ni-NTA prior to digestion is recommended.

Time-dependent inactivation experiments in the presence of reductants showed that two equivalents of dFdCDP per R1 (R1 is defined as a dimer (α_2)) are required for complete loss of R1 activity. At the same time, 1.73 equivalents of cytosine and 3.8 equivalents of fluoride were released. One possibility is that each active site of R1 dimer reacts with one equivalent of dFdCDP. Alternatively, the same active site could react sequentially with two equivalents of dFdCDP. One may be able to distinguish between these possibilities by quantifying the amount of cytosine and fluoride released in the reaction of C225S-R1/wt-R2 with dFdCDP and ATP since this mutant would not be expected to react with more than one equivalent of dFdCDP per active site. Thus, if ~ 2 equivalents of cytosine and ~ 4 equivalents of fluoride were released in the reaction with the C225S-R1 mutant, the results would indicate that both active sites are involved in the inhibition.

In the absence of reductants, two equivalents of dFdCDP were required for complete loss of R2 activity (R2 is defined as a dimer (β_2)) as revealed by time-dependent inactivation experiments. Monitoring of cytosine release by reverse phase HPLC revealed a broad region of radioactivity which was not associated with either the cytosine or the dFdC peak. Quantification of radioactivity in this region was difficult due to low counts which were spread over a large volume. The cytosine release quantification experiments should be repeated in the presence of NaBH_4 in an effort to trap any unstable intermediate(s) whose decomposition products may be associated with the broad radioactivity region. Additionally, fluoride measurements revealed 1.56 ± 0.4 equivalents were released. These measurements should be repeated using a voltmeter with accuracy of ± 0.1 mV to determine if the number of equivalents of fluoride release is closer to 1 or 2.

The new radical is nucleotide-based with one of the hyperfine interactions derived from the 1'-proton As discussed in Section 5.1, inhibition of wt-RNR by dFdCDP is reductant-dependent. During inactivations carried out in the absence of reductants, a new radical species is observable by EPR on the minute time scale. The radical is formed in the initial, fast phase of the inactivation. At 15 μM enzyme concentrations, the efficiency of conversion of tyrosyl radical into the new radical is $\sim 80\%$. Thus, the species accounts for a major part of the R2 inactivation process. The power at half saturation of the EPR signal is about 1.5 orders of magnitude lower than that of the tyrosyl radical on R2 for which the electron spin relaxation rate is considerably enhanced compared to that of free tyrosyl radicals due to the proximity to the diferric cluster. The saturation behavior suggests that the new radical is organic in nature and removed from the diferric cluster. The overall appearance of the signal at 9 GHz is that of a triplet with unequal intensities. The asymmetry of the signal suggests that it is the result of two overlapping doublet signals with hyperfine interactions of ~ 12 G which arise from the interaction with two spin 1/2 nuclei such as protons or fluorines. Previous studies by van der Donk *et al.* with perdeuterated-R1 ([U- ^2H]-R1) and in $^2\text{H}_2\text{O}$, and studies with perdeuterated R2 ([U- ^2H]-R2) described here, ruled out the possibility that either of the hyperfine interactions was derived from protons on R1, R2 or from solvent because no change of the hyperfine structure of the EPR signal was observed with these deuterations. Furthermore, the high-field EPR experiments allowed us to determine the principal g-values of the new radical. Both the g-values and the high-field spectrum of the radical proved strikingly similar to those observed for the 3 min radical in the reaction of E441Q-R1 with wt-R2, CDP, TTP and DTT described in Chapter 4. This similarity compelled us to probe whether the two radicals are analogous. Thus, the reaction of wt-R1, wt-R2, and ATP with [1'- ^2H]-dFdCDP was examined by 9 GHz EPR spectroscopy. The measurements revealed a collapse of the triplet signal into a doublet, confirming that one of the hyperfine interactions arises from the 1'-proton of dFdCDP. These results constitute the first definitive evidence that the new radical is nucleotide-based.

We further concentrated on determining whether the second hyperfine interaction could arise from a fluorine nucleus at the 2'-position. Available literature on α -fluorine couplings reveals that they are highly anisotropic.^{35,36} Typical values for A_{\perp} are in the range of 12–25 G while the values for A_{\parallel} are in the 180–300 G range. Therefore, reactions of either wt-R1 or C225S-R1 with wt-R2, ATP and either dFdCDP or [1'- ^2H]-dFdCDP were re-examined by 9 GHz EPR spectroscopy using a wide sweep-width of 700 G in order to look for additional features at the wings of the spectra. No additional peaks were detected under any conditions. Furthermore, since the literature examples show that the wing peaks due α -fluorine coupling are broad and low in intensity compared to the center-field peaks,^{35,36} the reactions were also re-examined using high modulation amplitude. Again, no difference in the spectra was detected at the wings. These results indicate that the second hyperfine interaction in the new radical is not derived from fluorine. If the radical is analogous to the 3 min radical detected in the reaction of E441Q-R1 with wt-R2, CDP, TTP and DTT described in Chapter 4, then the second coupling is most likely derived from the 4'-proton.

C225S is necessary for the mode of inactivation observed in the presence of reductants Previous studies in the Stubbe laboratory showed that C225S-R1 promotes $Y\cdot$ loss on R2 when incubated with dFdCDP and ATP in the absence of reductants.³³ The decay rates were shown to be similar to those observed in the reaction wt enzyme. However, this mutant had not been characterized by time-dependent inactivation or 9 GHz EPR experiments. In particular, its ability to promote $Y\cdot$ loss on R2, time-dependent inactivation of R2, or the formation of the new radical in the presence of reductants was not examined.

A mechanistic hypothesis was made that C225 and C462 may be necessary for the mode of inactivation observed in the presence of reductants. This hypothesis was formulated based on the results published by van der Donk *et al.* on the inactivation of C754S/C759S-R1/wt-R2 by dFdCDP in the presence of reductants.¹³ When incubated with TR/TRR/NADPH, this enzyme behaved the same as the wt-R1/wt-R2 enzyme in the absence of reductants. However, in the presence of DTT, C754S/C759S-R1/wt-R2 behaved as wt-R1/wt-R2 in the presence of reductants. These results indicate that the mode of inactivation observed in the presence of reductants requires delivery of reducing equivalents to the active site. To test whether C225 is necessary for the channeling of reducing equivalents during inactivations performed in the presence of reductants, time-dependent inactivation, 9 GHz EPR, and size-exclusion experiments were performed with the C225S-R1 mutant.

The first indication that C225 is necessary for the channeling of reducing equivalents, which are required for the mode of inactivation observed in the presence of reductants, came from time-dependent inactivation experiments. In these experiments, R2 activity loss was measured as a function of time in the presence of either TR/TRR/NADPH or DTT and compared to R2 activity loss when the same reaction was incubated in the absence of reductants. If C225 were not necessary for the channeling of reducing equivalents, then DTT could possibly deliver the required reducing equivalents to the active site, and one may be able to observe a difference in the inactivations carried out in the presence of DTT as compared to the inactivations carried out in the presence of TR/TRR/NADPH. No such difference was detected. In all cases, C225S-R1 promoted R2 activity loss that was identical to that observed in the wt enzyme in the absence of reductants.

Further confirmation that C225 is necessary for the channeling of reducing equivalents, which are required for the mode of inactivation observed in the presence of reductants, came from 9 GHz EPR experiments. The formation of the new triplet radical with C225S-R1 was detected both in the presence and in the absence of reductants unlike in the case of the wt enzyme. Moreover, the nature of the reductant did not make a difference. Together with the results of time-dependent inactivation experiments, these measurements indicate that C225 is necessary for the partitioning into the reductants pathway.

Bibliography

- [1] G. H. R. Pizzorno and Y. C. Cheng, *Cancer Medicine*, ch. Pyrimidine and purine antimetabolites, pp. 625–647. B. C. Decker, Inc., 5 ed., 2000.

- [2] W. Plunkett, P. Huang, and V. Gandhi, "Gemcitabine: actions and interactions," *Nucleosides & Nucleotides*, vol. 16, no. 7-9, pp. 1261–1270, 1997.
- [3] A. M. Bergman, H. M. Pinedo, and G. J. Peters, "Determinants of resistance to 2',2'-difluorodeoxycytidine (gemcitabine)," *Drug Resistance Updates*, vol. 5, no. 1, pp. 19–33, 2002.
- [4] E. S. Arner and S. Eriksson, "Mammalian deoxyribonuclease kinases," *Pharmacology & Therapeutics*, vol. 67, no. 2, pp. 155–186, 1995.
- [5] C.-H. Hsu, J.-Y. Liou, G. E. Dutschman, and Y.-C. Cheng, "Phosphorylation of cytidine, deoxycytidine, and their analog monophosphates by human UMP/CMP kinase is differentially regulated by ATP and magnesium," *Molecular Pharmacology*, vol. 67, no. 3, pp. 806–814, 2005.
- [6] A. R. Van Rompay, M. Johansson, and A. Karlsson, "Phosphorylation of deoxycytidine analog monophosphates by UMP-CMP kinase: molecular characterization of the human enzyme," *Molecular Pharmacology*, vol. 56, no. 3, pp. 562–569, 1999.
- [7] J.-Y. Liou, G. E. Dutschman, W. Lam, Z. Jiang, and Y.-C. Cheng, "Characterization of human UMP/CMP kinase and its phosphorylation of D- and L-form deoxycytidine analogue monophosphate," *Cancer Research*, vol. 62, no. 6, pp. 1624–1631, 2002.
- [8] E. J. Artin, "Stubbe laboratory year-end report," 2002.
- [9] P. Huang, S. Chubb, L. W. Hertel, G. B. Grindey, and W. Plunkett, "Action of 2',2'-difluorodeoxycytidine on DNA synthesis," *Cancer Research*, vol. 51, no. 22, pp. 6110–6117, 1991.
- [10] V. Gandhi and W. Plunkett, "Modulatory activity of 2',2'-difluorodeoxycytidine on the phosphorylation and cytotoxicity of arabinosyl nucleosides," *Cancer Research*, vol. 50, no. 12, pp. 3675–3680, 1990.
- [11] V. Heinemann, Y. Z. Xu, S. Chubb, A. Sen, L. W. Hertel, G. B. Grindey, and W. Plunkett, "Inhibition of ribonucleotide reduction in CCRF-CEM cells by 2',2'-difluorodeoxycytidine," *Molecular Pharmacology*, vol. 38, no. 4, pp. 567–572, 1990.
- [12] C. H. Baker, J. Banzon, J. M. Bollinger, J. Stubbe, V. Samano, M. J. Robins, B. Lippert, E. Jarvi, and R. Resvick, "2'-Deoxy-2'-methylene-cytidine and 2'-deoxy-2',2'-difluorocytidine 5'-diphosphates: potent mechanism-based inhibitors of ribonucleotide reductase," *Journal of Medicinal Chemistry*, vol. 34, no. 6, pp. 1879–1884, 1991.
- [13] W. A. van der Donk, G. Yu, L. Perez, R. Sanchez, J. Stubbe, V. Samano, and M. J. Robins, "Detection of a new substrate-derived radical during inactivation of ribonucleotide reductase from *Escherichia coli* by gemcitabine 5'-diphosphate," *Biochemistry*, vol. 37, no. 18, pp. 6419–6426, 1998.
- [14] V. Gandhi, P. Huang, Y. Z. Xu, V. Heinemann, and W. Plunkett, "Metabolism and action of 2',2'-difluorodeoxycytidine: self-potentialization of cytotoxicity," *Advances in Experimental Medicine and Biology*, vol. 309A, pp. 125–130, 1991.
- [15] J. D. Davidson, L. Ma, M. Flagella, S. Geeganage, L. M. Gelbert, and C. A. Slapak, "An increase in the expression of ribonucleotide reductase large subunit 1 is associated with gemcitabine resistance in non-small cell lung cancer cell lines," *Cancer Research*, vol. 64, no. 11, pp. 3761–3766, 2004.
- [16] M. S. Duxbury, H. Ito, M. J. Zinner, S. W. Ashley, and E. E. Whang, "RNA interference targeting the M2 subunit of ribonucleotide reductase enhances pancreatic adenocarcinoma chemosensitivity to gemcitabine," *Oncogene*, vol. 23, no. 8, pp. 1539–1548, 2004.
- [17] J. Ge, G. Yu, M. A. Ator, and J. Stubbe, "Pre-steady-state and steady-state kinetic analysis of *E. coli* class I ribonucleotide reductase," *Biochemistry*, vol. 42, no. 34, pp. 10071–10083, 2003.
- [18] S. Salowe, J. M. Bollinger, Jr., M. Ator, J. Stubbe, J. McCracken, J. Peisach, M. C. Samano, and M. J. Robins, "Alternative model for mechanism-based inhibition of *Escherichia coli* ribonucleotide reductase by 2'-azido-2'-deoxyuridine 5'-diphosphate," *Biochemistry*, vol. 32, no. 47, pp. 12749–12760, 1993.

- [19] S. P. Salowe and J. Stubbe, "Cloning, overproduction, and purification of the B2 subunit of ribonucleoside-diphosphate reductase," *Journal of Bacteriology*, vol. 165, no. 2, pp. 363–366, 1986.
- [20] J. M. Bollinger, Jr, D. E. Edmondson, B.-H. Huynh, J. Filley, J. R. Norton, and J. Stubbe, "Mechanism of assembly of the tyrosyl radical-dinuclear iron cluster cofactor of ribonucleotide reductase," *Science (Washington, DC)*, vol. 253, no. 5017, pp. 292–298, 1991.
- [21] M. Russel and P. Model, "Direct cloning of the *trxB* gene that encodes thioredoxin reductase," *Journal of Bacteriology*, vol. 163, no. 1, pp. 238–242, 1985.
- [22] J. C. Han and G. Y. Han, "A procedure for quantitative determination of tris(2-carboxyethyl)phosphine, an odorless reducing agent more stable and effective than dithiothreitol," *Analytical Biochemistry*, vol. 220, no. 1, pp. 5–10, 1994.
- [23] J. R. Steeper and C. D. Steuart, "Rapid assay for CDP reductase activity in mammalian cell extracts," *Analytical Biochemistry*, vol. 34, no. 1, pp. 123–130, 1970.
- [24] S. S. Mao, M. I. Johnston, J. M. Bollinger, and J. Stubbe, "Mechanism-based inhibition of a mutant *Escherichia coli* ribonucleotide reductase (cysteine-225 → serine) by its substrate CDP," *Proceedings of the National Academy of Sciences of the United States of America*, vol. 86, no. 5, pp. 1485–1489, 1989.
- [25] S. S. Mao, T. P. Holler, J. M. Bollinger, Jr., G. X. Yu, M. I. Johnston, and J. Stubbe, "Interaction of C225S-R1 mutant subunit of ribonucleotide reductase with R2 and nucleoside diphosphates: tales of a suicidal enzyme," *Biochemistry*, vol. 31, no. 40, pp. 9744–9751, 1992.
- [26] L. Thelander, B.-M. Sjöberg, and S. Eriksson, "Ribonucleoside diphosphate reductase (*Escherichia coli*)," *Methods in Enzymology*, vol. 51, pp. 227–237, 1978.
- [27] J. W. Kozarich, A. C. Chinault, and S. M. Hecht, "Ribonucleoside phosphates via phosphorimidazolidate intermediates. Synthesis of pseudoadenosine 5'-triphosphate," *Biochemistry*, vol. 12, no. 22, pp. 4458–4463, 1973.
- [28] W. E. O'Brien, "A continuous spectrophotometric assay for argininosuccinate synthetase based on pyrophosphate formation," *Analytical Biochemistry*, vol. 76, no. 2, pp. 423–430, 1976.
- [29] G. J. Lohman, "Stubbe laboratory year-end report," 2003.
- [30] M. Bennati, C. T. Farrar, J. A. Bryant, S. J. Inati, V. Weis, G. J. Gerfen, P. Riggs-Gelasco, J. Stubbe, and R. G. Griffin, "Pulsed electron-nuclear double resonance (ENDOR) at 140 GHz," *Journal of Magnetic Resonance*, vol. 138, no. 2, pp. 232–243, 1999.
- [31] S. Un, J. Bryant, and R. G. Griffin, "Precision field-sweep system for superconducting solenoids and its application to high-frequency EPR spectroscopy," *Journal of Magnetic Resonance, Series A*, vol. 101, no. 1, pp. 92–94, 1993.
- [32] C. S. Yee, "Mechanistic investigations of the radical initiation pathway of class I ribonucleotide reductase from *Escherichia coli*," *Massachusetts Institute of Technology*, 2004. PhD thesis.
- [33] G. Yu. Unpublished results.
- [34] A. N. I. Lin, G. W. Ashley, and J. Stubbe, "Location of the redox-active thiols of ribonucleotide reductase: sequence similarity between the *Escherichia coli* and *Lactobacillus leichmannii* enzymes," *Biochemistry*, vol. 26, no. 22, pp. 6905–6909, 1987.
- [35] M. Iwasaki, S. Noda, and K. Toriyama, "Electron spin resonance spectra of an irradiated single crystal of difluoromalonamide and hyperfine tensors of α -fluorine couplings.," *Molecular Physics*, vol. 18, no. 2, pp. 201–12, 1970.
- [36] K. Toriyama and M. Iwasaki, "Change with temperature of the electron spin resonance spectra of $\text{cf}_2\text{cf}_2[\text{radical}]$ trapped in irradiated poly(tetrafluoroethylene).," *Journal of Physical Chemistry*, vol. 73, no. 9, pp. 2919–24, 1969.

Appendix A

9 GHz EPR experiments on the time-course of *E. coli* RNR inactivation by N₃NDPs: optimization of conditions for PELDOR measurements

A.1 Introduction

Structural information about the spatial arrangement of radicals can be obtained by analyzing dipole-dipole interactions between unpaired electron spins using pulsed electron paramagnetic resonance (EPR) methods. For electron spins separated by distances greater than ~ 20 Å, dipole-dipole interactions are masked by the dominant contributions of inhomogeneous broadening, and they have a minor effect on the continuous wave (CW) EPR spectrum. With pulsed EPR methods, the effects of inhomogeneous broadening are minimized,¹ and the dipole-dipole interaction can be measured. The most common approach is to use a two-frequency pulse sequence, which avoids electron spin envelope echo modulation (ESEEM) effects. The two-frequency approach, referred to as either DEER (double electron-electron resonance) or ELDOR (electron-electron double resonance),^{2,3} is used for two-spin systems.

In a typical PELDOR experiment, the observed time trace consists of an oscillation superimposed on an echo decay. The frequency of the oscillation is determined after the subtraction of the echo decay (fitted to a monoexponential function) and subsequent Fourier transformation. The frequency thus obtained is related to the interspin distance through the expression for dipolar coupling in the high-field approximation.

PELDOR was successfully used to make the first direct measurement of the distance ($r = 33.1 \pm 0.2$ Å) between two tyrosyl radicals ($Y\cdot$) in a frozen solution of homodimeric *E. coli* R2 by Bennati *et al.*⁴ The experiment also provided the first direct evidence for two tyrosyl radicals in a single R2. In order to correlate the distance measured by PELDOR

spectroscopy to X-ray diffraction data, the centers of mass of spin density for tyrosines 122 in several R2 structures were calculated based on the coordinates from the PDB and the spin densities published by Hoganson *et al.*⁵

Building on the success of the initial measurements on R2, attention was focused on determining the distance between the R1 active site and the tyrosyl radical on R2 by labeling the R1 active site with mechanism-based inhibitors that generate well-characterized radicals, such as the nitrogen-centered radical (N·) described in Chapter 2. To this end, the reaction in which wt R1/R2 complex was incubated with 2'-azido-2'-deoxyuridine-5'-diphosphate (N₃UDP) was examined by 9 GHz EPR, and the ratio of nitrogen-centered radical to tyrosyl radical was determined as a function of time. A similar experiment was performed using C268S-R2 in place of wt R2. C268 is a residue on the surface of R2 which may be involved in the formation of intramolecular disulfide bonds. This mutant was shown to have 1.54 radicals per dimer as quantitated by EPR spectroscopy.⁶ Because of the greater radical-per-dimer content, the mutant is potentially useful in generating more of the active site-to-tyrosyl-radical spin pairs for a given enzyme and inhibitor concentration. Furthermore, the reaction of 2'-azido-2'-deoxycytidine-5'-diphosphate (N₃CDP) with wt RNR complex was examined as a function of time by 9 GHz EPR. Finally, the effect of 5 mM DTT on the kinetics of the wt RNR reaction with N₃UDP was examined also by 9 GHz EPR. Based on these studies, the first PELDOR measurement of the distance ($r = 48 \pm 1$ Å) between N· covalently bound to C225 in the active site of R1 (see Chapter 2) and Y· in R2 was measured by Bennati *et al.*⁷ This approach holds great promise for mapping the spatial arrangement and distances of catalytically important sites in RNR that have so far been inaccessible by crystallographic methods.

A.2 Calculations used for measuring distances between Y122 in each monomer of R2

For the comparison of the distance between the two tyrosyl radicals in a homodimer of R2 measured by the PELDOR EPR experiment with X-ray crystallographic data, distance calculations were performed on a series of structures using coordinates from the PDB. For the calculation of coordinates of the center of mass of spin density on each Y122 residue, equations A.1 through A.3 were used for the X , Y , and Z coordinate respectively. The X_1 through X_n in Equation A.1 refer to the X coordinates of atoms 1 through n used for the calculation, while m_1 through m_n represent the corresponding spin densities as published by Hoganson *et al.*⁵ and shown in Table A.1. Center of mass of spin density is abbreviated *csd*.

$$X_{csd} = \frac{m_1 X_1 + m_2 X_2 + \dots + m_n X_n}{m_1 + m_2 + \dots + m_n} \quad (\text{A.1})$$

$$Y_{csd} = \frac{m_1 Y_1 + m_2 Y_2 + \dots + m_n Y_n}{m_1 + m_2 + \dots + m_n} \quad (\text{A.2})$$

$$Z_{csd} = \frac{m_1 Z_1 + m_2 Z_2 + \dots + m_n Z_n}{m_1 + m_2 + \dots + m_n} \quad (\text{A.3})$$

The distance between the two centers of mass of spin density with coordinates (X_1, Y_1, Z_1) and (X_2, Y_2, Z_2) was then calculated using Equation A.4.

$$d = \sqrt{(X_2 - X_1)^2 + (Y_2 - Y_1)^2 + (Z_2 - Z_1)^2} \quad (\text{A.4})$$

Atom	Spin Density
O	0.29
C1	0.38
C2, C6	-0.08
C3, C5	0.25
C4	-0.05
C _{methylene}	0.03

Table A.1: π spin density distributions on Y122 of *E. coli* R2

For each of the following PDB files, a table with distances between the csd on Y122 of each monomer is given. For the first three entries in each table, the left column lists the identities of atoms used in the calculation of the center of mass of spin density according to equations A.1, A.2, and A.3 based on coordinates from the PDB file and the Hoganson spin densities. The right column lists the distances calculated between the centers of mass of spin density using equation A.4. For the last two entries in each table, the distances between the individual atoms, i.e. between the O or C₁ atoms of Y122 on each monomer, were determined using RasMol.

1RIB

Coordinates for the PDB entry 1RIB were deposited by Nordlund and Eklund in 1993.⁸ The resolution of this structure is 2.2 Å. The crystallization pH was omitted from the experimental section.

Atoms used in Distance Calc.	Distance (Å)
C ₁ through C ₆ , O, C _{methylene}	33.08
C ₁ through C ₆ , O	33.06
C ₁ , C ₃ , C ₅ , O	33.10
O	32.94
C ₁	33.72

Table A.2: Distances between the csd on Y122 of each monomer or between individual atoms for 1RIB

1PFR

The 1PFR R2 structure was solved and published by Logan *et al.*⁹ The crystals diffracted to 2.2 Å, and were obtained at pH 6.0.

Atoms used in Distance Calc.	Distance (Å)
C ₁ through C ₆ , O, C _{methylene}	32.91
C ₁ through C ₆ , O	32.88
C ₁ , C ₃ , C ₅ , O	32.93
O	32.52
C ₁	33.74

Table A.3: Distances between the csd on Y122 of each monomer or between individual atoms for 1PFR

1AV8

The 1AV8 structure was solved by Tong *et al.*¹⁰ The resolution of this structure is 2.8 Å. The crystallization was carried out at pH of 7.6.

1MXR

The 1MXR structure of *E. coli* R2 was published by Hogbom *et al.* in 2003.¹¹ The resolution of this structure is 1.42 Å. Crystals were obtained at pH 6.0.

Atoms used in Distance Calc.	Distance (Å)
C ₁ through C ₆ , O, C _{methylene}	32.81
C ₁ through C ₆ , O	32.79
C ₁ , C ₃ , C ₅ , O	32.82
O	32.61
C ₁	33.49

Table A.4: Distances between the csd on Y122 of each monomer or between individual atoms for 1AV8

Atoms used in Distance Calc.	Distance (Å)
C ₁ through C ₆ , O, C _{methylene}	32.38
C ₁ through C ₆ , O	32.34
C ₁ , C ₃ , C ₅ , O	32.41
O	31.72
C ₁	33.35

Table A.5: Distances between the csd on Y122 of each monomer or between individual atoms for 1MXR

A.3 Phosphorylation of 2'-azido-2'-deoxyuridine and 2'-azido-2'-deoxycytidine

N₃UDP was synthesized in 75% yield from 5 μmol of 2'-azido-2'-deoxyuridine (Sigma) by the enzymatic procedure described in Chapter 3 (¹H NMR (²H₂O) δ 4.05–4.17 (m, 2H), 4.25 (t, J = 5.3 Hz, 1H) 4.50 (t, J = 5.0 Hz, 1H), 5.85 (d, J = 8.1 Hz, 1H), 5.95 (d, J = 5.2 Hz, 1H), 7.85 (d, J = 8.0 Hz, 1H); ³¹P NMR (²H₂O) δ -10.17 (d, J = 21.1 Hz, 1P), -9.20 (d, J = 21.1 Hz, 1P)).

N₃CDP was synthesized in 83% from 5 μmol of 2'-azido-2'-deoxycytidine (Sigma) by the enzymatic procedure described in Chapter 3 (¹H NMR (²H₂O) δ 4.17 (m, 1H), 4.23 (m, 2H), 4.31 (t, J = 4.7 Hz, 1H), 4.6 (t, J = 5.0 Hz, 1H), 5.98 (d, J = 4.1 Hz, 1H), 6.10 (d, J = 7.6 Hz, 1H), 8.00 (d, J = 7.6 Hz, 1H); ³¹P NMR (²H₂O) δ -10.18 (d, J = 21.4 Hz, 1P), -8.05 (d, J = 21.4 Hz, 1P)).

A.4 Results of N₃NDP inactivation studies

All proteins were purified as described in Chapter 2.

In a final volume of 220 μL, reactions of wt RNR and wt R1/C268S R2 with N₃UDP contained 1 mM TTP, 1 mM N₃UDP, 360 μM R1 (pre-reduced, S.A. 2200–3000 nmol · mg⁻¹ · min⁻¹), either 300 μM wt R2 (S.A. 6000–7000 nmol · mg⁻¹ · min⁻¹, 1.2 Y · per dimer) or

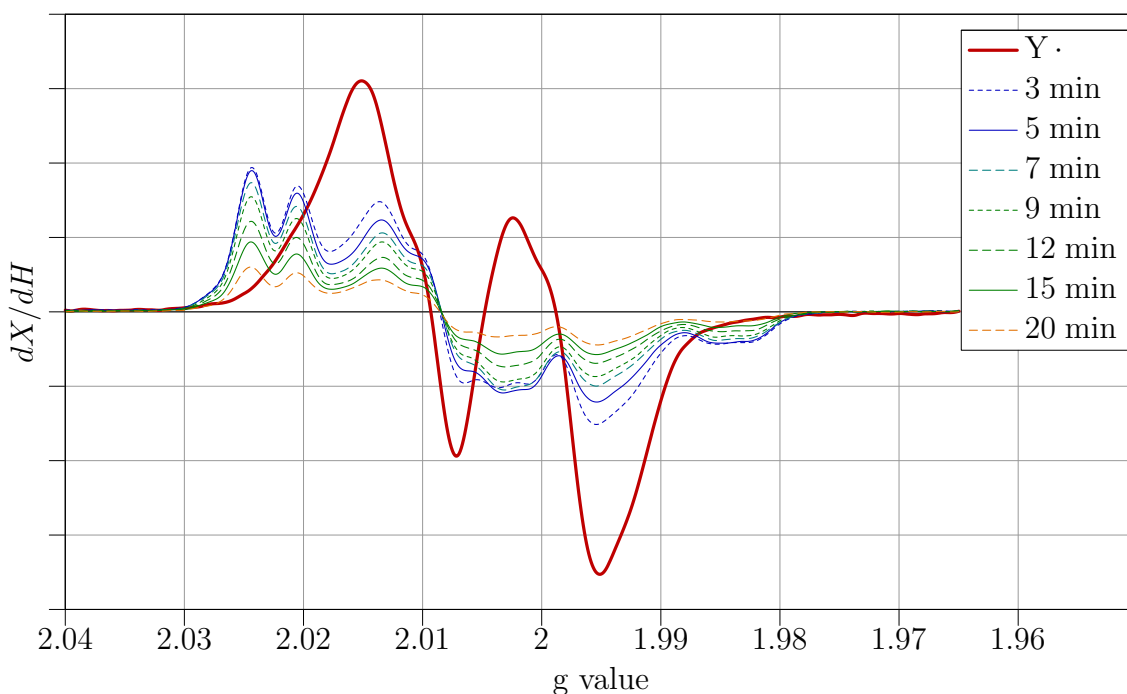


Figure A.1: 9 GHz EPR spectra of the reaction of wt *E. coli* RNR with N₃UDP as a function of time

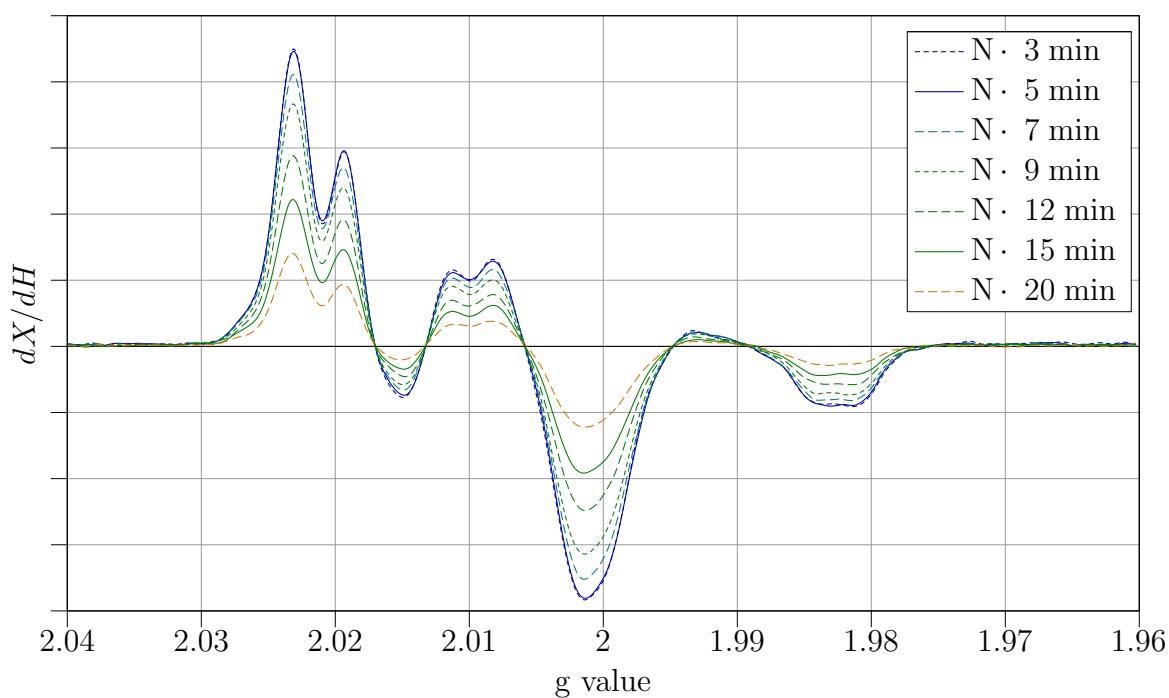
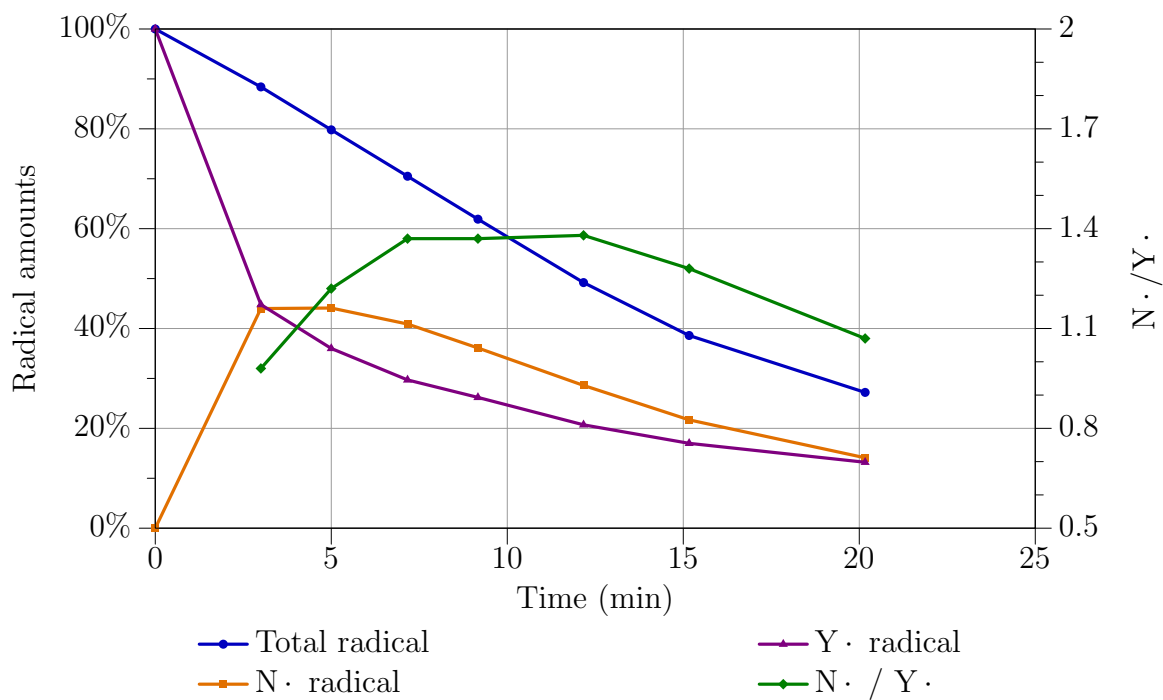
300 μM C268S-R2 (S.A. 12380 $\text{nmol} \cdot \text{mg}^{-1} \cdot \text{min}^{-1}$, 1.54 Y \cdot per dimer),⁶ 20 μM TR (S.A. 40 $\text{units} \cdot \text{mg}^{-1}$), 1 μM TRR (S.A. 1600 $\text{units} \cdot \text{mg}^{-1}$), and 0.8 mM NADPH all in 50 mM HEPES pH 7.6, 15 mM MgSO₄, 1 mM EDTA.

A control reaction of wt RNR and N₃UDP was run in the presence of DTT in place of TR/TRR/NADPH. In a final volume of 220 μL , the reaction contained 150 μM TTP, 1 mM N₃UDP, 60 μM R1 (pre-reduced, S.A. 2200–3000 $\text{nmol} \cdot \text{mg}^{-1} \cdot \text{min}^{-1}$), 50 μM wt R2 (S.A. 6000–7000 $\text{nmol} \cdot \text{mg}^{-1} \cdot \text{min}^{-1}$, 1.2 Y \cdot per dimer), and 5 mM DTT all in 50 mM HEPES pH 7.6, 15 mM MgSO₄, 1 mM EDTA.

Reactions of wt RNR with N₃CDP contained 0.5 mM TTP, 1 mM N₃CDP, 120 μM R1 (pre-reduced, S.A. 2200–3000 $\text{nmol} \cdot \text{mg}^{-1} \cdot \text{min}^{-1}$), 100 μM wt R2 (S.A. 6000–7000 $\text{nmol} \cdot \text{mg}^{-1} \cdot \text{min}^{-1}$, 1.2 Y \cdot per dimer), and 5 mM DTT all in 50 mM HEPES pH 7.6, 15 mM MgSO₄, 1 mM EDTA in a final volume of 220 μL .

For each reaction, all components except for the inhibitor were combined and equilibrated at 25 °C for 5 min. The reaction was started by the addition of the inhibitor and then transferred to a 706 PQ EPR tube (quartz, OD 4 mm, ID 2.4 mm, from Wilmad LabGlass) where it was frozen in liquid nitrogen. 9 GHz EPR experiments were performed as described in Chapter 2.

Shown in Figure A.1 are 9 GHz EPR spectra of the reaction of wt RNR with N₃UDP as a function of time. After subtraction of the unreacted tyrosyl radical (Y \cdot) spectrum

Figure A.2: $N\cdot$ spectra in the reaction of wt *E. coli* RNR with N_3 UDP as a function of timeFigure A.3: Decay curves for radical species in the reaction of wt *E. coli* RNR with N_3 UDP

Time (min)	Total radical	N·	Y·	N·/Y·
0	360 μM (100%)	0 μM (0%)	360 μM (100%)	0
3	320 μM (89%)	158 μM (44%)	161.3 μM (44.8%)	0.98
5	288 μM (80%)	158.9 μM (44%)	129.6 μM (36%)	1.22
7	254 μM (70.6%)	147.1 μM (41%)	106.9 μM (29.7%)	1.37
9	224 μM (62.3%)	129.8 μM (36%)	94.3 μM (26.2%)	1.37
12	178 μM (49.3%)	103.1 μM (28.6%)	74.5 μM (20.7%)	1.38
15	139 μM (38.7%)	78.1 μM (21.7%)	61.2 μM (17%)	1.28
20	98.5 μM (27.3%)	50.8 μM (14.1%)	47.5 μM (13.2%)	1.07

Table A.6: Time-course of the wt RNR reaction with N₃UDP

contribution from the spectrum at each time point (see Table A.6 for amounts), the spectra of the nitrogen-centered radical (N·) were obtained as shown in Figure A.2. Represented in percentage terms in Figure A.3 are the total amount of radical in the reaction, the amount of N· formed, and the amount of unreacted Y· remaining, as well as the dimensionless ratio of N· to Y· as a function of time. The highest N· to Y· ratio (1.4) is observed at 7–12 min into the reaction.

A similar experiment was performed using wt R1/C268S-R2 in place of wt RNR. The results are shown in Figure A.4. Spectra of N· were obtained after the subtraction of the unreacted Y· spectrum contribution from the spectrum at each time point (see Table A.7 for amounts) and are shown in Figure A.5. Represented in percentage terms in Figure A.3 are the total amount of radical in the reaction, the amount of N· formed, and the amount of unreacted Y· remaining, as well as the dimensionless ratio of N· to Y· as a function of time. The ratio of N· to Y· reaches a maximum of 1.55 at 20 min into the reaction.

To establish if change of the nitrogenous base of the inhibitor has an effect on the maximum ratio of N· to Y·, N₃CDP was synthesized and its reaction with wt RNR in the presence of TTP as the effector was examined by 9 GHz EPR spectroscopy. The results are shown in Figure A.7. To obtain the spectra of N· at each time point (Figure A.8), the contribution to the spectra of the unreacted Y· (see Table A.8 for amounts) was subtracted. In Figure A.9, the total amount of radical in the reaction, the amount of N· formed, and the amount of unreacted Y· remaining are shown in percent, as well as the dimensionless ratio of N· to Y· as a function of time. The ratio of N· to Y· reaches a maximum of 1.63 at 15 min into the reaction.

An additional control experiment was performed to determine if the presence of 5 mM 1,4-dithiothreitol (DTT) in the reaction of N₃UDP with wt RNR influences the maximum ratio of N· to Y·. The spectra of the reaction as a function of time are shown in Figure A.10. Spectra of N· were obtained after the subtraction of the unreacted Y· spectrum contribution from the spectrum at each time point (see Table A.9 for amounts) and are shown in Figure A.11. Represented in percentage terms in Figure A.12 are the total amount of radical in the reaction, the amount of N· formed, and the amount of unreacted Y· remaining, as well as

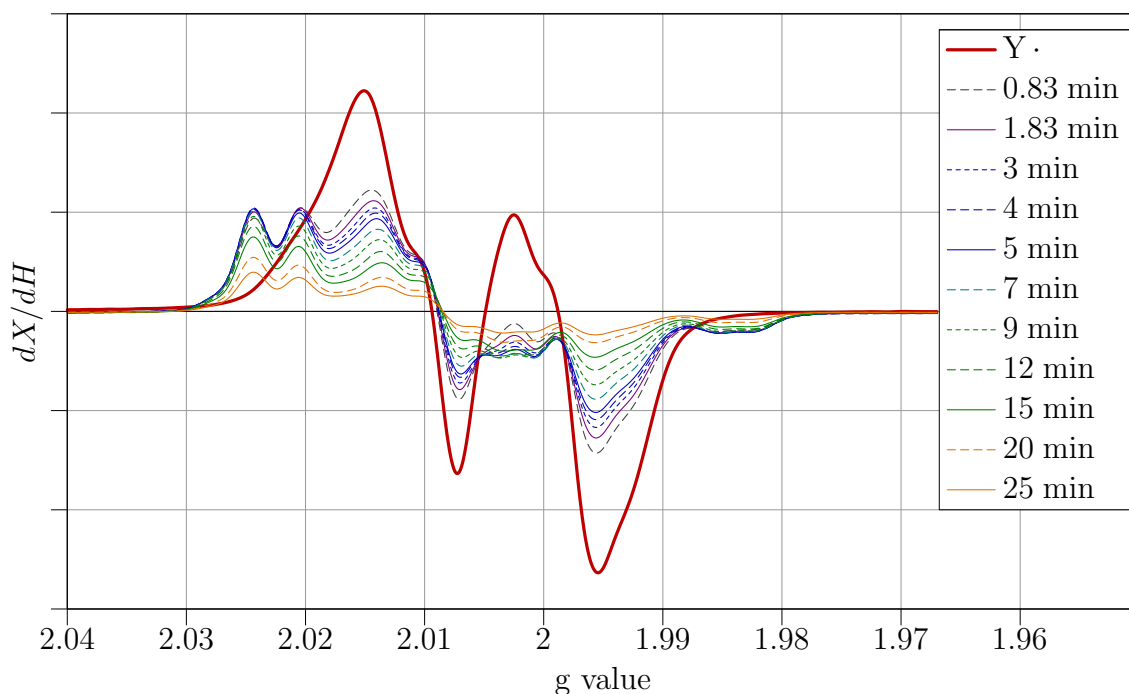


Figure A.4: 9 GHz EPR spectra of the reaction of wt R1/C268S-R2 *E. coli* RNR with N₃UDP as a function of time

Time (min)	Total radical	N·	Y·	N·/Y·
0	480 μM (100%)	0 μM (0%)	480 μM (100%)	0
0.83	417.12 μM (86.9%)	150.7 μM (31.4%)	266.4 μM (55.5%)	0.56
1.83	404.6 μM (84.3%)	165.6 μM (34.5%)	239 μM (49.8%)	0.69
3	392.6 μM (81.8%)	171.8 μM (35.8%)	220.32 μM (45.9%)	0.78
4	384 μM (80%)	177.1 μM (36.9%)	207.4 μM (43.2%)	0.85
5	370.1 μM (77.1%)	176.2 μM (36.7%)	193.9 μM (40.4%)	0.91
7	343.2 μM (77.5%)	173.76 μM (36.2%)	169.44 μM (35.3%)	1.02
9	309.6 μM (64.5%)	166.1 μM (34.6%)	143.5 μM (29.9%)	1.16
12	266.9 μM (55.6%)	150.72 μM (31.4%)	115.7 μM (24.1%)	1.30
15	225.1 μM (46.9%)	132.5 μM (27.6%)	92.2 μM (19.2%)	1.44
20	160.3 μM (33.4%)	97.4 μM (20.3%)	62.88 μM (13.1%)	1.55
25	118.1 μM (24.6%)	70.6 μM (14.7%)	47.6 μM (9.91%)	1.48

Table A.7: Time-course of the wt R1/C268S-R2 RNR reaction with N₃UDP

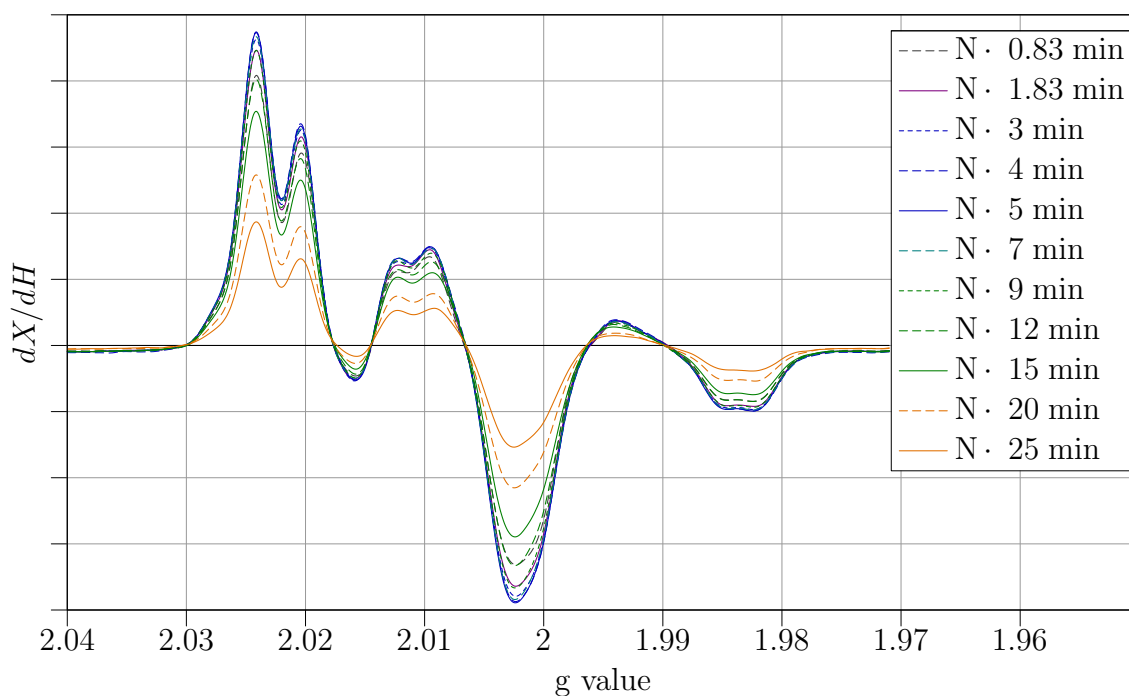


Figure A.5: N \cdot spectra in the reaction of wt R1/C268S-R2 *E. coli* RNR with N₃UDP as a function of time

Time (min)	Total radical	N \cdot	Y \cdot	N \cdot /Y \cdot
0	120 μ M (100%)	0 μ M (0%)	120 μ M (100%)	0
1	115 μ M (96.1%)	56.1 μ M (46.7%)	59.2 μ M (49.3%)	0.95
5	105 μ M (88%)	60.2 μ M (50.2%)	45.5 μ M (37.9%)	1.32
9	90 μ M (75.4%)	54.8 μ M (45.6%)	35.7 μ M (29.7%)	1.53
15	68.7 μ M (57.3%)	42.6 μ M (35.5%)	26.1 μ M (21.7%)	1.63

Table A.8: Timecourse of the wt RNR reaction with N₃CDP

Time (min)	Total radical	N \cdot	Y \cdot	N \cdot /Y \cdot
0	55 μ M (100%)	0 μ M (0%)	55 μ M (100%)	0
4	47.4 μ M (86.2%)	24.5 μ M (44.6%)	23.1 μ M (41.6%)	1.07
8	37.6 μ M (68.4%)	20.3 μ M (37%)	17.3 μ M (31.4%)	1.18
12	32.9 μ M (59.5%)	17.9 μ M (32.6%)	14.8 μ M (27%)	1.21

Table A.9: Time-course of the wt RNR reaction with N₃UDP in the presence of DTT

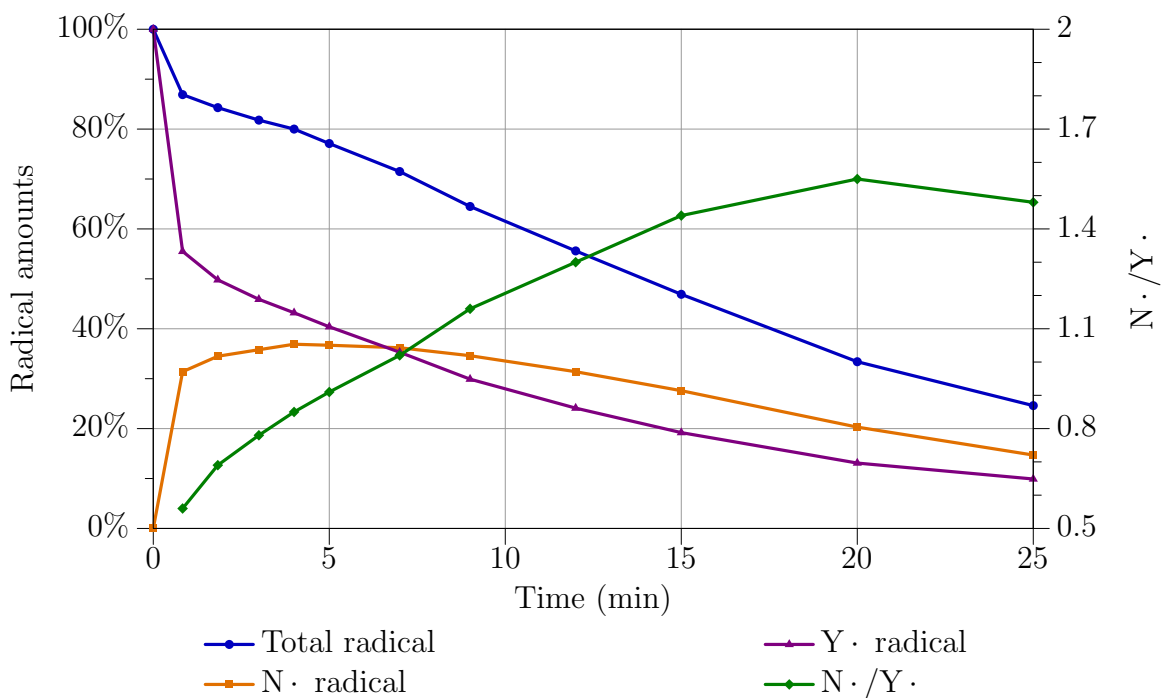


Figure A.6: Decay curves for radical species in the reaction of wt R1/C268S-R2 with N₃UDP

the dimensionless ratio of N· to Y· as a function of time. In the presence of DTT, the ratio of N· to Y· reaches a maximum of 1.2 at 12 min into the reaction.

Figures A.13, A.14, A.15, and A.16 show comparisons of the amounts of total radical, Y·, N· and the ratio of N· to Y·, respectively, as a function of time in all N₃NDP reactions. The percentage across experiments has not been normalized; rather, the percentage is always expressed relative to the starting amount of Y· in the reaction which depends on R2 concentration. For example, in Figure A.15, the amount of N· in the reaction of wt R1/C268S-R2 with N₃UDP at 0.83 min (0.83 min time-point) is 31% relative to the total amount of starting Y· and this percentage does not indicate that less radical is formed in absolute amounts relative to the reaction of wt RNR with N₃UDP (44%, 3 min time-point). The absolute amounts in the form of concentration of radicals in the reaction mixtures are shown in Tables A.6, A.7, A.8 and A.9.

Based on the calculated N· to Y· ratios, Bennati *et al.*⁷ designed PELDOR experiments to measure the distance between N· in the active site of R1 and Y· in R2.⁷ The distance was determined to be $48 \pm 1 \text{ \AA}$. Furthermore, no N· / N· pairs were observed.

These results have interesting implications when considered in the context of pre-steady state experiments published by Ge *et al.*¹² The pre-steady state experiments showed that 1.7 equivalents of dCDP were produced in a single kinetic phase (k_{obs} of 9 s^{-1}), indicating that each monomer of R1 is active.

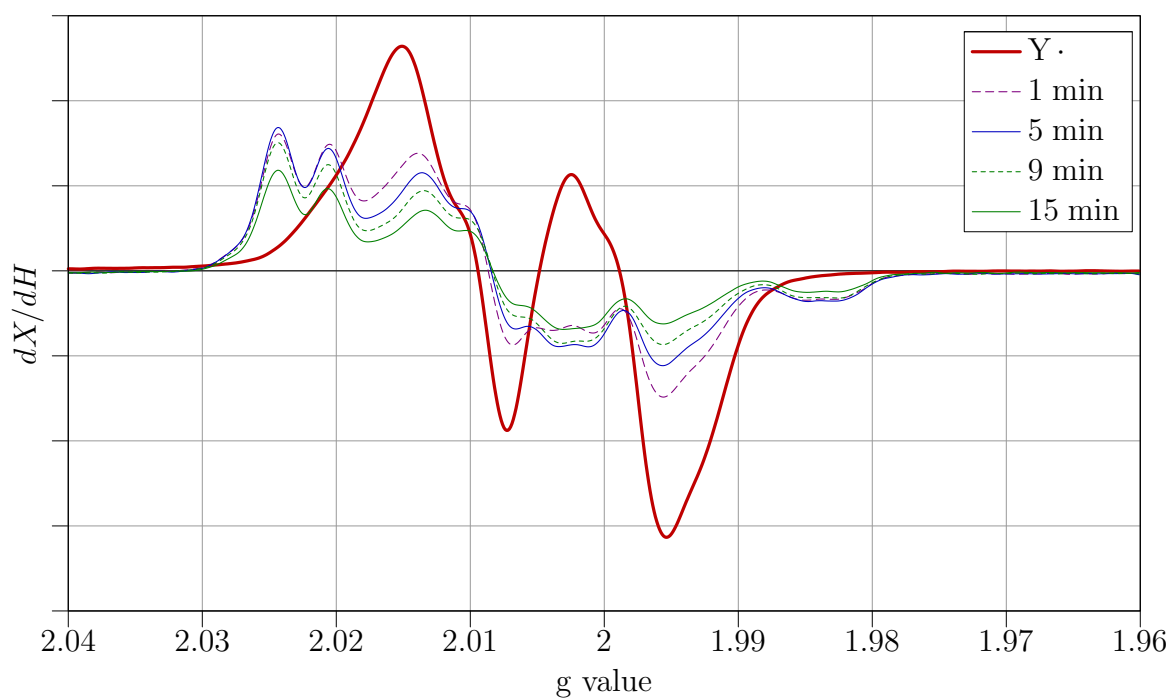
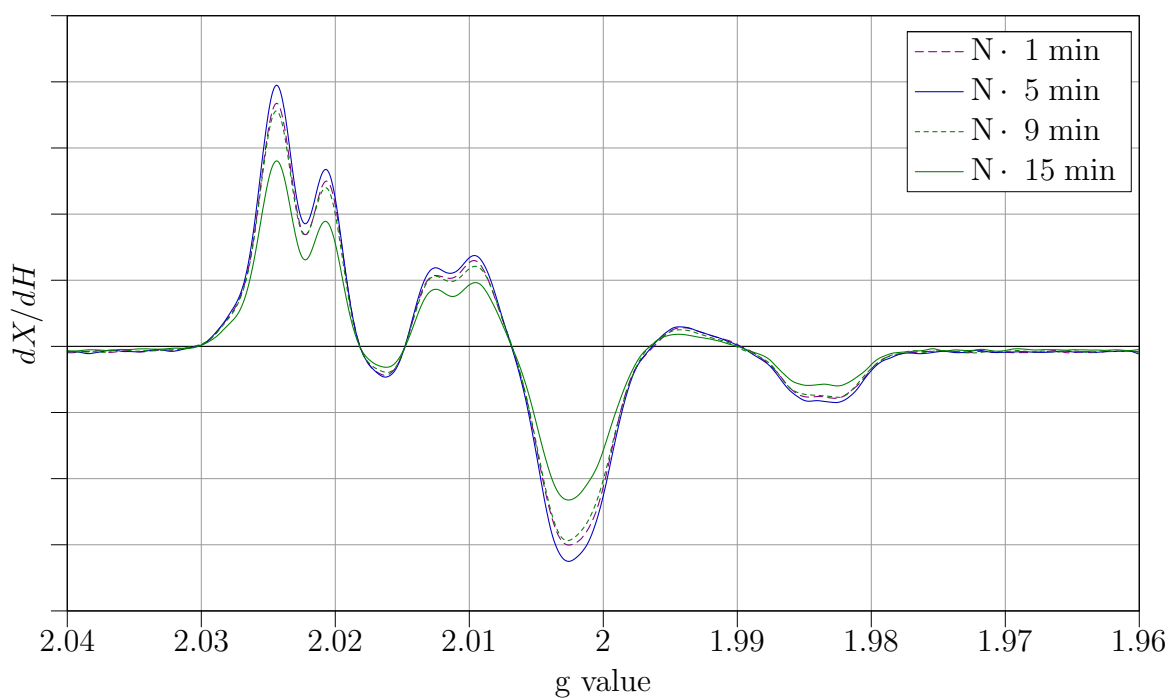
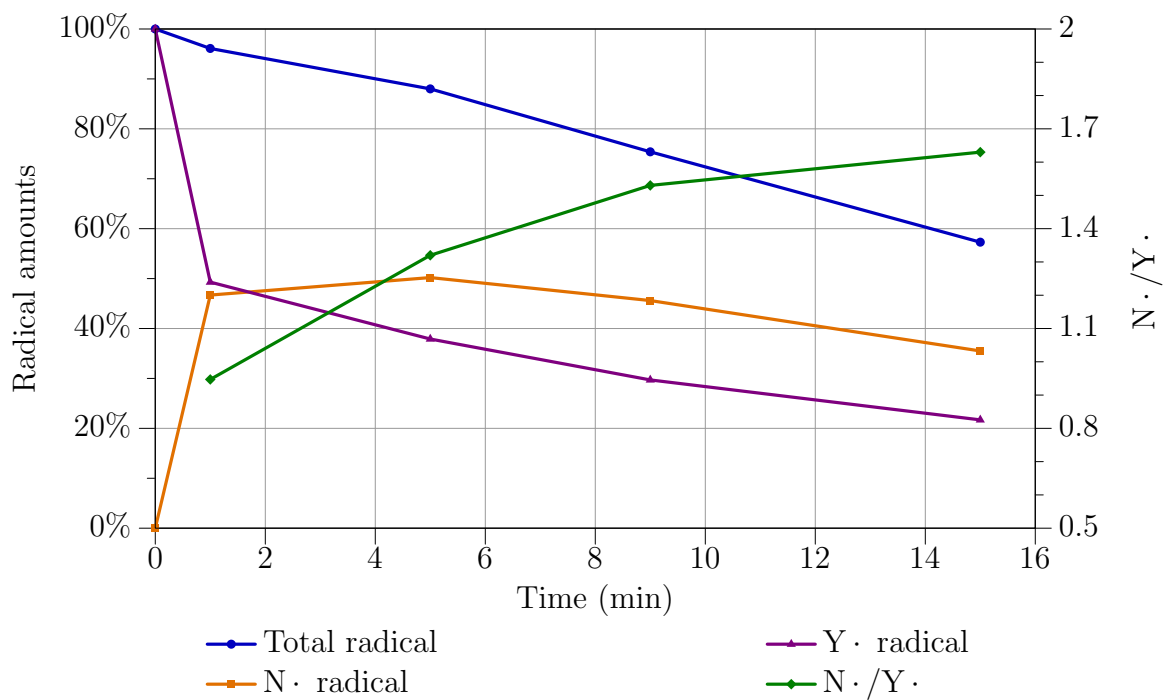


Figure A.7: 9 GHz EPR spectra of the reaction of wt *E. coli* RNR with N₃CDP as a function of time

Figure A.8: $N\cdot$ spectra in the reaction of wt *E. coli* RNR with N_3 CDP as a function of timeFigure A.9: Decay curves for radical species in the reaction of wt *E. coli* RNR with N_3 CDP

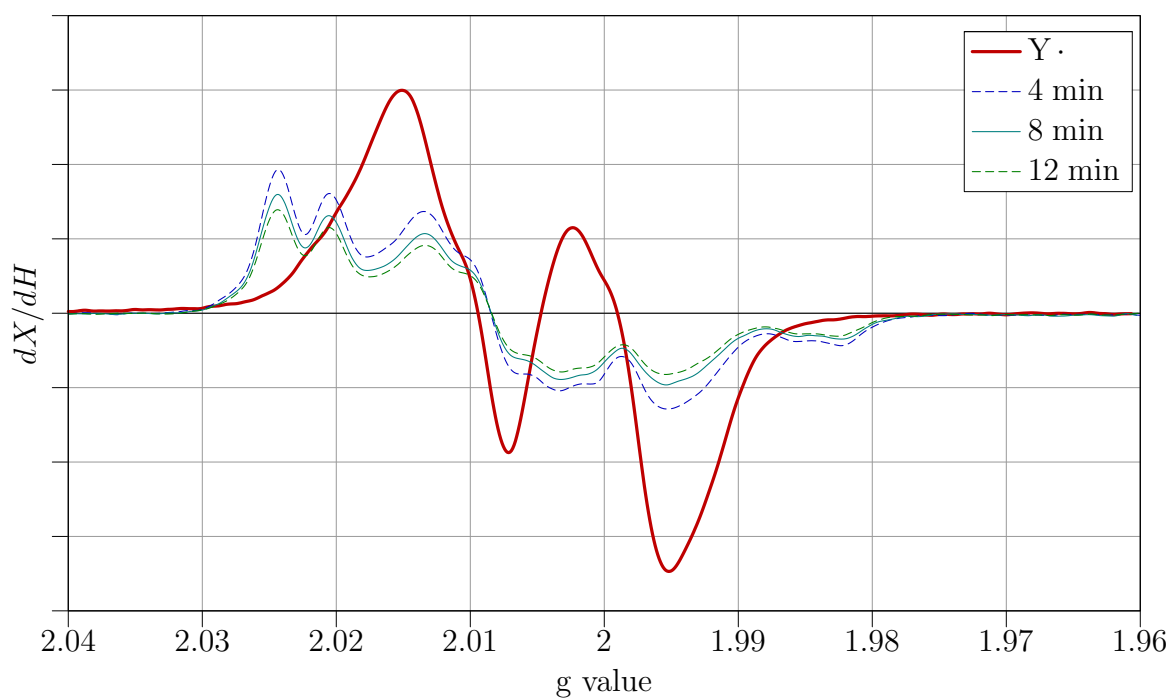


Figure A.10: 9 GHz EPR spectra of the reaction of wt *E. coli* RNR with N₃UDP as a function of time in the presence of DTT

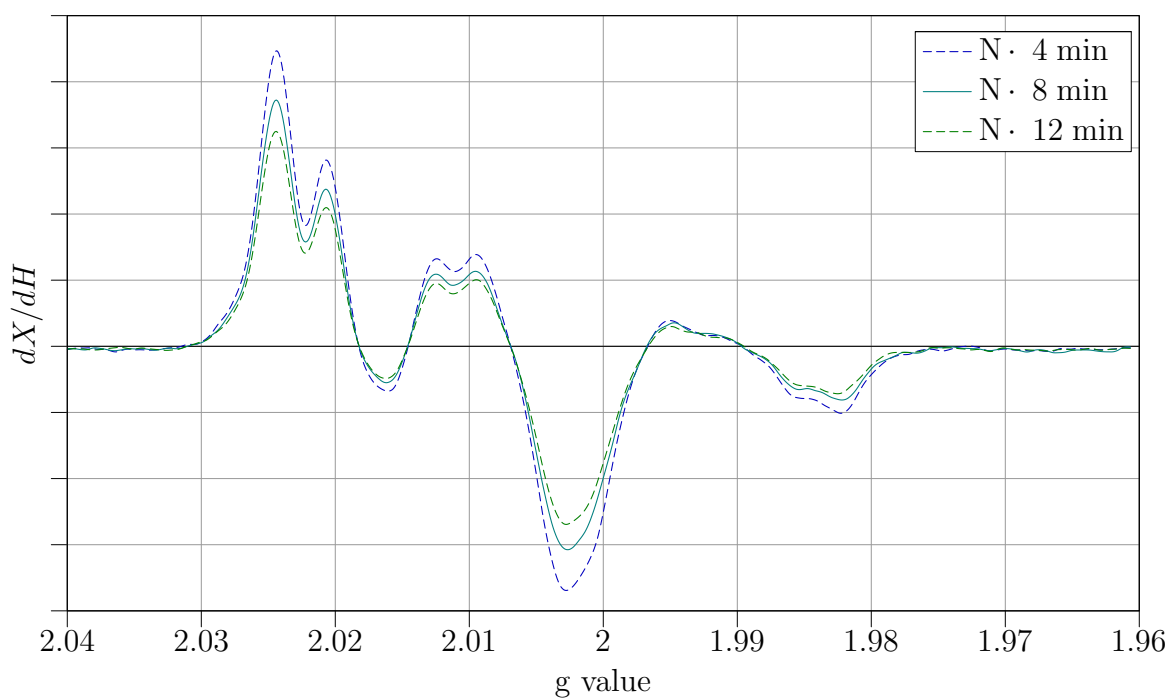


Figure A.11: $N\cdot$ spectra in the reaction of wt *E. coli* RNR with N_3 UDP as a function of time in the presence of DTT

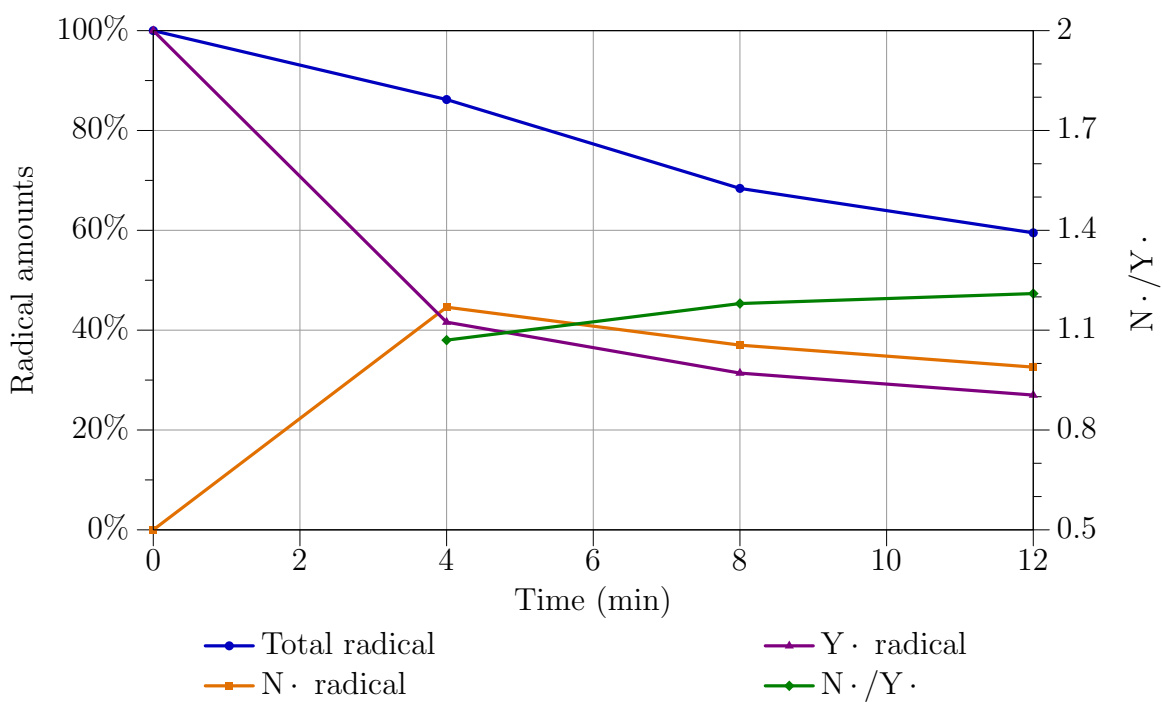
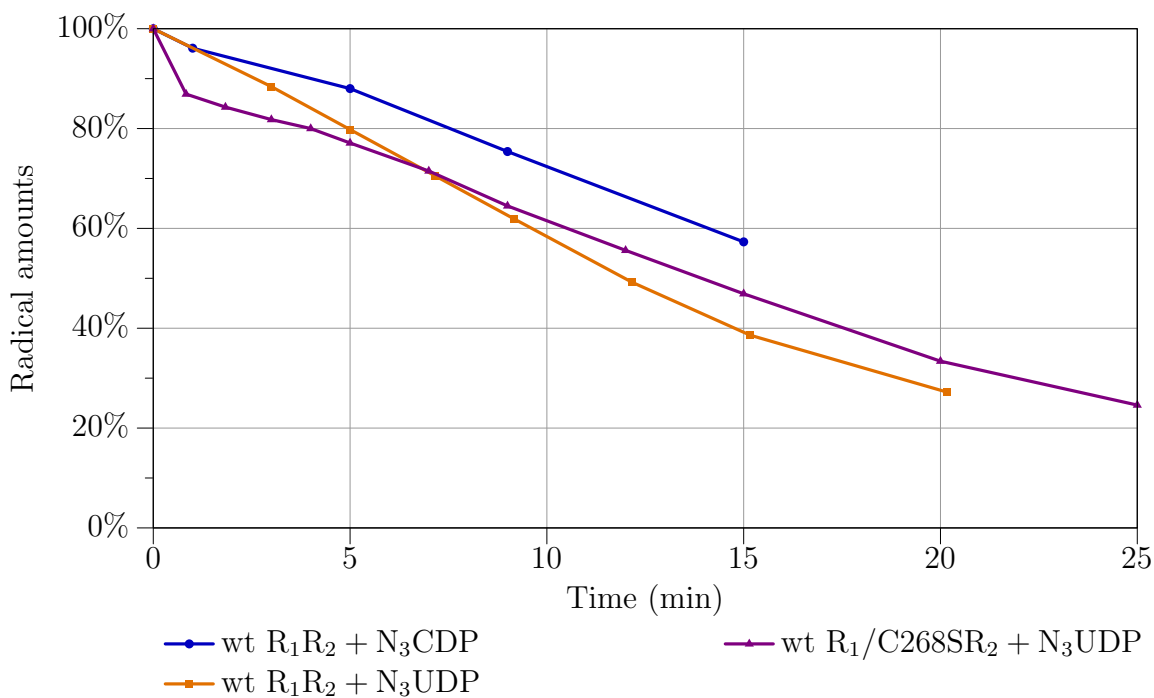
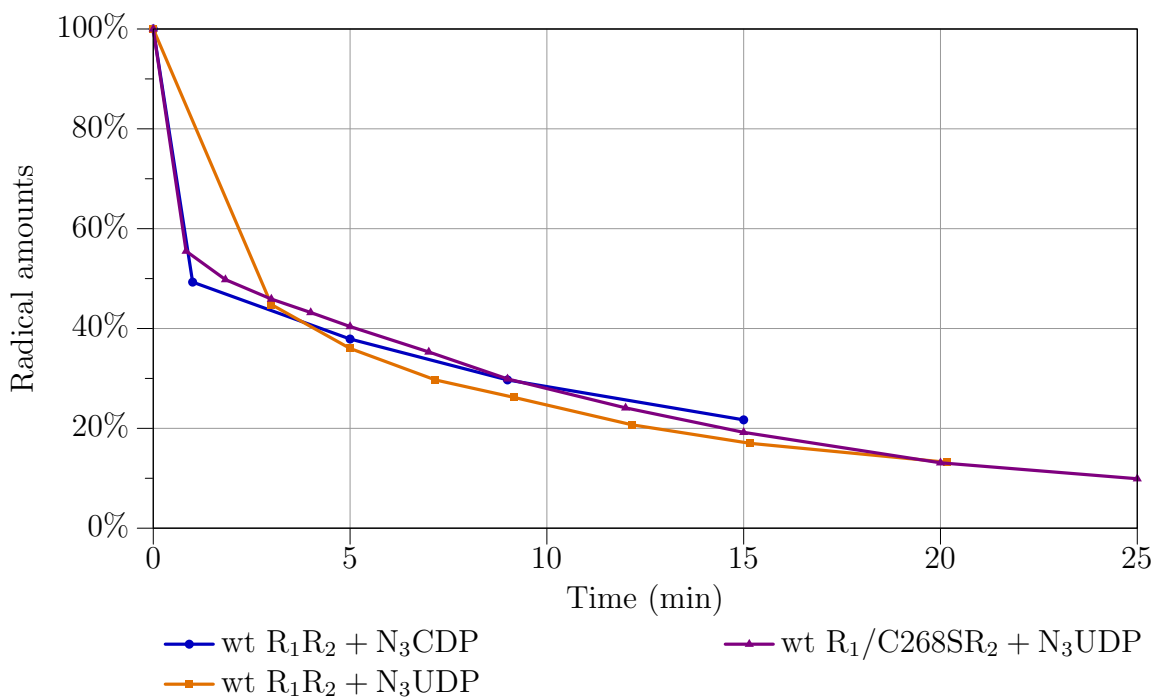
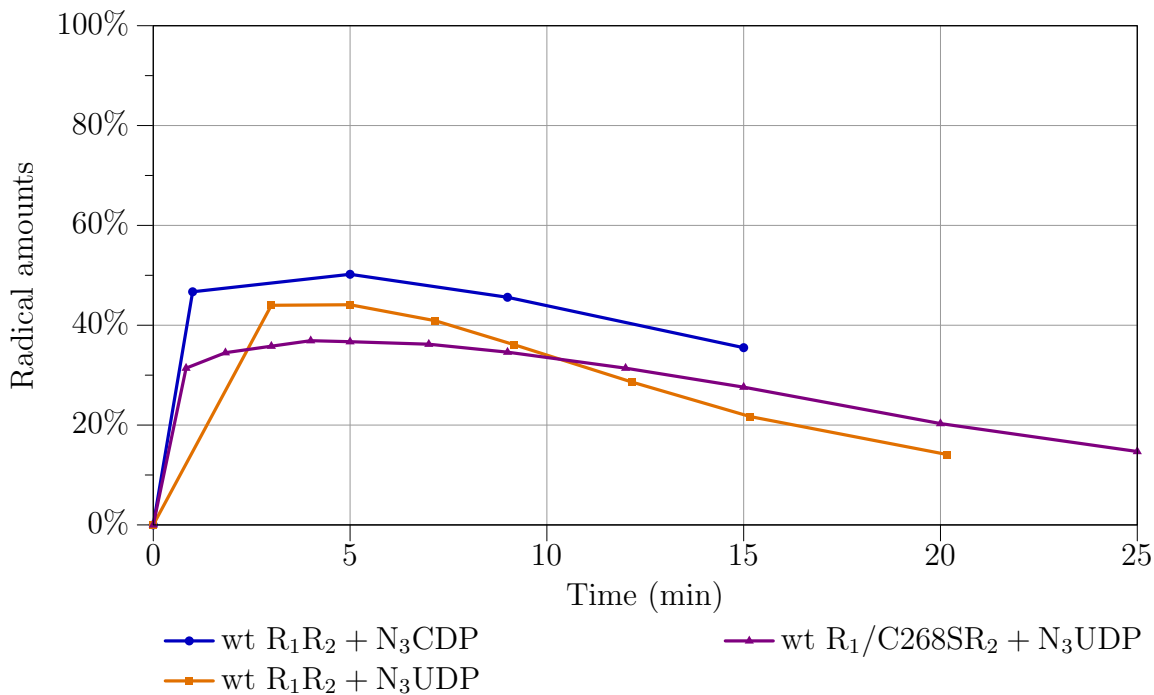
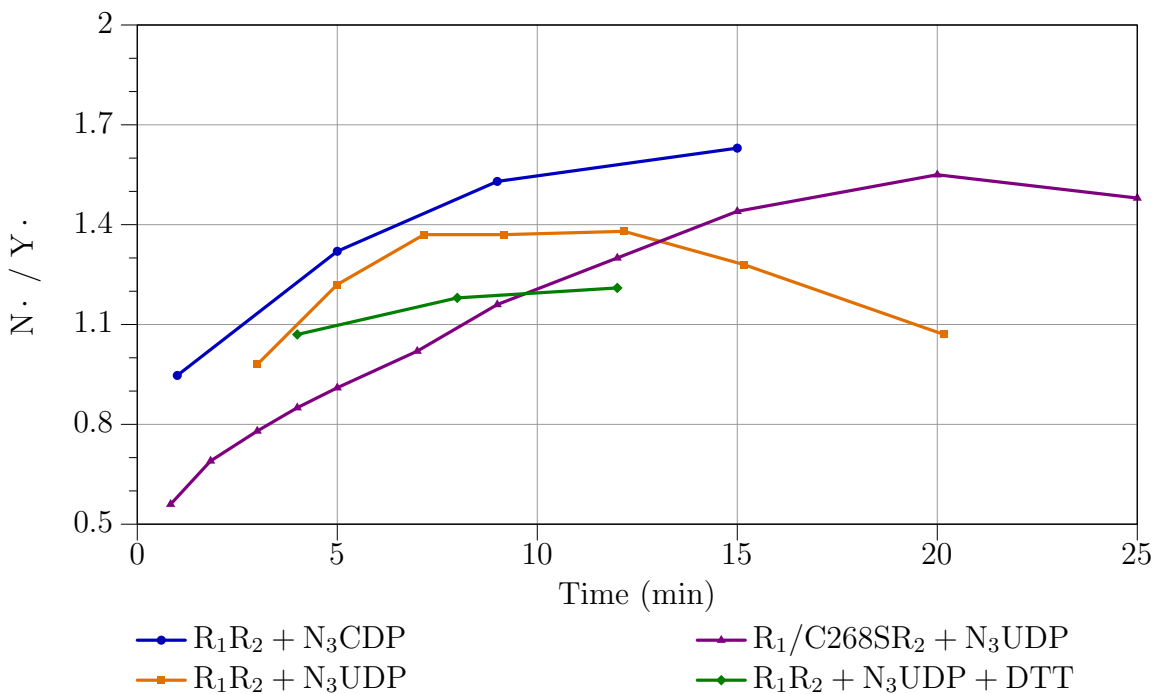


Figure A.12: Decay curves for radical species in the reaction of wt *E. coli* RNR with N₃UDP in the presence of DTT

Figure A.13: Decay curves for total radical in the reaction of RNR with N_3 NDPFigure A.14: Decay curves for $Y\cdot$ radical in the reaction of RNR with N_3 NDP

Figure A.15: Decay curves for $N\cdot$ in the reaction of RNR with N_3 NDPFigure A.16: Decay curves for $N\cdot / Y\cdot$ ratio in the reaction of RNR with N_3 NDP

The PELDOR studies show that $N\cdot / Y\cdot$ pairs are present in a single complex of RNR, and that $N\cdot / N\cdot$ pairs could not be detected. Thus, even though each monomer of R1 is active, the reduction chemistry in the monomers is not concerted. This observation is in accord with the fact that more than 1 equivalent of dCDP was formed per 1 equivalent of $Y\cdot$ (1.7 equivalents of dCDP per 1.1 equivalent of $Y\cdot$) in the pre-steady state studies carried out by Ge *et al.*¹²

Bibliography

- [1] E. L. Hahn, "Spin echoes," *Physical Review*, vol. 80, no. 4, pp. 580–594, 1950.
- [2] A. D. Milov, A. B. Ponomarev, and Y. D. Tsvetkov, "Electron-electron double resonance in electron spin echo: Model biradical systems and the sensitized photolysis of decalin," *Chemical Physics Letters*, vol. 110, no. 1, pp. 67–72, 1984.
- [3] R. G. Larsen and D. J. Singel, "Double electron-electron resonance spin-echo modulation: spectroscopic measurement of electron spin pair separations in orientationally disordered solids," *Journal of Chemical Physics*, vol. 98, no. 7, pp. 5134–5146, 1993.
- [4] M. Bennati, A. Weber, J. Antonic, D. L. Perlstein, J. Robblee, and J. Stubbe, "Pulsed ELDOR spectroscopy measures the distance between the two tyrosyl radicals in the R2 subunit of the *E. coli* ribonucleotide reductase," *Journal of the American Chemical Society*, vol. 125, no. 49, pp. 14988–14989, 2003.
- [5] C. W. Hoganson, M. Sahlin, B.-M. Sjöberg, and G. T. Babcock, "Electron magnetic resonance of the tyrosyl radical in ribonucleotide reductase from *Escherichia coli*," *Journal of the American Chemical Society*, vol. 118, no. 19, pp. 4672–4679, 1996.
- [6] C. S. Yee, "Mechanistic investigations of the radical initiation pathway of class I ribonucleotide reductase from *Escherichia coli*," *Massachusetts Institute of Technology*, 2004. PhD thesis.
- [7] M. Bennati, J. H. Robblee, V. Mugnaini, J. Stubbe, J. H. Freed, and P. Borbat, "EPR distance measurements support a model for long-range radical initiation in *E. coli* ribonucleotide reductase," *Journal of the American Chemical Society*, vol. 127, no. 43, pp. 15014–15015, 2005.
- [8] P. Nordlund and H. Eklund, "Structure and function of the *Escherichia coli* ribonucleotide reductase protein R2," *Journal of Molecular Biology*, vol. 232, no. 1, pp. 123–164, 1993.
- [9] D. T. Logan, X. D. Su, A. Aberg, K. Regnstrom, J. Hajdu, H. Eklund, and P. Nordlund, "Crystal structure of reduced protein R2 of ribonucleotide reductase: the structural basis for oxygen activation at a dinuclear iron site," *Structure (London)*, vol. 4, no. 9, pp. 1053–1064, 1996.
- [10] W. Tong, D. Burdi, P. Riggs-Gelasco, S. Chen, D. Edmondson, V. Huynh, J. Stubbe, S. Han, A. Arvai, and J. Tainer, "Characterization of Y122F R2 of *Escherichia coli* ribonucleotide reductase by time-resolved physical biochemical methods and X-ray crystallography," *Biochemistry*, vol. 37, no. 17, pp. 5840–5848, 1998.
- [11] M. Hogbom, M. Galander, M. Andersson, M. Kolberg, W. Hofbauer, G. Lassmann, P. Nordlund, and F. Lendzian, "Displacement of the tyrosyl radical cofactor in ribonucleotide reductase obtained by single-crystal high-field EPR and 1.4-Å X-ray data," *Proceedings of the National Academy of Sciences of the United States of America*, vol. 100, no. 6, pp. 3209–3214, 2003.
- [12] J. Ge, G. Yu, M. A. Ator, and J. Stubbe, "Pre-steady-state and steady-state kinetic analysis of *E. coli* class I ribonucleotide reductase," *Biochemistry*, vol. 42, no. 34, pp. 10071–10083, 2003.

Appendix B

Ab initio coupled cluster (CCSD(T)) calculations on HO–N•–SH and HO–CH₂–N•–SH structures

Table B.1 shows the HFC tensors for the small models obtained at CCSD(T) and DFT levels. Comparison of the constants revealed that influences of basis set and method are almost negligible for the dipolar HFCs (T_{ii}), whereas the isotropic HFC constants (A_{iso}) showed some dependence on both. DFT calculations, in particular the computations employing the IGLO-II basis set, systematically slightly underestimated the [¹⁴N] and [¹⁷O] isotropic HFC constants. For ONS-CUT (the name represents the structure as defined in Table B.1), the deviation between DFT and CCSD(T) [¹⁴N] isotropic HFC constants is up to about 5 G, but for CNS-CUT, the deviation is only 0.9 G. On the other hand, the effect on the [¹⁷O] isotropic HFC constant is more pronounced for the CNS-CUT model. These trends must be considered when comparing the results of calculations with the experimental data. Nevertheless, the *ab initio* validation study shows that the DFT computations employing the IGLO-II basis set yield satisfying spin densities and HFC constants for the systems under study, even though the Fermi contact contributions may be underestimated.

		HO – N · – SH (ONS - CUT)			HO – CH ₂ – N · – SH (CNS - CUT)		
		B3PW91	B3PW91	CCSD(T)	B3PW91	B3PW91	CCSD(T)
		IGLO-II	IGLO-III	IGLO-III	IGLO-II	IGLO-III	IGLO-III
¹⁴ N	A_{iso}	+9.43	+10.91	+14.56	+8.19	+9.16	+9.05
	T_{11}	-13.80	-14.05	-13.77	-11.41	-11.50	-10.30
	T_{22}	-12.90	-13.15	-12.94	-11.16	-11.27	-9.93
	T_{33}	+26.70	+27.20	+26.70	+22.57	+22.77	20.23
¹⁷ O	A_{iso}	-6.05	-6.35	-7.98	-3.46	-3.86	-5.87
	T_{11}	-20.34	-19.97	-17.90	-6.03	-5.96	-5.55
	T_{22}	+10.87	+10.65	+9.84	+3.16	+3.11	+2.55
	T_{33}	+9.47	+9.32	+8.07	+2.87	+2.85	3.00

Table B.1: Comparison between isotropic (A_{iso}) and dipolar (T_{ii}) hyperfine coupling constants obtained by UB3PW91/IGLO-II and IGLO-III and by *ab initio* CCSD(T)/IGLO-III calculations for ONS and CNS model substructures

Curriculum Vitae

Education

Massachusetts Institute of Technology (MIT), Cambridge, MA

Candidate for Ph.D. in Chemistry, June 2006, Research Supervisor: JoAnne Stubbe (1999–2006): “Mechanistic Studies of the Class I Ribonucleotide Reductase from *Escherichia coli*”; Thesis Committee: Robert Griffin, Catherine Drennan, Daniel Kemp

Mount Holyoke College (MHC), South Hadley, MA

Bachelor of Arts in Chemistry with minor in Mathematics, Cum Laude (1995–1999)

Awards

- Louisa Stone Stevenson Prize for excellence in Chemistry (outstanding chemistry major) (May 1998)
- American Chemical Society Undergraduate Award for achievement in Organic Chemistry (May 1997)
- Abbey Turner Award for excellence in Biochemistry (May 1996)

Selected Coursework

- MIT – Molecular Structure and Reactivity, Synthetic Organic Chemistry I & II, NMR Spectroscopy and Organic Structure Determination, Advanced Biological Chemistry, Enzymes: Structure and Mechanism
- MHC – Organometallic Chemistry and Catalysis, Chemical Thermodynamics, Quantum Chemistry, Protein Biochemistry, Nucleic Acid Biochemistry, Advanced Inorganic Chemistry, Group Theory, Organic Synthesis

Skills

- Spectroscopy – NMR, 9 GHz and 140 GHz CW and pulsed EPR, FTIR, UV-Vis absorption
- Biochemistry – Recombinant protein over-expression in bacterial systems; protein purification; size-exclusion, ion-exchange, hydrophobic, affinity, thin layer, flash and high performance liquid chromatography; execution of reactions under anaerobic conditions; development of spectrophotometric and radioactive enzyme activity and inhibition assays; rapid chemical quench; protein and DNA electrophoresis
- Synthetic Organic Chemistry – Multistep synthesis including execution of microscale reactions under inert atmosphere and handling of pyrophoric reagents; nucleotide analog chemistry
- Languages – Fluent in English; Fluent in Serbian (native)

Research Experience

Massachusetts Institute of Technology (MIT), Cambridge, MA

- Obtained direct evidence for a key intermediate in the reaction catalyzed by ribonucleotide reductase through judicious use of site-directed mutagenesis, synthesis of isotopically labeled nucleotides, and EPR spectroscopy
- Developed an enzymatic method for the phosphorylation of nucleoside analogues not amenable to standard phosphoramidate chemistry
- Determined the structure of a radical intermediate formed during inhibition of ribonucleotide reductase by 2'-azido-2'-deoxyuridine-5'-diphosphate (DFT calculations by Jörg Fritscher)
- Demonstrated that inhibition of ribonucleotide reductase by a clinically used nucleotide analog gemcitabine-5'-diphosphate (Gemzar) results from covalent modification of the enzyme

Mount Holyoke College (MHC), South Hadley, MA

- Carried out syntheses of bicyclic ring systems containing α -methylene- γ -butyrolactone functionality using organo-silicon reagents as key intermediates
- Demonstrated the utility of isotope-edited FTIR spectroscopy for the site-specific determination of secondary structure in short polypeptide sequences

Industry Experience

Merck Research Laboratories, Rahway, NJ

Department of Medicinal Chemistry, Summer 1999

Contributed to the development of a novel strategy for the combinatorial and parallel solid-phase synthesis of potential inhibitors of the mur-pathway enzymes

Department of Biochemistry, Summer 1998

Worked on the γ -secretase cloning project doing protein isolation and assays

Department of Analytical Chemistry, Summer 1997

Developed a method for the chiral separation of deprotected amino acids using capillary electrophoresis and imprinted gel synthesis

Teaching Experience

MIT

- General Chemistry – Led a tutorial (1999)
- Intermediate Chemical Experimentation – Led two laboratory sessions (2000)

MHC

- Organic Chemistry I and II – Led tutorials and laboratory sessions (1996 – 1999) NMR lab assistant – Instructed students on the use of a Bruker spectrometer (1997 – 1998)

Selected Publications

- Fritscher, J; Artin, E; Wnuk, S; Bar, G; Robblee, JH; Kacprzak, S; Kaupp, M; Griffin, RG; Bennati, M; Stubbe, J, Structure of the nitrogen-centered radical formed during inactivation of E. coli Ribonucleotide reductase by 2'-azido-2'-deoxyuridine-5'-diphosphate: trapping of the 3'-ketonucleotide, JACS, 127(21), 7729-38 (2005)

Published as Jelena Antonic:

- Maletic, M; Antonic, J; Leeman, A; Santorelli, G; Waddell, S, Preparation of potential inhibitors of the mur-pathway enzymes on solid support using an acetal linker, Bioorg. Med. Chem. Lett., 13(6), 1125-28 (2003)

- Decatur, SM; Antonic, J, Isotope-Edited Infrared Spectroscopy of Helical Peptides, JACS, 121(50), 11914-15 (1999)

Activities and Public Service

Amateur radio (KB1FMS)

- Provided emergency radio communications: Head of the Charles Regatta (2001–2004); Boston Marathon (2001–2002); Walk for Hunger (2001–2002); Jimmy Fund Walk (2001); Boston Half Marathon (2001)
- MIT UHF Repeater Association (W1XM), Treasurer (2001–2004)
- MIT Radio Society (W1MX), Treasurer (2001–2004)

Chemistry Outreach Program

- Showcased Chemistry demonstrations at local high schools (2004, 2005)
- Women in Research Day, Museum of Science Boston: introduced the fields of Chemistry and Biochemistry to high school female students (2004, 2005)